University of Southampton

MONO- AND BI-DENTATE GROUP 15 AND 16 LIGAND COMPLEXES OF MAIN GROUP METAL HALIDES

by Anthony Richard John Genge

A Thesis Submitted for the Degree of Doctor of Philosophy
Department of Chemistry

October 1999

UNIVERSITY OF SOUTHAMPTON

ABSTRACT

FACULTY OF SCIENCE

CHEMISTRY

Doctor of Philosophy

Mono- and Bi-dentate Group 15 and 16 Ligand Complexes
Of Main Group Metal Halides

by Anthony Richard John Genge

The synthesis and properties of tin(IV) and bismuth(III) halide complexes of mono- and bi-dentate ligands of groups 15 and 16 are described.

The complexes of SnX_4 (X = Cl, Br) with group 16 ligands of type R_2E (R = Me or Ph for E = S, Se; R = Me for E = Te), $RE(CH_2)_nER$ (E = S, Se or Te, R = Me or Ph, n = 1 – 3; n ≠ 1 or 2 for E = Te) and o-$C_6H_4(EMe)_2$ (E = S, Se or Te) have been synthesised and characterised by multinuclear NMR (^1H, ^{119}Sn,^{77}Se, ^{125}Te) spectroscopy, IR spectroscopy and elemental analysis. SnI_4 adducts were also studied. Single crystal X-ray diffraction has been employed to structurally characterise $[SnX_4(Me_2Se)_2]$ (X = Cl or Br), $[SnCl_4\{MeECH_2EMe\}]$ (E = S or Se), $[SnCl_4\{MeE(CH_2)_nEMe\}]$ (n = 2 for E = S, n = 3 for E = S or Se), $[SnX_4\{o\text{-}C_6H_4(EMe)_2\}]$ (X = Cl for E = S; X = Cl or Br for E = Se or Te), $[SnCl_4\{PhE(CH_2)_nEPh\}]$ (n = 3 for E = S; n = 2 for E = Se) and $[SnBr_4\{MeS(CH_2)_3SMe\}]$, and reveals a distorted octahedral geometry at the Sn^{IV} centre. This is also observed for $[SnCl_4(MeECH_2EMe)]$ (E = S or Se), where a highly strained four-membered chelate ring is formed. Multinuclear NMR spectroscopy and X-ray diffraction proved highly complementary, and allow a number of trends with donor and acceptor to be derived. A structural analysis was also obtained for $[SnI_4\{\eta^1\text{-}O\text{-}MeS(O)(CH_2)_3SMe\}_2]$, exhibiting an octahedral Sn^{IV} centre with two monodentate ligands bound through the sulfoxide donor.

An analogous series of complexes of phosphine and arsine ligands were also studied. The complexes of SnX_4 (X = Cl, Br or I) with the ligands Me_3P, $RE(CH_2)_2ER$ (R = Me or Ph for E = P; R = Ph for E = As), o-$C_6H_4(PPh_2)_2$ and o-$C_6H_4(AsMe_2)_2$ were produced and characterised using multinuclear NMR (^1H, ^{31}P, ^{119}Sn) and IR spectroscopies, elemental analysis. The chemical shifts observed were consistent with an octahedral geometry at Sn^{IV} and this was confirmed by the structural analysis of $[SnI_4\{o\text{-}C_6H_4(AsMe)_2\}]$, showing the ligand to chelate forming six-coordinate Sn^{IV}. The combination of techniques again allow trends with donor and acceptor to be identified. The oxidised complexes of o-$C_6H_4(PPh_2)_2$ were also studied for comparison and the structural analysis of solvated and unsolvated $[SnI_4\{o\text{-}C_6H_4(P(O)Ph_2)_2\}]$ reveal an unusual seven-membered chelate ring.

Complexes were also formed by reaction of certain of these group 15 and 16 bidentate ligands and with BiX_3 (X = Cl, Br or I). Characterisation of a number of the complexes was achieved by single crystal X-ray diffraction studies which reveal a wide range highly unusual and unexpected structural motifs ranging from seven-coordinate chelate species ($[BiBr_3\{MeS(CH_2)_2SMe\}_2]$), Bi_2X_6 dimers with chelating ligands ($[Bi_2I_6\{o\text{-}C_6H_4(AsMe_2)_2\}_2]$), or bridging ligands forming polymeric sheets with 1:1 ($[BiBr_3\{MeE(CH_2)_3EMe\}]_n$ (E = S or Se)), or 1:2 Bi : donor atom stoichiometries, ($[Bi_2Br_6\{PhS(CH_2)_2SPh\}]_n$), and the highly unusual complex $[Bi_4Cl_{12}\{MeS(CH_2)_3SMe\}_4]_n$, consisting of Bi_4Cl_4 pseudo-cuboids linked in a three-dimensional network by bridging ligands.

Acknowledgements

First and foremost, I should like to thank Professor Bill Levason and Dr Gill Reid for their help, support and enthusiasm during the years of this research, particularly for dedicating many an hour of their time to the collection of NMR spectra. Thanks are also due to Bill for the elemental analyses of the more sensitive materials within this report.

Special mention is due for Dr Mike Webster in particular, but also Gill for all their help in teaching me the mystical art of single crystal X-ray diffraction. Mike deserves special credit for introducing me to the wonders of the Hamilton R-factor statistical test for absolute configuration (wet towel and stiff drink obligatory!). Thanks also to Dr Sandra Dann for collecting MASNMR data.

Thanks to Nick Holmes for surviving two years in a lab with me, I'll make sure I get you next time! Prior to that Jeff Quirk is deserving of mention for spending hours on topics of little importance and providing me with the ideal role model.

Thanks to all other members of the Levason/Reid collective, from the 7th floor of the old department to the shiny new building, including Simon Pope, Julie Connolly, Andy Barton, Bhavesh Patel (has he broken the diffractometer yet?) and, prior to his defection, Doug Booth, all of whom have been the source of chemicals and distractions.

Everyone at the Church Lane residence; Adam Healy, Rich 'Tommy' Needs, Jon (Electrochemist!) Amphlett and Nic (Stato) Gibbard (and Kenny!). I'm grateful to the lads for hours of tedious footballing televisual entertainment, and Nic for replacing this with Coronation Street!

All the other reprobates who have, at one time or other, frequented the inorganic department; Adam, Tommy, Geoff, Kenny, Radar, Eric, Paul, Arran, Ant, Durrell, Steve, Julia, Sandra and Chris Rudkin. Particular thanks should go to all who have managed to avoid me on the mountains in France or Southampton; Kenny, Nick, Chris Rudkin, Eric and Doug.

Finally, I must acknowledge the Department of Chemistry for four years of funding as X-ray technician and PhD research student.

"If we knew what we were doing,
it wouldn't be called research, would it?"

Albert Einstein (1879-1955)

Contents

Page

Chapter 1

Chapter 2

Chapter 3

Chapter 4

Chapter 5

Chapter 6

Page

Chapter 1

Chapter 2

Chapter 3

Chapter 4

Chapter 5

Chapter 6

ABBREVIATIONS

Techniques

MASNMR	Magic Angle Spinning Nuclear Magnetic Resonance
NMR	Nuclear Magnetic Resonance
IR	Infra Red

Ligands - Acyclic

L	Monodentate ligand
L-L	Bidentate ligand
R	Ligand substituent
E	Donor atom

Ph - phenyl Me - methyl

Pr^n - n-propyl Bu - butyl

Et - ethyl

dppe	1,2-Bis(diphenylphosphino)ethane
dmpe	1,2-Bis(dimethylphosphino)ethane
dppm	Bis(diphenylphosphino)methane
dpae	Bis(diphenylarsino)ethane
diars	o-$C_6H_4(AsMe_2)_2$
triars	$CH_3C(CH_2AsMe_2)_3$

Ligands – Macrocyclic (general)

y – crown – n	oxygen-donor macrocycle where:
	y – number of atoms in ring
	n – number of donor atoms
[y]aneX_n	y, n as for oxygen-donor macrocycle
	X – donor heteroatom

Miscellaneous

CH_2Cl_2	Dichloromethane	$CHCl_3$	Chloroform
thf	Tetrahydrofuran	dmso	Dimethylsulfoxide
MeCN	Acetonitrile	$MeNO_2$	Nitromethane
Me_2CO	Acetone	acac	Acetylacetonate
TMS	Tetramethylsilane		

Chapter 1

Introduction

1.1 Main Group Chemistry – Overview

It is difficult to compile an overview of the main group elements as no two elements are alike, even within the groups of the periodic table. The p-block is the only block to contain non-metals, and as well as these it also contains metalloids whose properties share characteristics of both metals and non-metals (Figure 1.1). In general the metallic elements (Al, Sn, Pb etc.) lie in the bottom left of the block with non-metals (C, N, O, halogens etc.) occupying the top right separated by the metalloid elements (Si, Ge, As etc.). While extensive reviews have been produced on the main group elements[1] this study concentrates on the heavier p-block elements, whose coordination chemistry is the subject of this thesis. Previous, relevant studies on the coordination chemistry of their halides are discussed at the start of each chapter. The overview of the area and the properties of the starting halides are discussed here.

Figure 1.1. P-Block elements illustrating metals (white), metalloids (circled) and non-metals (grey). (taken from ref. 1)

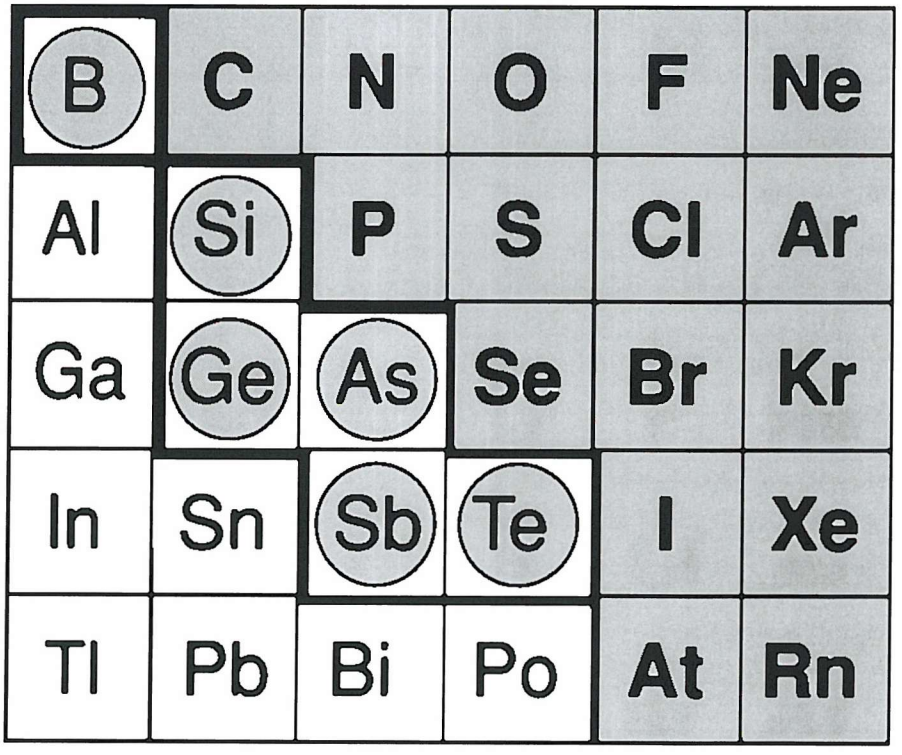

1.1.1. Group 14 Elements – Si, Ge and Sn

Nowhere is this enormous discontinuity in general properties between the first- and second-row elements as obvious as group 14, and this is followed by a transition through metalloids to metallic elements at the bottom of the group. This is well illustrated by their varying physical properties (Table 1.1). There is very little that can be taken from the chemistry of carbon and applied in detail to the chemistry of silicon. Carbon is a non-metallic element, silicon is essentially non-metallic, germanium is classed a metalloid and tin and lead are metallic in nature.

Table 1.1. Some properties of the Group 14 elements.[2a]

Element	Electronic structure	mp (° C)	bp (° C)	Ionisation enthalpies (kJ mol^{-1}) 1st	2nd	3rd	4th	Electro-Negativity	Covalent radius[a] (Å)
C	$[He]2s^2 2p^2$	>3550[b]	4827	1086	2353	4618	6512	2.5 – 2.6	0.77
Si	$[Ne]3s^2 3p^2$	1410	2355	786.3	1577	3228	4355	1.8 – 1.9	1.17
Ge	$[Ar]3d^{10}4s^2 4p^2$	937	2830	760	1537	3301	4410	1.8 – 1.9	1.22
Sn	$[Kr]4d^{10}5s^2 5p^2$	231.9	2260	708.2	1411	2942	3928	1.8 – 1.9	1.40[c]
Pb	$[Xe]4f^{14}5d^{10}6s^2 6p^2$	327.5	1744	715.3	1450	3080	4082	1.8	1.44[d]

a. Tetrahedral (i.e., sp^3 radii).
b. Diamond.
c. Covalent radius of Sn^{II}, 1.63 Å.
d. Ionic radius of Pb^{2+}, 1.33 (CN 6); of Pb^{4+}, 0.775 Å.

The group 14 elements form two series of halides, MX_2 and MX_4. The stability of MX_2 increases down group 14; $SiX_2 < GeX_2 < SnX_2 < PbX_2$, with the trend reversed for MX_4; $SiX_4 > GeX_4 > SnX_4 > PbX_4$. Silicon(IV) halides are formed as colourless, volatile liquids by reaction of silicon or silicon carbide with any halogen. Germanium(IV) halides are easily produced by reaction of GeO_2 with aqueous HX. The fluorides, SiF_4 and GeF_4 (produced by the thermal decomposition of $BaGeF_6$), are gaseous. All these halides consist of discrete tetrahedral units. SnF_4, which is produced by reaction of fluorine with tin, is different from the other group 14

tetrafluorides in being a white crystalline compound. The structure is polymeric (Figure 1.2) with octahedral coordination about the tin with SnF_6 units joined into planar layers by edge-sharing of four equatorial F atoms (Sn-F_μ 2.02 Å) with two further terminal F atoms mutually *trans* (Sn-F_t 1.88 Å).[3] The other tin(IV) halides are produced by reaction of elemental tin with the halogen under anhydrous conditions. These other tin(IV) halides follow the observed trend of discrete tetrahedral molecules with $SnCl_4$ a colourless liquid, while $SnBr_4$ is a colourless, crystalline solid and SnI_4 is an orange crystalline solid. All the group 14 tetrahalides are hygroscopic, and are immediately and completely hydrolysed by water. Controlled hydrolysis is possible with SiX_4 forming $X_3SiOSiX_3$ and $(X_3SiO)_2SiX_2$, GeX_4 is partially hydrolysed to give equilibria involving species of the type $[Ge(OH)_nCl_{6-n}]^{2-}$, and in the case of the tin(IV) halides, a number of hydrates of varying stoichiometries have been identified.[4]

There is also a clear trend of increasing Lewis acidity progressing down the group 14 elements. The MX_4 molecules are able to act as electron acceptors as they possess two vacant *d*-orbitals. Together with the s- and p-orbitals, these hybridise to form a set of six d^2sp^3 hybrids,[1] adopting the octahedral geometry commonly found in adducts of these MX_4 compounds.[5] There is also an observed decrease in Lewis acidity with halide type, F > Cl > Br > I as the M-X bond becomes less polar and the effective charge on the M centre increases.[6] This has also dictated the types of ligands that have been studied for these systems. In the vast majority of cases the ligands have been those with O-[5-7] or N-donor[5,6,8,9] systems. In contrast, the number of systems involving the softer P-[10] and S-donor[5,11,12] systems are few, As-[13] and Se-donor[12] systems rarer still, and for Te, systems of this nature have not been studied at all. Those that have been studied are discussed in detail in the introductions of the relevant chapters (S, chapter 2; Se, chapter 3; P/As, chapter 5).

Figure 1.2. View of the polymeric SnF_4 structure

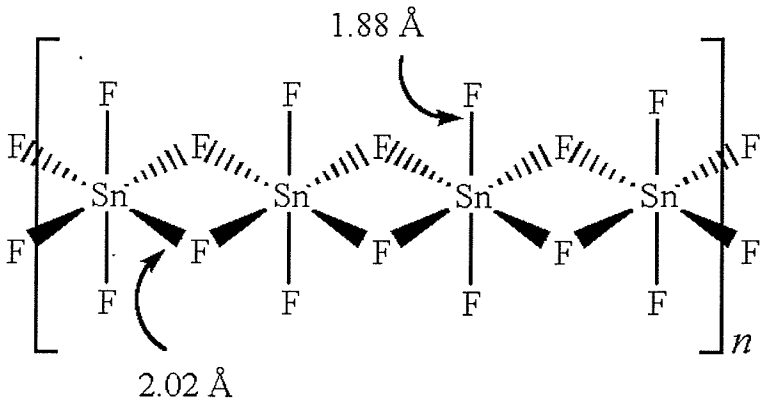

Industrial uses of the group 14 elements are widespread. The principal uses of silicon are within solid state electronics (silicon based transistor circuitry forms the basis for all modern electrical devices), ceramics, and polymers.[14] Germanium is also a key constituent within the solid state electronics industry (transistor action was first discovered in germanium), but also within optics (germanium is transparent in the infrared region of the spectrum) and other smaller applications (alloys, strain gauges, and superconductors).[15] Industrially, tin has a great deal of uses. Free radical reactions of organotin compounds are widespread and are reviewed briefly by A.G.Davies[16] and in greater detail in other reviews.[17] Tin(IV) oxide has interesting surface chemistry with a porous nature, which has been studied by Sharygin *et al.*,[18] and this leads to uses in catalysis and gas sensing. Organotins of oxidation states +II and +IV have a wide variety of uses and effects in biological chemistry, these are reviewed for general aspects,[19] environmental problems[20] and biochemistry and toxicology.[21]

1.1.2. Group 15 elements - Bi

As with the group 14 elements, the properties and characteristics of the group 15 elements vary greatly from top to bottom. This is again seen in the physical properties of the elements (Table 1.2). Nitrogen (which has the obvious distinction of being gaseous under normal conditions) is not included, as there is little resemblance between the characteristics it displays and the other group 15, elements except for the stoichiometries of some simple ionic compounds (e.g. NH_3, PH_3, NCl_3, $BiCl_3$). The elements of group 15 form two series of halides MX_3 and MX_5. In the case of bismuth the +3 oxidation state is far more stable than the +5 oxidation state.

In the gas phase the bismuth(III) halides studied here are pyramidal molecules.[22] In the normal solid, crystalline state however, there are additional near neighbours and weak, secondary Bi···X interactions form.[23,24] It is proposed that these interactions are formed about the site of the lone pair of electrons. In a review of SbX_3 complexes, Sawyer and Gillespie[25] found the same weak interactions forming. They too postulate that these interactions are formed around the direction of maximum electron density of the lone pair, but not directly over it. Complexes of BiX_3 are discussed in Chapter 6. With no visible spectroscopy or nuclei suitable for study by NMR, the coordination chemistry of BiX_3 is very limited and most of what has been studied dates back to the 1960s, when characterisation techniques were limited.[26] The vast majority of characterised complexes of BiX_3 adopt octahedral Bi^{III} centres, suggesting the lone pair is not stereochemically active, but there are numerous examples of other stoichiometries where there is a clear void left within the coordination sphere, consistent with the lone pair being stereochemically active in these cases. It is difficult to predict when the lone pair of electrons will be stereochemically active though certain general trends for the group 15 elements are apparent. Stereochemical activity of the lone pair is found to decrease according to As > Sb > Bi[2c] and also with increasing coordination number and increasing atomic number of the halogen.

Table 1.2. Physical properties of the Group 15 elements.[2b]

Element	Electronic structure	mp (° C)	Sum of 1st three ionisation enthalpies (kJ mol^{-1})/10^3	Electro-negativity	Covalent radius[a] (Å)
P	$[Ne]3s^23p^3$	44.1	5.83	2.06	1.10
As	$[Ar]3d^{10}4s^24p^3$	813 (36 atm)	5.60	2.20	1.21
Sb	$[Kr]4d^{10}5s^25p^3$	630.5	5.05	1.82	1.41
Bi	$[Xe]4f^{14}5d^{10}6s^26p^3$	271.3	5.02	1.67	1.52

a. For trivalent state.

Figure 1.3. View of the structure, with bond lengths, of SbF_3 (reproduced from ref. 23)

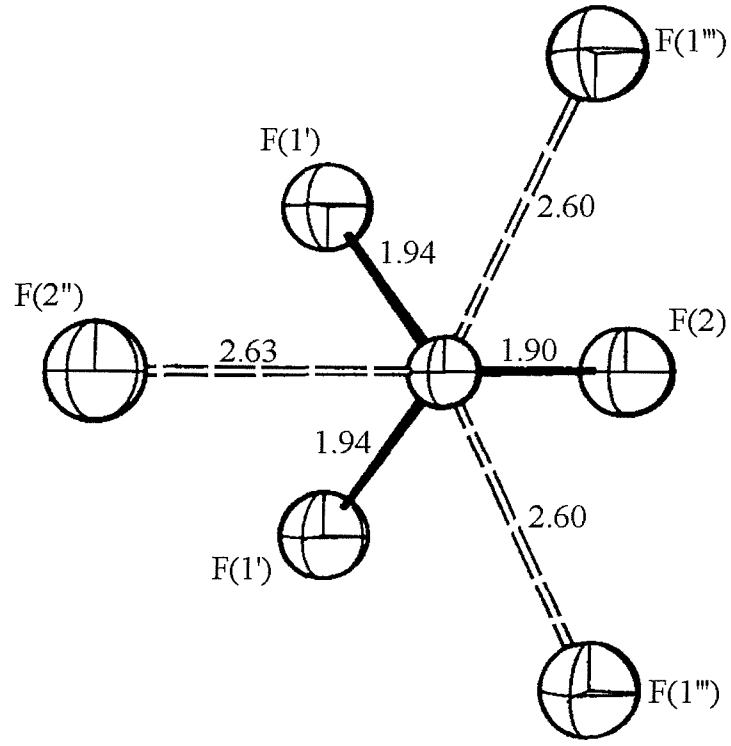

As a general rule the Lewis acidity for the BiX_3 compounds will decrease with increasing halide, F > Cl > Br > I, as the electron density is drawn closer to the Bi^{III} centre, reducing the attraction towards electron donors.

1.2. Ligands

1.2.1. Group 15 Ligands

Phosphines have been the centre of a great deal of research in recent years, mainly because of their importance in a number of key industrial process such as hydrogenation of alkenes (Wilkinson's complex[27]) or hydroformylation of alkenes.[28] In most cases the study of phosphine donors has involved mono- or bi-dentate tertiary phosphine ligands, and more recently interest has arisen in macrocyclic phosphines.[29] In this research the tin(IV) halide complexes of the group 15 donors are studied. The study carries on previous research of tin(IV) halide-phosphine complexes,[30] which warrants further studies as the results would appear to indicate the formation of phosphine-oxide complexes rather than the desired tin-diphosphine complexes.

1.2.2. M-P/As Bonding

In discussing group 15 ligand binding properties, the generally accepted description of phosphine bonding is that for transition metal complexes was first proposed by Chatt.[31] While this model holds for middle to late transition metals, it should be noted that the binding in early transition metals and main group metals is different due to their lack of suitable, filled π orbitals.

In transition metal-phosphine bonding the lone pair on the phosphine is donated into an empty metal d orbital forming a σ bond. The phosphine also possesses empty 3d orbitals into which π backbonding can occur from electrons of filled metal d orbitals of suitable symmetry, the effect being mutually reinforcing (synergic). While this model was applied extensively some workers suggested that a number of the properties observed in phosphine coordination could be explained purely in terms of σ bonding. It was argued that the 3d orbitals of the phosphorus donor are too high in energy and too diffuse to contribute significantly to bonding. There do remain certain aspects, such as the stabilisation of zerovalent metal phosphine complexes and the high spectrochemical position of phosphines, which cannot be explained by σ bonding alone. The general consensus, therefore, is that the bonding is dominated by σ bonding, and may be supplemented by a small π bonding component when the phosphine carries electronegative substituents.

The σ-donor power was traditionally quoted in terms of proton basicity [pK_a(H_2O)], determined either experimentally or estimated from Hammett σ_p or Kabachnik σ^{ϕ} constants.[32] Since then, gas-phase photoelectron spectroscopy (PES) has been used to measure directly the binding energy of the phosphorus lone pair.[33] The results of the PES studies show that electron binding energy decreases with more electronegative substituents such that PPh_3 > PPh_2Me > $PPhMe_2$ > PMe_3, opposite to the order expected and that obtained from pK_a measurements.[34,34] The nature of the π bonding has also been questioned and consequently changed. Early work had assumed that the π bond was M(dπ)-P(3dπ), but subsequent molecular orbital calculations[35] and PES experiments[36] have shown that these phosphorus 3d orbitals are not involved in π bonding. With this and other data collected from X-ray crystallography, the π backbonding from the metal is now considered to be accepted by the P-X (X = H or C) σ* orbital.[37]

For main group metals, the lack of suitable, filled π-bonding orbitals means that the bonding between the phosphine and the metal centre is purely σ-donor in character.

From studies on $[(C_5H_5)Fe(CO)_2]^+$ complexes with monodentate group 15 ligands, ER_3 (where E = N, P, As, Sb or Bi), the σ-donor ability of the ligands, based on ligand exchange experiments, was found to decrease down group 15 in the order E = P > As > Sb > N > Bi.[38] Steric effects due to the donor atom increase down the group, PR_3 < AsR_3 < SbR_3 < BiR_3, while the steric effects due to the substituents, R, decreases down the group, PR_3 > AsR_3 > SbR_3 > BiR_3.[2]

Until *ca.* 1970 the trends in metal-phosphine bonding were almost entirely attributed to the electronic effects discussed previously. However, the steric effects of the substituents are also significant and the accepted model for this was proposed by Tolman,[39] who described the cone angle (Θ) created by the substituents. Changes in the M-P or P-C bond lengths have little effect on the value of the cone angle. The largest changes are seen where rotation about the P-C bonds is possible and marked variations in the cone angles are observed. Since the concept of a cone angle treats the entire ligand as a solid cone, intermeshing of neighbouring substituents is not allowed for, and the resulting steric effect of the ligand is usually overestimated. This has lead to considerably more sophisticated methods of describing the cone angle.[40] What Tolman's cone angle does allow, however, is a simple, semiquantitative way of discussing the relative steric effects of different ligands. The advent of X-ray crystallography has created a wealth of data with which to work. Oliver and Smith[41]

have used these data to compare thirty platinum(II) complexes of PCy_3 to examine the steric effects. They showed that steric overcrowding in such molecules was accommodated in several ways, most importantly in lengthening the M-P bond.

Figure 1.4. Schematic diagram showing the cone angle, Θ.

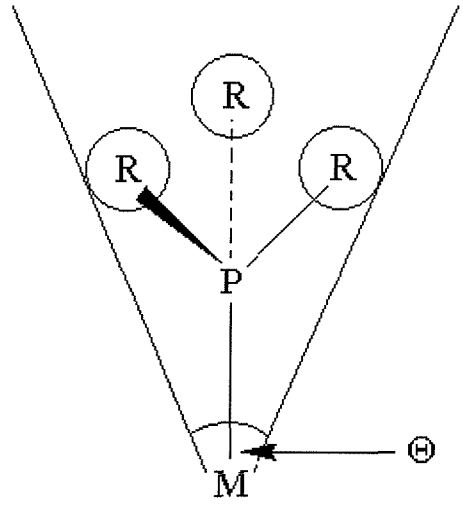

1.2.3. Group 16 Ligands - M-S/Se/Te Bonding

The general electronic configuration of the group 16 elements is ns^2, np^4, nd^0. Hence in the case of dialkylated species such as thioethers, selenoethers and telluroethers there are two of these valence electrons involved in bonding interactions with the alkyl groups, leaving four electrons in non-bonding orbitals on the heteroatom. In a review of thioether complexes of transition metals Murray and Hartley[42] describe the orbitals on the group 16 elements as varying from sp^3 hybridised on oxygen, to an s and three p orbitals on tellurium, with sulphur and selenium lying somewhere between these two extremes. In the case of thioethers they consider sulfur to be sp^3 hybridised resulting in two lone pairs. One or both of these may be involved in a coordinate bond to an electron acceptor.

If only one lone pair is involved in bonding then the other may either remain non-bonding resulting in stereoelectronic repulsion, or take part in π donation by rehybridisation to sp^2 followed by π donation of the lone pair from a p orbital to the

electron acceptor. In theoretical studies, Schumann and Hoffmann[43] predicted that the M-L (L = S, Se or Te) bond strengths increase as group 16 is descended. Within the same study[43] on complexes of $[C_5H_5Fe(CO)_2]^+$, ligand exchange experiments indicated that the M-E bond strengths increase as group 16 is descended. This is in contrast to group 15 where the opposite is found.[43] In more recent studies,[44] the same conclusions are drawn from observed ν(CO) force constants of low valent Mn(I), Re(I), Cr(0), Mo(0) and W(0) carbonyl complexes. The trend that arises from these is that the CO bond weakens in the order S $\rightarrow$ Se $\rightarrow$ Te, the suggested reasoning being that with decreasing electronegativity down group 16 an increase in π backdonation from the metal centre results in weakening CO bonds. For metal halide systems, there is evidence that Se offers stronger binding than S, but Te ligands appear to bond more weakly as the metal oxidation state increases.[45] The rationale for this being that the overlap between the large Te σ-donor orbital and the contracted metal orbitals is poorer for Te than for Se.

As well as filled valence orbitals, all group 16 elements have empty n*d* orbitals, providing the possibility for π back-donation from metal to ligand, if the orbitals are of the correct symmetry and energy. The importance of this π back-donation is ill-defined but should increase down the group. However, in all cases, it is less important than for phosphines, arsines and stibines. For thioethers, as with group 15 ligands, suitably oriented S-C σ^* orbitals are considered to be the most likely acceptors of π backbonding.[46] In a review of structurally characterised examples of late transition metal complexes of [9]aneS_3 (1,4,7-trithiacyclononane), Blower *et al.*[46] argue that they observe increasing S-C bond lengths consistent with π backbonding into these σ^* orbitals. In the most extreme example, $[Re([9]aneS_3)_2]^{2+}$, it was suggested that this effect was strong enough to break the S-C bonds, releasing ethene, forming $[Re([9]aneS_3)(SCH_2CH_2SCH_2CH_2S)]^+$.

With no strong π back-donation, modest σ donor abilities and any stereoelectronic effects arising from the non-bonding pair of electrons, group 16 ethers are considered poor ligands relative to group 15 ligands. As discussed for the group 15 donor ligands, the lack of suitable, filled π orbitals on the main group metals studied in this thesis means that π backbonding in these systems is not an option and bonding is restricted to σ donation.

1.2.4. Pyramidal Inversion

Since the thio-, seleno- and telluro-ethers used in this study can bind *via* one of two lone pairs, there are different invertomers that can be formed for $[SnX_4(L\text{-}L)]$. In solution the molecules are able to switch between invertomers, either by a dissociative route or *via* pyramidal inversion. Pyramidal inversion at sulfur atoms was first studied in 1966 by Abel *et al.*[47] using ^1H NMR spectroscopy with $[PtCl_2\{MeS(CH_2)_2SMe\}]$. It was found that the inversion process occurred slowly on the NMR timescale, such that the protons were nonequivalent and the *meso* and *dl* invertomers (Figure 1.5) could be identified.

Figure 1.5. *meso* and *dl* invertomers for $[PtCl_2\{MeS(CH_2)_2SMe\}]$ (taken form ref. 47)

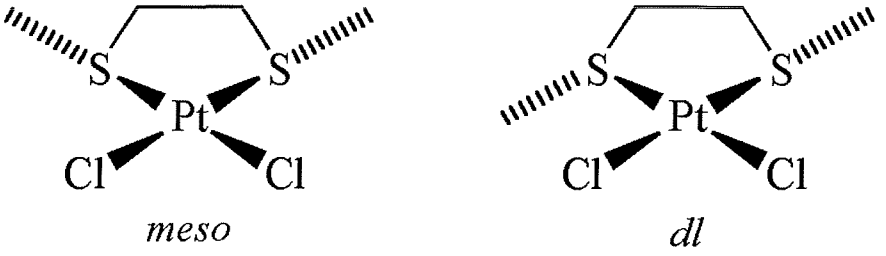

Typical activation energies are in the range 35 – 100 kJ mol^{-1}.[48] Since the activation energy for this process is low, and ^{195}Pt-^1H coupling is retained at higher temperatures, the mechanism proposed for this process is *via* a planar transition state (Figure 1.6) with both lone pairs bonded to the metal.[49,50] The onset of pyramidal inversion in bidentate complexes occurs at significantly higher temperatures than for *trans* monodentate complexes. The *trans* effect on the inversion barriers seen for halide ions in these complexes is found to be in the order Cl > Br > I.[42]

Figure 1.6. Proposed mechanism for pyramidal inversion in $[PtCl_2\{MeS(CH_2)_2SMe\}]$[49,50]

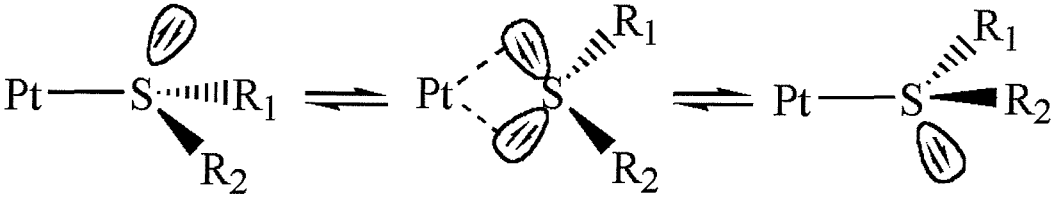

1.3. Physical Measurements

The complexes formed in this study were all characterised using a combination of techniques. Microanalyses were collected for all solids isolated. The other means of characterisation were infrared (IR) spectroscopy, nuclear magnetic resonance (NMR) spectroscopy and single crystal X-ray diffraction. The following is a brief overview of these three techniques which, for the purposes of this study, prove highly complementary.

1.3.1. Single Crystal X-ray Diffraction

Figure 1.7. Rigaku AFC7S four circle diffractometer

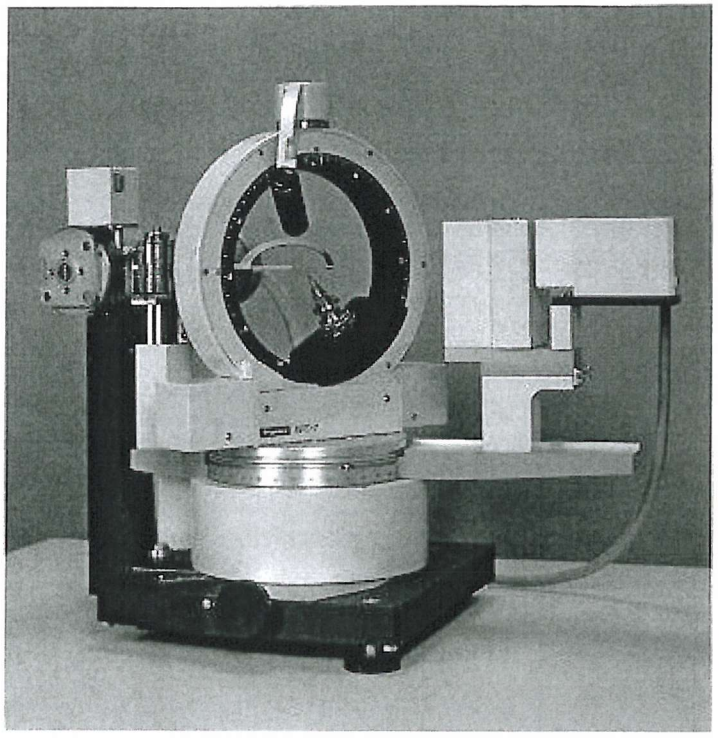

The data for the X-ray structural analyses within this study were, in the majority of cases, collected on a Rigaku AFC7S four-circle diffractometer (Figure 1.7) using a sealed Mo-Kα X-ray tube with radiation of wavelength 0.71073 Å. However, in the case of $[BiBr_3\{MeS(CH_2)_3SMe\}]$ the crystals obtained were smaller and the data were collected instead on an Enraf-Nonius KappaCCD diffractometer (Figure 1.8) that uses a

Nonius FR591 rotating anode X-ray generator. By rotating the anode within the X-ray source a more powerful beam is possible and the heat generated is dispersed across a much larger area relative to the anode found in a sealed tube. The increased power possible from a rotating anode source means that smaller, and less strongly diffracting, crystals may be analysed. The collection strategies are also very different for the four-circle and the KappaCCD diffractometer. The Rigaku AFC7S collects intensities of reflections using a scintillation counter. This contains a material, such as thallium-doped sodium iodide, which produces light when X-rays fall on it. This light is, in turn, detected and amplified by a photomultiplier, such that an electrical pulse is produced for every X-ray photon that is incident on the detector face, which is normally a few millimetres in diameter. In contrast the KappaCCD diffractometer uses an area detector. This uses a technology more commonly found in video cameras where a CCD (charge-coupled device) is used to measure the incident X-ray photons. Rather than direct recording of the X-ray photons, a phosphor is fibre-optically coupled to the CCD chip and the incident radiation produces an electron-hole pair on the semiconductor. The CCD has a detection area of a few centimetres in diameter and collects several reflections simultaneously as an image for computer analysis.

Figure 1.8. Enraf-Nonius KappaCCD area detector diffractometer

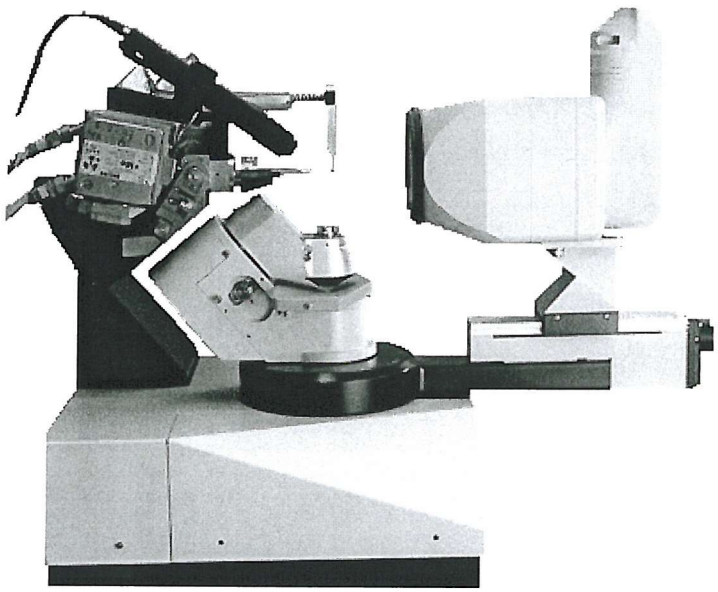

Data Collection

The crystal is mounted on a goniometer which allows adjustment of the position in three dimensions and is placed at the centre of the diffractometer. The different sizes of detector area employed by the diffractometers also leads to different collection strategies. The four-circle diffractometer needs four full rotation axes (χ, ϕ, ω and θ; Figure 1.9a) in order to position the goniometer for all the necessary reflections. The KappaCCD, with a larger detector area does not need to use full circles. Instead ϕ, ω and θ are used along with a partial κ axis (Figure 1.9b). The principal advantages of using a CCD based diffractometer are the reduced time periods required to collect a full dataset (hours compared to days for the scintillation counter) and the ability to obtain structural analyses of much smaller, less strongly diffracting samples.

The most crucial part of data collection is, without doubt, selection of a suitable crystal. The morphology of the crystal (well defined faces/edges) is a good indicator of quality, but better still are the optical characteristic of the crystal when viewed under plane-polarized light. While viewed under polarized light, if the crystal is rotated the light should be extinguished in certain directions and allowed through at 90° to this direction. Once selected the crystal is mounted on the goniometer head. If the material is sensitive to moisture or air it can be mounted within a capilliary tube, though usually a coating of an inert oil, followed by rapid cooling in a stream of cold N_2 gas is sufficient. The crystal is then aligned in the centre of the X-ray beam. If the data is to be collected at room temperature the crystal needs to mounted with a glue to prevent movement, but more normally collection is at low temperature (e.g. 150 K), to reduce molecular vibrations, so a grease, which freezes solid, is sufficient.

Figure 1.9. Schematic diagrams of a) four-circle diffractometer and b) Enraf-Nonius KappaCCD diffractometer (taken from ref. 51)

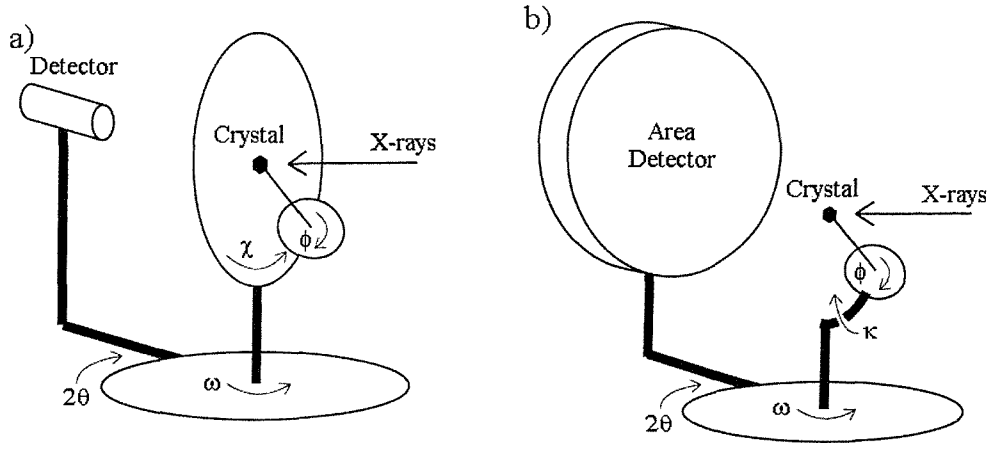

The first stage of collection is then to identify the unit cell. On the four circle diffractometers this is achieved by finding > 15 reflections by scanning randomly across the crystal. The ability of the CCD detector to collect several reflections simultaneously speeds this process up. From these the simplest unit cell that connects the reflections is calculated, together with an orientation matrix which relates the position of the crystal with the Miller indices, hkl. The initial pattern can also be used to identify symmetry elements present within the cell. The symmetry elements are checked by measuring independent reflections which would be expected to be equivalent due to the symmetry. From this a Laue group may be assigned which can reduce the amount of data that needs to be collected. At this point on the four-circle diffractometer a psi-scan is collected by measuring the intensity of one reflection while rotating the crystal about 360 ° in the diffraction vector (ψ). This can be used to correct for irregular absorption arising from the crystal morphology. Heavier atoms will absorb more radiation and, in some cases, the psi-scan does not provide an adequate correction. In these cases an empirical absorption correction may be applied during structure solution, e.g. DIFABS.[52] For the KappaCCD the nature of the rotation axes prevent psi-scan measurements. Instead an empirical absorption correction is calculated based on symmetry equivalent reflection that have been collected (SORTAV[53]). During collection on the four circle diffractometer standard reflections are collected every 150 reflections which may be compared to calculate the degree of decay which may arise from decomposition by the environment or, for heavily absorbing crystals, the X-ray radiation. The intensities (I(hkl) and observed structure amplitudes ($|F_o|$) of the required reflections are measured.

Structure Solution

Once collected, the reflections are ordered according to hkl and from the characteristic systematic absences arising from the symmetry a space group can be assigned. At this point it is possible to gauge the quality of the data according to what percentage of the maximum possible data has been observed and, if equivalent reflections have been measured, a comparison of these can be calculated (R_{int}). Once sorted, the data are solved using one of two strategies, direct methods or Patterson synthesis. The phases of the reflections are unknown. In the Patterson synthesis this problem is avoided by calculating the Fourier transform of the squared amplitudes F_o^2 with all phases set equal to zero. The Patterson map produced by this represents a map

of vectors between the atoms in the structure. Thus for two atoms at (x_1, y_1, z_1) and (x_2, y_2, z_2) there will be a peaks in the Patterson map at (x_1-x_2, y_1-y_2, z_1-z_2) and (x_2-x_1, y_2-y_1, z_2-z_1). From this it can be said that for a peak in the map at (u, v, w) there must be two atoms whose x coordinates differ by u, y coordinates differ by v and z coordinates differ by z. A Patterson map contains a total of $n^2 - n$ reflections and while these resemble electron density peaks they are more spread out and overlap. This means that Patterson synthesis is best suited to structures containing heavy atoms.

Direct methods attempts to obtain approximate reflection phases from the measured intensities. Several factors help in this process. Firstly while the wave has half its value positive and half negative, the electron density within the structure must be positive or zero, it cannot be negative. Secondly the electron density is not evenly distributed, but localised at the sites of the atoms. This means that the waves must be added together in such a way as to maximise the positive regions and minimise the negative regions. Direct methods involve selecting the most important reflections which contribute most to the Fourier transform, working out the probable phase relationships between these, and then calculating the remaining relationships. The most promising solution is then used to calculate a Fourier transform from the observed amplitudes. If successful recognisable features of the molecules should be found in the electron density map calculated. Unlike the Patterson synthesis atom size is unimportant so this method is suitable for all structures.

Structure Refinement

Once a solution has been found the structure must be refined. This is done by least-squares analysis. From the parameters that have been defined during solution (these include x, y, z, occupancy, and a description of the atoms thermal motion) the reverse procedure is carried out and a Fourier transform is calculated for the data to produce the amplitudes that would be observed for this structure $|F_c|$. The refinement process defines the 'best fit' of the two sets of data ($|F_o|$ and $|F_c|$) as that which minimises the least-squares sum:

$$\Sigma\, w_i(|F_o|_i - |F_c|_i)^2$$

Where w_i is a weighting factor applied to each reflection calculated according to its reliability, for the structures in this thesis this is based on the e.s.d.s, $1/\sigma^2(F_o^2)$ is used.

From this, a comparison can be made between the calculated model and the observed data. This is normally done by calculating an *R*-factor (residual factor) defined as:

$$R = \frac{\sum(|F_o|_i - |F_c|_i)}{\sum|F_o|_i}$$

The same *R*-factor is calculated but with weighting. This weighted *R*-factor is defined as:

$$R_w = \sqrt{\frac{\sum w_i(|F_o|_i - |F_c|_i)^2}{\sum w_i |F_o|_i^2}}$$

Another commonly quoted comparison is the goodness of fit (GOF) which is calculated based on similar principles and is defined as:

$$GOF = \frac{\sum(|F_o|_i - |F_c|_i)/\sigma_i}{(n-m)} \approx 1$$

Where n = the number and reflections used

m = the number of variables refined

Iterative cycles of least-squares refinements are used until these values are minimised. Typically the *R*-factor has a value of 0.02 – 0.07 for a satisfactory solution. Once refinement is complete the residual peaks and troughs remaining in the Fourier difference map should be minimised such that they are close to zero.

1.3.2. Nuclear Magnetic Resonance (NMR) Spectroscopy

For all of these compounds a major characterisation technique has been NMR spectroscopy, both in solution and in the solid state. Using multinuclear NMR spectroscopy, with low temperature attachment, it is possible to probe the dynamic processes occuring in solution. There follows a brief discussion of the nuclei studied.

^{31}P NMR Spectroscopy[54]

Phosphorus has a 100 % abundance of ^{31}P with spin I = ½ and a relative receptivity to hydrogen of 6.6 x 10^{-2} and is therefore an excellent nucleus for NMR spectroscopic studies of metal-phosphine complexes. Chemical shifts are normally referenced to an external 85 % aqueous H_3PO_4 solution. The chemical shift of the phosphines is largely governed by the nature of the substituent. If the substituents are electron-rich a lower frequency shift is observed, while electron-poor substituents have the opposite effect and a high frequency shift is found. When a phosphine is coordinated to a metal centre the formation of a M-P σ bond involves the movement of electrons away from the phosphine to the metal deshielding the ^{31}P nucleus. The result is that a shift to higher frequency is usually observed for coordinated phosphines. In the case of the diphosphines the size of the chelate-ring formed is an important factor. Garrou[55] has reviewed the chelate-ring parameter, ΔR. This is defined as the difference between the coordination chemical shift, Δ, of the *cis*-coordinated monodentate complex (*cis*-[$SnX_4(Me_3P)_2$]), and the observed coordination chemical shift of an equivalent *cis*-coordinated bidentate chelate complex (e.g. Δ(*cis*-[$SnX_4(Me_3P)_2$]) – Δ([SnX_4(dmpe)]). Generally, for a five-membered chelate-ring ΔR is found to be positive while for four- and six-membered chelate-rings a negative ΔR is observed. This is best illustrated for the series [$PtMe_2\{Ph_2P(CH_2)_nPPh_2\}$] where ΔR values of –52.2, +24.1, -14.1 and –0.7 are observed for n = 1 to 4, representing four- to seven-membered chelate rings.[55] The reason for this effect is not clear and there are exceptions. One highly relevant example for this main group metal study is that of Siegl, Schier and Schmidbaur[56] who see a coordination shift to low frequency in the ^{31}P NMR spectrum of the o-$C_6H_4(PPh_2)_2$ complex of indium(III) chloride.

^{77}Se NMR Spectroscopy[57]

Selenium has six naturally occuring isotopes. ^{77}Se, with natural abundance 7.6 %, has spin I = ½ and a relative receptivity to hydrogen of 5.26 x 10^{-4} making it suitable for study by NMR spectroscopy. ^{77}Se chemical shift are referenced to the ^{77}Se resonance of neat Me_2Se which is assigned δ 0.[58] As for ^{31}P NMR chemical shifts, a high frequency shift is observed with electron rich substituents. When an M-Se σ bond is formed on coordination the Se centre is deshielded and the resulting shift is usually to high frequency.

The coordination shift, ΔR, reviewed by Garrou[55] can also be applied to selenoether systems and corresponding shifts have been observed in transition metal complexes.[59]

^{125}Te NMR Spectroscopy[57]

Tellurium has seven naturally occuring isotopes of which it is ^{125}Te, with spin I = ½, natural abundance 7.0 % and a relative receptivity to hydrogen of 2.21 x 10^{-3}, which is used in NMR spectroscopic studies. Detracting from this is the negative magnetogyric ratio (γ = -8.453 x 10^7 rad T^{-1} s^{-1}) which may lead to signal diminuation *via* the Nuclear Overhauser Effect (NOE) (discussed in the ^{119}Sn NMR spectroscopy).[57] Resonances for ^{125}Te are referenced to the resonance of neat Me_2Te. The same high frequency shifts discussed for other nuclei are observed with electron-rich substituents. With coordination, a low frequency shift is observed as the tellurium nucleus is deshielded.

^{73}Ge NMR Spectroscopy[57]

^{73}Ge NMR spectroscopy is hampered by the combination of a very low NMR frequency, 3.488 MHz, and a quadrupole moment arising from the spin of $^9/_2$. This means that the difference in energy between the ground and excited states is small and the signals obtained are consequently weak. The quadrupole moment then has the effect of broadening the lines. Combined with these problems ^{73}Ge also possesses a negative magnetogyric ratio which also decreases the signal strength. The net effect of this is that only molecules with high symmetry (e.g. GeX_4, GeX_6^{2-}) have linewidths narrow enough to be discernible from background. In this study $GeCl_4$ is observed at +30.9 ppm and this is unchanged in the presence of a chelating ligand ($MeS(CH_2)_2SMe$) suggesting that no adduct formation occurs that would lower the symmetry and increase the linewidth.

^{119}Sn NMR spectroscopy[57]

Tin has three nuclei suitable for study by NMR spectroscopy, ^{115}Sn, ^{117}Sn and ^{119}Sn. All three nuclei have spin I = ½. Of these, ^{115}Sn is rarely used due to its low natural abundance, 0.35 %. ^{117}Sn and ^{119}Sn both have similar relative receptivities to hydrogen, ^{117}Sn = 3.5 x 10^{-3}, ^{119}Sn = 4.5 x 10^{-3}, and similar natural abundances, ^{117}Sn 7.6 %, ^{119}Sn 8.6 %, but it is ^{119}Sn which is commonly studied as it is slightly superior in both aspects. ^{119}Sn resonances are referenced relative to that of neat Me_4Sn (δ 0 ppm).

Very distinct regions are observed in the tin(IV) halides dictated by the halide donor. Thus with the chloride, $SnCl_4$ is observed at δ –150 ppm and the complexes formed in this study are typically in the range δ –500 to –600 ppm. In contrast, $SnBr_4$ is observed at δ –638 ppm with complexes formed observed in the range δ –1100 to –1300.

^{119}Sn also possesses a large negative magnetogyric ratio, γ = -9.9707 x 10^7 rad T^{-1} s^{-1}, which means that the resonances observed are heavily affected by signal diminuation from the NOE.[57] For most nuclei this ratio is positive and has the effect of enhancing the signal by an amount defined by:

$$NOE_{\max} = 1 + \frac{\chi_s}{2\chi_I}$$

χ_s = magnetogyric ratio of observed species

χ_I = magnetogyric ratio of irradiated species

When the negative magnetogyric ratio is placed in this equation a negative effect is observed, i.e. signal diminuation. For spectra of this nucleus, a paramagnetic centre, such as $Cr(acac)_3$, is added to the solution to reduce very long spin-lattice relaxation times and remove the NOE. This is achieved by providing a second relaxation mechanism which over-rides the nuclear dipole-dipole relaxation process.

1.3.3. Infra-red Spectroscopy

Previous studies of tin(IV) halides[11] had shown that the ν(Sn-X) bands lie within the regions 290 – 340 cm^{-1} for X = Cl and 190 – 240 cm^{-1} for X = Br. Therefore in order to access this region nujol mulls of the samples are supported on caesium iodide windows, which are transparent across the range 4000 – 200 cm^{-1}, and used either a Perkin-Elmer 983G grating spectrophotometer or a Perkin-Elmer FTIR 1710 spectrophotometer which employs caesium iodide beam splitter and covers the same range. The bismuth(III) chloride complexes were found to show several features assigned as ν(Bi-Cl) in the range 230 – 280 cm^{-1}. The heavier bromine atom meant that the analogous ν(Bi-Br) bands fall below the cut-off point of the caesium iodide windows.

For the tin(IV) halide systems studied two different symmetries are anticipated. For the monodentate systems, *trans*-[SnX_4L_2] is the expected form and would exhibit D_{4h} symmetry, while for the bidentate systems the chelate, *cis*-[SnX_4(L-L)], with C_{2v} symmetry is expected. By applying the reduction formula (Figure 1.10) to the reducible representation of symmetry operations within the molecules it is possible to find the IR active bands to be expected.

Figure 1.10. Infrared Reduction Formula

$$n_i = \frac{1}{h}\sum g_i \times \chi_I \times \chi_r$$

h = number of operations in the group

g_i = number of symmetry operations in the class

χ_I = character of the irreducible representation

χ_r = character of the reducible representation

Thus for molecules of the type *cis*-[SnX_4(L-L)] with C_{2v} symmetry the reducible representation is:

C_{2v}	E	C_2	σ_v	σ_v'
$\Gamma_{Sn\text{-}X}$	4	0	2	2

Which, when the reduction formula is applied predicts four active bands ($2A_1$ + B_1 + B_2) in the infrared.

For the $BiCl_3$ complexes the bands are observed in the region 230 – 280 cm^{-1}, however, as is seen from the literature the number of different structural motifs observed in this coordination chemistry,[26] even within one reaction mixture, makes prediction of bands for these systems hazardous.

1.4. Aims of this study

The aims of this research study were to synthesise and characterise a variety of main group metal complexes with mono- and bi-dentate ligands of groups 15 and 16. These complexes have been characterised using spectroscopic techniques and, in a number of cases, structurally using single crystal X-ray diffraction.

By using multinuclear NMR spectroscopic techniques incorporating variable temperature studies, it has been possible to study the dynamic processes of ligand dissociation and pyramidal inversion that occurs in solution for the tin(IV) halide complexes with group 16 donor ligands. The data obtained for a wide variety of complexes from their X-ray structural analysis has permitted correlations to be drawn between the solution and solid states. By studying the analogous thio-, seleno- and telluro-ether complexes of the tin(IV) halides it has been possible to draw conclusions about their relative stabilities. The effects of altering the halide species, ligand substituent and chelate-ring size have also been studied and conclusions have been drawn from the results about the relative stabilities of the complexes formed.

The same spectroscopic techniques have been used to study the tin(IV) halide complexes with group 15 donor ligands, and allowed conclusions to be made on the relative stabilities of the complexes formed. X-ray structural analysis has also been used to study characteristics in the solid state. The tin(IV) halide complexes of the oxidised ligand o-$C_6H_4(P(O)Ph_2)_2$ were synthesised to allow comparison with the phosphine complexes in solution.

The same group 15 and 16 bidentate ligands have been studied with the bismuth(III) halides. The main emphasis of this study has been on structural analysis which has revealed a large variety of structural motifs including seven-coordinate monomers, halide-bridged dimers, and extended polymeric arrays incorporating dimers and pseudo-cuboids.

References

[1] N. C. Norman, in J. Evans (Editor), *Periodicity and the p-Block Elements*, Oxford University Press, Oxford.

[2] Advanced Inorganic Chemistry, F. A. Cotton and G. Wilkinson, 5th Edition, Wiley, New York, p. 266 (a); p. 383 (b); p. 398 (c).

[3] R. Hoppe and W. Dähne, *Naturwissenschaften*, 1962, **49**, 254.

[4] G. Valle, A. Cassol and U. Russo, *Inorg. Chim. Acta*, 1984, **82**, 81.

[5] J-M. Dumas and M. Gomel, *Bull. Soc. Chim. France*, 1974, **10**, 1885.

[6] P. G. Harrison, in P. G. Harrison (Editor), *The Chemistry of Tin*, Blackie, New York, 1989, p. 30.

[7] C. Y. Wong and J. D. Woollins, *Coord. Chem. Rev.*, 1994, **130**, 175 and references therein.

[8] D. Tudela, V. Fernandez, J. D. Tornero and A. Vegas, *Z. Anorg. Allg. Chem.*, 1986, **532**, 215.

[9] D. Tudela, M. A. Khan and J. J. Zuckerman, *J. Chem. Soc., Dalton Trans.*, 1991, 999 and references therein.

[10] F. Sarikhaya, *Synth. React. Inorg. Met. Org. Chem.*, 1989, **19**, 641 and references therein.

[11] I.R. Beattie and L. Rule, *J. Chem. Soc.*, 1964, 3267; S.J. Ruzicka and A.E. Merbach, *Inorg. Chim. Acta*, 1976, **20**, 221; C.T.G. Knight and A.E. Merbach, *J. Am. Chem. Soc.*, 1984, **106**, 804; C.T.G. Knight and A.E. Merbach, *Inorg. Chem.*, 1985, **24**, 576; N. Bricklebank, S. M. Godfrey, C. A. McAuliffe and R. G. Pritchard, *J. Chem. Soc., Chem. Commun.*, 1994, 695; G.T. Morgan and W. Ledbury, *J. Chem. Soc.*, 1922, 2882; G.R. Willey, A. Jarvis, J. Palin and W. Errington, *J. Chem. Soc., Dalton Trans.*, 1994, 255; M. M. Olmstead, K. A. Williams and W.K. Musker, *J. Am. Chem. Soc.*, 1982, **104**, 5567.

[12] S.J. Ruzicka and A.E. Merbach, *Inorg. Chim. Acta*, 1977, **22**, 191; S.J. Ruzicka, C.M.P. Favez and A.E. Merbach, *Inorg. Chim. Acta*, 1977, **23**, 239; E.W. Abel, S.K. Bhargava, K.G. Orrell and V. Sik, *Inorg. Chim. Acta*, 1981 , **49** , 25.

[13] J. A. C. Allison and F. G. Mann, *J. Chem. Soc.*, 1949, 2915; P. G. Harrison, B. C. Lane and J. J. Zuckerman, *Inorg. Chem.*, 1972, **11**, 1537; D. Cunningham, M. J. Frazer and J. D. Donaldson, *J. Chem. Soc. A*, 1971, 2049; R. Rivest, S. Singh and C. Abraham, *Can. J. Chem.*, 1967, **45**, 3137; N. Ohkaku and K. Nakamoto, *Inorg. Chem.*, 1973, **12**, 2446; R. J. H. Clark, *J. Chem. Soc.*, 1965, 5699.

[14] Kirk-Othmer Encyclopaedia of Chemical Technology, 2nd Edition, 1969, **18**, 46 (Silica, silicon and silicides; Silicon compounds); 3rd Edition, 1979, **5**, 234 (Ceramics), 290 (Ceramics as electrical materials); 3rd Edition, 1979, **6**, 190 (Clays).

[15] Kirk-Othmer Encyclopaedia of Chemical Technology, 3rd Edition, 1980, **11**, 791 (Germanium and germanium compounds).

[16] "Organotin Compounds: New Chemistry and Applications", J.J. Zuckerman, *Adv. Chem. Ser.*, American Chemical Society, Washington, DC, 1976, **157**, 26.

[17] "Tin in Organic Synthesis", M. Pereyre, J. Quintard and A. Rahm, Pergamon, London, 1986; "Radicals in Organic Synthesis: Formation of Carbon - Carbon Bonds", B. Geise, Pergamon, London, 1986.

[18] L.M. Sharygin and V.F. Gonchar, *Kinet. Catal.*, 1974, **15**, 123; *ibid.*, 1974, **15**, 404; L.M. Sharygin, V.F. Gonchar and V.M.Galkin, *Kinet. Catal.*, 1974, **15**, 1125; L.M. Sharygin, V.F. Gonchar and A.P. Shtin, *Kinet. Catal.*, 1975, **16**, 178.

[19] "Organometallic Compounds and Living Organisms", J.S. Thayer, Academic Press, Orlando and London, 1984.

[20] S.J. Blunden, L.A. Hobbs and P.J. Smith, *Environmental Chemistry- RSC Spec. Periodical Rept.*, 1984, **3**, 49.

[21] W.N. Aldridge, in *Proc. 2nd Int. Conf. on Si, Ge, Sn and Pb Compounds*, "Rev. Si, Ge, Sn and Pb Cmpds, Special Issue", M. Gielen and P.G. Harrison, Freund Publishing House, Tel Aviv, 1978, **9**; A.K. Saxena, *Appl. Organomet. Chem.*, 1987, **1**, 39; *Tin as a Vital Nutrient: Implications in Cancer Prophylaxis and Other Physiological Processes*, N.F. Cardarelli, CRC Press, Boca Raton, Florida, 1986.

[22] H. A. Skinner and L. E. Sutton, *Trans. Faraday Soc.*, 1940, **36**, 681.

[23] S. C. Nyburg, G. A. Ozin and J. T. Szymanski, *Acta Crystallogr., Sect. B*, 1971, **27**, 2298.

[24] A. K. Cheetham and N. Norma, *Acta Chem. Scand., Ser. A,* 1974, **28**, 55.

[25] J. F. Sawyer and R. J. Gillespie, *Prog. Inorg. Chem.*, 1986, **34**, 65.

[26] N. C. Norman and N. L. Pickett, *Coord. Chem. Rev.*, 1995, **145**, 27; S. M. Godfrey, C. A. McAuliffe, A. G. Mackie and R. G. Pritchard in *Chemistry of Arsenic, Antimony and Bismuth*, N. C. Norman (Editor), Blackie, New York, 1997, p. 159.

[27] J. A. Osborn, F. H. Jardine, J. F. Young and G. Wilkinson, *J. Chem. Soc.*, 1966, 1711.

[28] C. A. McAuliffe and W. Levason, *Transition Metal Complexes of Phosphorus, Arsenic and Antimony Ligands,* C. A. McAuliffe (Editor), MacMillan, London, 1973.

[29] A.-M. Caminade and J. P. Majoral, *Chem. Rev.*, 1994, **94**, 1183 and references therein.

[30] V. S. Petrosyan, N. S. Yashina and E. J. Gefel, *Silicon Germanium Tin Lead Compd.*, 1985, **9**, 1387.

[31] J. Chatt, *Nature Lond.*, 1950, **165**, 637; J. Chatt and A. A. Williams, *J. Chem. Soc.*, 1951, 3061.

[32] M. J. Kabachnik and T. A. Mastryukova, *Russ. Chem. Rev.*, 1969, **38**, 795.

[33] J. Behan, R. A. W. Johnstone, and R. J. Puddephatt, *J. Chem. Soc., Chem. Commun.*, 1978, 444; R. J. Puddephatt, G. M. Bancroft and T. Chan, *Inorg. Chim. Acta*, 1983, **73**, 83.

[34] B. L. Shaw, *J. Chem. Soc., Chem Commun.*, 1979, 104.

[35] S-X. Xiao, W. C. Taylor, D. E. Ellis and Z. Bewrkowitch-Yellin, *J. Am. Chem. Soc.*, 1983, **105**, 7033.

[36] J. A. Tossell, J. H. Moore and J. C. Giordan, *Inorg. Chem.*, 1985, **24**, 1100.

[37] A. G. Orpen and N. G. Connolly, *J. Chem. Soc., Chem. Commun.*, 1985, 1310.

[38] H. Schumann, *Chem.-Ztg.*, 1986, **111**, 121; H. Schumann and L. Eguran, *J. Organomet. Chem.*, 1991, **403**, 183.

[39] C.A. Tolman, *J. Am. Chem. Soc.*, 1970, **92**, 2956; C. A. Tolman, *Chem. Rev.*, 1977, **77**, 313.

[40] G. Ferguson, P. J. Roberts, E. C. Alyea and M. Khan, *Inorg. Chem.*, 1978, **17**, 2965; E. C. Alyea, G. Ferguson and A. Somogyvari, *Inorg. Chem.*, 1982, **21**, 1369; A. Immirzi and A. Musco, *Inorg. Chim. Acta*, 1977, **25**, L41.

[41] J. D. Smith and J. D. Oliver, *Inorg. Chem.*, 1978, **17**, 2585.

[42] S.G. Murray and F.R. Hartley, *Chem. Rev.*, 1981, **81**, 365.

[43] H. Schumann, A. A. Arif, A. L. Rheingold, C. Janiak, R. Hoffmann and N. Kuhn, *Inorg. Chem.*, 1991, **30**, 1618.

[44] W. Levason, S. D. Orchard and G. Reid, *Organometallics*, 1999, **18**, 1275.

[45] E. G. Hope and W. Levason, *Coord. Chem. Rev.*, 1993, **122**, 109.

[46] G. D. Mullen, M. J. Went, S. Wocadlo, A. K. Powell and P. J. Blower, *Angew. Chem. Int. Ed. Engl.*, 1997, **36**, 1205.

[47] E. W. Abel, R. P. Bush, F. J. Hopton and C. R. Jenkins, *J. Chem. Soc., Chem. Commun.*, 1966, 58.

[48] E. W. Abel, S. K. Bhargava and K. G. Orrell, *Prog. Inorg. Chem.*, 1984, **32**, 1.

[49] P. Haake and P. C. Turley, *J. Am. Chem. Soc.*, 1967, **89**, 4611; *ibid.*, 1967, **89**, 4617.

[50] J. H. Eekhof, H. Hoegeveen, R. M. Kellogg and E. Klei, *J. Organomet. Chem.*, 1978, **161**, 183.

[51] W. Clegg, in J. Evans (Editor), *Crystal Structure Determination*, Oxford University Press, Oxford.

[52] N. Walker and D. Stuart, *Acta Crystallogr., Sect A.*, 1983, **39**, 158.

[53] SORTAV, R. H. Blessing, *Acta Crystallogr., Sect A.*, 1995, **51**, 33; R. H. Blessing, *J. Appl. Cryst.*, 1997, **30**, 421.

[54] *Multinuclear NMR*, J. Mason (Editor), Plenum, New York, 1987.

[55] P. E. Garrou, *Chem. Rev.*, 1981, **81**, 229.

[56] M. Sigl, A. Schier and H. Schmidbaur, *Eur. J. Inorg. Chem.*, 1998, 203.

[57] *NMR and the Periodic Table*, R. K. Harris and B. E. Mann (Editors), Academic Press, London, 1978, p. 402 (^{77}Se); p. 412 (^{125}Te); p. 10 (NOE); p.340 (^{73}Ge); p. 342 (^{119}Sn).

[58] D. W. Anderson, E. A. V. Ebsworth, G. D. Meikle and D. W. H. Rankin, *Mol. Phys.*, 1973, **25**, 381.

[59] E. G. Hope and W. Levason, *Coord. Chem. Rev.*, 1993, **122**, 109.

Chapter 2

Group 14 Halide Complexes With Mono- and Bidentate Thioethers

2.1 Introduction

Studies of complexes of the tin(IV) halides with neutral thioether donors are rare, although not unknown. The bulk of work carried out previously has looked at monodentate dialkyl sulfides. A review of group 14 complexes, including thioethers, was compiled by Dumas & Gomel (1974).[1] Of particular interest in these SnX_4L_2 1:2 adducts is the *cis/trans* isomerisation mechanisms which occur in solution. Beattie and Rule (1964) first studied this process as part of a general study of *cis/trans* isomerisation in octahedral 1:2 adducts using infrared spectroscopy.[2] In this study the patterns in the caesium bromide region in both solution and in the solid state (nujol mull) were investigated. In the cases of diethyl and dibutyl sulfides the compounds are assigned as the *trans* adduct in the solid state. This line of investigation was continued by Ruzicka and Merbach (1976)[3] who carried out a vibrational study of the *cis/trans* isomerism in solution. As well as diethyl sulfide, they also studied the dimethyl sulfide complexes. Using solid state IR and Raman spectroscopy they confirm the previous assignments of the *trans* isomer for these systems. Using solution Raman spectroscopy however, they were able to observe more absorption bands signifying a *cis/trans* equilibrium as a result of both *cis-trans* isomerisation and ligand exchange. Merbach *et al.*[4,5] continued these studies using NMR spectroscopy. Firstly, from studies using variable temperature ^1H NMR spectroscopy on solutions containing an excess of ligand, they were able to establish that the *cis* isomer was the more labile of the two, with the dissociative mechanisms involving the free ligand starting at lower temperatures than the *trans* isomer. However these experiments revealed little about the *cis-trans* isomerisation mechanisms in solution. By carrying out a combination of variable pressure proton NMR and magnetisation transfer ^{119}Sn NMR spectroscopy experiments[6,7] they were able to study this intermolecular *cis-trans* isomerisation process. When an adduct undergoes an intra-molecular ligand exchange process with free ligand there should be a corresponding change in the pressure of the system. The intramolecule ligand exchange of the *cis* isomer was seen to commence at *ca.* 223 K and when Merbach *et al.*[7] varied the pressure of the system at this temperature a cessation of the process was observed to the point where $^{117/119}Sn$ satellites are partially resolved. The same would be true for the *trans* isomer if intramolecular ligand exchanges were the dominant process. However, since this is not seen, intermolecular exchange was assigned as the dominant process. Further confirmation of this came

from the ^{119}Sn magnetisation transfer NMR spectroscopy experiments. By selectively saturating one signal in the ^{119}Sn NMR spectra by using a selective 180° pulse and then observing the spectra over time, Merbach *et al.*[7] were able to observe the return of the magnetisation to equilibrium (Figure 2.1). A decrease in the *trans* isomer intensity was observed as the equilibrium was restored, with increasing *cis* intensity proving the presence of the *cis-trans* isomerisation process. From these studies they were able to isolate trends within the system. They observe an increased lability for the *cis* isomer over the *trans* isomer which is assigned to the increased *trans* effect of the halide anion over that of another neutral donor atom. The increased lability of the bromide over the chloride systems is also observed and assigned to the reduced effective charge on the tin.

Figure 2.1. ^{119}Sn-{^{1}H} NMR spectra of $[SnCl_4(Me_2S)_2]$ in CD_2Cl_2 solution at 285 K as a function of the time interval *t* between the inversion pulse train and the observation pulse. (taken from ref. 7)

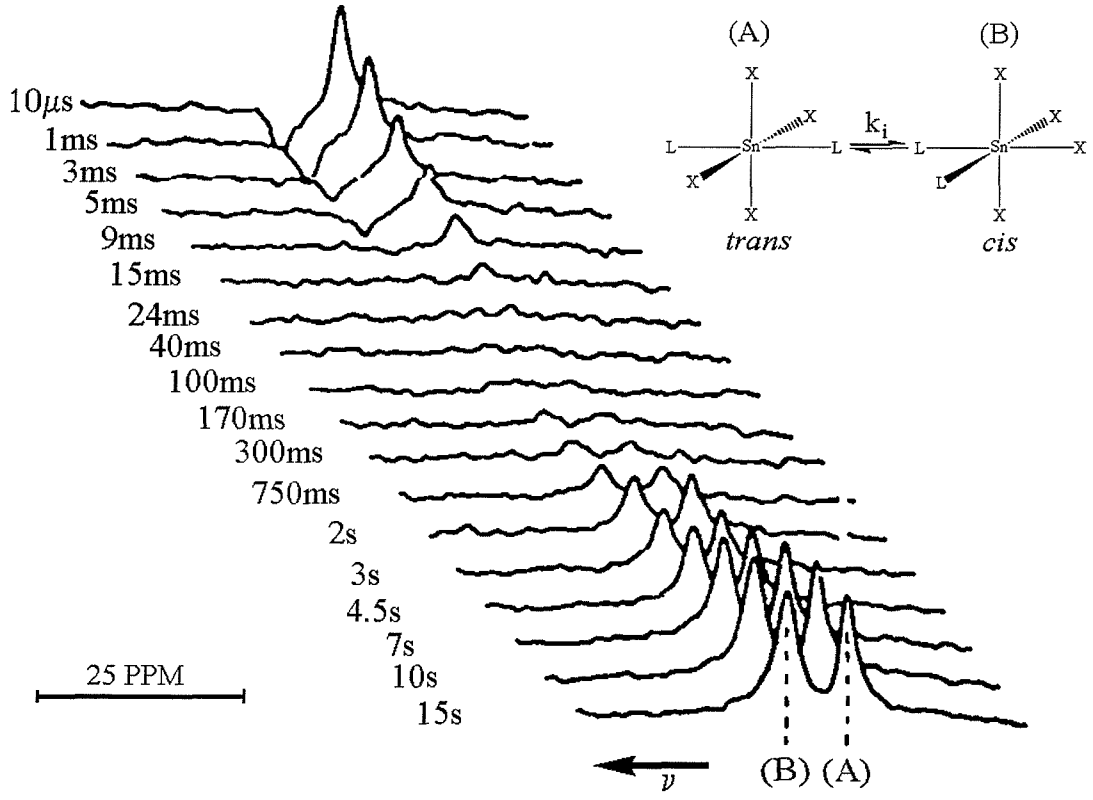

The other process occurring within these systems is the pyramidal inversion of the donor ligand. This was studied for these monodentate systems by Abel *et al.*[8], again using variable temperature NMR spectroscopy. This was done *via* proton NMR spectra for systems with a prochiral methylene group and observing the resonances resulting from the two protons H_A and H_B. If rapid interchange of the two sulfur lone pairs (i.e. pyramidal inversion) is occurring, these two protons will appear equivalent, but if this inversion can be slowed, these protons become non-equivalent on an NMR timescale and give rise to an AB quartet. To further clarify this behaviour Abel *et al.* used systems where further proton coupling did not occur (e.g. $(C_6H_5CH_2)_2S$, $((CH_3)_3SiCH_2)_2S$ and $((CH_3)_3SiCH_2)_2Se$), providing a clean AB quartet. At *ca.* 173 K two distinct AB quartets were observed for the *cis* and *trans* isomers with the cessation of pyramidal inversion along with a single sharp signal corresponding to free ligand. As Merbach *et al.*[3,4,5,6,7] had observed, the *cis* isomer was the more labile with pyramidal inversion beginning at *ca.* 191 K leading to a broad singlet as the protons became equivalent. At *ca.* 237 K the AB quartet arising from the *trans* isomer had also collapsed to a singlet, but remained separate from the free ligand/*cis* isomer signal. The crystal structure of *trans*-$[SnBr_4(Me_2S)_2]$,[9] produced by the reaction of tin metal with Me_2SBr_2, has also been reported.

Complexes involving bidentate thioether ligands are much less well studied. The first example dates back to 1922 when Morgan and Ledbury reported the synthesis of $[SnCl_4\{MeS(CH_2)_2SMe\}]$, albeit with very little spectroscopic evidence.[10] Further work was conducted by Abel *et al.*, who have studied pyramidal inversion processes in this and similar compounds.[8] The 2,5-dithiahexane complex of $SnCl_4$ was found to be either too insoluble or too unstable in solution to make these studies possible, hence two other related complexes, $[SnCl_3Ph\{MeS(CH_2)_2SMe\}]$ and $[SnCl_4\{(CH_3S)_2C_6H_3(CH_3)\}]$ were studied instead. Below *ca.* 178 K they were able to distinguish the various *meso* and *dl* isomers for these complexes. Above this temperature coalescence takes place in the ^1H NMR spectrum. Adapting the findings of Merbach *et al.*[5] they assign this observation to the onset of both pyramidal inversion at sulfur and ligand exchange processes with the conclusion that k (ligand exchange) $\approx$ k_i (atomic inversion).

The only other multidentate thioether ligands to be studied with tin tetrahalides are macrocyclic ligands. Willey *et al.*[11] have studied the complexes formed between tin(IV) chloride and 1,4,7-trithiacyclononane ([9]aneS_3) and 1,4,7,10,13,16-hexathiacyclooctadecane ([18]aneS_6). Reaction of [9]aneS_3 with $SnCl_4$ yields

$[SnCl_3([9]aneS_3)]_2[SnCl_6]$ (cation shown in Figure 2.2). The cation features tridentate binding to $SnCl_3^+$. The [18]aneS$_6$ complex involves *cis* bidentate exocyclic binding of [18]aneS$_6$ to two molecules of $SnCl_4$. The *trans* complex of tin(IV) chloride with 1,5-dithiacyclooctane has also been studied, and this also features a distorted octahedral tin(IV) centre.[12]

Figure 2.2. View of the structure of $[SnCl_3([9]aneS_3]^+$ (taken from ref. 11)

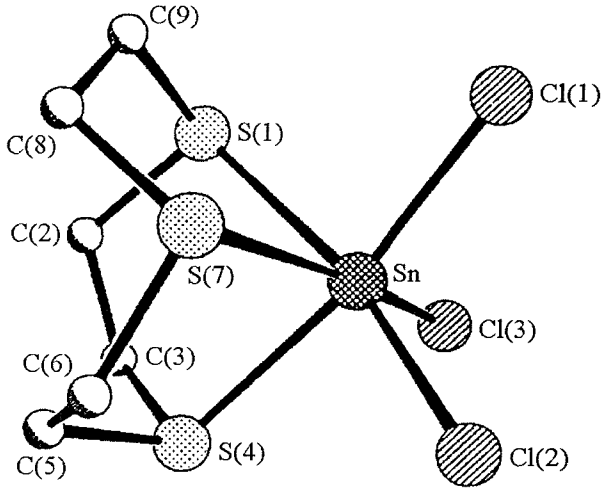

The following work provides a detailed investigation into the behaviour of the tin(IV) halides with monodentate ligands (R_2S where R = Me or Ph) and bidentate ligands of the type $RS(CH_2)_nSR$ (where R = Me or Ph for n = 2 or 3; R = Me for n = 1) and o-$C_6H_4(SMe)_2$ forming part of a study of the coordination of group16 ligands to Sn(IV) halides both in solution and in the solid state. The effects of changing halide and ligand interdonor linkage and substituents are studied. Variable temperature ^1H and ^{119}Sn NMR spectra have been recorded to investigate the pyramidal inversion and ligand exchange processes in these systems. Infrared spectroscopy, ^{119}Sn MASNMR spectroscopy and single crystal X-ray diffraction have been used to study the behaviour of these complexes in the solid state. The analogous selenoether complexes will be discussed in chapter 3, with the telluroether complexes and overall trends and comparisons brought together in chapter 4.

2.2 Results & Discussion

2.2.1. Synthesis and Properties of Monodentate Thioether Complexes

A range of complexes of type $[SnX_4L_2]$ (where X = Cl, Br or I; L = Me_2S or Ph_2S) has been prepared by reaction of SnX_4 with two molar equivalents of thioether ligand L in strictly anhydrous, degassed CH_2Cl_2. For the chloro derivatives, IR spectra of the solid complexes formed all showed one broad peak around 300 cm^{-1} for ν(SnCl) probably corresponding to the *trans* isomer (D_{4h} symmetry) and indicating that this is the principal isomer present in the solid state. There was no evidence of ligand oxidation (ν(S=O) 900 – 1300 cm^{-1}).[13-17] Similarly, no bands were present in the region 400 - 470 cm^{-1} characteristic of ν(SnO) stretching frequencies.[18] IR spectroscopic and analytical data are presented in Table 2.1. The compounds formed were hydrolytically unstable and were stored and manipulated in a dry, dinitrogen purged glove box.

Table 2.1. Analytical and spectroscopic data for $[SnX_4(R_2S)_2]$ complexes

Complex	Colour	%C[a]	%H	ν(Sn-X)[b] (cm^{-1})
$[SnCl_4(Me_2S)_2]$	Pale cream	12.5(12.4)	3.1(3.2)	306
$[SnCl_4(Ph_2S)_2]$	Pale cream	45.7(45.5)	3.1(3.1)	306
$[SnBr_4(Me_2S)_2]$	Pale yellow	8.6(8.5)	2.1(2.1)	230
$[SnBr_4(Ph_2S)_2]$	Yellow	35.4(35.6)	2.5(2.5)	232

a. Calculated values in parentheses
b. Nujol mulls.

2.2.2. Variable Temperature $^{119}Sn\{^1H\}$ NMR Spectroscopy

$^{119}Sn\text{-}\{^1H\}$ NMR spectroscopic data are presented in Table 2.2. The $[SnCl_4(Me_2S)_2]$ + Me_2S system recorded in CH_2Cl_2 solution at room temperature, exhibits two resonances at δ –572 and δ –578 ppm, attributable to the *cis* and *trans* isomers respectively (Figure 2.3). On cooling the system there is little change except for a sharpening of the signals and slight shifts due to the temperature change. This system has already been studied in the presence of excess Me_2S by Knight and

Merbach,[7] who assigned the processes (in order of decreasing rate) as Me_2S exchange with the *cis* isomer, *cis-trans* isomerisation, and Me_2S exchange with the *trans* isomer.

The analogous $SnBr_4$ system was also examined as part of this study. In the ^{119}Sn-$\{^1H\}$ NMR spectra of the 1:2 complex at room temperature, no signals are observed. On lowering the temperature to 280 K, a single broad resonance appears which broadens on further cooling and splits into two below *ca.* 240 K. At 180 K two sharp resonances of approximately equal intensity are present at δ –1174 and δ –1222 ppm, assignable to *cis* and *trans* forms. The same solution with an excess of Me_2S shows the same two sharp resonances of δ –1179 and δ –1228 ppm at 180 K. On warming to *ca.* 230 K the higher frequency resonance arising from the *cis* isomer broadens and then sharpens on further heating. At *ca.* 250 K the same behaviour is observed in the *trans* isomer. However in the presence of excess ligand the two resonances arising from the two geometric isomers are still observable at room temperature.

Figure 2.3. **^{119}Sn-$\{^1H\}$ NMR spectrum of $[SnCl_4(Me_2S)_2]$ in CD_2Cl_2 solution**

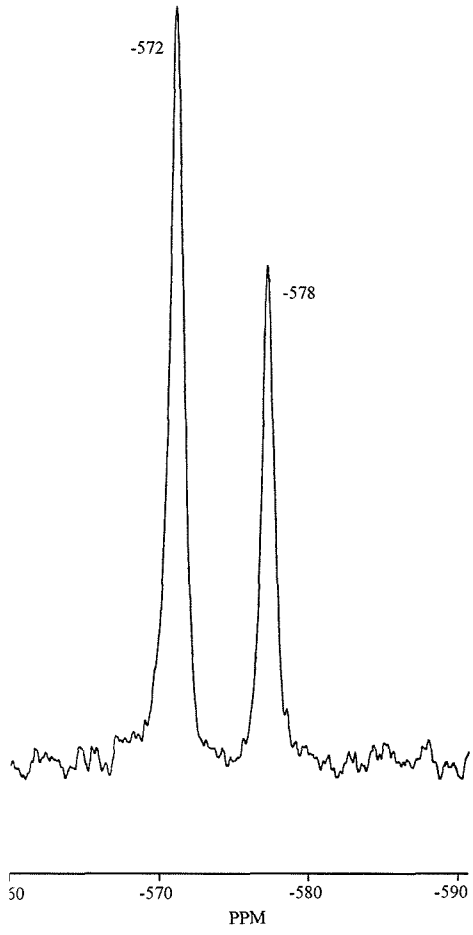

Continuing this trend of increased lability with weakening Lewis acid no resonances for the SnI_4-thioether 1:2 complex were seen at any accessible temperature (173 – 300 K), either as a 1:2 mixture or with an excess of ligand.

The effects of altering the substituent was also studied by looking at the complexes of the tin(IV) halides with Ph_2S. A CH_2Cl_2 solution of $SnCl_4$ with an excess of Ph_2S displays a broad $^{119}Sn\{^1H\}$ resonance at δ –599 ppm at 190 K that broadens rapidly and disappears above *ca.* 200 K. As would be predicted from the observations of the methyl substituted systems no resonances were observed for the corresponding $SnBr_4$-Ph_2S-CH_2Cl_2 systems even at 190 K.

SnF_4 does not dissolve in CH_2Cl_2 even in the presence of a large excess of Me_2S and *in situ* $^{119}Sn\{^1H\}$ NMR spectra again show no resonances at any temperatures.

Table 2.2. ^{119}Sn-$\{^1H\}$ NMR spectroscopic data for $[SnX_4(Me_2S)_2]$ complexes

	^{119}Sn-$\{^1H\}$ (δ)[a]		
Complex	300 K	180 K	*cis*:*trans*
$[SnCl_4(Me_2S)_2]$	-572, -578	-561, -572	2:1
$[SnBr_4(Me_2S)_2]$	n.o.[b]	-1174, -1222	1:1
$[SnI_4(Me_2S)_2]$	n.o.	n.o.	—

a. Relative to external $SnMe_4$ in CH_2Cl_2-CD_2Cl_2 solution.
n.o. = No resonance observed

2.2.3. ^{119}Sn Magic Angle Spinning NMR Spectroscopy

The ^{119}Sn Magic Angle Spinning NMR (MASNMR) spectrum of $[SnCl_4(Me_2S)_2]$ was also studied (Figure 2.4). A single broad resonance was observed at δ –626.7 ppm. This resonance is typical of a six-co-ordinate tin(IV) chloro species[19] and the chemical shift difference of ~65 ppm between solid state and solution NMR studies are probably attributable to solvent effects.[20] The chemical shift range of solution ^{119}Sn NMR spectroscopy is some 4000 ppm,[21] which suggest that significant differences might be expected in δ(^{119}Sn) on going from solution to the solid state. For example, studies on $[Sn(C_6H_{11})_3(OH)]$[20] have shown δ(^{119}Sn) 11.6 ppm in $CDCl_3$ solution and δ –217 ppm in the solid state. Although the most dramatic differences are expected when a change in co-ordination occurs on going into solution, even slight geometrical changes can cause a shift of 50 – 100 ppm.[20]

Figure 2.4. ^{119}Sn MASNMR spectrum of $[SnCl_4(Me_2S)_2]$

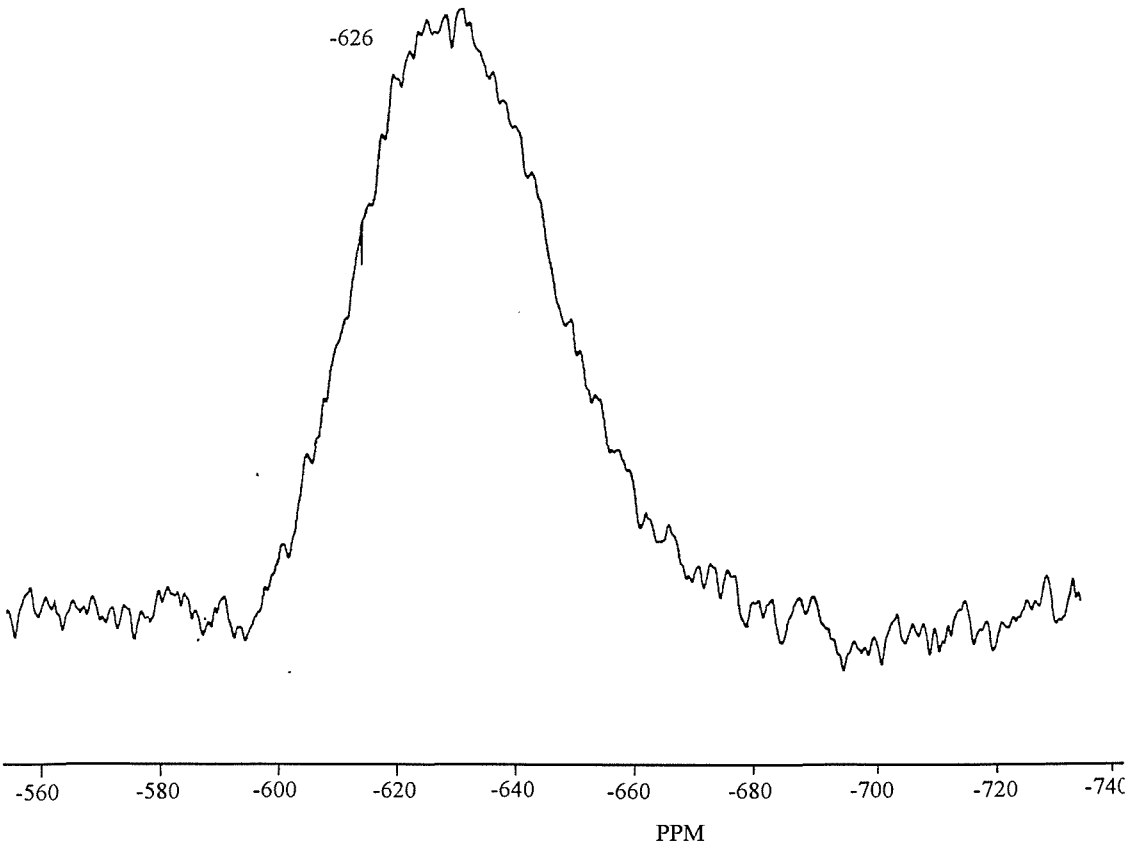

2.2.4. Synthesis and Properties of Bidentate Thioether Complexes

A range of complexes of type $[SnX_4\{L\text{-}L\}]$ (where X = Cl, Br or I; L-L = $MeSCH_2SMe$, o-$C_6H_4(SMe)_2$ or $RS(CH_2)_nSR$; where R = Ph or Me, n = 2 or 3) have been prepared by reaction of SnX_4 with a molar equivalent of thioether ligand L-L in degassed $CHCl_3$. In most cases this gave precipitates of powdered white solids (Me substituted ligands), or crystalline solids (Ph substituted ligands), in good yield. In the case of $[SnBr_4\{PhS(CH_2)_3SPh\}]$ a viscous yellow solution was formed from which it was not possible to isolate a solid, and no solids were isolable for reactions involving SnI_4. Due to the extreme moisture sensitivity of the tin(IV) halides all reactions were carried out under an atmosphere of dry dinitrogen using standard Schlenk techniques. While these complexes were found to be stable over a period of several months in the solid state they were susceptible to hydrolysis in solution, necessitating the use of dry solvents when studied in solution. If dry solvents are not used hydrolysis occurs readily resulting in the formation of hydrates of varying stoichiometries or oxidation of the ligand as discussed later within this chapter. SnF_4 was also studied with the methyl substituted ligands $MeS(CH_2)_nSMe$ (n = 2 or 3). Previous complexes of SnF_4[22,23] with harder oxygen- and nitrogen-donor ligands such as pyridine, triethylamine, acetonitrile and tetrahydrofuran (thf) suggested that SnF_4 only achieved reasonable solubility in warm thf solution. This method was employed with the dithioether systems but failed to yield any solid product which displayed either ν(Sn-F) bands in the IR spectrum or any ^{119}Sn NMR resonances at any accessible temperature (173 – 300 K).

IR spectra of the solid complexes formed all showed the expected four ν(Sn-Cl) bands (theory: $2A_1 + B_1 + B_2$) in the range 300 - 340 cm^{-1} consistent with C_{2v} symmetry. The presence of strong bands from the nujol the complexes were studied in made assignment of associated ligand bands difficult. When the spectrum of $[SnCl_4\{MeS(CH_2)_3SMe\}]$ was recorded as a CsI disc, the disc turned a dark brown very rapidly, suggesting a reaction had occurred between the complex and the CsI. There were no strong bands present in the range 900 - 1300 cm^{-1} as have been reported for complexes incorporating sulfoxide (S=O) functions.[13-17] Similarly, there were no bands in the region 400 - 470 cm^{-1} characteristic of the associated ν(SnO) stretching frequencies.[18] IR spectroscopic and analytical data are presented in Table 2.3

As tin has the greatest number of naturally occurring isotopes of any element, mass spectrometry would seem to be an extremely effective means of identifying the

tin species present. Unfortunately despite trying a variety of matrices, no peaks with the required isotope patterns were observed either by fast atom bombardment, or by positive electrospray. This is most likely to be due to the sensitivity of the compounds which decompose in the solvent or matrix media.

Table 2.3. Analytical and spectroscopic data for $[SnX_4(dithioether)]$ complexes

Complex	Colour	%C[a]	%H	ν(Sn-X)[b] (cm^{-1})
$[SnCl_4\{MeS(CH_2)_2SMe\}]$	White	12.5(12.6)	2.4(2.6)	326, 316, 307, 301
$[SnCl_4\{MeS(CH_2)_3SMe\}]$	Yellow	15.3(15.1)	2.9(3.1)	331, 321, 315, 308
$[SnCl_4\{PhS(CH_2)_2PhMe\}]$	Yellow	33.0(33.2)	3.0(2.8)	334, 327, 315, 302
$[SnCl_4\{PhS(CH_2)_2PhMe\}]$	Orange	34.8(34.6)	3.4(3.1)	339, 323, 316, 309
$[SnCl_4(o\text{-}C_6H_4(SMe)_2\}]$	White	21.8(22.3)	2.2(2.3)	332, 320, 311, 304
$[SnBr_4\{MeS(CH_2)_2SMe\}]$	Yellow	8.8(8.5)	2.0(1.8)	238, 220, 216, 209
$[SnBr_4\{MeS(CH_2)_3SMe\}]$	Yellow	10.3(10.4)	1.9(2.1)	241, 220, 206, 200
$[SnBr_4(o\text{-}C_6H_4(SMe)_2\}]$	Yellow	15.5(15.8)	1.3(1.6)	236, 224, 221, 212

a. Calculated values in parentheses
b. Nujol mulls

2.2.5. Single Crystal X-ray Diffraction Studies

Prior to this work, structurally characterised examples of thioether complexes with tin(IV) had been restricted to the monodentate ligand Me_2S, and the multidentate cyclic thioethers [9]aneS_3,[11] [18]aneS_6,[11] and 1,5-dithiacyclooctane.[12] In order to attempt to identify trends in their geometric parameters, and to correlate these with their observed behaviour within solution (by variable temperature $^{119}Sn\{^1H\}$ and ^1H NMR spectroscopy) single crystal X-ray structure analyses on several of the products were undertaken.

Figure 2.5. View of the structure of $[SnCl_4\{MeS(CH_2)_2SMe\}]$ with the numbering scheme adopted. Ellipsoids are shown at 40 % probability and atoms marked with an asterisk are related by a crystallographic two-fold axis at (½, 0, z)

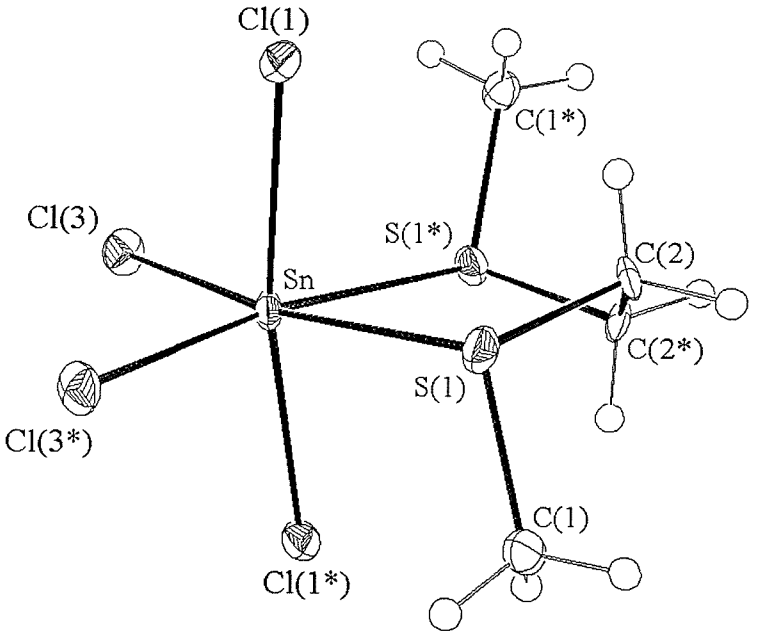

Table 2.4. Selected bond lengths (Å) with e.s.d's for the [SnX_4{dithioether}] complexes

Compound	Sn-X(1)[a]	Sn-X(2)[a]	Sn-X(3)[b]	Sn-X(4)[b]	Sn-S(1)	Sn-S(2)
[$SnCl_4${$MeSCH_2SMe$}]	2.402(2)	2.390(2)	2.343(2)	2.362(2)	2.647(2)	2.710(2)
[$SnCl_4${$MeS(CH_2)_2SMe$}]	2.413(3)	(–)[c]	2.372(4)	(–)[c]	2.619(4)	(–)[c]
[$SnCl_4${$MeS(CH_2)_3SMe$}]	2.409(2)	(–)[d]	2.378(2)	(–)[d]	2.667(2)	(–)[d]
[$SnBr_4${$MeS(CH_2)_3SMe$}]	2.562(3)	(–)[d]	2.533(3)	(–)[d]	2.700(7)	(–)[d]
[$SnCl_4${o-$C_6H_4(SMe)_2$}]	2.401(2)	2.383(2)	2.357(2)	2.357(2)	2.659(2)	2.677(2)
[$SnCl_4${$PhS(CH_2)_3SPh$}]	2.385(5)	2.379(6)	2.376(4)	2.380(5)	2.724(5)	2.725(5)

a. X atoms *trans* X atoms
b. X atoms *trans* S atoms
c. Atoms related by crystallographic two-fold axis at (½, 0, z)
d. Atoms related by crystallographic two-fold axis at (1, 0, z)

Table 2.5 Selected bond angles (°) for the [SnX_4{dithioether}] complexes

Compound	[$SnCl_4${$MeSCH_2SMe$}]	[$SnCl_4${$MeS(CH_2)_2SMe$}][a]	[$SnCl_4${$MeS(CH_2)_3SMe$}][b]
X(1)-Sn-X(2)	167.15(5)	169.9(2)	172.04(8)
X(1)-Sn-X(3)	93.94(6)	93.2(1)	94.94(6)
X(1)-Sn-X(4)	94.69(5)	–[a]	–[b]
X(1)-Sn-S(1)	88.08(5)	91.3(1)	89.27(6)
X(1)-Sn-S(2)	78.70(5)	81.2(1)	84.80(6)
X(2)-Sn-X(3)	95.45(6)	93.4(1)	90.37(6)
X(2)-Sn-X(4)	92.39(5)	–	–
X(2)-Sn-S(1)	82.09(5)	–	–
X(2)-Sn-S(2)	89.90(5)	–	–
X(3)-Sn-X(4)	99.51(6)	98.2(2)	96.32(8)
X(3)-Sn-S(1)	97.05(5)	89.04(10)	89.27(6)
X(3)-Sn-S(2)	163.15(6)	171.1(1)	172.24(6)
X(4)-Sn-S(1)	162.97(5)	–	–
X(4)-Sn-S(2)	96.20(5)	–	–
S(1)-Sn-S(2)	67.82(5)	84.2(2)	83.73(7)

Compound	[$SnBr_4${$MeS(CH_2)_3SMe$}][b]	[$SnCl_4${o-$C_6H_4(SMe)_2$}]	[$SnCl_4${$PhS(CH_2)_3SPh$}]
X(1)-Sn-X(2)	172.3(1)	169.00(7)	167.69(5)
X(1)-Sn-X(3)	94.71(9)	93.14(7)	94.6(2)
X(1)-Sn-X(4)	–[b]	91.79(7)	94.1(2)
X(1)-Sn-S(1)	89.9(2)	83.28(6)	84.0(2)
X(1)-Sn-S(2)	84.3(2)	83.17(6)	86.7(2)
X(2)-Sn-X(3)	90.46(9)	95.57(8)	94.4(2)
X(2)-Sn-X(4)	–	92.83(7)	93.2(2)
X(2)-Sn-S(1)	–	89.87(6)	87.5(2)
X(2)-Sn-S(2)	–	86.70(7)	83.3(2)
X(3)-Sn-X(4)	95.9(1)	102.73(7)	96.55(5)
X(3)-Sn-S(1)	91.0(2)	90.95(6)	90.6(2)
X(3)-Sn-S(2)	171.7(2)	165.01(6)	172.0(2)
X(4)-Sn-S(1)	-	165.72(7)	172.7(2)
X(4)-Sn-S(2)	–	91.93(6)	91.2(2)
S(1)-Sn-S(2)	82.5(3)	74.21(6)	81.67(4)

a. X(2) and X(4) refer to Cl(1*) and Cl(3*) in the numbering scheme adopted, related by a crystallographic two-fold axis at (½, 0, z)

b. X(2) and X(4) refer to X(1*) and X(3*) in the numbering scheme adopted, related by a crystallographic two-fold axis at (1, 0, z)

Figure 2.6. View of the structure of $[SnCl_4\{MeS(CH_2)_3SMe\}]$ with the numbering scheme adopted. Ellipsoids are shown at 40 % probability and atoms marked by an asterisk are related by a crystallographic two-fold axis at (1, 0, z)

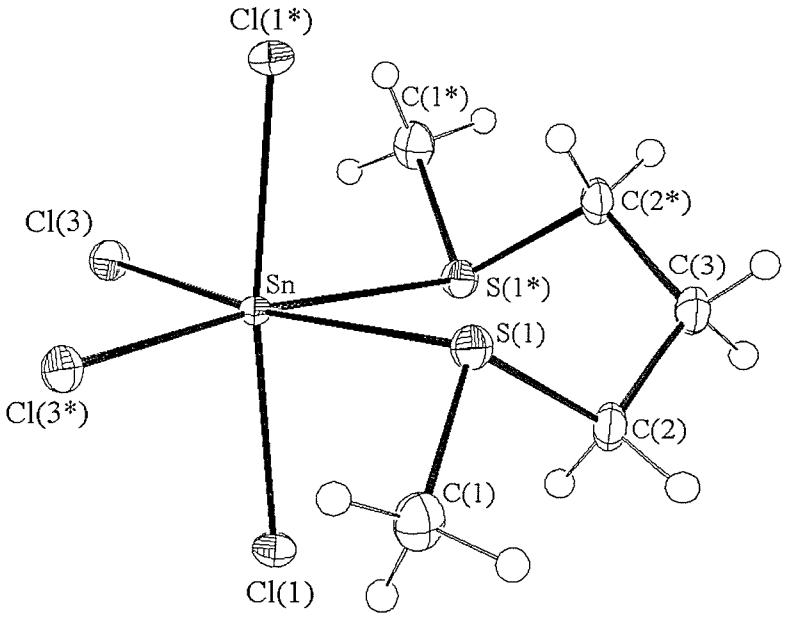

The structure for $[SnCl_4\{MeS(CH_2)_2SMe\}]$ (Figure 2.5) shows a distorted octahedral arrangement with the tin centre occupying a crystallographic 2-fold axis (0.5, 0, z). Similarly the structure for $[SnCl_4\{MeS(CH_2)_3SMe\}]$ (Figure 2.6) also shows a distorted octahedral arrangement with the tin centre, and carbon (3), occupying a crystallographic 2-fold axis (1, 0, z), and the tin(IV) bromide system, $[SnBr_4\{MeS(CH_2)_3SMe\}]$, is isostructural with this (Figure 2.7). The other structures for $[SnCl_4(MeSCH_2SMe)]$ (Figure 2.8), $[SnCl_4\{o\text{-}C_6H_4(SMe)_2\}]$ (Figure 2.9) and $[SnCl_4\{PhS(CH_2)_3SPh\}]$ (Figure 2.10) also show distorted octahedral arrangements but in these structures the tin centres occupy crystallographic general positions.

Selected bond lengths (Å) and angles (°) are presented for these structures in Tables 2.4 and 2.5 respectively. The Sn-S and Sn-X distances determined from these studies (Sn-S 2.619(4) – 2.725(5), Sn-Cl 2.372(4) – 2.409(2), Sn-Br 2.533(3) & 2.562(3) Å) are in good agreement with the few structurally characterised examples in the literature, *e.g.* $[SnCl_3([9]aneS_3)]^+$ [Sn-S 2.618(3), 2.636(3) and 2.657(4), Sn-Cl 2.366(4), 2.369(3) and 2.371(4) Å],[11] $2SnCl_4.[18]aneS_6$ [Sn-S 2.535(10), 2.56(2), 2.687(13) and 2.689(13), Sn-Cl 2.30(2), 2.31(2), 2.38(2), 2.391(2), 2.421(2) and

Figure 2.7. View of the structure of [$SnBr_4${$MeS(CH_2)_3SMe$}] with numbering scheme adopted. Details as in Figure 2.5

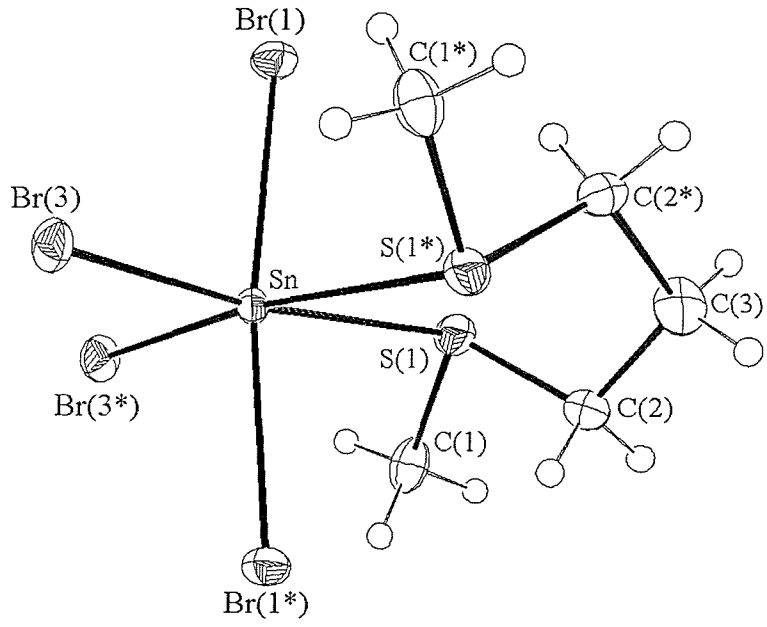

2.42(2)][11] *cis*-[$SnBr_4(Me_2S)_2$] [Sn-S 2.692(8) and 2.692(9), Sn-Br 2.554(4), 2.532(4), 2.557(4) and 2.539(4) Å][9] and *trans*-[$SnCl_4(\eta\,\S\text{-}C_6H_{12}S_2\text{-}1,5)_2$] ($C_6H_{12}S_2$-1,5 = 1,5-dithiacyclooctane) [Sn-S 2.602(1), Sn-Cl 2.414(1), 2.428(1) Å].[12] However, the number of structures determined in this work allow comparisons to be drawn and, from these, a number of observations can be made on the stability of the complexes. In all cases there are variations in the Sn-X bond distances with d(Sn-Cl) for Cl *trans* to Cl being longer than those *trans* to S (e.g. 2.372(4) and 2.413(3) Å respectively in [$SnCl_4${$MeS(CH_2)_2SMe$}]) presumably reflecting the greater *trans* influence of Cl over S(thioether) in these hard Sn(IV) species that was suggested by Ruzicka and Merbach.[3,4,5] This is a trend that is also observed in the complexes [$(SnCl_4)_2$([18]aneS_6)][11] (*cf.* Sn-Cl(*trans* Cl) 2.421(2) and 2.391(2) Å *vs.* Sn-Cl(*trans* S) 2.30(2) and 2.31(2) Å) and *cis*-[$SnBr_4(Me_2S)_2$][9] (*cf.* Sn-Br(*trans* Br) 2.557(4) and 2.554(4) Å *vs.* Sn-Br(*trans* S) 2.532(4) and 2.539(4) Å). It is also noted that there is a distortion in the octahedral geometry with the mutually *trans* halides tilted towards the coordinated dithioether ligand (e.g. 169.9° in [$SnCl_4${$MeS(CH_2)_2SMe$}]). Also of interest are the Sn-S bond distances which shed some light on the relative stabilities of the various systems studied.

Figure 2.8. View of the structure of $[SnCl_4(MeSCH_2SMe)]$ with numbering scheme adopted. Ellipsoids are shown at 40 % probability

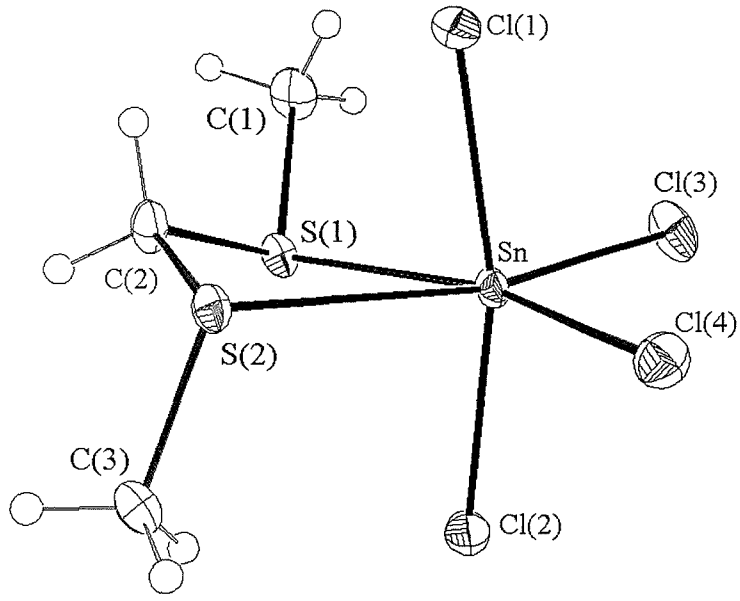

There are significant variations in these Sn-S bond distances across the series of complexes. Comparing the three different chelate ring-sizes studied with tin(IV) chloride (four, five and six membered chelates), we see that the shortest distance occurs for the five membered chelate ring, $[SnCl_4\{MeS(CH_2)_2SMe\}]$ 2.619(4) Å. The next shortest is seen for six membered chelate, $[SnCl_4\{MeS(CH_2)_3SMe\}]$ 2.667(2) Å, with the longest Sn-S bond distances seen in the four membered chelate system, $[SnCl_4(MeSCH_2SMe)]$ 2.647(2) and 2.710(2) Å suggesting that the five-membered chelate-ring is preferred to the six-member chelate ring, with the four-membered chelate-ring least favourable, as would be expected due to the ring strain in this system.

The presence of the more rigid o-C_6H_4 backbone within $[SnCl_4\{o\text{-}C_6H_4(SMe)_2\}]$ also has the effect of reducing the stability of the five-membered chelate-ring so the Sn-S bond distances here (2.659(2) and 2.677(2) Å) are significantly longer than those of $[SnCl_4\{MeS(CH_2)_2SMe\}]$, with the more flexible backbone (2.619(4) Å).

The Sn-S bond distances observed for the Ph substituted species, $[SnCl_4\{PhS(CH_2)_3SPh\}]$ [Sn-S 2.724(5) and 2.725(5) Å], are significantly longer than those of the methyl substituted analogue, $[SnCl_4\{MeS(CH_2)_3SMe\}]$ [Sn-S 2.667(2) Å].

This increase in *d*(Sn-S) parallels the observed decrease in stability observed in solution in the NMR studies that follow.

Figure 2.9. View of the structure of [$SnCl_4${o-$C_6H_4(SMe)_2$}] with the numbering scheme adopted. Ellipsoids are shown at 40 % probability

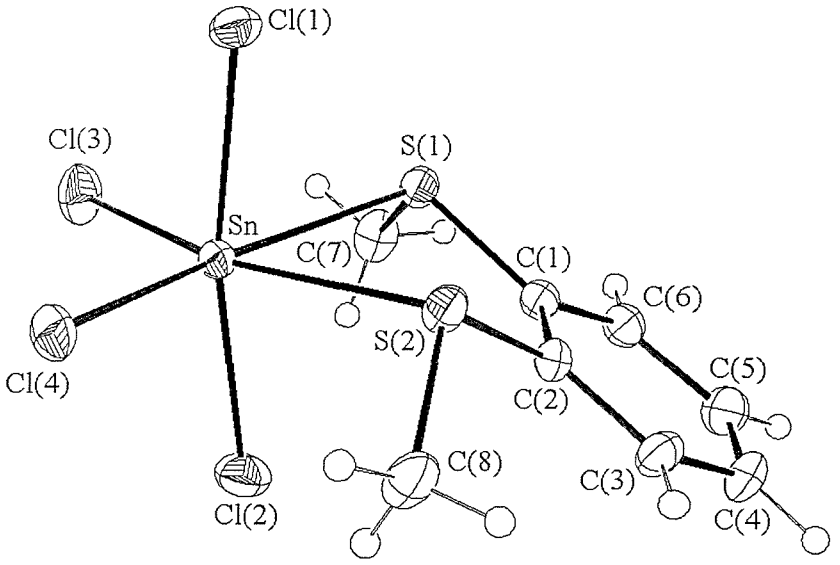

The highly strained nature of the complex of $MeSCH_2SMe$ with tin(IV) chloride leading to the high lability of this complex in solution is well illustrated by the X-ray diffraction study. The S-Sn-S angle of 67.82(5)° is significantly more acute than the ideal octahedral angle of 90°, and is markedly more strained than the other two Me-substituted dithioether systems studied. This is the first example of a chelating methylene linked dithio-, diseleno or ditelluro-ether. Previously characterised examples with this methylene linked dithioether ligand have featured η^1-coordination within systems of the type $[ML_2Cl_2]$[24] (where M = Pd or Pt; L = $PhSCH_2SPh$, $MeSCH_2SMe$) or bridging ligands interlinking the $SnCl_4$ units oligomers seen previously for Cu^I and Ag^I systems.[25] [$SnCl_4${$MeS(CH_2)_2SMe$}] with an S-Sn-S angle of 84.2(2)° is closer to this ideal than [$SnCl_4${$MeS(CH_2)_3SMe$}] with an angle of 83.73(7)° showing that the five membered chelate ring is preferred in terms of strain over the six membered ring with the four membered chelate ring worst of all.

Comparison between the $SnCl_4$ and $SnBr_4$ adducts with $MeS(CH_2)_3SMe$ shows a variation in the Sn-S bond distances, those of the chloride [Sn-S 2.667(2) Å] being significantly shorter than those of the bromide [2.700(7) Å]. Whether for steric or electronic reasons this shows that the bond between tin and sulfur is weaker in the bromide complex so it is of no surprise that the phenyl substituted ligands, that have been seen to be poorer donors, form no isolable solid adducts.

Figure 2.10. View of the structure of $[SnCl_4\{PhS(CH_2)_3SPh\}]$ with numbering scheme adopted. Ellipsoids are shown at 40 % probability

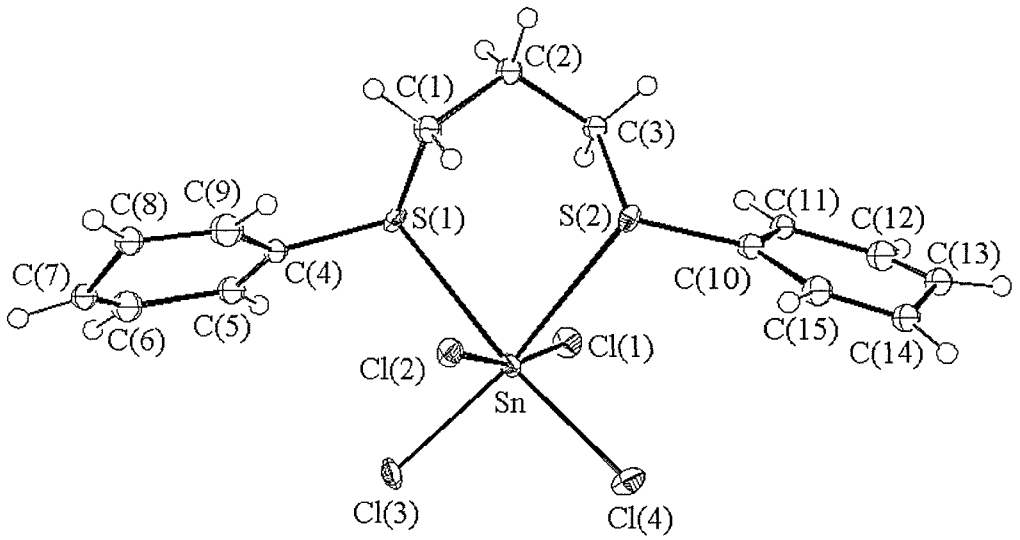

2.2.6. Variable Temperature Solution ^{1}H NMR Studies

At room temperature these bidentate dithioether complexes are expected to undergo exchange *via* a dissociative process and also sulfur inversion, both of which are rapid on an NMR timescale. As a result, in the NMR spectra recorded at room temperature protons, which in the absence of these processes are magnetically non-equivalent, appear equivalent and the resulting spectra appear very simple. On lowering the temperature to *ca.* 200 K the ligand exchange is slowed to a rate observable by NMR and, in some cases, the sulfur inversion process is also slowed sufficiently that the resultant isomers are distinguishable. The sulfurs undergo inversion independently to give the *dl* and *meso* configurations.

Table 2.6. ^{1}H NMR spectroscopic data for methyl substituted [SnX_4{dithioether}] complexes

	^{1}H (δ)[a]		
Compound	300 K	175 K	*dl*:*meso*
[$SnCl_4${$MeS(CH_2)_2SMe$}]	2.50	2.48, 2.61	2:1
[$SnCl_4${$MeS(CH_2)_3SMe$}]	2.37	2.48, 2.64	1:2
[$SnCl_4${o-$C_6H_4(SMe)_2$}]	2.75	2.80, 3.05	1:10
[$SnBr_4${$MeS(CH_2)_2SMe$}]	2.24	2.26, 2.41	1:1
[$SnBr_4${$MeS(CH_2)_3SMe$}]	2.18	2.05, 2.41	3:1
[$SnBr_4${o-$C_6H_4(SMe)_2$}]	2.50	2.86	—

a. In CD_2Cl_2, Me resonances only.

For the methyl substituted complexes of $SnCl_4$ ([$SnCl_4${$MeS(CH_2)_nSMe$}], n = 2 or 3; [$SnCl_4${o-$C_6H_4(SMe)_2$}]) the δ(CH_2) resonances for each complex can clearly be seen to broaden on cooling, before splitting into two separate doublet resonances (< *ca.* 200 K) representing the AB coupling of the two separate diastereoisomers. Also at low

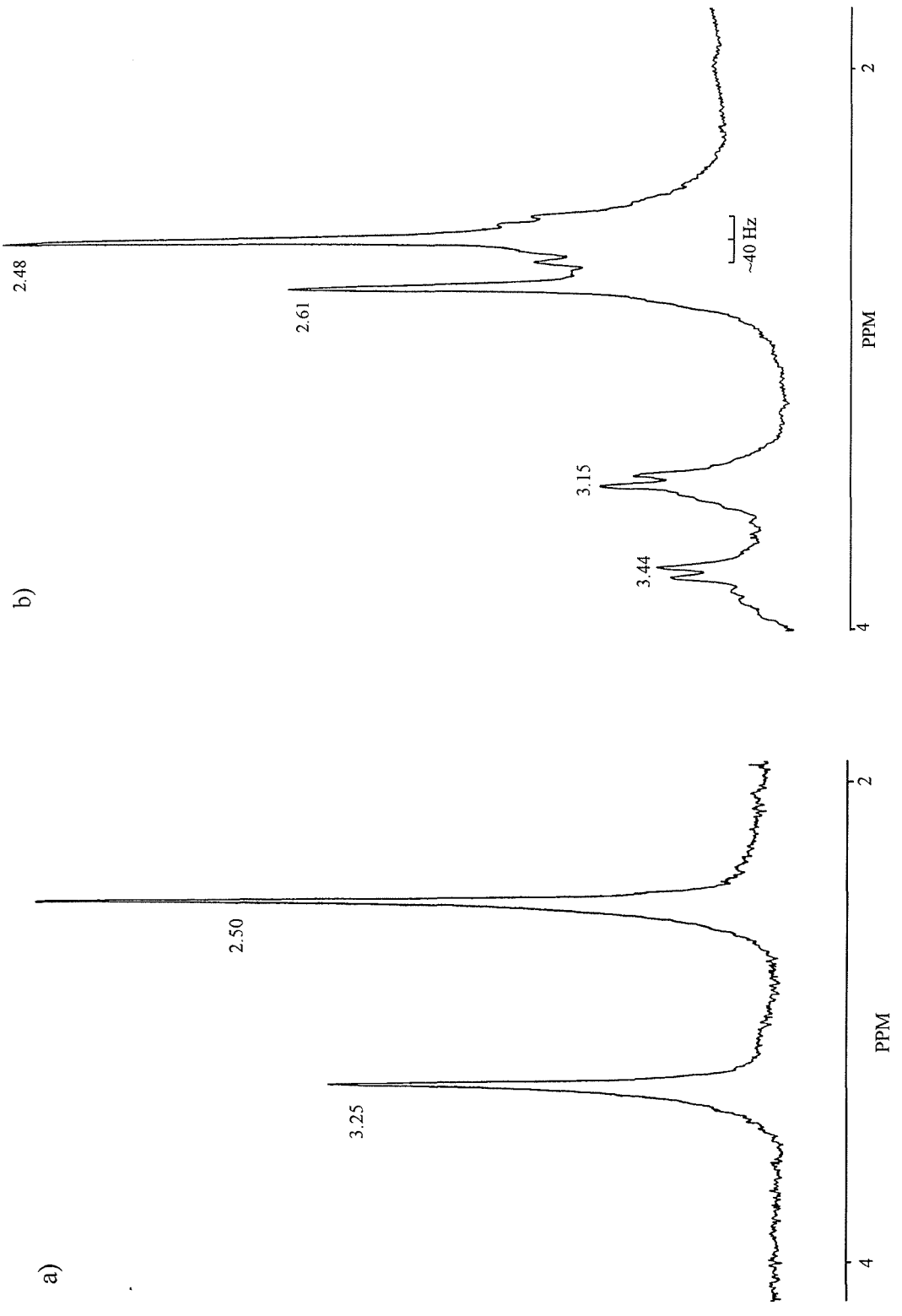

Figure 2.11. ^{1}**H NMR spectra of [$SnCl_4${$MeS(CH_2)_2SMe$}] in CD_2Cl_2 solution at a) 300 K and b) 175 K**

temperature it is possible to observe coupling to the tin isotopes with I = $^1/_2$ ($^3J(^{117/119}Sn - ^1H) \sim 40$ Hz, Figure 2.11). At *ca.* 220 K these tin satellites are lost, indicating that at this temperature ligand dissociation mechanisms also become important in the exchange processes. For complexes of $SnBr_4$ the same patterns are seen for the complexes of with alkyl backbones ($MeS(CH_2)_nSMe$), with invertomers observable at the lowest temperature studied (180 K). However, even at this temperature, the δ(Me) resonance for the o-phenylene ligand (o-$C_6H_4(SMe)_2$) merely broadens signifying that for this system the low temperature limiting spectrum has not been reached. In the case of complexes of SnI_4, where no solid is isolable, it was not possible to identify any signals at all in an *in situ* experiment over the entire temperature range (175 – 300 K).

The approximate ratios of *meso* : *dl* isomers can also be determined from the ^1H NMR (CD_2Cl_2, 180 K) spectra of the methyl substituted complexes. For the complexes [$SnCl_4\{MeS(CH_2)_nSMe\}$] the ratio *meso* : *dl* are 1 : 2 (n = 2) and 2 : 1 (n = 3). However for the complex [$SnCl_4\{o\text{-}C_6H_4(SMe)_2\}$] the ratio is approximately 10 : 1.

In the cases of the phenyl substituted complexes ([$SnCl_4\{PhS(CH_2)_nSPh\}$]; n = 2 or 3) the resonances from the phenyl rings are not very informative. The information can be gained instead by examining the δ(CH_2) resonances. For [$SnCl_4\{PhS(CH_2)_2SPh\}$], the δ(CH_2) resonance can clearly be seen to broaden on lowering the temperature, before splitting and sharpening on lowering the temperature down to 180 K. For the species [$SnCl_4\{PhS(CH_2)_3SPh\}$] it was only possible to produce a broad, single peak even at the lowest temperature achieved (175 K). This indicates that the low temperature limiting spectrum has not been reached and the inversion barrier is lowered by having a phenyl group rather than a methyl group bound to the inverting atom. This may be due to the increased steric bulk or the electronic effects of the phenyl ring. This is in accordance with the observations reported by Abel *et al.*[8] who also assign the ligands in this order of decreasing inversion barrier and also the results of our single crystal X-ray diffraction studies where the Sn-S bond distances were seen to increase with the poorer phenyl substituted donors. As was observed for the bromide systems of the methyl substituted ligands, the phenyl substituted complexes of tin(IV) bromide proved too labile in solution to reach the low temperature limiting spectrum, and this is in accordance with the observation that no solid was isolable for the $SnBr_4$ – $PhS(CH_2)_3SPh$ system, and consistent with the X-ray diffraction study where the Sn-S bond distance for the $SnBr_4$ system is longer than those of the $SnCl_4$ systems. Continuing the pattern there was no obvious reaction

between these phenyl substituted ligands and tin(IV) iodide either in the reaction mix or in terms of resonance shifts in the ^{1}H NMR spectra which would correspond to co-ordination.

2.2.7. Variable Temperature Solution ^{119}Sn NMR Studies

As has been observed[8,9] for related species the solubility of these complexes in chlorocarbon solvents is extremely poor. A range of other solvents was also examined, including $MeNO_2$, Me_2CO, thf and propane-1,2-diol carbonate, but these proved unsatisfactory and there was some evidence that the observed resonances were due to adducts with O-donors[26] and displacement of the dithioether ligand. CD_2Cl_2 was therefore used even although the compounds were not very soluble in this solvent.

The $^{119}Sn\{^{1}H\}$ NMR spectra (134.2 MHz, CD_2Cl_2) were recorded over a range of temperatures (300 - 180 K) in order to observe the effects of ligand exchange by dissociation and sulfur inversion. Resonances for the various tin(IV) species were observed in characteristic regions. Resonances for the tin(IV) chloride-dithioether complexes were observed within the range δ -500 to δ -600 ppm, similar to the chemical shifts observed for the *cis* and *trans* isomers of $[SnCl_4(Me_2S)_2]$ by Merbach *et al.* (δ -569 and δ -574 respectively)[6,7] and also similar to $\delta(^{119}Sn)$ for the six co-ordinate tin system, $[SnCl_4(PBu_3)_2]$, (δ -573 ppm).[27] The complexes of tin(IV) bromide were characteristically observed over the range δ –1100 to δ -1300 ppm. Complexes of tin(IV) iodide fall in the region δ –2600 to δ -2800 ppm where the closest characterised analogue is the resonance at –1701 ppm for tin(IV) iodide in CS_2 solution.[27]

Over the entire temperature range studied (300 K – 180 K) the resonances for these complexes were weak, due to the poor solubility of the compounds in CH_2Cl_2. Variable temperature $^{119}Sn\text{-}\{^{1}H\}$ NMR data are presented in Table 2.7.

The complexes of $MeSCH_2SMe$, were rather more soluble in CD_2Cl_2, possibly due to ring opening in this strained molecule. No signal is observed in the $^{119}Sn\{^{1}H\}$ NMR spectrum above 230 K. Below this a single broad resonance becomes observable, which then sharpens on cooling and eventually splits at 180 K to show two distinct resonances for *dl* and *meso* invertomers at δ -585.3 and -585.7 ppm. This is within the same region of the spectra as the other $[SnCl_4(L\text{-}L)]$ species studied confirming a chelate is formed in solution as well as the solid state. Given the highly strained nature of the four-membered chelate-ring formed this is a surprise.

Above 230 K the ligand is probably dissociating rapidly to give a mix of chelate and η^1 co-ordination.

Table 2.7. Variable temperature ^{119}Sn-{^{1}H} NMR spectroscopic data for [SnX_4{dithiother}] complexes.

	^{119}Sn-{^{1}H} (δ)[a]	
Compound	300 K	180 K
[$SnCl_4$($MeSCH_2SMe$)]	n.o.[b]	-585.3, -585.7
[$SnCl_4${$MeS(CH_2)_2SMe$}]	-572, -578	-548.5, -549.0
[$SnCl_4${$MeS(CH_2)_3SMe$}]	-560 (br)	-558.0, -563.0
[$SnCl_4${o-$C_6H_4(SMe)_2$}]	-567 (br)	-504.2, -504.9 (sh)
[$SnCl_4${$PhS(CH_2)_2SPh$}]	n.o.	-515.0, -516.2
[$SnCl_4${$PhS(CH_2)_3SPh$}]	n.o.	-570.3
[$SnBr_4${$MeS(CH_2)_2SMe$}]	n.o.	-1123.2, -1124.0
[$SnBr_4${$MeS(CH_2)_3SMe$}]	n.o.	-1179, -1180 (br)
[$SnBr_4${o-$C_6H_4(SMe)_2$}]	n.o.	n.o.
[$SnBr_4${$PhS(CH_2)_2SPh$}]	n.o.	-1127
[$SnBr_4${$PhS(CH_2)_3SPh$}]	n.o.	n.o.
[SnI_4{$MeS(CH_2)_2SMe$}]	n.o.	-2725
[SnI_4{$MeS(CH_2)_3SMe$}]	n.o.	-2645

a. Relative to neat external $SnMe_4$ in CH_2Cl_2-CD_2Cl_2 solution.
b. n.o. = No resonance observed.

For the compound [$SnCl_4${$MeS(CH_2)_2SMe$}] at 300 K a single resonance was observed at δ –560 ppm. Lowering the temperature to 250 K results in a small shift in the resonance, probably due to temperature drift. This continues until at the lowest observed temperature (180 K) there are two discernible resonances at δ –549.0 ppm and δ –548.6 ppm. On warming the solution again, the two signals merge once more.

The same behaviour was observed for the complex $[SnCl_4\{MeS(CH_2)_3SMe\}]$ with a single resonance at δ –567 ppm at 300 K (Figure 2.12a). Cooling the sample to 250 K produces a slight shift to δ –564 ppm and this continued until at *ca.* 220 K the resonance was seen to split into two closely spaced resonances attributable to the *meso* and *dl* invertomers at δ –563 ppm and δ –558 ppm (Figure 2.12b). The two signals once again merge into one upon warming. The complex of $SnCl_4$ with o-$C_6H_4(SMe)_2$, showed no resonance at 300 K. Ligand exchange in solution at this temperature is rapid resulting in no resonance being observed until the temperature is lowered to *ca.* 240 K. At this point the exchange processes occurring are slowed sufficiently to allow this resonance to be observed on the NMR timescale. At this temperature a signal was observed at δ –507 ppm which, on further cooling to 180 K, split into two separate resonances at δ –504.2 ppm and δ –504.9 ppm for the *meso* and *dl* invertomers.

The analogous phenyl substituted systems, $PhS(CH_2)_nSPh$ (n = 2 or 3), of $SnCl_4$ prove still more labile, consistent with the observed increase in Sn-S bond distances observed in the solid state X-ray diffraction studies. For the complex $[SnCl_4\{PhS(CH_2)_2SPh\}]$ no signals are evident at 300 K. At 220 K a very broad resonance was observed at *ca.* δ –518 ppm. At 200 K this resonance sharpened and was clearly discernible at δ –517.8 ppm. Further cooling to 180 K eventually slowed inversion sufficiently so that two resonances were now seen at δ –516.2 ppm and δ –515.0 ppm. $PhS(CH_2)_3SPh$ proved to be the weakest donor of all. For this ligand no signals were observed until the very lowest temperature reached, 180 K, when a resonance was seen at δ –570 ppm. The fact that the signals for the phenyl substituted ligand systems were not observed until lower temperatures shows that these ligands are more labile than their methyl substituted analogues, resulting in dissociative ligand exchange processes beginning at lower temperatures.

Figure 2.12. **^{119}Sn-{^{1}H} NMR spectra of [$SnCl_4${$MeS(CH_2)_3SMe$}] in CH_2Cl_2-CD_2Cl_2 solution at a) 300 K and b) 180 K. Poor solubility and short accumulation periods restrict resolution**

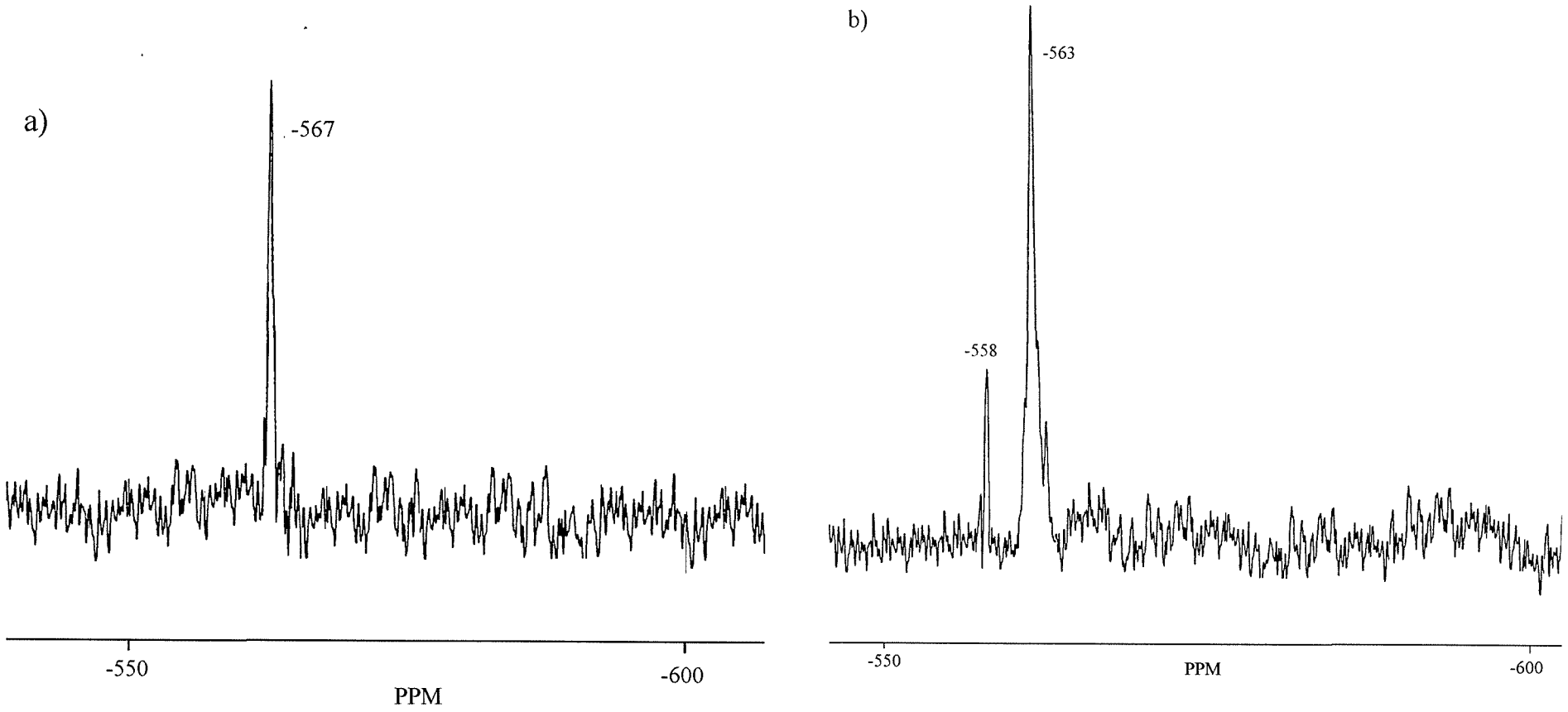

For the systems of $SnBr_4$ the same general trends are observed, but with the dynamic processes in solution commencing at lower temperatures. This overall trend is in accordance with the X-ray diffraction results that show significantly longer bond distances for the bromide systems compared to the analogous chloride systems. $[SnBr_4(MeSCH_2SMe)]$ is again extremely soluble in CH_2Cl_2 as the ligand is labile so even at the lowest recorded temperatures, no signals are observed within the $^{119}Sn\{^1H\}$ spectra. For $[SnBr_4\{MeS(CH_2)_2SMe\}]$ a resonance only became evident at *ca.* 230 K. At this temperature a weak resonance was observed at δ –1121 ppm and at 180 K, this split giving two distinct resonances at δ –1124.0 ppm and δ –1123.2 ppm for the two invertomers. The same pattern was observed for $[SnBr_4\{MeS(CH_2)_3SMe\}]$ with the first signal observed at δ –1188 ppm at *ca.* 230 K and again at 180 K two resonances assigned to the two invertomers were observed at δ –1180.0 ppm and δ –1178.8 ppm. The difference between the chloride and bromide complexes was most clearly seen in the cases of the o-$C_6H_4(SMe)_2$ and $PhS(CH_2)_nSPh$ complexes. The only resonance to be observed was for $[SnBr_4\{PhS(CH_2)_2SPh\}]$ in the presence of excess ligand at 175 K, with a broad resonance at δ –1127 ppm. Further evidence for the increased lability of these phenyl substituted ligands comes from the fact that it was not possible to isolate a solid product from the reaction of $SnBr_4$ with $PhS(CH_2)_3SPh$.

As expected, these trends are continued in the complexes of SnI_4. No solid complexes were isolable for any of these products, so all NMR studies were performed *in situ*. SnI_4 dissolves in CH_2Cl_2 solution readily in the presence of an excess of $MeS(CH_2)_nSMe$ (n = 2 or 3). At 180 K broad resonances were observed at δ – 2725 ppm (n = 2) and δ –2645 ppm (n = 3) which are assigned to the formation of an SnI_4S_2 adduct (*cf.* SnI_4 in CS_2 has δ –1701 ppm).[27] Both resonances were lost above 190 K.

Although problems arising from the onset of ligand dissociation and pyramidal inversion at similar temperatures (as observed previously by Abel *et al.*[8]) precludes more detailed and quantitative analyses, there are a number of qualitative observations that can be made and trends that have become apparent within these systems. The inversion barrier for *meso/dl* isomerisation is affected by altering both the ligand and the tin(IV) halide species. Of the two terminal substituents on the sulfur (Me and Ph) it is clear that the methyl substituted ligand is less labile, leading to these dynamic processes occurring at higher temperatures relative to the phenyl substituted ligand complexes. Altering the ligand backbone has the same effect, with the inversion barrier lowered for the less favoured six and four-membered chelates. Adding unsaturation to

the backbone in the form of an o-phenylene ring also lowers the inversion barriers relative to the dimethylene backbone, with pyramidal inversion and ligand dissociation starting at lower temperatures. These inversion barriers also lower with weakening Lewis acidity, thus tin(IV) chloride forms the most stable complexes, followed by tin(IV) bromide, with tin(IV) iodide adducts only observable *in situ* at lower temperatures. All of these observations are consistent with the conclusions drawn from the single crystal X-ray diffraction studies of these systems, indicating the complimentarity of the two analytical techniques.

2.2.8. ^{119}Sn Magic Angle Spinning NMR Spectroscopy

The $SnCl_4$-dithioether species were also investigated in the solid state using ^{119}Sn magic angle spinning NMR spectroscopy. Resonances were observed in the range –600 to –660 ppm for the systems studied. The ^{119}Sn MASNMR spectroscopic data is presented in Table 2.8.

Table 2.8. ^{119}Sn Magic Angle Spinning NMR spectroscopic data for [$SnCl_4${dithioether}] complexes

Compound	^{119}Sn (δ)
[$SnCl_4${$MeS(CH_2)_2SMe$}]	-630
[$SnCl_4${$MeS(CH_2)_3SMe$}]	-654
[$SnCl_4${o-$C_6H_4(SMe)_2$}]	-617
[$SnCl_4${$PhS(CH_2)_2SPh$}]	-618
[$SnCl_4${$PhS(CH_2)_3SPh$}]	-653

Of note is the small chemical shift range observed for the various $SnCl_4$-dithioether species (40 ppm) in the solid state, and these are shifted by up to 100 ppm from the observed solution resonances. The observed resonances at δ *ca.* –600 ppm are typical of a six-co-ordinate tin(IV) chloro species.[19] In the solid state the small chemical shift range observed between all the $SnCl_4$-dithioether complexes suggests that the tin centres are in very similar environments.

In all cases a singlet was observed for the $SnCl_4$-dithioether systems studied. The resonance broadens with the lowering symmetry in the molecular crystal structure, *e.g.* [$SnCl_4${$MeS(CH_2)_3SMe$}] (Figure 2.13, tetragonal space group, C_2 local symmetry at tin, δ –654 ppm, full width half height (f.w.h.m.) 335.7 Hz) and [$SnCl_4${o-$C_6H_4(SMe)_2$}] (triclinic space group, C_1 local symmetry at tin, δ –617 ppm, f.w.h.m. 4476.4 Hz). In addition to the resonances broadening on reduction of the symmetry, additional spinning side bands appeared which did not collapse even at the highest possible spinning rate (6.5 kHz). The appearance of spinning side bands in the solid-state spectra is also indicative of a more anisotropic environment.

The observation of a single broad line in the solid-state spectra contrasts markedly with the low temperature solution spectra which exhibit two sharp lines (separated by 1 – 2 ppm, attributed to the *dl* and *meso* isomers), and precludes identification of stereoisomers in the solid state.

No resonance was observed in the solid state for any of the $SnBr_4$-dithioether series despite long acquisition times and a variety of pulse/delay routines.

Figure 2.13. MAS ^{119}Sn NMR spectrum of [$SnCl_4${$MeS(CH_2)_3SMe$}] recorded at 4.5 KHz

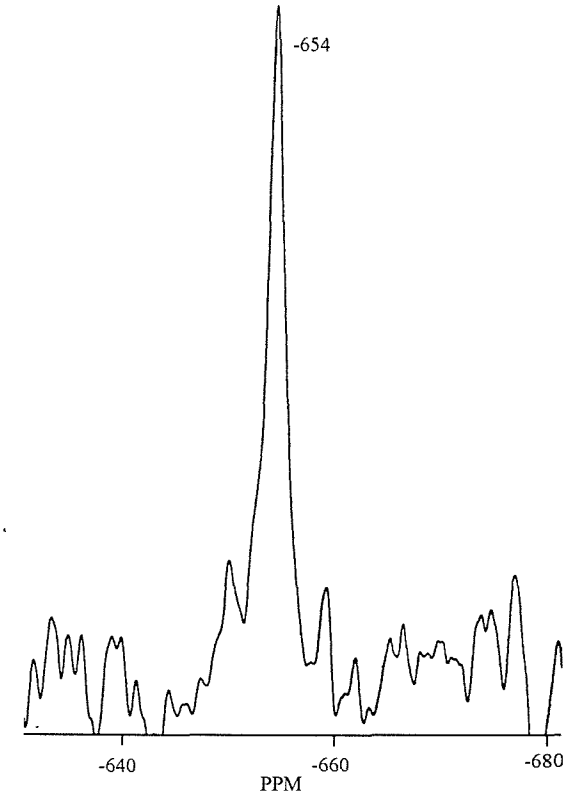

2.2.9. Attempted Synthesis of Bidentate Thioether Complexes With Germanium(IV) and Silicon(IV) Halides

In addition to the bidentate thioether complexes of the tin(IV) halides reported here, similar reactions were attempted with silicon(IV) and germanium(IV) halides. The same general method of synthesis was employed as for the tin(IV) halide complexes, i.e. direct reaction of MCl_4 (M = Si or Ge) with one mole equivalent of ligand in dry, degassed CH_2Cl_2. No evidence was observed for the formation of any adducts by variable temperature ^1H NMR spectroscopy, contrasting with the immediate reactions seen for the $SnCl_4$ and $SnBr_4$ chemistry. The ^1H NMR spectra showed only free ligand with no change in chemical shift occurring as the temperature was varied between 180 – 300 K. Similar results were observed by ^{73}Ge-$\{^1H\}$ and ^{29}Si-$\{^1H\}$ NMR spectroscopy which only showed the presence of the free MCl_4 species.

2.2.10. Crystal Structure of *cis*-[$SnI_4\{\eta^1$-*O*-$MeS(O)(CH_2)_3SMe_2$]

The formation of [$SnI_4\{MeS(CH_2)_3SMe\}$] was achieved *in situ* and confirmed by solution ^{119}Sn-{^1H} NMR spectroscopy with a single resonance at δ –2645 ppm. In an effort to obtain a crystal suitable for an X-ray structure analysis, a $CHCl_3$ solution containing a 1:1 molar ratio of SnI_4 and $MeS(CH_2)_3SMe$ was allowed to evaporate slowly. This resulted in a viscous orange oil with a few red-orange crystals forming on further evaporation. While there were too few of these crystals to permit detailed spectroscopic characterisation, they were of suitable quality for an X-ray crystallographic analysis.

The structure obtained from this analysis (Figure 2.14) showed that during crystallisation oxidation of the ligand had occurred forming $MeS(O)(CH_2)_3SMe$. The structure shows that the material isolated was in fact *cis*-[$SnI_4\{\eta^1$-*O*-$MeS(O)(CH_2)_3SMe\}_2$], involving a distorted octahedral arrangement at Sn(IV) *via* four iodide ligands and two mutually *cis* $MeS(O)(CH_2)_3SMe$ ligands both of which are coordinated *via* the O-donor of the sulfoxide function.

Figure 2.14. View of the structure of *cis*-[$SnI_4\{\eta^1$-*O*-$MeS(O)(CH_2)_3SMe\}_2$] with the numbering scheme adopted. Ellipsoids are shown at 40 % probability

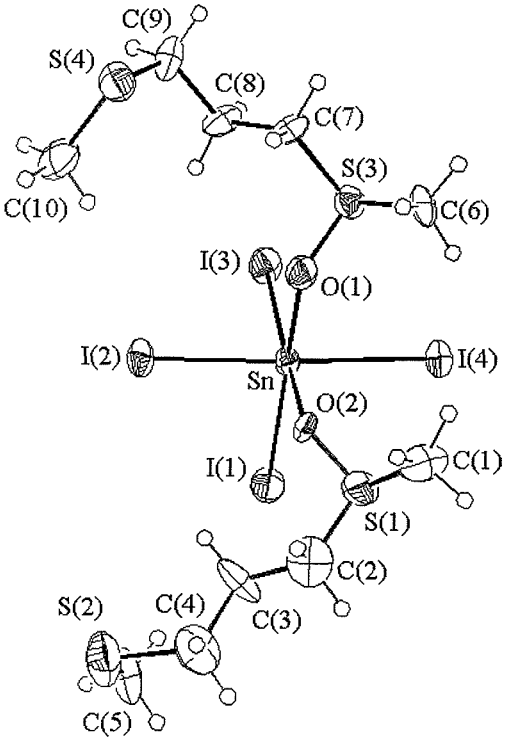

Selected bond angles (°) are presented in Table 2.10. The Sn-I bond distances (Table 2.9) and Sn-O bond distances (Table 2.9) are in good agreement with other literature examples of tin(IV) sulfoxide adducts.[28-30] However, *cis*-[$SnI_4\{\eta^1$-*O*-$MeS(O)(CH_2)_3SMe\}_2$] is unusual in that the monosulfoxide formed by oxidation of the dithioether in the presence of SnI_4. This presumably occurred as a result of trace amounts of water and iodine in the reaction mixture. Attempts to reproduce this reaction using wet solvents failed, with unreacted tin(IV) iodide recovered at the end.

Table 2.9. Bond lengths (Å) with e.s.d.s for *cis*-[$SnI_4\{\eta^1$-*O*-$MeS(O)(CH_2)_3SMe\}_2$]

I(1)	Sn	2.789(4)	S(2)	C(5)	1.75(5)
I(2)	Sn	2.762(4)	S(3)	O(2)	1.52(2)
I(3)	Sn	2.780(4)	S(3)	C(6)	1.80(3)
I(4)	Sn	2.802(4)	S(3)	C(7)	1.79(3)
Sn	O(1)	2.21(3)	S(4)	C(9)	1.80(4)
Sn	O(2)	2.18(2)	S(4)	C(10)	1.76(5)
S(1)	O(1)	1.47(2)	C(2)	C(3)	1.47(5)
S(1)	C(1)	1.78(4)	C(3)	C(4)	1.53(6)
S(1)	C(2)	1.78(5)	C(7)	C(8)	1.49(4)
S(2)	C(4)	1.79(4)	C(8)	C(9)	1.55(5)

Table 2.10. Selected bond angles (°) with e.s.d.s for *cis*-[$SnI_4\{\eta^1$-*O*-$MeS(O)(CH_2)_3SMe\}_2$]

I(1)	Sn	I(2)	93.21(7)	I(1)	Sn	I(3)	97.13(7)
I(1)	Sn	I(4)	93.74(7)	I(1)	Sn	O(1)	92.0(4)
I(1)	Sn	O(2)	169.6(3)	I(2)	Sn	I(3)	93.64(6)
I(2)	Sn	I(4)	170.27(7)	I(2)	Sn	O(1)	92.0(4)
I(2)	Sn	O(2)	83.6(4)	I(3)	Sn	I(4)	92.25(7)
I(3)	Sn	O(1)	170.7(4)	I(3)	Sn	O(2)	92.9(3)
I(4)	Sn	O(1)	88.9(3)	I(4)	Sn	(O2)	88.4(4)
O(1)	Sn	O(2)	77.9(5)	O(1)	S(1)	C(1)	102(1)
O(1)	Sn	C(2)	102(1)	O(2)	S(3)	C(6)	103.6(9)
O(2)	S(3)	C(7)	101.5(9)				

2.3. Conclusions

The products $[SnX_4(R_2S)]$ (where X = Cl, Br or I; R = Me or Ph) and $[SnX_4\{MeS(CH_2)_nSMe\}]$ (where n = 1, 2 or 3), $[SnX_4\{PhS(CH_2)_nSPh\}]$ (where n = 2 or 3) and $[SnX_4\{o\text{-}C_6H_4(SMe)_2\}]$ have been prepared in high yield. A detailed examination of the variable temperature ^1H and $^{119}Sn\text{-}\{^1H\}$ NMR spectroscopy over the temperature range 300 – 180 K has been presented. Particular emphasis for the bidentate systems has been on the study of the dynamic processes occurring in solution. The onset of pyramidal inversion and ligand dissociation have been detected, both of which begin at similar temperatures. It was possible to distinguish the *dl* and *meso* isomers within the NMR spectra at low temperature (180 K) for the majority of the systems, and a number of qualitative trends have been identified. Examples involving phenyl substituents are typically less stable than those with methyl substituents, and the stability of the complexes formed decreases with the SnX_4 acceptor: X = Cl > Br > I. The results also confirmed that five-membered chelate-ring systems are more stable than six membered chelates with the highly strained four membered chelate least favoured. Both single crystal X-ray diffraction studies on $[SnCl_4\{MeS(CH_2)_2SMe\}]$, $[SnX_4\{MeS(CH_2)_3SMe\}]$ (where X = Cl or Br), $[SnCl_4\{o\text{-}C_6H_4(SMe)_2\}]$, $[SnCl_4\{PhS(CH_2)_3SPh\}]$ and the highly strained four-membered chelate-ring species, and ^{119}Sn MASNMR spectroscopy were also used with both proving highly complementary to the solution studies and providing further support for the trends seen.

The crystal structure of *cis*-$[SnI_4\{\eta^1\text{-}O\text{-}MeS(O)(CH_2)_3SMe\}_2]$ is also reported which features the selective oxidation of one S-donor of the dithioether ligand giving a sulfoxide which binds *via* the O-donor to the hard Sn(IV) centre.

2.4. Experimental

The tin(IV) chloride, bromide and iodide and the ligands Me_2S, Ph_2S and $MeSCH_2SMe$ were purchased from *Aldrich Chemicals*. The ligands $MeS(CH_2)_nSMe$[31], $PhS(CH_2)_nSPh$[31] (where n = 2 or 3) and o-$C_6H_4(SMe)_2$[32] were prepared by following literature methods. Tin(IV) fluoride was prepared by Dr. Andrew Hector by reaction of tin powder with fluorine at 300 °C/ 3 atm. in a Monel autoclave.

Single Crystal X-ray Diffraction

Single crystals of $[SnCl_4\{MeS(CH_2)_2SMe\}]$, $[SnCl_4\{MeS(CH_2)_3SMe)\}]$, $[SnCl_4\{PhS(CH_2)_3SPh\}]$ and $[SnBr_4\{MeS(CH_2)_3SMe\}]$ were obtained by slow evaporation from a solution of the appropriate complex in Me_2CO, $[SnCl_4\{o\text{-}C_6H_4(SMe)_2\}]$ by slow cooling of the reaction mixture in CH_2Cl_2 and $[SnCl_4(MeSCH_2SMe)]$ by slow evaporation of a CH_2Cl_2 solution. For each compound the selected crystal was coated with mineral oil and mounted on a glass fibre. Data collection used a Rigaku AFC7S four-circle diffractometer equipped with an Oxford Cryostreams low temperature attachment operating at 150 K, using graphite-monochromated Mo-K_α X-radiation (~ = 0.71073 Å), T = 150 K, ω-2θ scans. The intensities of three standard reflections were monitored every 150 reflections. No significant crystal decay or movement was observed. As there were no identifiable faces the raw data were corrected for absorption using psi-scans. The weighting scheme $w^{-1} = \sigma^2(F)$ gave satisfactory agreement analyses in each case. Crystallographic data is presented in Table 2.11.

The structures of $[SnCl_4\{MeS(CH_2)_2SMe\}]$, $[SnCl_4\{MeS(CH_2)_3SMe)\}]$, $[SnCl_4\{o\text{-}C_6H_4(SMe)_2\}]$ were solved by direct methods[33], while the structures of $[SnCl_4\{PhS(CH_2)_3SPh\}]$ and $[SnBr_4\{MeS(CH_2)_3SMe\}]$ were solved by heavy atom methods.[34] All of the structures were then developed by iterative cycles of full-matrix least-squares refinement and difference Fourier syntheses which located all non-H atoms in the asymmetric unit.[35] In each case all non-H atoms in the structures were refined anisotropically and H-atoms were placed in fixed, calculated positions. For $[SnCl_4\{MeS(CH_2)_3SMe\}]$ and $[SnBr_4\{MeS(CH_2)_3SMe\}]$, both of which crystallise in the polar space group $I\bar{4}2d$, the absolute configuration was confirmed by inverting and translating the co-ordinates and re-refining to convergence. In both cases, the enantiomorph chosen gave lower R-factors and e.s.d.s associated with the atomic

Table 2.11. Crystallographic data

Compound	$[SnCl_4\{MeS(CH_2)_2SMe\}]$	$[SnCl_4\{MeS(CH_2)_3SMe\}]$	$[SnCl_4\{o\text{-}C_6H_4(SMe)_2\}]$	$[SnCl_4\{PhS(CH_2)_3SPh\}]$	$[SnBr_4\{MeS(CH_2)_3SMe\}]$	$[SnI_4\{MeS(O)(CH_2)_3SMe\}_2]$
Formula	$C_4H_{10}Cl_4S_2Sn$	$C_5H_{12}Cl_4S_2Sn$	$C_8H_{10}Cl_4S_2Sn$	$C_{15}H_{16}Cl_4S_2Sn$	$C_5H_{12}Br_4S_2Sn$	$C_{10}H_{24}I_4O_2S_4Sn$
Formula Weight	382.74	396.77	430.79	520.91	574.58	930.85
Colour, morphology	colourless block	colourless block	colourless, column	yellow, block	colourless, block	orange, column
Crystal dimensions/mm	0.30 x 0.25 x 0.10	0.40 x 0.20 x 0.20	0.50 x 0.20 x 0.10	0.40 x 0.30 x 0.15	0.30 x 0.30 x 0.20	0.20 x 0.20 x 0.05
Crystal System	orthorhonmbic	tetragonal	triclinic	monoclinic	tetragonal	triclinic
Space Group	*Aba*2	*I*-42*d*	*P*-1	*Cc*	*I*-42*d*	*P*-1
a/Å	11.605(2)	10.107(2)	8.245(3)	7.763(2)	10.330(5)	10.545(6)
b/Å	8.918(3)	10.107	11.241(4)	13.893(3)	10.330	15.24(1)
c/Å	11.790(2)	24.726(3)	8.162(2)	17.611(2)	25.867(8)	8.284(5)
α/°	90	90	90.55(3)	90	90	95.42(5)
β/°	90	90	98.01(3)	93.75(2)	90	94.15(5)
γ/°	90	90	109.69(2)	90	90	108.69(5)
U/Å^3	1220.2(5)	2525.8(9)	703.9(4)	1895.2(6)	2760(2)	1247(1)
Z	4	8	2	4	8	2
Scan Type	ω-2θ	ω-2θ	ω-2θ	ω-2θ	ω-2θ	ω-2θ
F(000)	736	1536	416	1024	2112	852
D_c/g cm^{-3}	2.083	2.087	2.032	1.825	2.765	2.478
μ(Mo-Ka)/cm^{-1}	32.56	31.50	28.42	21.24	137.25	63.10
Transmission factors (max. and min.)	1.000, 0.721	1.000, 0.906	1.000, 0.686	1.000, 0.783	1.000, 0.578	1.000, 0.661
No. of Unique obs. reflections	640	685	2479	1893	756	4405
R_{int} (based on F^2)	-	-	0.013	0.045	-	0.048
Unique obs. Reflections with $[I_o > 2.0\sigma(I_o)]$	531	583	2203	1450	509	2107
No. of parameters	51	56	136	124	56	190
Goodness of fit	3.99	1.84	3.25	1.19	1.84	1.82
$R(F_o)$	0.031	0.023	0.039	0.023	0.047	0.051
$R_w(F_o)$	0.035	0.032	0.042	0.031	0.056	0.054
Max. residual peak/eÅ^{-3}	1.66	0.70	1.22	0.44	1.43	1.75
Max. residual trough/eÅ^{-3}	-0.86	-0.48	-2.42	-0.80	-1.15	-1.82

$$R = \Sigma\,(|F_{obs}|_i - |F_{calc}|_i)/\Sigma\,|F_{obs}|_i$$

$$R_w = \sqrt{[\Sigma\, w_i(|F_{obs}|_i - |F_{calc}|_i)^2 / \Sigma\, w_i|F_{obs}|_i^2]}$$

$$GOF = [\Sigma\,(|F_{obs}|_i - |F_{calc}|_i)/\sigma_i]/(n - m) \approx 1$$

positions. The Hamilton R-factor ratio statistical check[36] was also used to determine a significance value for each of the chosen configurations. The structure chosen for $[SnCl_4\{MeS(CH_2)_3SMe\}]$ was determined to be significant to 99.5 % and that for $[SnBr_4\{MeS(CH_2)_3SMe\}]$ 95 %, confirming the assignments made.

Complex Synthesis

$[SnCl_4(Me_2S)_2]$

Dimethyl sulfide (0.024 g, 2 mmol) was dissolved in degassed $CHCl_3$ ($5cm^3$) in a 3-neck RB flask under an atmosphere of dry N_2 and the solution further degassed. Addition of $SnCl_4$ (0.26 g, 1 mmol) to the solution gave a very exothermic reaction with the immediate formation of a pale cream precipitate. This was filtered and dried *in vacuo*. 0.134 g, 93 %.

$[SnCl_4(Ph_2S)_2]$

Diphenyl sulfide (0.037 g, 2 mmol) was dissolved in degassed $CHCl_3$ ($5cm^3$), addition of $SnCl_4$ (0.26 g, 1 mmol) producing a pale cream precipitate. 0.249 g, 84 %.

$[SnBr_4(Me_2S)_2]$

Similar reaction between dimethyl sulfide (0.024 g, 2 mmol) and $SnBr_4$ (0.44 g, 1 mmol) in degassed $CHCl_3$ ($5cm^3$) gave a pale cream precipitate. 0.403 g, 87 %.

$[SnBr_4(Ph_2S)_2]$

Diphenyl sulfide (0.037 g, 2 mmol) with $SnBr_4$ (0.44 g, 1 mmol) in degassed $CHCl_3$ ($5cm^3$) formed a pale cream precipitate. 0.362 g, 76 %.

$[SnCl_4\{MeS(CH_2)_2SMe\}]$

2,5-Dithiahexane (0.12 g, 1 mmol) was added to degassed $CHCl_3$ ($5\ cm^3$) in a 3-neck RB flask under an atmosphere of dry N_2 and the solution was further degassed. $SnCl_4$ (0.26 g, 1 mmol) was added to the flask with stirring. A violently exothermic reaction occured as the $SnCl_4$ was added and a white precipitate was seen to form from solution immediately. This was filtered through a Schlenk filter and dried *in vacuo*. 0.277 g, 73 %. ^1H NMR spectrum (360 MHz, CD_2Cl_2, 300 K): 3.25 (s, CH_2, 4H), 2.50(s, SMe, 6H) ppm.

[$SnCl_4${$MeS(CH_2)_3SMe$}]

Addition of $SnCl_4$ (0.26 g, 1 mmol) to a solution of 1,3-bis(methylthio)propane (0.13 g, 1 mmol) formed a yellow precipitate immediately. This was filtered through a Schlenk filter and dried *in vacuo*. 0.33 g, 83 %. ^1H NMR spectrum (360 MHz, CD_2Cl_2, 300 K): 2.95 (SCH_2, 4H), 2.37(SMe, 6H), 2.12(CH_2, 2H) ppm.

[$SnCl_4${$PhS(CH_2)_2SPh$}]

Addition of $SnCl_4$ (0.26 g, 1 mmol) to a solution of 1,2-bis(phenylthio)ethane (0.242 g, 1 mmol) in $CHCl_3$ (5 cm^3) formed a yellow precipitate immediately from solution. This was filtered through a Schlenk filter, washed with $CHCl_3$ to remove unreacted solid ligand, and dried *in vacuo*. 0.39 g, 77 %. ^1H NMR spectrum (360 MHz, CD_2Cl_2, 300 K): 7.3(m, 5H, SPh), 3.43 (s, 2H, CH_2).

[$SnCl_4${$PhS(CH_2)_3SPh$}]

Addition of $SnCl_4$ (0.26 g, 1 mmol) to a solution of 1,3-bis(phenylthio)propane (0.244 g, 1 mmol) in $CHCl_3$ (10 cm^3) formed a crop of orange crystals from solution. These were filtered through a Schlenk filter and dried *in vacuo*. 0.38 g, 73 %. ^1H NMR spectrum (360 MHz, CD_2Cl_2, 300 K): 7.3(m, 10H, SPh), 3.12(m, 4H, SCH_2), 1.93(m, 2H, CH_2) ppm.

[$SnCl_4$(o-$C_6H_4(SMe)_2$}]

Addition of $SnCl_4$ (0.26 g, 1 mmol) to a solution of o-$C_6H_4(SMe)_2$ (0.17 g, 1 mmol) in $CHCl_3$ (10 cm^3) formed a white crystalline from solution. This was filtered through a Schlenk filter and dried *in vacuo*. 0.34 g, 79 %. ^1H NMR spectrum (360 MHz, CD_2Cl_2, 300 K): 7.5(m, 4H C_6H_4), 2.75(s, 6H, SMe).

[$SnBr_4${$MeS(CH_2)_2SMe$}]

$SnBr_4$ (0.88 g, 2 mmol) was dissolved in degassed $CHCl_3$ (10 cm^3) in a 3-neck RB flask under an atmosphere of dry N_2. 2,5-Dithiahexane (0.24 g, 2 mmol) was dissolved in degassed $CHCl_3$ (10 cm^3). This solution was added dropwise with stirring to the $SnBr_4$ solution. A yellow precipitate was seen to form from solution immediately. This precipitate was filtered through a Schlenk filter and dried *in vacuo*. 0.67 g, 60 %. Found: C, 8.8; H, 2.0. ^1H NMR spectrum (360 MHz, CD_2Cl_2, 300 K): 2.80 (s, CH_2, 4H), 2.24(s, SMe, 6H) ppm.

[$SnBr_4${$MeS(CH_2)_3SMe$}]

Addition of a solution of 1,3-bis(methylthio)propane (0.26 g, 2 mmol) in $CHCl_3$ (10 cm^3) to a solution of $SnBr_4$ (0.88 g, 2 mmol) formed a yellow precipitate immediately from solution. This precipitate was filtered through a Schlenk filter and dried *in vacuo*. 0.69 g, 61 %. ^1H NMR spectrum (360 MHz, CD_2Cl_2, 300 K): 2.72(t, SCH_2, 4H), 2.18(s, SMe, 6H), 1.91(d, CH_2, 2H) ppm.

[$SnBr_4${o-$C_6H_4(SMe)_2$}]

Addition of o-$C_6H_4(SMe)_2$ (0.34 g, 2 mmol) in $CHCl_3$ (10 cm^3) to a solution of $SnBr_4$ (0.88 g, 2mmol) gave a yellow precipitate which formed immediately from solution. This precipitate was filtered through a Schlenk filter and dried *in vacuo*. 0.70 g, 58 %. ^1H NMR spectrum (360 MHz, CD_2Cl_2, 300 K): ~7.3(C_6H_4, 4H), 2.5(s, SMe, 6H) ppm.

References

[1] J-M. Dumas and M. Gomel, *Bull. Soc. Chim. France*, 1974, **10**, 1885.

[2] I.R. Beattie and L. Rule, *J. Chem. Soc.*, 1964, 3267.

[3] S.J. Ruzicka and A.E. Merbach, *Inorg. Chim. Acta*, 1976, **20**, 221.

[4] S.J. Ruzicka and A.E. Merbach, *Inorg. Chim. Acta*, 1977, **22**, 191.

[5] S.J. Ruzicka, C.M.P. Favez and A.E. Merbach, *Inorg. Chim. Acta*, 1977, **23**, 239.

[6] C.T.G. Knight and A.E. Merbach, *J. Am. Chem. Soc.*, 1984, **106**, 804.

[7] C.T.G. Knight and A.E. Merbach, *Inorg. Chem.*, 1985, **24**, 576.

[8] E.W. Abel, S.K. Bhargava, K.G. Orrell and V. Sik, *Inorg. Chim. Acta*, 1981 , **49** , 25.

[9] N. Bricklebank, S. M. Godfrey, C. A. McAuliffe and R. G. Pritchard, *J. Chem. Soc., Chem. Commun.*, 1994, 695.

[10] G.T. Morgan and W. Ledbury, *J. Chem. Soc.*, 1922, 2882.

[11] G.R. Willey, A. Jarvis, J. Palin and W. Errington, *J. Chem. Soc., Dalton Trans.*, 1994, 255.

[12] M. M. Olmstead, K. A. Williams and W.K. Musker, *J. Am. Chem. Soc.*, 1982, **104**, 5567.

[13] D. Tudela, V. Fernandez, J.D. Tornero and A. Vegas, *Z. Anorg. Allg. Chem.*, 1986, **532**, 215.

[14] E.W. Randall, C.M.S. Yoder and J.J. Zuckerman, *Inorg. Chem.*, 1966, **5**, 2240.

[15] T.N. Srivastava, S.K. Tandon and N. Bhakru, *J. Inorg. Nucl. Chem.*, 1976, **38**, 2311.

[16] A.R. Bassoteli, A.C.D. Angelo, E. Tfouni and N.R. Stradiotto, *Polyhedron*, 1984, **3**, 627.

[17] C. H. Schumacher, F. Weller and K. Dehnicke, *Z. Anorg. Allg. Chem.*, 1984, **508**, 79.

[18] T. Tanaka, *Inorg. Chem.*, 1967, **1**, 217.

[19] K. W. Zilm, G. A. Lawless, R. M. Merrill, J. N. Nillar and G. G. Webb, *J. Am. Chem. Soc.*, 1987, **109**, 7236.

[20] R. K. Harris and A. Sebald, *Organometallics*, 1988, **7**, 388.

[21] W. Petz, *Chem. Rev.*, 1986, **86**, 1019.

[22] I. R. Beattie, *Q. Rev. Chem. Soc.*, 1963, **17**, 382.

[23] E. L. Muetterties, *J.Am. Chem. Soc.*, 1960, **82**, 1082.

[24] A. F. Chiffey, J. Evans, W. Levason and M. Webster, *J. Chem. Soc., Dalton Trans.*, 1994, 2835.

[25] J. R. Black, N. R. Champness, W. Levason and G. Reid, *Inorg. Chem.*, 1996, **35**, 4432.

[26] S.J. Blunden, D. Searle and P.J. Smith, *Inorg. Chim. Acta*, 1985, **98**, 185.

[27] R. Colton, D. Dakternieks and C-A. Harvey, *Inorg. Chim. Acta*, 1982, **61**, 1.

[28] J. M. Kisenyi, G. R. Willey and M. G. B. Drew, *Acta Crystallogr., Sect. C*, 1985, **41**, 700.

[29] M. Gregorkiewitz and D. Tudela, *Acta Crystallogr., Sect. C*, 1990, **46**, 210.

[30] A. V. Jatsenko, S. V. Medvedev, K. A. Paseshnitchenko and L. A. Aslanov, *J. Organomet. Chem.*, 1985, **284**, 181.

[31] F. R. Hartley, S.G. Murray, W. Levason, H. E. Soutter and C. A. McAuliffe, *Inorg. Chim. Acta*, 1979, **35**, 265.

[32] T. Kemmitt and W. Levason, *Organometallics*, 1989, **8**, 1303.

[33] SHELXS-86, program for crystal structure solution, G. M. Sheldrick, *Acta Crystallogr., Sect. A*, 1990, **46**, 467.

[34] PATTY, The DIRDIF Program System, P. T. Beurskens, G. Admiraal, G. Beurskens, W. P. Bosman, S. Garcia-Granda, R. O. Gould, J. M. M. Smits and C. Smykalla. Technical Report of the Crystallography Laboratory, University of Nijmegen, The Netherlands, 1992.

[35] TEXSAN, Crystal Structure Analysis Package, Molecular Structure Corporation, Houston, TX, 1992.

[36] W. C. Hamilton, *Acta Crystallogr.*, 1965, **18**, 502.

Chapter 3

Group 14 Halide Complexes With Mono- and Bidentate Selenoethers

3.1. Introduction

Compared to the thioether complexes studied in chapter 2 very little prior work has been done on selenoether complexes of the tin(IV) halides. The only prior reports of selenoether complexes are studies of $[SnX_4(R_2Se)_2]$ (where X = Cl or Br, R = Me[1-3] or Me_3SiCH_2[3]). In the first series of studies on these systems Ruzicka and Merbach[1] used infrared and Raman spectroscopy to investigate the vibrational spectra in the solid and solution states and compared this system with these containing a range of other ligand types. In the solid state the *trans* isomer was identified as predominant, while solution Raman spectroscopy identified the presence of a *cis/trans* equilibrium, again with the *trans* isomer preferred. They continued to study the same system using ^{119}Sn-{^{1}H} NMR spectroscopy and arrived at a number of conclusions for these systems.[2] As discussed in chapter 2, they observed an increased lability for the *cis* isomer, attributed to the larger *trans* effect of the halide anion over a neutral donor in the *trans* isomer, and increased lability for bromide systems, assigned to the reduced effective charge on the tin(IV) centre.

Abel *et al.*[3] repeated and confirmed these results using ^{119}Sn-{^{1}H} NMR spectroscopy but also observed the cessation of pyramidal inversion at the selenium at temperatures below *ca.* 200 K.

The following work provides a detailed investigation into the behaviour of the tin(IV) halides with monodentate ligands of type R_2Se (where R = Me or Ph) and bidentate ligands of the type $RSe(CH_2)_nSeR$ (where R = Me for n = 1, 2 or 3; R = Ph for n = 2 or 3) and o-$C_6H_4(SeMe)_2$ continuing a study of group 16 ligand complexes, both in solution and in the solid state. The effects of changing halide and ligand interdonor linkage and substituents are studied. Variable temperature ^{1}H, ^{119}Sn-{^{1}H} and ^{77}Se-{^{1}H} NMR spectra have been recorded investigating the pyramidal inversion and ligand exchange processes in solution for these systems, with infrared spectroscopy and single crystal X-ray diffraction used to study the behaviour of these complexes in the solid state. The analogous thioether complexes were discussed in chapter 2 and the telluroether complexes and overall trends and comparisons will be brought together in chapter 4.

3.2. Results & Discussion

3.2.1. Synthesis and Properties of Monodentate Selenoether Complexes

Complexes of the type $[SnX_4(R_2Se)_2]$ (where X = Cl, Br, R = Me or Ph; X = I, R = Me) have been prepared by reaction of SnX_4 with two molar equivalents of R_2Se in degassed CH_2Cl_2. Only complexes of the Me_2Se ligand with $SnCl_4$ and $SnBr_4$ were isolable as solids. For these solid complexes IR spectra showed one broad peak at 300 (ν(SnCl)) or 220 cm^{-1} (ν(SnBr)) probably corresponding to the *trans* isomer (D_{4h} symmetry) being the principal isomer present in the solid state. There was no evidence of ligand oxidation, no bands were present in the region 400 - 470 cm^{-1} characteristic of ν(SnO) stretching frequencies.[4] Satisfactory microanalyses were collected for all species isolated.

3.2.2. Single Crystal X-ray Diffraction Studies

Prior to this study there were no structurally characterised examples of tin(IV) halide-selenoether complexes, so an analysis was carried out on crystals of $[SnCl_4(Me_2Se)_2]$ (Figure 3.1) and $[SnBr_4(Me_2Se)_2]$ (Figure 3.2) to allow comparison between the solid state and solution. The analogous thioether complex, $[SnBr_4(Me_2S)_2]$, synthesised by reaction of tin metal with Me_2SBr_2, has been structurally characterised by Bricklebank *et al.*[5] and features both the *cis* and *trans* forms within the unit cell.

Table 3.1. Bond lengths (Å) with e.s.d.s for *trans*-$[SnX_4(Me_2Se)_2]$

Complex	*trans*-$[SnCl_4(Me_2Se)_2]$	*trans*-$[SnBr_4(Me_2Se)_2]$
Sn-X(1)	2.7001(9)	2.576(2)
Sn-X(2)	2.413(2)	2.587(2)
Sn-Se(1)	2.427(2)	2.731(2)
Se(1)-C(1)	1.957(10)	1.96(2)
Se(1)-C(2)	1.952(9)	1.94(2)

Table 3.2. Bond angles (°) with e.s.d.s for *trans*-[$SnX_4(Me_2Se)_2$]

Complex	*trans*-[$SnCl_4(Me_2Se)_2$]	*trans*-[$SnBr_4(Me_2Se)_2$]
X(1)-Sn-X(2)	89.54(8)	90.47(5)
X(1)-Sn-Se(1)	89.40(6)	90.63(5)
X(2)-Sn-Se(1)	91.25(6)	88.46(5)
Sn-Se(1)-C(1)	100.7(3)	100.9(4)
Sn-Se(1)-C(2)	100.2(3)	102.2(5)
C(1)-Se(1)-C(2)	97.3(4)	96.9(7)

Both Me_2Se complexes are isostructural, with the same space group and with unit cells of similar sizes, with the bromide slightly larger, consistent with the increased radii of the bromine atoms over the chlorine. In both structures the central Sn(IV) occupies a crystallographic inversion centre, co-ordinated *via* four precisely planar X atoms, with two mutually *trans* Me_2Se ligands completing the slightly distorted octahedral geometry. In both cases the angles around the central tin atom are very close to the 90 and 180° angles expected for a regular octahedron.

Bond lengths (Å) and angles (°) for *trans*-[$SnX_4(Me_2Se)_2$] (X = Cl and Br) are presented in Table 3.1 and 3.2 respectively. The Sn-X distances for these two structures are in good agreement with the few structurally characterised examples of thioether complexes of tin(IV) halides discussed in chapter 2, *e.g.* $[SnCl_3([9]aneS_3)]^+$ [Sn-Cl 2.366(4), 2.369(3) and 2.371(4) Å],[6] $2SnCl_4.[18]aneS_6$ [Sn-Cl 2.30(2), 2.31(2), 2.38(2), 2.391(2), 2.421(2) and 2.42(2)][6] *cis*-[$SnBr_4(Me_2S)_2$] [Sn-Br 2.554(4), 2.532(4), 2.557(4) and 2.539(4) Å][5] and *trans*-[$SnCl_4(\eta^1\text{-}C_6H_{12}S_2\text{-}1,5)_2$] [Sn-Cl 2.414(1), 2.428(1) Å].[7]

As was observed for *trans*-[$SnBr_4(Me_2S)_2$],[5] the bond distance Sn-E (E = S or Se) is longer for the bromide complex, most likely a consequence of $SnBr_4$ being a poorer acceptor than $SnCl_4$. Comparison of the Sn-Br bond lengths in *trans*-[$SnBr_4(Me_2Se)_2$] with those in *trans*-[$SnBr_4(Me_2S)_2$][5] shows that they are very similar and the Sn-Se distances are *ca.* 0.1 Å longer than the Sn-S distances, consistent with the larger radius of Se over S.

Figure 3.1. View of the structure of *trans*-[$SnCl_4(Me_2Se)_2$] with numbering scheme adopted. Ellipsoids are shown at 40 % probability and atoms marked with an asterisk are related by a crystallographic inversion centre

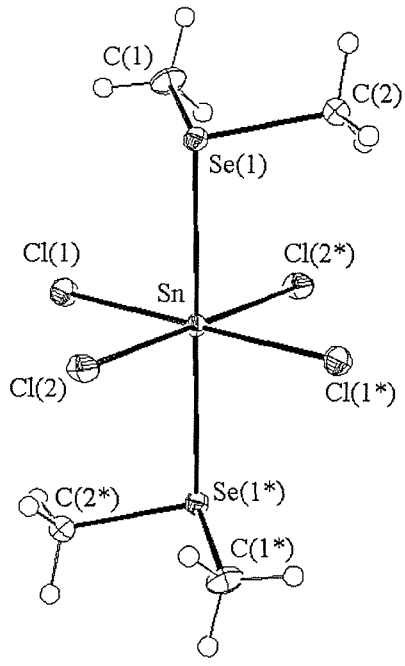

Figure 3.2. View of the structure of *trans*-[$SnBr_4(Me_2Se)_2$] with numbering scheme adopted. Details as for Fig. 3.1

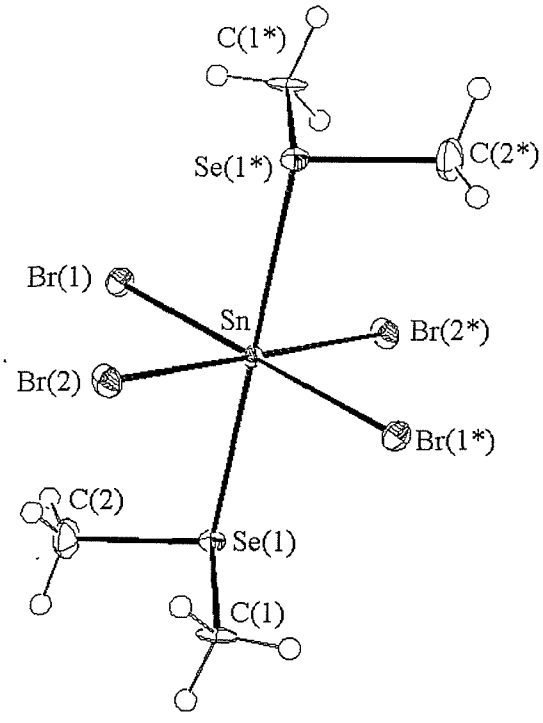

3.2.3. Variable Temperature ^{1}H NMR Spectroscopy

The SnX_4/Me_2Se (X = Cl or Br) systems have previously been examined *via* ^{1}H NMR spectroscopy.[1-3] A solution of $[SnCl_4(Me_2Se)_2]$ with excess Me_2Se in CD_2Cl_2 at 300 K exhibits a single δ(Me) at 2.51 ppm. At this temperature there is no evidence of $^3J(^1H - ^{117/119}Sn)$ satellites. However, on cooling the solution to *ca.* 250 K the resonance is seen to split, giving two resonances due to the *trans* and *cis* isomers, and ill defined satellites are also seen to appear. At the lowest temperature studied, 180 K, the two resonances are present in the ratio *ca.* 1.5 : 1 due to *trans* and *cis* isomers at δ 2.44 and 2.54 ppm respectively, with $^3J(^1H - ^{117/119}Sn)$ couplings of *ca.* 50-60 Hz now clearly defined.

The ^{1}H NMR spectrum of $[SnBr_4(Me_2Se)_2]$ in CD_2Cl_2 with an excess of Me_2Se at 300 K consists of a single broad resonance at δ 2.36 ppm. On lowering the temperature to 250 K the signal splits to give two resonances for the *cis* and *trans* isomers. At 180 K these two resonances have sharpened at δ 2.26 and 2.40 ppm respectively and the $^3J(^1H - ^{117/119}Sn)$ satellites are seen with couplings of *ca.* 50-60 Hz. For this complex the *trans* and *cis* isomers are observed in the ratio *ca.* 3 : 1. This is to be expected for the larger $SnBr_4$ compared to $SnCl_4$, with the *trans* isomer preferred sterically.

Studies of SnF_4 and SnI_4 with an excess of Me_2Se in CD_2Cl_2 solution exhibit no evidence for adduct formation even at the lowest temperatures studied (173 K).

Reaction of tin(IV) halides with the monodentate ligand Ph_2Se yielded no isolable solid products, although colour changes were evident for tin(IV) chloride and bromide. In the ^{1}H NMR spectra no resonances consistent with adduct formation were observed for any of the species even at the lowest studied temperature (173 K).

3.2.4. Variable Temperature ^{119}Sn-{^{1}H} NMR Spectroscopy

As has been observed[2,5] the solubility of these complexes in CH_2Cl_2 is extremely poor. A range of other solvents was also examined including $MeNO_2$, Me_2CO, thf and propane-1,2-diol carbonate, but these proved unsatisfactory and there was a possibility that the observed resonances were due to adducts with O-donors.[8] CD_2Cl_2 was therefore again used even though the compounds were not very soluble in this solvent, necessitating long data collection times.

At 300 K the system $[SnCl_4(Me_2Se)_2]$ in CD_2Cl_2 exhibits a single broad resonance at δ –693 ppm, shifted to low frequency by 100 – 150 ppm from the region of the spectrum observed for the $SnCl_4$-thioether complexes studied in chapter 2. On cooling the system the resonance is seen to split at *ca.* 260 K where resonances attributable to the *cis* and *trans* isomers are observed. On cooling further the resonances sharpen to give two signals at δ –691 and 695 ppm for the *cis* and *trans* isomers respectively. At this temperature $^{1}J(^{119}Sn\text{-}^{77}Se)$ couplings of *ca.* 460 – 490 Hz are also clearly seen (Figure 3.3). In contrast no resonance is observed for the species $[SnBr_4(Me_2Se)_2]$ in CH_2Cl_2 at 300 K due to rapid exchange in solution. A single resonance becomes apparent on cooling to *ca.* 280 K at δ -1360 ppm which then splits on further cooling and resolves clearly at 180 K to show the two resonances expected for *cis* and *trans* isomers at δ -1296 and –1319 ppm respectively. Also present is similar $^{1}J(^{119}Sn\text{-}^{77}Se)$ coupling to that observed in the $[SnCl_4(Me_2Se)_2]$ system, with values of *ca.* 500 – 550 Hz.

These two $[SnX_4(Me_2Se)_2]$ (X = Cl or Br) systems were also studied with an excess of Me_2Se in CH_2Cl_2 solution over the temperature range 180 – 300 K. At 180 K in the ^{119}Sn-{^{1}H} NMR spectrum of the chloride species both *cis* and *trans* resonances are observed at δ –690.5 and –694.0 ppm with the $^{1}J(^{119}Sn\text{-}^{77}Se)$ coupling again present. Warming the solution results in the signal for the *cis* isomer broadening as exchange with free ligand starts at *ca.* 230 K before disappearing at *ca.* 270 K. The *trans* isomer remains largely unchanged until ambient temperatures are reached consistent with a higher barrier to exchange in the *trans* isomer. The corresponding $SnBr_4$ species displayed largely similar behaviour, at 180 K the two resonances for *cis* and *trans* isomers are observed at δ –1293 and –1315 ppm in the ^{119}Sn-{^{1}H} NMR spectrum with the $^{1}J(^{119}Sn\text{-}^{77}Se)$ coupling present. For this system the onset of ligand exchange with free ligand in the *cis* isomer begins at *ca.* 210 K when the *cis* resonance

weakens and broadens before disappearing at *ca.* 245 K. The *trans* resonance starts to weaken and broaden with ligand exchange at *ca.* 250 K and at ambient temperatures has become unresolvable. These results are qualitatively again consistent with the results of the analogous $[SnX_4(Me_2S)_2]$-Me_2S systems studied by Knight and Merbach,[9] discussed in chapter 2. The onset of ligand exchange at lower temperatures in the $[SnBr_4(Me_2Se)_2]$-Me_2Se system relative to the chloride system is consistent with the observations made in chapter 2 that $SnBr_4$ is a poorer acceptor than the chloride.

While no isolable solids were produced from the reactions of SnI_4 or SnF_4 with Me_2Se *in situ* ^{119}Sn-$\{^1H\}$ NMR studies were tried. SnF_4 proved to insoluble in non-co-ordinating solvent, precluding studies of these systems. For SnI_4 no resonances resulting from adduct formation were observed even at 175 K, again consistent with the results of chapter 2 where these tin species were assigned as poorer acceptors than $SnCl_4$ and $SnBr_4$.

Figure 3.3. ^{119}Sn-$\{^1H\}$ NMR spectrum of $[SnCl_4(Me_2Se)_2]$ in CD_2Cl_2 solution at 180 K

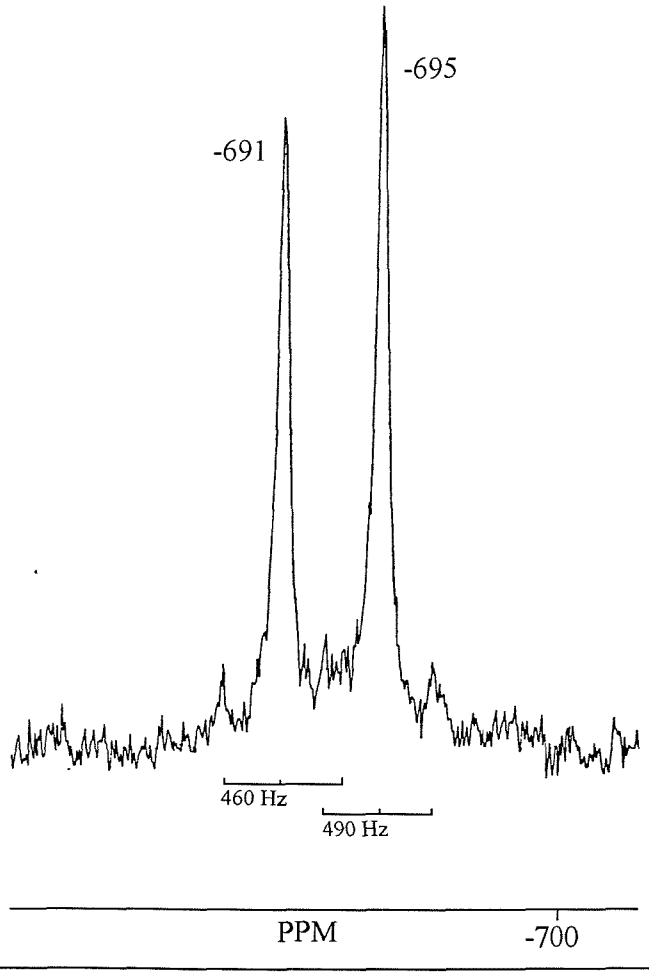

3.2.5. Variable Temperature ^{77}Se-{^{1}H} NMR Spectroscopy

The presence of selenium within the ligand provides another nucleus (^{77}Se) with spin I = ½ (abundance = 7.6 %) and these complexes can therefore be studied using ^{77}Se-{^{1}H} NMR spectroscopy and corresponding $^{1}J(^{119}\text{Sn-}^{77}\text{Se})$ couplings in the ^{119}Sn-{^{1}H} NMR spectra have already been observed.

In the ^{77}Se-{^{1}H} NMR spectra of both the chloride and bromide systems large high-frequency co-ordination shifts Δ (= $\delta_{complex} - \delta_{ligand}$) of approximately +200 are observed, with the resonance of the *cis* isomer slightly to high frequency of the *trans* isomer. In general, the behaviour in the ^{77}Se-{^{1}H} NMR spectra mirrored those of the ^{119}Sn-{^{1}H} NMR spectra. At 300 K the spectrum of $[SnCl_4(Me_2Se)_2]$ in CD_2Cl_2 exhibits a single resonance at δ +176 ppm, indicating that ligand exchange is too rapid to resolve the two isomers. Upon lowering the temperature to *ca.* 240 K the signal broadens and splits to give the two resonances for *cis* and *trans* isomers at δ +199 and +180 ppm, and these become sharper as the temperature is lowered further. Eventually, at 180 K, the resonances are at δ +204 and 185 ppm with satellites due to $^{1}J(^{77}\text{Se-}^{117/119}\text{Sn})$ coupling clearly resolved (Figure 3.4). These couplings are consistent with those observed in the ^{119}Sn-{^{1}H} NMR spectra with values of *ca.* 460 – 490 Hz. Since tin has two nuclei with spin I = ½ and similar abundances (^{117}Sn and ^{119}Sn), we were unable to resolve two sets of satellites. Since the $\gamma(^{119}\text{Sn}) : \gamma(^{117}\text{Sn})$ ratio is 0.956 : 1, these couplings are nearly coincident and often cannot be resolved.

The behaviour observed for $[SnBr_4(Me_2Se)_2]$ in the ^{77}Se-{^{1}H} NMR spectra again mirrors that in the ^{119}Sn-{^{1}H} NMR spectra. At 300 K no resonance is seen due to rapid ligand exchange at this temperature. A resonance first appears at *ca.* 280 K at δ 195 ppm. At *ca.* 220 K a second broad signal at δ ~216 ppm begins to appear, as the *cis* and *trans* isomers become resolved. At 200 K both resonances are observed clearly and at 180 K both resonances at δ 204.0 and 218.8 ppm display $^{1}J(^{77}\text{Se-}^{117/119}\text{Sn})$ couplings with values consistent with those observed in the ^{119}Sn NMR spectra, 500 and 550 Hz respectively.

The behaviour of the systems in the presence of an excess of Me_2Se again mirror that observed in the ^{119}Sn-{^{1}H} NMR spectra. However, in the ^{77}Se-{^{1}H} NMR spectra the free ligand (Me_2Se δ 0 ppm) is also observed. At 300 K only one resonance at δ 174 ppm is seen in the spectrum of $[SnCl_4(Me_2Se)]$-Me_2Se as exchange between the adduct and free ligand is rapid. At *ca.* 240 K two separate resonances are evident at

Figure 3.4. Variable temperature ^{77}Se-{^{1}H} NMR spectrum of $[SnCl_4(Me_2Se)_2]$ in CH_2Cl_2-CD_2Cl_2 solution

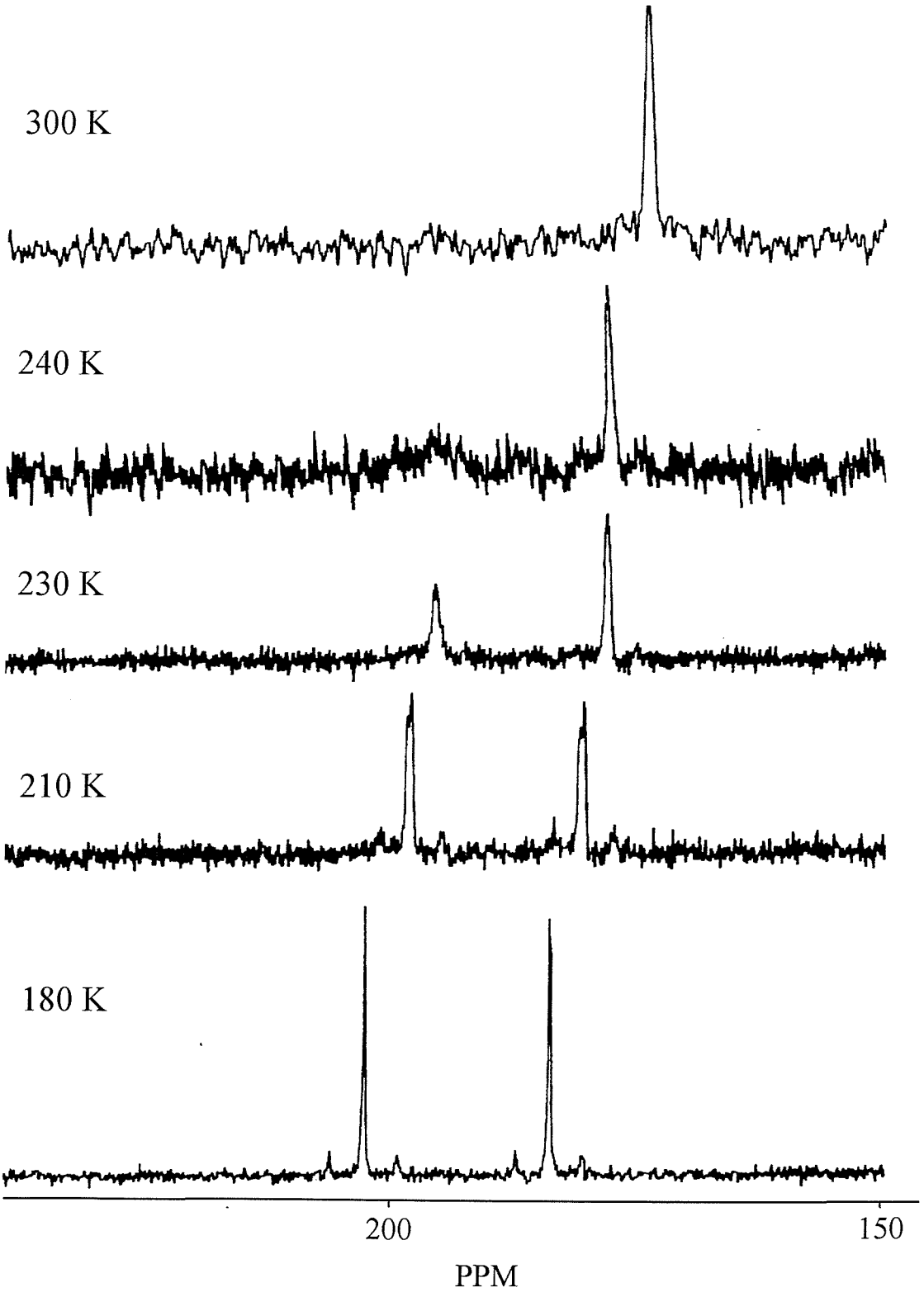

δ 177 and –8.9 ppm for the complex and free ligand respectively, the shift from δ 0 to -8.9 ppm arising from temperature effects. At *ca.* 220 K all three species are observed, and at 180 K resonances are clearly resolved at δ 204, 189 and –8.5 ppm for *cis* and *trans* isomers and free ligand. The $^{1}J(^{77}Se\text{-}^{117/119}Sn)$ coupling is also clearly resolved with values, *ca.* 500 – 550 Hz, consistent with the previous observed couplings. The bromide system, $[SnBr_4(Me_2Se)_2]$-Me_2Se, again mirrors the results from the $^{119}Sn\text{-}\{^{1}H\}$ NMR spectra and follows the same behaviour as the chloride system. At 300 K the only resonance observed is an averaged signal at δ 9 ppm. At *ca.* 260 K this signal has broadened and diminished with a second sharp resonance forming at δ 196 ppm, for the *trans* isomer. At *ca.* 240 K the free ligand resonance has sharpened again as ligand exchange with the *trans* isomer is slowed. At *ca.* 200 K the resonance of the *cis* isomer is seen, and at 180 K all three species are clearly resolved at δ 219, 204 and –7 ppm for the *cis*, *trans* isomers and free ligand, with $^{1}J(^{77}Se\text{-}^{117/119}Sn)$ couplings clearly observed for the *cis* and *trans* isomers, values of *ca.* 500 – 560 Hz again consistent with the observation in the $^{119}Sn\text{-}\{^{1}H\}$ NMR spectra. On returning to ambient temperatures the same behaviour is seen in reverse, with the onset of ligand exchange in the *cis* isomer occurring first, followed by exchange in the *trans* isomer, before these mechanisms become too fast to be observed on the NMR timescale. The onset of exchange at lower temperatures in the bromide systems is again consistent with $SnBr_4$ being a poorer acceptor than $SnCl_4$. All of these results are consistent with those for the analogous thioether system studied by Knight and Merbach.[9]

Although the ^{119}Sn NMR spectra of SnI_4 and SnF_4 with Me_2Se showed no resonances over the temperature range 173 – 300 K, the $^{77}Se\text{-}\{^{1}H\}$ NMR spectra of SnI_4 in the presence of a large excess of Me_2Se shows a single resonance at δ 152 ppm at 180 K. It is likely that this resonance is representative of adduct formation, probably *trans*-$[SnI_4(Me_2Se)_2]$, in solution at these low temperatures. This is consistent with the weaker Lewis acid, SnI_4, being a poorer acceptor than $SnBr_4$ and $SnCl_4$ as seen in chapter 2.

Attempts were made to record the $^{77}Se\text{-}\{^{1}H\}$ NMR spectra of the corresponding Ph_2Se systems, $[SnX_4(Ph_2Se)_2]$ (where X = Cl or Br), over the temperature range 173 – 300 K. No resonances were observed for either of the systems at any temperature with only free ligand observed at δ 413 ppm. This result supports the conclusion of chapter 2 where phenyl substituted ligands were assigned as poorer donors than the methyl

substituted analogues, though whether this is due to steric or electronic effects has not been established.

3.2.6. Synthesis and Properties of Bidentate Selenoether Complexes

A range of complexes of type $[SnX_4\{L\text{-}L\}]$ (where X = Cl or Br; L-L = $MeSeCH_2SeMe$, o-$C_6H_4(SeMe)_2$ or $RSe(CH_2)_nSeR$; where R = Ph or Me, n = 2 or 3) have been prepared by reaction of SnX_4 with a molar equivalent of thioether ligand L-L in degassed CH_2Cl_2. In most cases this gave precipitates of powdered white or yellow solids (Me substituted ligands), or orange crystalline solids (Ph substituted ligands), in good yield. In the case of the $[SnBr_4\{PhSe(CH_2)_nSePh\}]$ species, viscous yellow solutions were formed from which it was not possible to isolate a solid, and no solids were isolable for reactions involving SnI_4. Due to the extreme moisture sensitivity of the tin(IV) halides, all reactions were carried out under an atmosphere of dry dinitrogen using standard Schlenk techniques. Whereas the thioether complexes of the tin(IV) halides were found to be stable over a period of months in the solid state, the corresponding selenoether complexes prove to be far more sensitive to hydrolysis and decompose to dark oils over a period of days. As a result, all complexes were stored in a dry-box under an atmosphere of dry nitrogen. If dry solvents are not used hydrolysis occurs resulting in the formation of hydrates of varying stoichiometries or oxidation of the ligand as discussed later within this chapter.

IR spectra of the solid complexes formed all showed the expected four ν(Sn-Cl) bands (theory: $2A_1 + B_1 + B_2$) in the range 300 - 340 cm^{-1} consistent with C_{2v} symmetry. Satisfactory microanalyses were recorded for all solid $[SnX_4(L\text{-}L)]$ produced.

3.2.7. Single Crystal X-ray Diffraction Studies

Prior to this study there were no structurally characterised examples of selenoether complexes of any tin(IV) halides, and the two structures of *trans*-$[SnCl_4(Me_2Se)_2]$ (Section 3.2.2, Figure 3.1) and *trans*-$[SnBr_4(Me_2Se)_2]$ (Section 3.2.2, Figure 3.2) are the only examples of selenoether complexes available for comparison.[10] In order to attempt to identify trends in their geometric parameters, and to correlate these with their behaviour observed in solution (by variable temperature $^{119}Sn\text{-}\{^1H\}$, $^{77}Se\text{-}\{^1H\}$ and ^1H NMR spectroscopy), single crystal X-ray structure analyses were undertaken on several of the products.

Single crystal X-ray diffraction studies were carried out on the two complexes of the orthophenylene selenoethers, $[SnX_4\{o\text{-}C_6H_4(SeMe)_2\}]$ [where X = Cl (Figure 3.5) or Br (Figure 3.6)], and the single methylene backboned species $[SnCl_4\{MeSeCH_2SeMe\}]$ (Figure 3.7), which features a highly strained four-membered chelate-ring system that has not been seen before for this ligand. All structures feature distorted octahedral arrangements. In the cases of $[SnBr_4\{o\text{-}C_6H_4(SeMe)_2]$ (Figure 3.6) and $[SnCl_4\{MeSeCH_2SeMe\}]$ (Figure 3.7) only half the molecule is found in the asymmetric cell with the second half generated by a mirror plane (x, 0.5 – y, z) upon which the tin atom and two axial halide atoms lie. Single crystals of $[SnCl_4\{MeSe(CH_2)_3SeMe\}]$ (Figure 3.8) and $[SnCl_4\{PhSe(CH_2)_2SePh\}]$ (Figure 3.9) were also studied but they were of rather poor quality and weakly diffracting and consequently the overall data quality was low. However, the analyses were sufficient to confirm unambiguously that these two complexes feature chelating ligands both of which adopt the *dl* configuration.

Figure 3.5. View of the structure of $[SnCl_4\{o\text{-}C_6H_4(SeMe)_2\}]$ with numbering scheme adopted. Ellipsoids are shown at 40 % probability

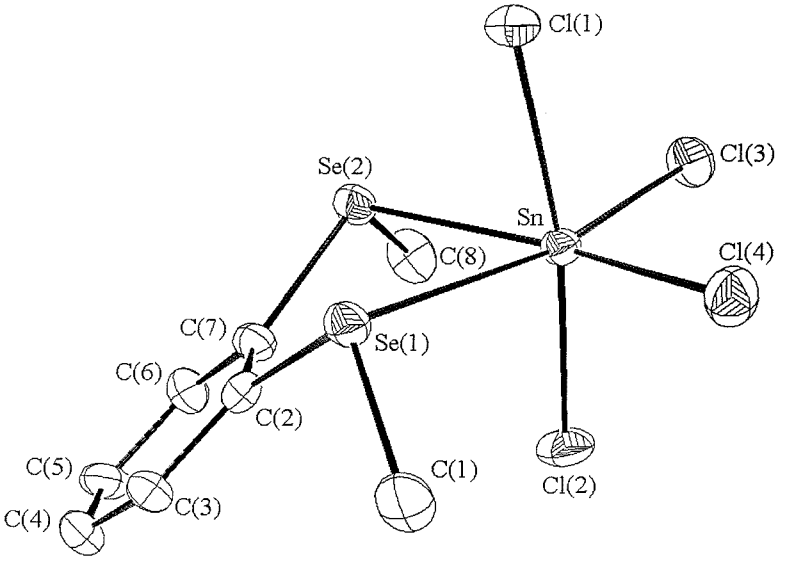

Selected bond lengths (Å) and angles are presented in Tables 3.3 and 3.4 respectively. The Sn-X distances for these structures are again in good agreement with the thioether analogues, *e.g.* $[SnCl_3([9]aneS_3)]^+$ [Sn-Cl 2.366(4), 2.369(3) and 2.371(4) Å],[6] $2SnCl_4.[18]aneS_6$ [Sn-Cl 2.30(2), 2.31(2), 2.38(2), 2.391(2), 2.421(2) and 2.42(2)],[6] *cis*-$[SnBr_4(Me_2S)_2]$ [Sn-Br 2.554(4), 2.532(4), 2.557(4) and 2.539(4) Å][5] and *trans*-$[SnCl_4(\eta^1\text{-}C_6H_{12}S_2\text{-}1,5)_2]$ [Sn-Cl 2.414(1), 2.428(1) Å].[7]

Table 3.3. Bond lengths (Å) with e.s.d.s for $[SnX_4\{diselenoether\}]$ complexes

Complex	$[SnCl_4(MeSeCH_2SeMe)]$	$[SnCl_4\{o\text{-}C_6H_4(SeMe)_2\}]$	$[SnBr_4\{o\text{-}C_6H_4(SeMe)_2\}]$
Sn-X(1)	2.406(4)	2.426(3)	2.600(2)
Sn-X(2)	2.407(4)	2.389(3)	2.547(2)
Sn-X(3)	2.376(3)	2.360(3)	2.512(1)
Sn-X(4)	– [a]	2.364(3)	– [a]
Sn-Se(1)	2.782(1)	2.749(1)	2.841(2)
Sn-Se(2)	– [b]	2.787(2)	– [b]

a. atom related to X(3), in the numbering scheme adopted, by crystallographic mirror plane
b. atom related to Se(1), in the numbering scheme adopted, by crystallographic mirror plane

Figure 3.6. View of the structure of $[SnBr_4\{o\text{-}C_6H_4(SeMe)_2\}]$ with numbering scheme adopted. Ellipsoids are shown at 40 % probability and atoms marked with an asterisk are related by a crystallographic mirror plane

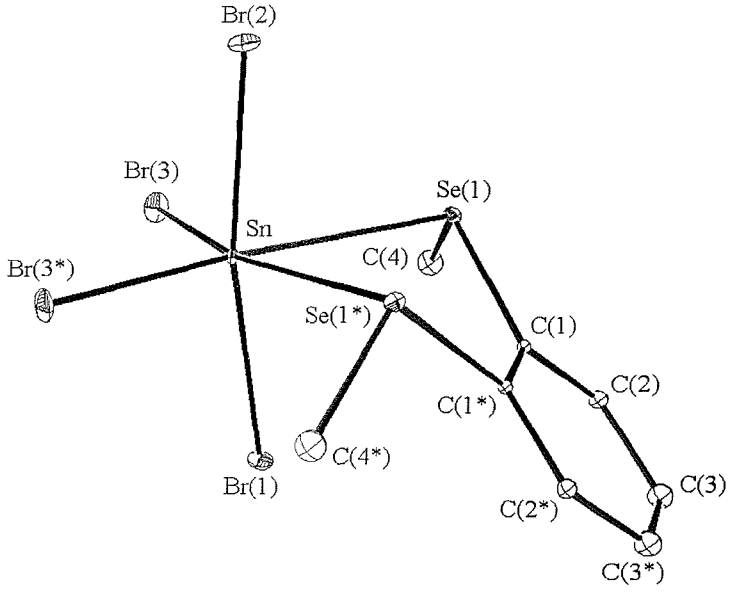

Table 3.4. Selected bond angles (°) with e.s.d.s for [SnX_4{diselenoether}] complexes

Complex	$[SnCl_4(MeSeCH_2SeMe)]$[a]	$[SnCl_4\{o\text{-}C_6H_4(SeMe)_2\}]$	$[SnBr_4\{o\text{-}C_6H_4(SeMe)_2\}]$[a]
X(1)-Sn-X(2)	175.5(1)	169.7(1)	169.12(7)
X(1)-Sn-X(3)	91.77(9)	91.4(1)	92.44(5)
X(1)-Sn-X(4)	–[a]	95.4(1)	–
X(1)-Sn-Se(1)	87.53(8)	82.41(8)	87.81(5)
X(1)-Sn-Se(2)	–	83.16(8)	–
X(2)-Sn-X(3)	91.05(9)	93.0(1)	94.40(5)
X(2)-Sn-X(4)	–	95.4(1)	–
X(2)-Sn-Se(1)	88.75(8)	91.27(9)	83.38(5)
X(2)-Sn-Se(2)	–	87.40(9)	–
X(3)-Sn-X(4)	102.6(1)	101.7(1)	102.08(7)
X(3)-Sn-Se(1)	163.26(7)	166.60(9)	164.74(5)
X(3)-Sn-Se(2)	94.15(7)	91.41(9)	93.15(4)
X(4)-Sn-Se(1)	–	90.50(9)	–
X(4)-Sn-Se(2)	–	166.37(9)	–
Se(1)-Sn-Se(2)	69.11(5)	76.08(4)	71.60(6)

a. X(4) refers to X(3*), and is related to X(3) by a crystallographic mirror plane.

As was observed in the analogous thioether complexes in chapter 2 there are variations in the Sn-X bond distances. *d*(Sn-X) for halides that are *trans* to another halide atom are consistently longer than those *trans* to an Se donor atom. This is reflected when compared to the Sn-X distances of the monodentate selenoether complexes characterised earlier. In those cases all halide atoms are *trans* to another halide atom and closely match those *trans* to another halide in these chelate systems *e.g.* *trans*-$[SnCl_4(Me_2Se)_2]$ [Figure 3.1, Sn-Cl 2.413(2) and 2.427(2) Å] and *trans*-$[SnBr_4(Me_2Se)_2]$ [Figure 3.2, Sn-Br 2.576(2) and 2.587(2) Å]. Again this presumably reflects the greater *trans* influence of a halide over selenoether.[2] Further evidence for this is seen in the Sn-Se distances when compared between monodentate and bidentate systems. In the bidentate systems the Se donor atoms are *trans* to a halide and are consequently markedly longer than those *trans* to another Se donor atom as observed for the monodentate systems, the influence of the *trans* atoms being less (*cf.* *d*(Sn-Se) *trans* Se, 2.7001(9) and 2.731(2) Å *vs.* *d*(Sn-Se) *trans* X 2.749(1), 2.782(1), 2.787(2) and 2.841(2) Å). Again the distortion of the octahedron has the axial halide atoms

leaning towards the Se_2 donor system resembling the tetrahedral geometry of the starting tin(IV) halide, where the *trans*-$[SnX_4(Me_2Se)_2]$ complexes had featured almost ideal octahedra. However, as was seen in the thioether systems it is the Sn-Se distances and Se-Sn-Se angles that provide the best indicators of the relative stabilities of the complexes.

Figure 3.7. View of the structure of $[SnCl_4(MeSeCH_2SeMe)]$ with numbering scheme adopted. Details as for Fig. 3.6

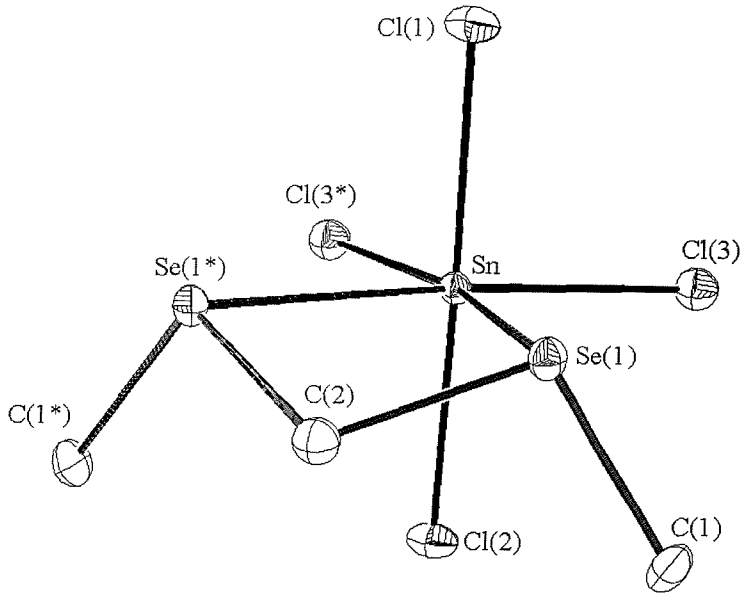

The strain in the four-membered chelate-ring system in $[SnCl_4(MeSeCH_2SeMe)]$ (Figure 3.7) which has not been observed before for an acyclic selenoether ligand, is clear to see when compared to the other chloride characterised, $[SnCl_4\{o\text{-}C_6H_4(SeMe)_2\}]$ (Figure 3.5), which features a five-membered chelate-ring. The *d*(Sn-Se) is markedly longer for the four-membered chelate-ring system (2.782(1) Å) than that seen for the five-membered chelate-ring (2.749(1) Å). The bond angle Se-Sn-Se is also markedly more strained for the four-membered chelate-ring at 69.11(5)° relative to the angle of 76.08(4)° for the five-membered chelate-ring which is still well short of the 90° ideal. It is also worth noting that for the thioether study this unsaturated phenylene system was seen to be more strained than the

Figure 3.8. View of the structure of $[SnCl_4\{MeSe(CH_2)_3SeMe\}]$ with numbering scheme adopted. Ellipsoids are shown at 40 % probability and atoms marked with an asterisk are related by a crystallographic two-fold axis at (-x, ½ -y, z)

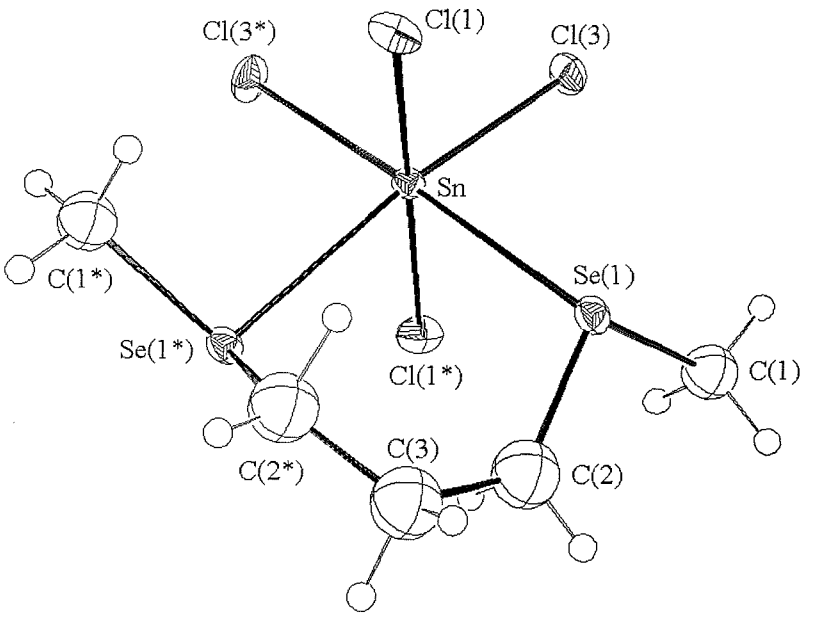

saturated five and six-membered chelate-ring systems. The structures of $[SnCl_4\{MeSe(CH_2)_3SeMe\}]$ (Figure 3.8) and $[SnCl_4\{PhSe(CH_2)_2SePh\}]$ (Figure 3.9) have Se-Sn-Se angles of 85.9° and 86.1°, and while the overall data quality was not good it is probable that these are representative.

Comparing Sn-Se bond distances within the two comparable structures, $[SnCl_4\{o\text{-}C_6H_4(SeMe)_2\}]$ and $[SnBr_4\{o\text{-}C_6H_4(SeMe)_2\}]$, further evidence is found for $SnBr_4$ being a poorer acceptor than $SnCl_4$. The *d*(Sn-Se) for $[SnBr_4\{o\text{-}C_6H_4(SeMe)_2\}]$, 2.841(1) Å, is markedly longer than those seen in either $[SnCl_4\{o\text{-}C_6H_4(SeMe)_2\}]$ or $[SnCl_4(MeSeCH_2SeMe)]$, 2.749(1) and 2.782(1) Å respectively. The Se-Sn-Se bond angle is also considerably more strained (71.60(6)°) than that in the corresponding chloride (76.08(4)°).

Figure 3.9. View of the structure of $[SnCl_4\{PhSe(CH_2)_2SePh\}]$ with numbering scheme adopted. Ellipsoids are shown at 40 % probability

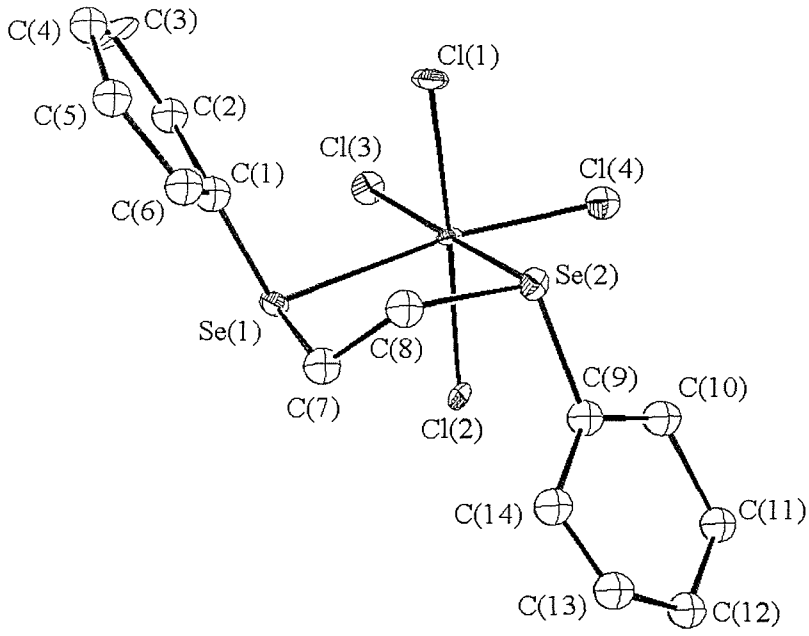

3.2.8. Variable Temperature ^{1}H NMR Studies

As was found for the corresponding thioether complexes, the selenoether complexes prove to be extremely poorly soluble in CD_2Cl_2. A variety of other solvents including thf and acetone were tried and offered better solubility. However, the spectra obtained were significantly different to those observed in CD_2Cl_2, so it seems likely that these harder oxygen donor solvents provide alternative ligands for the tin,[11] so these studies were not pursued.

Table 3.5. Variable temperature ^{1}H NMR spectroscopic data for [SnX_4{diselenoether}] complexes

	^{1}H (δ)[a]		
Complex	300 K	180 K	approximate ratio (*meso*:*dl*)
[$SnCl_4${$MeSe(CH_2)_2SeMe$}]	2.48 (3 H), 3.30 (2 H)	2.40, 2.46, 3.10, 3.40	1:1
[$SnCl_4${$MeSe(CH_2)_3SeMe$}]	2.30 (1 H), 2.46 (3 H), 3.2 (2 H)	2.40, 2.45, 2.51, 3.11, 3.42	1:5
[$SnCl_4${o-$C_6H_4(SeMe)_2$}]	2.83 (3 H), 7.5, 7.65 (2 H)	2.99, 2.79, 7.55	1:3
[$SnCl_4${$PhSe(CH_2)_2SePh$}]	3.39 (2 H), 7.2-7.7 (5 H)	3.5, 3.8, 7.0-7.8	1:1
[$SnCl_4${$PhSe(CH_2)_3SePh$}]	2.10 (1 H), 3.25 (2 H), 7.2-7.7 (5 H)	Ill defined (see text)	
[$SnBr_4${$MeSe(CH_2)_2SeMe$}]	2.25 (3 H), 3.15 (2 H)	2.21, 2.30, 3.10, 3.30	2:1
[$SnBr_4${$MeSe(CH_2)_3SeMe$}]	2.41 (1 H + 3 H), 3.1 (2 H)	2.38, 2.44, 3.05, 3.25	1:5
[$SnBr_4${o-$C_6H_4(SeMe)_2$}]	2.45 (3 H), 7.25, 7.38 (2 H)	2.76 [2.55 (sh)], 7.47	

a. In CD_2Cl_2 solution

As for a thioether, the presence of two lone pairs of electrons on the selenium donor atoms in these selenoethers results in the occurrence of diastereoisomers (*dl* and *meso* configurations). At 300 K the exchange and inversion processes are too fast on an NMR timescale to distinguish between them. If the temperature is reduced however, the exchange mechanisms and then the inversion processes are slowed sufficiently that the resultant isomers, that appeared equivalent, become resolvable. Variable temperature ^{1}H NMR spectroscopic data are presented in Table 3.5.

The ^{1}H NMR spectrum of [$SnCl_4$($MeSeCH_2SeMe$)] shows no splitting at any temperature studied (173 - 300 K). The four-membered chelate-ring that is seen to be highly strained in the X-ray diffraction analysis, is still undergoing rapid ring opening and ligand exchange in solution, even at 173 K. At 300 K the ^{1}H NMR spectrum of [$SnCl_4${$MeSe(CH_2)_2SeMe$}] exhibits two resonances for δ(Me) and δ(CH_2). On reducing the temperature to *ca.* 250 K the resonances are seen to split as the ligand exchange and inversion processes are slowed to show the AB –CH_2 coupling of the two separate diastereoisomers. At 180 K the peaks are clearly resolved for the *dl* and *meso* isomers. However, they are not clear enough to distinguish the $^3J(^{117/119}Sn - ^1H)$ coupling that was seen for the thioether systems. For [$SnCl_4${$MeSe(CH_2)_3SeMe$}] three resonances are observed at 300 K for the three different proton environments. These resonances do not split until *ca.* 220 K where the dynamic processes in solution are slowed sufficiently, and $^3J(^{117/119}Sn - ^1H)$ coupling is again unobserved even at 180 K. For the phenyl substituted system, [$SnCl_4${$PhSe(CH_2)_2SePh$}], no splitting is seen in the proton NMR spectra until 180 K, where splitting becomes obvious in the δ(CH_2) resonance, while for the trimethylene backboned species [$SnCl_4${$PhSe(CH_2)_3SePh$}] the resonances remain broad even at the lowest temperature studied (173 K). [$SnCl_4${o-$C_6H_4(SeMe)_2$}] was found to be more soluble in CD_2Cl_2, so the resulting spectra were clearer. The δ(Me) resonance observed for this species splits at *ca.* 230 K and at 175 K $^3J(^{117/119}Sn - ^1H)$ coupling of *ca.* 40 Hz can be distinguished.

In general, the behaviour seen in the bromide systems mirrors that of the chloride, but with the onset of pyramidal inversion and ligand exchange beginning at lower temperatures such that no splitting can be seen for the phenyl substituted adducts even at 173 K and for [$SnBr_4${o-$C_6H_4(SeMe)_2$}] the splitting is only present as a weak shoulder that is not fully resolved.

A number of trends become apparent from these results. The fact that no splitting can be distinguished for [$SnCl_4$($MeSeCH_2SeMe$)] shows the extreme

lability of this ligand, and is consistent with the highly strained nature of the four-membered chelate-ring that was observed in the X-ray crystallography. The observation that the bromide systems undergo exchange mechanisms at lower temperatures is consistent with the observation that has already been made for the monodentate systems, and the $[SnX_4\{o\text{-}C_6H_4(SeMe)_2\}]$ (where X = Cl or Br) systems from the X-ray crystallographic study, that $SnBr_4$ is a poorer acceptor than $SnCl_4$. This is also consistent with the overall trends found for the thioether systems in chapter 2.

3.2.9. Variable Temperature ^{119}Sn-{^{1}H} NMR Spectroscopy

The $^{119}Sn\{^1H\}$ NMR spectra (134.2 MHz, CD_2Cl_2) were recorded over a range of temperatures (300 - 180 K) in order to observe the effects of ligand exchange by dissociation and selenium inversion. Resonances for the various tin(IV) species were observed in characteristic regions. Tin(IV) chloride complexes were observed over the range δ -600 to δ -700 ppm which is consistent with the range observed for the *cis* and *trans* isomers of $[SnCl_4(Me_2Se)_2]$ (δ –691 and –695 ppm) discussed earlier and the chemical shift is approximately 110 – 150 ppm to lower frequency to those observed for the thioether systems (δ –500 to δ –600 ppm). The complexes of tin(IV) bromide were characteristically observed over the range δ –1200 to δ -1350 ppm, consistent with the shift of $[SnBr_4(Me_2Se)_2]$ (δ –1296 and –1319 ppm) and again shifted by approximately 100 ppm to lower frequency than the thioether analogues. $^{119}Sn\text{-}\{^1H\}$ NMR spectroscopic data at 180 K for these $[SnX_4\{diselenoether\}]$ complexes are presented in Table 3.6.

These complexes again proved extremely poorly soluble in chlorocarbon solvents. This resulted in spectra with relatively poor signal-to-noise ratios even after long accumulations, and prevented identification of satellites from $^1J(^{119}Sn - ^{77}Se)$ coupling. Coordinating solvents were again avoided to prevent risk of displacing the selenoether

As for the thioether analogue, the exception to this insolubility was the $MeSeCH_2SeMe$ complex of $SnCl_4$. The extremely strained nature of the four-membered chelate-ring, characterised by X-ray crystallography, leads to this complex being very labile in solution. The result is that no resonance is observed over the entire temperature range, supporting the observation that the selenoether ligands are poorer donors than the thioether analogues.

None of the other $SnCl_4$ complexes exhibit a resonance at 300 K, most likely due to reversible ring opening occurring rapidly in solution. In all cases resolved resonances are not seen in the ^{119}Sn-{^1H} spectra until very low temperatures (< 200 K) are reached. The *dl* and *meso* isomers can be resolved for the $SnCl_4$ species [$SnCl_4${$MeSe(CH_2)_nSeMe$}] (where n = 2 or 3) and at 180 K the resonance for [$SnCl_4${o-$C_6H_4(SeMe)_2$}] is evident in the appearance of splitting, with a resonance at δ –632 ppm with a second resonance becoming discernible at δ –635 ppm. Consistent with the observed trend that phenyl substituted ligands are poorer donors, no splitting was seen in the resonances of the [$SnCl_4${$PhSe(CH_2)_nSePh$}] species even at 173 K.

Table 3.6. ^{119}Sn-{^1H} and ^{77}Se-{^1H} NMR spectroscopic data at 180 K for [SnX_4{diselenoether}] complexes.[a]

Compound	^{119}Sn-{^1H} (δ)[b]	^{77}Se-{^1H} (δ)[c]
[$SnCl_4(MeSeCH_2SeMe)$]	n.o.[d]	n.o.
[$SnCl_4${$MeSe(CH_2)_2SeMe$}]	-680, -682	482, 487 (1:1)
[$SnCl_4${$MeSe(CH_2)_3SeMe$}]	-685, -686.5	231, 232 (5:1)
[$SnCl_4${o-$C_6H_4(SeMe)_2$}]	-632, -635	323, 338 (1:5)
[$SnCl_4${$PhSe(CH_2)_2SePh$}]	n.o.	436
[$SnBr_4${$MeSe(CH_2)_2SeMe$}]	-1238, -1288	493, 496 (2:1)
[$SnBr_4${$MeSe(CH_2)_3SeMe$}]	-1305, -1308	261, 263 (1:2)
[$SnBr_4${o-$C_6H_4(SeMe)_2$}]	-1258 (br)	355

Free selenoether: δ(^{77}Se) $MeSe(CH_2)_2SeMe$, 121; $MeSe(CH_2)_3SeMe$, 74; $PhSe(CH_2)_2SePh$, 340; o-$C_6H_4(SeMe)_2$, 202.[14]

a. In anhydrous CH_2Cl_2-CD_2Cl_2 solution containing [$Cr(acac)_3$].
b. Relative to neat external $SnMe_4$.
c. Relative to neat external Me_2Se, approximate *dl*:*meso* ratios in parentheses.
d. n.o. = not observed

The ^{119}Sn-{^{1}H} NMR spectra of the complexes of $SnBr_4$ exhibit largely similar behaviour to the $SnCl_4$ systems. Once again exchange mechanisms begin at lower temperatures for these systems meaning splitting is now not seen for the phenylene example, [$SnBr_4${o-$C_6H_4(SeMe)_2$}]. Even at 173 K the resonance for this system is still extremely broad. For [$SnBr_4${$PhSe(CH_2)_2SePh$}] a resonance is observed at 180 K but it is not possible to resolve splitting for the two diastereoisomers. While a visible colour change in solution may indicate adduct formation, no solid was isolated from the attempted synthesis of [$SnBr_4${$PhSe(CH_2)_3SePh$}], and no resonances were observed in the *in situ* ^{119}Sn-{^{1}H} NMR spectra over the entire temperature range studied, again consistent with phenyl substituted ligands being poorer donors.

The synthesis of [SnI_4{$MeSe(CH_2)_2SeMe$}] was also attempted. Despite a vivid colour change from orange to red when the ligand was added to the solution of SnI_4 in CH_2Cl_2 no solid was isolated. *In situ* ^{119}Sn-{^{1}H} NMR spectra over the temperature range 180 – 300 K exhibited no resonance indicative of adduct formation, presumably as exchange mechanisms at this temperature are too rapid on an NMR timescale. The analogous thioether complex was only observed at 180 K, so this again supports the observed trend that these selenoethers are poorer ligands than their corresponding thioether analogues.

3.2.10. Variable Temperature ^{77}Se-{^{1}H} NMR Spectroscopy

The ^{77}Se-{^{1}H} NMR spectra of the complexes formed were studied over the temperature range 173 – 300 K. As in the ^{119}Sn-{^{1}H} NMR spectroscopy the aim is to slow ligand exchange and pyramidal inversion sufficiently to observe separate resonances for the *dl* and *meso* diastereoisomers. ^{77}Se-{^{1}H} NMR spectroscopic data at 180 K for these [SnX_4{diselenoether}] complexes are presented in Table 3.6.

For the complex [$SnCl_4(MeSeCH_2SeMe)$] no resonance was observed in the ^{77}Se-{^{1}H} NMR spectra over the entire temperature range. This result is consistent with this ligand being highly labile and has already been seen to form a highly strained four-membered chelate-ring from the X-ray crystallographic study. At 300 K a single resonance at δ 486 ppm is observed in the spectrum of [$SnCl_4${$MeSe(CH_2)_2SeMe$}], which splits below *ca.* 200 K giving peaks at δ 482 and 487 ppm assigned to the two diastereoisomers. Nothing is observed at 300 K for [$SnCl_4${$MeSe(CH_2)_3SeMe$}], a resonance only becoming obvious at *ca.* 255 K, and it is not until *ca.* 180 K that the resonance is seen to split as exchange and inversion is reduced sufficiently and the

diastereoisomers are observed. Neither of the phenyl substituted systems $[SnCl_4\{PhSe(CH_2)_nSePh\}]$ (n = 2 or 3) exhibit splitting even at 173 K. For $[SnCl_4\{PhSe(CH_2)_2SePh\}]$ a single resonance is observed at δ 436 ppm, while no resonance for $[SnCl_4\{PhSe(CH_2)_3SePh\}]$ is observed at any temperature, supporting the assignment of these phenyl substituted ligands as poorer than the methyl substituted equivalents, and also with the five-membered chelate-ring being preferred over the six-membered chelate-ring. The $^{77}Se-\{^1H\}$ NMR spectrum of $[SnCl_4\{o\text{-}C_6H_4(SeMe)_2\}]$ was run in the presence of excess ligand. At 180 K three resonances are observed at δ 323, 338 and 193 ppm consistent with the two diastereoisomers and free ligand. Raising the temperature to *ca.* 220 K the signals were clearly broadening, and by 235 K had disappeared showing fast ligand exchange at this temperature.

The bromide systems again display the onset of exchange and inversion at lower temperatures. For the methyl substituted system, $[SnBr_4\{MeSe(CH_2)_2SeMe\}]$, a resonance is not observed until *ca.* 225 K at δ 496 ppm, with splitting not observed until below *ca.* 200 K. For $[SnBr_4\{MeSe(CH_2)_3SeMe\}]$ the recorded temperatures are lower still, a resonance at δ 261 ppm only apparent at *ca.* 200 K and splitting not until 180 K. Even at 180 K the $^{77}Se-\{^1H\}$ NMR spectrum of $[SnBr_4\{o\text{-}C_6H_4(SeMe)_2\}]$ displays a single resonance at δ 355 ppm with no evidence for splitting. No solid was isolated from the attempted synthesis of $[SnBr_4\{PhSe(CH_2)_2SePh\}]$ but a resonance was observed at δ 440 ppm indicative of adduct formation at lowest temperatures. Exchange was still too rapid to allow a resonance to be observed for $[SnBr_4\{PhSe(CH_2)_3SePh\}]$ at any temperature.

As for the $^{119}Sn-\{^1H\}$ NMR spectrum, no evidence of adduct formation was seen at any temperature in a solution containing SnI_4 and $MeSe(CH_2)_2SeMe$.

One trend arising from the $^{77}Se-\{^1H\}$ NMR data is the large changes in co-ordination shift with chelate-ring size. These large changes have previously been studied for transition metal complexes of selenoethers[12] and since data has been obtained on monodentate systems as well as bidentate systems incorporating chelate-rings of varying sizes, it is possible to identify similar trends here. Following the approach first employed by Garrou[13] for diphosphine complexes, the coordination shift Δ for each of the complexes is calculated as $\Delta = \delta_{complex} - \delta_{ligand}$. The chelate-ring-parameter ΔR is then defined as Δ(chelate complex) – Δ(equivalent monodentate complex). For the purposes of this study the species *cis*-$[SnX_4(Me_2Se)_2]$ are considered

to be the "equivalent monodentate complex" for the complexes $[SnX_4\{MeSe(CH_2)_nSeMe\}]$ (n = 2 or 3).

Free $MeSe(CH_2)_2SeMe$ has δ 121 ppm,[14] leading to co-ordination shifts (Δ) of 365 for the $SnCl_4$ complex and 374 for the corresponding bromide complex. From these the values of ΔR for these five-membered chelate-ring systems are 161 and 155 for the chloride and bromide complexes respectively. When applied to the six-membered chelate-ring system $[SnX_4\{MeSe(CH_2)_3SeMe\}]$, free ligand has δ 74 ppm, leading to Δ 158 and Δ 188 for the chloride and bromide complexes and chelate-ring-parameters of ΔR –46 and ΔR –31 respectively. These negative shifts for six-membered chelate-rings and positive shifts for the corresponding five-membered chelate-rings provide clear evidence for the presence of a chelate-ring-parameter effect in the selenium chemical shift values. This is the first time this has been established in complexes of a main-group metal, though the trends are similar to those observed in d-block metal complexes.[12] The origins of the chelate-ring effect is unclear even in the much studied diphosphine systems,[15] but the observation of such an effect in the tin complexes here, where the metal is behaving as a simple σ acceptor, supports the suggestion that it involves the strain in different ring sizes.[14] The degree of straining in these systems relative to the octahedral ideal has been seen in the X-ray crystallography discussed earlier and, by analogy, in the diffraction studies on thioethers in chapter 2.

Since the complexes of PhMeSe, which would be considered the "equivalent monodentate complex" for the complexes of $PhSe(CH_2)_2SePh$ and $\underline{o}\text{-}C_6H_4(SeMe)_2$, were not studied similar, calculations of ΔR cannot be carried out for these bidentate compounds. However, for $[SnX_4\{\underline{o}\text{-}C_6H_4(SeMe)_2\}]$ the substantial high frequency co-ordination shifts in themselves strongly suggest that the chelate structures identified by X-ray crystallography are also retained in solution.

3.3. Conclusions

The products $[SnX_4(R_2Se)_2]$ (where X = Cl or Br; R = Me or Ph) arising from the reactions of SnX_4 with monodentate selenoethers and those with bidentate selenoethers, $[SnX_4\{MeSe(CH_2)_nSeMe\}]$ (where n = 1, 2 or 3), $[SnX_4\{PhSe(CH_2)_nSePh\}]$ (where n = 2 or 3) and $[SnX_4\{o\text{-}C_6H_4(SeMe)_2\}]$ have been prepared in high yield, including a highly strained four-membered chelate-ring species involving the $MeSeCH_2SeMe$ ligand. A detailed examination of the variable temperature ^1H, $^{119}Sn\text{-}\{^1H\}$ and $^{77}Se\text{-}\{^1H\}$ NMR spectroscopy over the temperature range 300 – 180 K has been presented. As with the thioether systems of chapter 2, particular emphasis for the bidentate systems has been on the study of the dynamic processes occurring in solution. The variable temperature NMR studies again identified the onset of pyramidal inversion and ligand dissociation in a number of the complexes, both beginning at similar temperatures preventing quantitative analysis. It was possible to distinguish the *dl* and *meso* isomers within the NMR spectra at low temperature (180 K) for a large number of the systems and the onset of these observations allowed a number of qualitative trends to be identified. The trends observed were consistent with those of the thioether analogues in chapter 2, examples involving phenyl substituents are typically less stable than those with methyl substituents, that the stability of the complexes formed decreases with the SnX_4 acceptor: X = Cl > Br >> I. The results again confirmed that five-membered chelate-ring systems are more stable than six-membered chelate-rings with the highly strained four-membered chelate-ring least favoured. Single crystal X-ray diffraction studies again proved highly complementary to the solution studies and providing further support for the trends seen.

3.4. Experimental

The tin(IV) chloride, bromide and iodide were purchased from *Aldrich Chemicals*. The ligands Me_2Se, Ph_2Se, $MeSe(CH_2)_nSeMe$ (where n = 1, 2 or 3), $PhSe(CH_2)_nSePh$ (where n = 2 or 3) and o-$C_6H_4(SeMe)_2$ were prepared by following literature methods.[14,16] Tin(IV) fluoride was prepared by Dr. Andrew Hector by reaction of tin powder with fluorine at 300 °C/ 3 atm. in a Monel autoclave.

Tin(IV) halides are moisture sensitive, therefore all of the reactions were carried out under an atmosphere of dry nitrogen, using standard Schlenk, vacuum-line and dry box techniques.

Single Crystal X-ray Diffraction

Single crystals of $[SnCl_4(Me_2Se)_2]$, $[SnBr_4(Me_2Se)_2]$, $[SnCl_4\{o\text{-}C_6H_4(SeMe)_2\}]$, $[SnBr_4\{o\text{-}C_6H_4(SeMe)_2\}]$ were obtained from a solution of the appropriate complex in $CHCl_3$. The compounds were extremely sensitive to hydrolysis on exposure to moist air. Therefore, in each case the selected crystal was coated in mineral oil, mounted on a glass fibre using silicone grease as adhesive, and immediately placed in a stream of cold nitrogen gas and cooled to 150 K. Data collection used a Rigaku AFC7S four-circle diffractometer equipped with an Oxford Cryostreams low temperature attachment operating at 150 K, using graphite-monochromated Mo-K_α X-radiation ($\sim$ = 0.71073 Å), T = 150 K, ω-2θ scans. The intensities of three standard reflections were monitored every 150 reflections. No significant crystal decay or movement was observed. As there were no identifiable faces the raw data were corrected for absorption using psi-scans. The weighting scheme $w^{-1} = \sigma^2$ (F) gave satisfactory agreement analyses in each case.

All four structures were solved by direct methods,[17] and then developed by iterative cycles of full-matrix least-squares refinement (based on *F*) and difference Fourier syntheses which located all non-H atoms in the asymmetric unit.[18] For $[SnBr_4(Me_2Se)_2]$ and $[SnBr_4\{o\text{-}C_6H_4(SeMe)_2\}]$ an empirical absorption correction using DIFABS[19] was applied to the raw data at isotropic convergence. All non-H atoms in the structures were refined anisotropically (with the exception of $[SnBr_4\{o\text{-}C_6H_4(SeMe)_2\}]$ for which the C atoms were refined isotropically), and H atoms were placed in fixed, calculated positions with *d*(C-H) = 0.96 Å.

Data collection was also undertaken on poorly diffracting crystals of $[SnCl_4\{MeSe(CH_2)_3SeMe\}]$ and $[SnCl_4\{PhSe(CH_2)_2SePh\}]$ both obtained by the same method as the other complexes using solutions of the appropriate complex in $CHCl_3$. The overall data quality was poor and the residuals rather high, preventing satisfactory refinement, but the analysis was sufficient to confirm unambiguously that the compounds do contain a chelating ligand in the *dl* arrangement for both complexes.

Crystallographic data for these structures are presented in Table 3.7.

Table 3.7. Crystallographic data

Compound	*trans*-[$SnCl_4(Me_2Se)_2$]	*trans*-[$SnBr_4(Me_2Se)_2$]	[$SnCl_4${o-$C_6H_4(SeMe)_2$}]	[$SnBr_4${o-$C_6H_4(SeMe)_2$}]	[$SnCl_4${$MeSe(CH_2)_3SeMe$}]	[$SnCl_4${$PhSe(CH_2)_2SePh$}]
Formula	$C_4H_{12}Cl_4Se_2Sn$	$C_4H_{12}Br_4Se_2Sn$	$C_8H_{10}Cl_4Se_2Sn$	$C_8H_{10}Br_4Se_2Sn$	$C_5H_{12}Cl_4Se_2Sn$	$C_{14}H_{14}Cl_4Se_2Sn$
Formula Weight	478.56	656.36	524.59	702.39	490.57	600.69
Colour, morphology	Colourless, block	Yellow, rhomboid	Colourless, block	Yellow, block	Colourless, prism	Colourless, plate
Crystal dimensions/mm	0.25 x 0.10 x 0.10	0.45 x 0.40 x 0.20	0.30 x 0.15 x 0.12	0.30 x 0.20 x 0.20	0.25 x 0.24 x 0.15	0.30 x 0.15 x 0.07
Crystal System	Monoclinic	Monoclinic	Triclinic	Monoclinic	Tetragonal	Monoclinic
Space Group	$P2_1/n$	$P2_1/n$	P-1	$P2_1/m$	$I4_1/a$	$P2_1/a$
a/Å	6.539(2)	6.768(3)	8.419(2)	6.826(3)	10.062(6)	13.330(4)
b/Å	12.610(3)	13.000(3)	11.323(3)	11.324(2)	10.062	7.006(3)
c/Å	8.111(2)	8.373(3)	8.251(1)	9.936(2)	25.702(10)	20.28(3)
α/°			90.32(2)			
β/°	107.67(2)	108.47(3)	98.17(2)	100.67(2)		91.75(4)
γ/°			109.68(2)			
U/Å^3	637.2(2)	698.7(4)	731.8(3)	754.7(3)	2602(3)	1892(1)
Z	2	2	2	2	8	4
Scan Type	ω-2θ	ω-2θ	ω-2θ	ω-2θ	ω-2θ	ω-2θ
F(000)	444	588	488	632	1824	1136
D_c/g cm^{-3}	2.494	3.119	2.380	3.119	2.504	2.11
μ(Mo-Ka)/cm^{-1}	85.04	184.63	73.85	184.63	83.32	57.51
Transmission factors (max. and min.)	1.000, 0.694	1.000, 0.645	1.000, 0.717	1.000, 0.645	1.000, 0.662	1.000, 0.53
No. of Unique obs. reflections	1189	1289	2563	1402	1187	3637
R_{int} (based on F^2)	0.031	0.132	0.028	0.043	0.083	0.124
Unique obs. reflections with [$I_o > 2.0\ \sigma(I_o)$]	925	1039	1763	1143	841	1752
No. of parameters	52	52	136	50	43	190
Goodness of fit	2.29	4.35	1.97	3.49	6.83	4.06
$R(F_o)$	0.036	0.050	0.045	0.049	0.108	0.110
$R_w(F_o)$	0.043	0.057	0.052	0.062	0.156	0.151
Max. residual peak/eÅ^{-3}	1.19	1.66	1.33	2.49	3.41	3.29
Max. residual trough/eÅ^{-3}	-1.66	-2.15	-2.10	-2.91	-2.68	-2.58

$$R = \Sigma\ (|F_{obs}|_i - |F_{calc}|_i)/\Sigma\ |F_{obs}|_i$$

$$R_w = \sqrt{[\Sigma\ w_i(|F_{obs}|_i - |F_{calc}|_i)^2\ /\Sigma\ w_i|F_{obs}|_i^2]}$$

$$GOF = [\Sigma\ (|F_{obs}|_i - |F_{calc}|_i)/\sigma_i]/(n - m) \approx 1$$

Complex Synthesis

$[SnCl_4(Me_2Se)_2]$

Tin(IV) chloride (0.26 g, 1 mmol) was added to a solution of Me_2Se (0.22 g, 2 mmol) in chloroform (10 cm^3). The complex formed immediately as a white precipitate which was filtered off and dried *in vacuo.* The product was stored in a nitrogen dry-box. Yield 0.44 g, 92 %. Found: C, 9.75; H 2.7. Calculated for $C_4H_{12}Cl_4Se_2Sn$: C, 10.05; H, 2.5 %. IR spectrum (nujol mull) ν/cm^{-1} (Sn-Cl) 312.

$[SnBr_4(Me_2Se)_2]$

A saturated solution of tin(IV) bromide (0.44 g, 1 mmol) in chloroform (5 cm^3) was added dropwise to a solution of Me_2Se (0.22 g, 2 mmol) in chloroform (5 cm^3). On reducing the volume *in vacuo* the complex slowly formed as yellow crystals that were filtered off and dried *in vacuo.* Yield 0.54 g, 82 %. Found: C, 7.4; H, 1.9. Calculated for $C_4H_{12}Br_4Se_2Sn$: C, 7.3; H, 1.85 %. IR spectrum (nujol mull) ν/cm^{-1} (Sn-Br) 220.

$[SnCl_4\{MeSeCH_2SeMe\}]$

Tin(IV) chloride (0.52 g, 2 mmol) was added to a solution of $MeSeCH_2SeMe$ (0.40 g, 2 mmol) in anhydrous CH_2Cl_2 (10 cm^3). Stirring at room temperature followed by concentration of the solution *in vacuo*, afforded a yellow precipitate which was collected by filtration and dried *in vacuo.* Yield 0.5 g, 54 %. Found: C, 7.9; H, 2.0. Calculated for $C_3H_8Cl_4Se_2Sn$: C, 7.8; H, 1.7 %. IR spectrum (nujol mull) ν/cm^{-1} (Sn-Cl) 326(br).

$[SnCl_4\{MeSe(CH_2)_2SeMe\}]$

Tin(IV) chloride (0.26 g, 1 mmol) was added to a solution of $MeSe(CH_2)_2SeMe$ (0.22 g, 1 mmol) in chloroform (10 cm^3). The complex formed as a white powder which was filtered off and dried *in vacuo.* Yield 0.45 g, 72 %. Found: C, 10.3; H, 2.5. Calculated for $C_4H_{10}Cl_4Se_2Sn$: C, 10.1; H, 2.1 %. IR spectrum (nujol mull) ν/cm^{-1} (Sn-Cl) 339, 331, 320 and 312.

[$SnCl_4${$MeSe(CH_2)_3SeMe$}]

Addition of $SnCl_4$ (0.26 g, 1 mmol) to a solution of $MeSe(CH_2)_3SeMe$ (0.23 g, 1 mmol) formed a white precipitate immediately. This was filtered off and dried *in vacuo*. Yield 0.72 g, 93 %. Found: C, 12.5; H, 2.6. Calculated for $C_5H_{12}Cl_4Se_2Sn$: C, 12.25; H, 2.45 %. IR spectrum (nujol mull) ν/cm^{-1} (Sn-Cl) 336, 331, 325 and 313.

[$SnCl_4${$PhSe(CH_2)_2SePh$}]

Addition of $SnCl_4$ (0.26 g, 1 mmol) to a solution of $PhSe(CH_2)_2SePh$ (0.34 g, 1 mmol) formed a yellow crystalline product immediately. This was filtered off and dried *in vacuo*. Yield 0.59 g, 81 %. Found: C, 27.2; H, 2.5. Calculated for $C_{14}H_{14}Cl_4Se_2Sn$: C, 28.0; H, 2.35 %. IR spectrum (nujol mull) ν/cm^{-1} (Sn-Cl) 330, 324, 319 and 313.

[$SnCl_4${$PhSe(CH_2)_3SePh$}]

Addition of $SnCl_4$ (0.26 g, 1 mmol) to a solution of $PhSe(CH_2)_3SePh$ (0.35 g, 1 mmol) formed an orange crystalline product immediately. This was filtered off and dried *in vacuo*. Yield 0.53 g, 86 %. Found: C, 29.5; H, 2.7. Calculated for $C_{15}H_{16}Cl_4Se_2Sn$: C, 29.8; H, 2.65 %. IR spectrum (nujol mull) ν/cm^{-1} (Sn-Cl) 330, 324, 315 and 304.

[$SnCl_4${o-$C_6H_4(SeMe)_2$}

Addition of $SnCl_4$ (0.26 g, 1 mmol) to a solution of o-$C_6H_4(SeMe)_2$ (0.26 g, 1 mmol) formed a white crystalline product immediately. This was filtered off and dried *in vacuo*. Yield 0.49 g, 94 %. Found: C, 18.35; H, 2.0. Calculated for $C_8H_{10}Cl_4Se_2Sn$: C, 18.3; H, 1.9 %. IR spectrum (nujol mull) ν/cm^{-1} (Sn-Cl) 338, 328, 323 and 317.

[$SnBr_4${$MeSe(CH_2)_2SeMe$}]

A saturated solution of tin(IV) bromide (0.44 g, 1mmol) in chloroform (5 cm^3) was added dropwise to a solution of $MeSe(CH_2)_2SeMe$ (0.22 g, 1 mmol) in chloroform (5 cm^3). A pale yellow precipitate formed immediately which was filtered off and dried *in vacuo*. Yield 0.50 g, 69 %. Found: C, 7.5; H, 1.8. Calculated for $C_4H_{10}Br_4Se_2Sn$: C, 7.35; H, 1.55 %. IR spectrum (nujol mull) ν/cm^{-1} (Sn-Br) 220, 218, 216 and 214.

[$SnBr_4${$MeSe(CH_2)_3SeMe$}]

Addition of $SnBr_4$ (0.44 g, 1 mmol) to a solution of $MeSe(CH_2)_3SeMe$ (0.23 g, 1 mmol) formed a yellow precipitate immediately. This was filtered off and dried *in vacuo*. Yield 0.48 g, 81 %. Found: C, 9.3; H, 1.9. Calculated for $C_5H_{12}Br_4Se_2Sn$: C, 9.0; H, 1.8 %. IR spectrum (nujol mull) ν/cm^{-1} (Sn-Br) 219, 214, 206 and 201.

[$SnBr_4${o-$C_6H_4(SeMe)_2$}]

Addition of $SnBr_4$ (0.44 g, 1 mmol) to a solution of o-$C_6H_4(SeMe)_2$ (0.26 g, 1 mmol) formed an orange crystalline product slowly from solution. This was filtered off and dried *in vacuo*. Yield 0.67 g, 86 %. Found: C, 13.9; H, 1.7. Calculated for $C_8H_{10}Br_4Se_2Sn$: C, 13.65; H, 1.4 %. IR spectrum (nujol mull) ν/cm^{-1} (Sn-Br) 230, 228, 224 and 222.

References

[1] S. J. Ruzicka and A. E. Merbach, *Inorg. Chim. Acta.*, 1976, **20**, 221; 1977, **22**, 191.

[2] S. J. Ruzicka, C. M. P. Favez and A. E. Merbach, *Inorg. Chim. Acta.*, 1977, **23**, 239

[3] E. W. Abel, S. K. Bhargava, K. G. Orrell and V. Sik, *Inorg. Chim. Acta*, 1981, **49**, 25.

[4] T. Tanaka, *Inorg. Chem.*, 1967, **1**, 217.

[5] N. Bricklebank, S. M. Godfrey, C. A. McAuliffe and R. G. Pritchard, *J. Chem. Soc., Chem. Commun.*, 1994, 695.

[6] G.R. Willey, A. Jarvis, J. Palin and W. Errington, *J. Chem. Soc., Dalton Trans.*, 1994, 255.

[7] M. M. Olmstead, K. A. Williams and W.K. Musker, *J. Am. Chem. Soc.*, 1982, **104**, 5567.

[8] S.J. Blunden, D. Searle and P.J. Smith, *Inorg. Chim. Acta*, 1985, **98**, 185.

[9] C. T. G. Knight and A. E. Merbach, *Inorg. Chem.*, 1985, **24**, 576.

[10] S. E. Dann, A. R. J. Genge, W. Levason and G. Reid, *J. Chem. Soc., Dalton Trans.*, 1997, 2207.

[11] S.J. Blunden, D. Searle and P.J. Smith, *Inorg. Chim. Acta*, 1985, **98**, 185.

[12] E. G. Hope and W. Levason, *Coord. Chem. Rev.*, 1993, **122**, 109.

[13] P.E. Garrou, *Chem. Rev.*, 1981, **81**, 229.

[14] D. J. Gulliver, E. G. Hope, W. Levason, S. G. Murray, D. M. Potter and G. L. Marshall, *J. Chem. Soc., Perkin Trans. 2*, 1984, 429.

[15] J. G. Verkade and L. D. Quin (Editors), *Phosphorus-31 NMR Spectroscopy in Stereochemical Analysis,* VCH, Deerfield Beach, FL, 1987.

[16] E. G. Hope, T. Kemmitt and W. Levason, *J. Chem. Soc., Perkin Trans. 2*, 1987, 487.

[17] SHELXS-86, program for crystal structure solution, G. M. Sheldrick, *Acta Crystallogr., Sect. A*, 1990, **46**, 467.

[18] TEXSAN, Crystal Structure Analysis Package, Molecular Structure Corporation, Houston, TX, 1992.

[19] N. Walker and D. Stuart, *Acta Crystallogr., Sect A.*, 1983, **39**, 158.

Chapter 4

Group 14 Halide Complexes With Mono- and Bidentate Telluroethers

4.1. Introduction

In chapters 2 and 3 the group 14 halide complexes of thioethers and selenoethers were characterised and trends identified. No tin telluroethers appear in the literature, although RTe-Sn bonds are established.[1]

The following work provides a detailed investigation into the behaviour of the tin(IV) halides (Cl, Br or I) with the monodentate ligand Me_2Te, and bidentate ligands of the type $RTe(CH_2)_3TeR$ (where R = Me or Ph) and o-$C_6H_4(TeMe)_2$. The effects of changing halide and ligand interdonor linkage and substituents are studied. Variable temperature ^{1}H, ^{119}Sn and ^{125}Te NMR spectra have been recorded in attempts to investigate the pyramidal inversion and ligand exchange processes in these systems. IR spectroscopy and single crystal X-ray diffraction have been used to study the behaviour of these complexes in the solid state. Overall trends observed for these tin(IV) halide complexes of group 16 ligands will be discussed here.

4.2. Results & Discussion

4.2.1. Synthesis and Properties of Monodentate Telluroether Complexes

The complexes $[SnCl_4(Me_2Te)_2]$ and $[SnBr_4(Me_2Te)_2]$ have been prepared by reaction of the appropriate SnX_4 with two molar equivalents of Me_2Te in thoroughly degassed, anhydrous CH_2Cl_2. The solids formed are hydrolysed easily, even the briefest exposure to the laboratory atmosphere causing them to turn orange-red with liberation of Me_2Te, and then cream with oxidation of the ligand. All complexes were therefore stored and handled in a dinitrogen filled dry-box. Even here the compounds decompose to give dark brown solids. The far-IR spectrum of the chloride complex shows one broad peak at 312 cm^{-1} for ν(SnCl) probably corresponding to the *trans* isomer (D_{4h}) being the principal isomer present in the solid state (compare *trans*-$[SnCl_4(Me_2Se)_2]$ 312 cm^{-1} in chapter 3). The same observation is made for the bromide species with a broad band observed at 220 cm^{-1} (compare *trans*-$[SnBr_4(Me_2Se)_2]$ 220 cm^{-1}, chapter 3). Satisfactory elemental analyses were obtained for both species.

Reaction of SnI_4 with Me_2Te in CH_2Cl_2 solution was also tried and produced a brown precipitate immediately. The product was tentatively assigned as the adduct, $[SnI_4(Me_2Te)_2]$, but while it was isolable due to its low solubility in CH_2Cl_2, the complex proved extremely susceptible to hydrolysis decomposing immediately in the laboratory atmosphere, and overnight in the dinitrogen filled dry-box. *In situ* NMR experiments displayed no peaks other than those corresponding to hydrolysed product, presumably due to trace amounts of water in the solvents.

4.2.2. Variable Temperature ^1H NMR Spectroscopy

^1H NMR spectroscopic data are presented in Table 4.1. The ^1H NMR spectrum of a solution of $[SnCl_4(Me_2Te)_2]$ in CD_2Cl_2 at 300 K (Figure 4.1a) consists of a single resonance at δ 3.0 ppm. This is little changed on cooling the solution to 200 K, but on further cooling the resonance broadens, and at 180 K it is seen to split into two distinct resonances at δ 3.04 and 3.06 ppm (Figure 4.1b). Even at the lowest attainable temperature obtainable in this solvent (*ca.* 175 K) no $^{117/119}Sn$ satellites are observed. These satellites were observed at 180 K for the analogous selenoether system allowing them to be assigned as the two possible geometric isomers. However, the two species

here have relative intensity 1:2, and are tentatively assigned as the *cis* and *trans* isomers for this $SnCl_4L_2$ system (δ for free Me_2Te is 1.90 ppm).

For a solution of $[SnCl_4(Me_2Te)_2]$ with excess Me_2Te only one single resonance is observed over the entire temperature range studied (175 – 300 K). This is consistent with fast exchange between free and coordinated telluroether and also with the observed trend of weaker binding to hard acceptors as group 16 is descended.

The ^1H NMR spectra of $[SnBr_4(Me_2Te)_2]$ studied over the same temperature range (175 – 300 K) exhibits a single resonance at δ 3.25 ppm. No splitting indicative of the presence of *cis* and *trans* isomers is observed at any temperature again consistent with the observed trend from chapters 2 and 3 that the complex is more labile when the Lewis acid is $SnBr_4$. The experiment was also run in the presence of excess ligand, again a single resonance is observed at all temperatures with fast exchange between free and co-ordinated telluroether.

A product was isolated for the reaction of SnI_4 with Me_2Te, but proved too hydrolytically unstable in solution to observe the species in the ^1H NMR spectrum.

Table 4.1. Variable Temperature ^1H NMR Spectroscopic Data

	δ(Me)[a]	
	300K	180 K
$[SnCl_4(Me_2Te)_2]$	3.0	3.04, 3.06 (1:2)
$[SnBr_4(Me_2Te)_2]$	3.25	3.17
$[SnI_4(Me_2Te)_2]$	n.o.[b]	n.o.[b]

[a] In CD_2Cl_2, approximate *cis/trans* ratios in parentheses. [b] n.o. = not observed

4.2.3. Variable Temperature ^{119}Sn-{^1H} and ^{125}Te-{^1H} NMR Spectroscopy

A solution of $[SnCl_4(Me_2Te)_2]$ in CH_2Cl_2 solution with *ca.* 10 % CD_2Cl_2 exhibited no resonances in either the ^{119}Sn-{^1H} or ^{125}Te-{^1H} NMR spectra at any temperature. Significantly, when the ^{125}Te-{^1H} NMR spectra were recollected with approximately a two-fold excess of Me_2Te present, no resonance was observed for either free or co-ordinated telluroether, confirming exchange in solution that is so rapid

that the NMR resonances are broadened and not observed. In contrast, the analogous selenoether complex with excess ligand displayed two resonances in the ^{77}Se-{^{1}H} and ^{119}Sn-{^{1}H} NMR spectra at 300 K with the resonances for the adduct seen to split below *ca.* 250 K to two distinct resonances for *cis* and *trans* isomers. These observations are again consistent with weakening Sn-L binding, Te < Se.

As expected for the weakening Lewis acids, no resonances were observed for the analogous $SnBr_4$ or SnI_4 complexes in either the ^{119}Sn-{^{1}H} or ^{125}Te-{^{1}H} NMR spectra.

Figure 4.1. ^{1}H NMR spectrum of $[SnCl_4(Me_2Te)_2]$ in CD_2Cl_2 solution at a) 300 K and b) 180 K

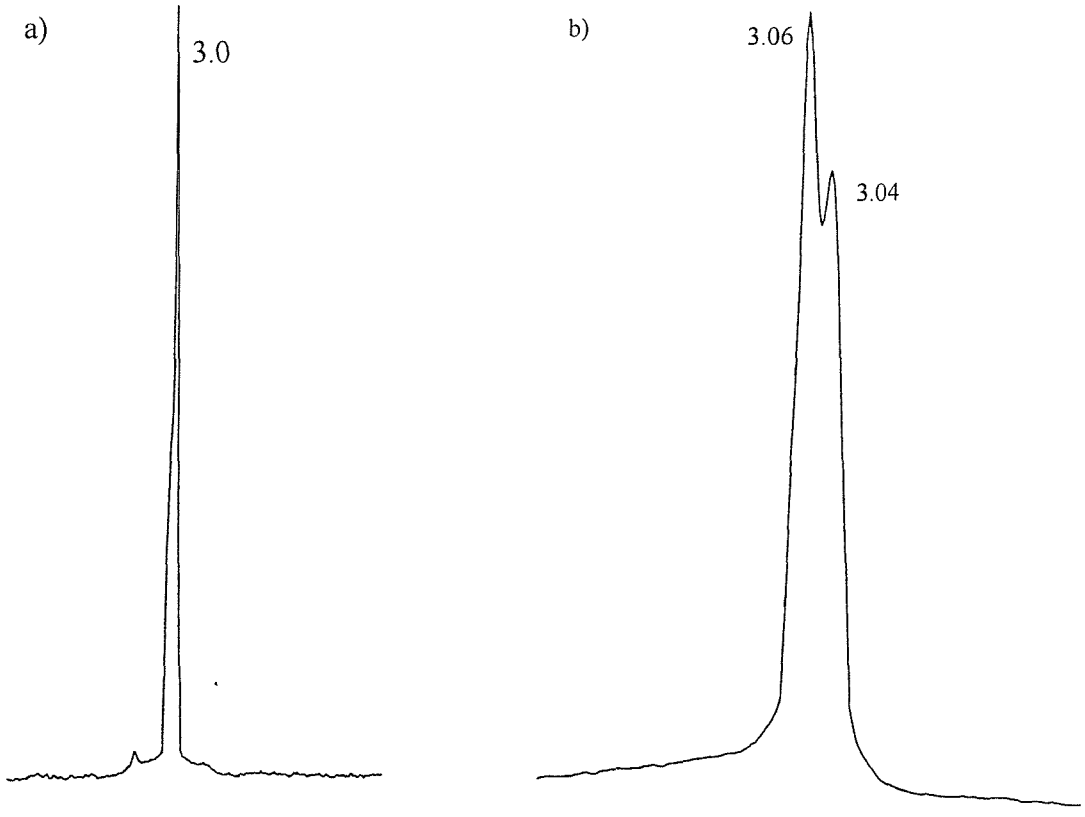

4.2.4. Synthesis and Properties of Bidentate Telluroether Complexes

A range of complexes of type SnX_4L_2 (where X = Cl, Br or I; L = $MeTe(CH_2)_3TeMe$, $PhTe(CH_2)_3TePh$ and o-$C_6H_4(TeMe)_2$) have been isolated from reaction in CH_2Cl_2. The range of telluroether ligands used is restricted since $RTe(CH_2)_2TeR$ ligands are not known (their attempted synthesis producing only R_2Te_2[2]). In most cases the poor solubility of the SnX_4-ditelluroether complexes meant that the products formed immediately from solution as powdered precipitates, the exception being for complexes of o-$C_6H_4(TeMe)_2$ where the products form gradually as a crystalline material upon slow evaporation. Due to the extreme moisture sensitivity of the tin(IV) halides and telluroethers, all reactions were carried out under an atmosphere of dry dinitrogen using standard Schlenk techniques. As for the SnX_4L_2 monodentate systems these complexes prove very easily hydrolysed, rapidly turning black in moist air, and the same effect is observed over a few weeks in a dinitrogen dry box. Satisfactory microanalyses were obtained for all products isolated.

IR spectra of the $SnCl_4$ complexes formed all showed the expected four ν(Sn-Cl) bands (theory: $2A_1 + B_1 + B_2$) in the range 300 - 340 cm^{-1} consistent with C_{2v} symmetry. Similarly, the bromide systems also show four ν(Sn-Br) bands in the range 190 – 230 cm^{-1} consistent with C_{2v} symmetry in these products as well. For the iodide systems the ν(Sn-I) bands are below the cut-off point of the spectrometer used (> 180 cm^{-1}) but the IR spectra show bands attributable to the telluroethers similar to those observed in previously studied Pd^{II} and Pt^{II} telluroether systems.[3]

The iodide complexes were isolated and satisfactory microanalyses were obtained. However, they prove too unstable in solution with hydrolysis the principal problem. Though even in high purity solvent the complexes are still seen to decompose in solution.

4.2.5. Single Crystal X-ray Diffraction Studies

Prior to this study there were no structurally characterised examples of telluroether complexes of any tin(IV) halides In order to attempt to identify trends in their geometric parameters, single crystal X-ray structure analyses on [$SnCl_4${o-$C_6H_4(TeMe)_2$}] and [$SnBr_4${o-$C_6H_4(TeMe)_2$}] were undertaken.

Figure 4.2. View of the structure of [$SnCl_4${o-$C_6H_4(TeMe)_2$}] with the numbering scheme adopted. Ellipsoids are shown at 40 % probability

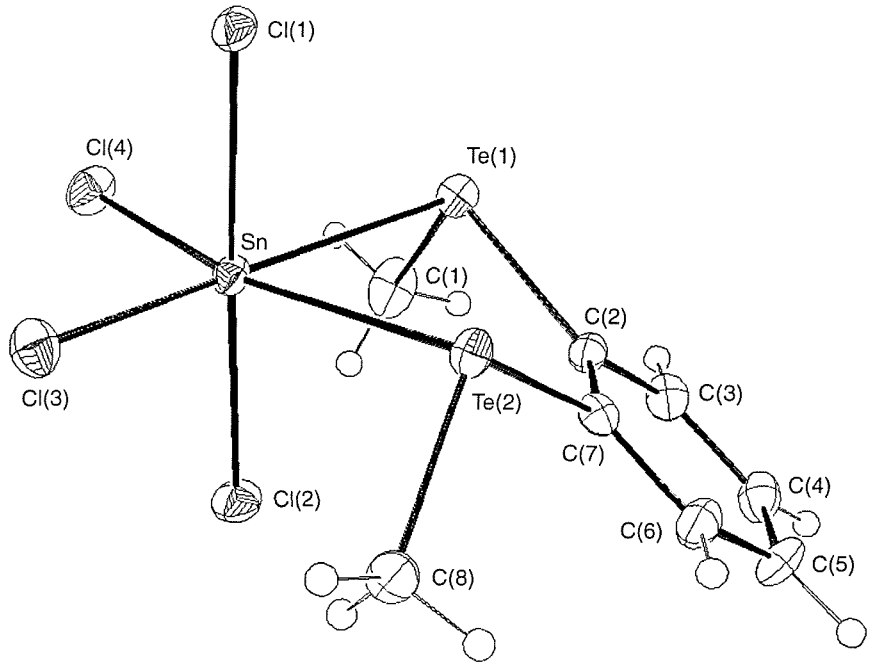

The structures for $[SnCl_4\{o\text{-}C_6H_4(TeMe)_2\}]$ and $[SnBr_4\{o\text{-}C_6H_4(TeMe)_2\}]$ are shown in Figures 4.2 and 4.3 respectively. Selected bond distances (Å) are presented in Tables 4.2 and angles (°) for $[SnX_4\{o\text{-}C_6H_4(TeMe)_2\}]$ are presented in Tables 4.3 (X = Cl) and 4.4 (X = Br). In each case the structure shows a discrete tin(IV) species involving a chelating $o\text{-}C_6H_4(TeMe)_2$ ligand, giving a distorted octahedral molecule as was observed previously in the cases of the thioether and selenoether analogues. As with the analogous thio- and selenoether systems the distortion has the axial halides bending towards the bidentate donor set. An alternative rationalisation might be distortion towards the tetrahedral geometry of the free SnX_4, arising from the weakened binding to the ditelluroether over halide atoms. In both compounds the ligand adopts a *meso* arrangement, with both methyl substituents directed to the same side of the SnX_4Te_2 plane. In the case of the bromide species, $[SnBr_4\{o\text{-}C_6H_4(TeMe)_2\}]$, only half the molecule is found in the asymmetric cell, the second half generated by a mirror plane (x, ½ - y, z) upon which the tin atom and two axial halide atoms lie. This is isostructural with the selenoether analogue, $[SnBr_4\{o\text{-}C_6H_4(SeMe)_2\}]$.

No other tin(IV) halide-telluroether complexes are known and thus there are no data with which to compare bond distances. However, the Sn-Te bond distances observed (2.908(1) – 2.981(2) Å) are approximately 0.1 Å longer than the analogous Sn-Se bond distances (2.749(1) – 2.841(2) Å), consistent with the larger radius of Te over Se. A similar difference was observed between the selenoether and thioether systems.

Once again variations are observed in the Sn-X bond distances (Table 4.2). In all cases *d*(Sn-X) for X *trans* to X are longer than those for X *trans* to Te, again suggesting that the *trans* influence of the halide atoms in these hard SnX_4 adducts is greater than that of the telluroether donor. This is in contrast with the usual trend observed in transition-metal complexes involving these ligands where the telluroether function exerts a greater *trans* influence than halogen atoms.[1]

Table 4.2. Selected Bond Distances (Å) for [$SnCl_4${o-$C_6H_4(TeMe)_2$}] and [$SnBr_4${o-$C_6H_4(TeMe)_2$}]

	[$SnCl_4${o-$C_6H_4(TeMe)_2$}]	[$SnBr_4${o-$C_6H_4(TeMe)_2$}]
Sn-Te(1)	2.908(1)	2.981(2)[a]
Sn-Te(2)	2.9222(8)	
Sn-X(1)	2.457(2)	2.567(2)
Sn-X(2)	2.433(2)	2.622(2)
Sn-X(3)	2.384(2)	2.526(2)[a]
Sn-X(4)	2.390(2)	

a. Second atom generated by crystallographic mirror plane, (x, ½ - y, z)

Figure 4.3. View of the structure of [$SnBr_4${o-$C_6H_4(TeMe)_2$}] with the numbering scheme adopted. Ellipsoids are shown at 40 % probability and atoms marked with an asterisk are related by a crystallographic mirror plane (x, ½ -y, z)

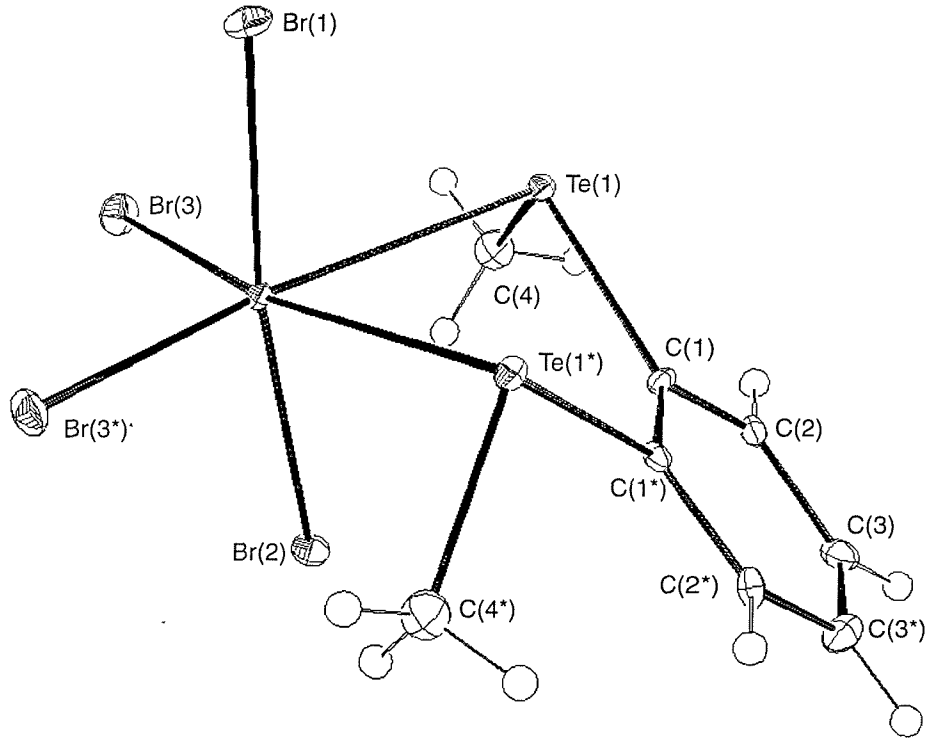

The Sn-Te bond distances (Table 4.2) are also markedly different for the two structures studied. *d*(Sn-Te) for the bromide system is approximately 0.6 Å longer than that of the chloride system. This is consistent with the observed trends of the analogous thio- and selenoether systems, but whether this is as a result of the weaker Lewis acid or largely a steric effect is not known. This also has the effect of creating a more strained chelate-ring (Table 4.3). Angles of 81.67(2) and 74.99(7)°, for the chloro and bromo species respectively, show that the shorter Sn-Te distances present within the chloro complexes creates a less strained arrangement within the five-membered chelate-ring compared to the bromo species, and hence a smaller distortion from the ideal 90°.

Table 4.3. Selected Bond Angles (°) for [$SnCl_4${o-$C_6H_4(TeMe)_2$}]

Te(1)-Sn-Te(2)	81.67(2)
Te(1)-Sn-Cl(1)	88.55(5)
Te(1)-Sn-Cl(2)	90.53(5)
Te(1)-Sn-Cl(3)	174.10(6)
Te(1)-Sn-Cl(4)	87.51(6)
Te(2)-Sn-Cl(1)	86.54(5)
Te(2)-Sn-Cl(2)	91.30(5)
Te(2)-Sn-Cl(3)	92.73(6)
Te(2)-Sn-Cl(4)	168.44(6)
Cl(1)-Sn-Cl(2)	177.75(7)
Cl(1)-Sn-Cl(3)	89.25(7)
Cl(1)-Sn-Cl(4)	89.13(7)
Cl(2)-Sn-Cl(3)	91.47(8)
Cl(2)-Sn-Cl(4)	92.88(7)
Cl(3)-Sn-Cl(4)	97.93(8)

Table 4.4. Selected Bond Angles (°) for $[SnBr_4\{o\text{-}C_6H_4(TeMe)_2\}]$

Te(1)-Sn-Te(1*)	74.99(7)[a]
Te(1)-Sn-Br(1)	84.36(7)
Te(1)-Sn-Br(2)	88.96(7)
Te(1)-Sn-Br(3)	92.66(7)
Te(1*)-Sn-Br(3)	167.64(4)[a]
Br(1)-Sn-Br(2)	171.58(7)
Br(1)-Sn-Br(3)	93.91(7)
Br(2)-Sn-Br(3)	91.51(6)
Br(3)-Sn-Br(3*)	99.68(9)[a]

a. Atom generated by (x, ½ -y, z) mirror plane

4.2.6. Variable Temperature NMR Spectroscopy

As described in section 4.2.4 these complexes exhibit very poor solubility in chlorocarbon solvents, and it is only the complexes $[SnX_4\{o\text{-}C_6H_4(TeMe)_2\}]$ which dissolve sparingly in CH_2Cl_2. $[SnX_4\{RTe(CH_2)_3TeR\}]$, especially when R = Me, prove insoluble in chlorocarbons, and this continues the trend observed in the thio- and selenoether systems of decreasing solubility for $[SnX_4\{MeE(CH_2)_3EMe\}]$ (S > Se). It is this low solubility, rather than increased stability, that leads to the isolation of complexes such as $[SnBr_4\{PhTe(CH_2)_3TePh\}]$ and SnI_4 complexes which had not been isolable for the thio- or selenoether analogous systems. Solubility is higher in dry acetone or tetrahydrofuran, but it is likely that the O-donor solvent partially displaces the tellurium ligand, since the ^1H NMR spectra of such solutions reveal several species present.

This poor solubility in chlorocarbon solvents means that no useful data could be obtained for the $[SnX_4\{RTe(CH_2)_3TeR\}]$ species in either the ^1H, $^{119}Sn\text{-}\{^1H\}$ or $^{125}Te\text{-}\{^1H\}$ NMR spectra. Resonances were observed for $[SnCl_4\{o\text{-}C_6H_4(TeMe)_2\}]$ in CD_2Cl_2 though the poor solubility meant the spectra (Figure 4.4) were not well refined. Longer accumulation periods were not available to allow for the solubility problem. At 300 K the ^1H NMR spectrum shows a single δ(Me) at 2.45 ppm (Figure 4.4a) which broadens on cooling and, at 180 K, two distinct resonances δ 2.61 and 2.71 ppm were present in a ratio *ca.* 3:1 (Figure 4.4b). These are attributable to the *meso* and *DL* diastereoisomers, showing that for this system reversible ring opening and pyramidal inversion is slowed sufficiently at this temperature. The solubility of the complex means that even at 180 K the signal-to-noise ratio was relatively poor and $^{117/119}Sn$ satellites were not observed. The ^1H NMR spectra of $[SnBr_4\{o\text{-}C_6H_4(TeMe)_2\}]$ only shows a singlet δ(Me) resonance over the range 180 – 300 K, consistent with the weaker Lewis acid leading to increased lability.

Neither of the $[SnX_4\{o\text{-}C_6H_4(TeMe)_2\}]$ systems exhibits any resonances in the $^{119}Sn\text{-}\{^1H\}$ or $^{125}Te\text{-}\{^1H\}$ NMR spectra at any temperature studied. Whilst the poor solubility of these complexes would make observation of these nuclei very difficult, separate experiments in which mixtures of $[SnCl_4\{o\text{-}C_6H_4(TeMe)_2\}]$ and $o\text{-}C_6H_4(TeMe)_2$ were studied failed to show any $^{125}Te\text{-}\{^1H\}$ resonance, even for the readily soluble free ditelluroether, demonstrating that fast exchange on the NMR time-scale is resulting in the resonances becoming unobservably broad. Although similar

exchange occurs in the analogous thio- and selenoether systems at 300 K, the exchange is slowed on cooling and $^{117/119}$Sn-{^{1}H} or ^{77}Se-{^{1}H} resonances are easily observed at lower temperatures. The fact that this is not possible for the telluroether systems is consistent with these being poorer donors to Sn(IV) and hence leading to more labile systems.

Figure 4.4. ^{1}H NMR spectra for [$SnCl_4${o-$C_6H_4(TeMe)_2$}] in CD_2Cl_2 solution at a) 300 K and b) 180 K

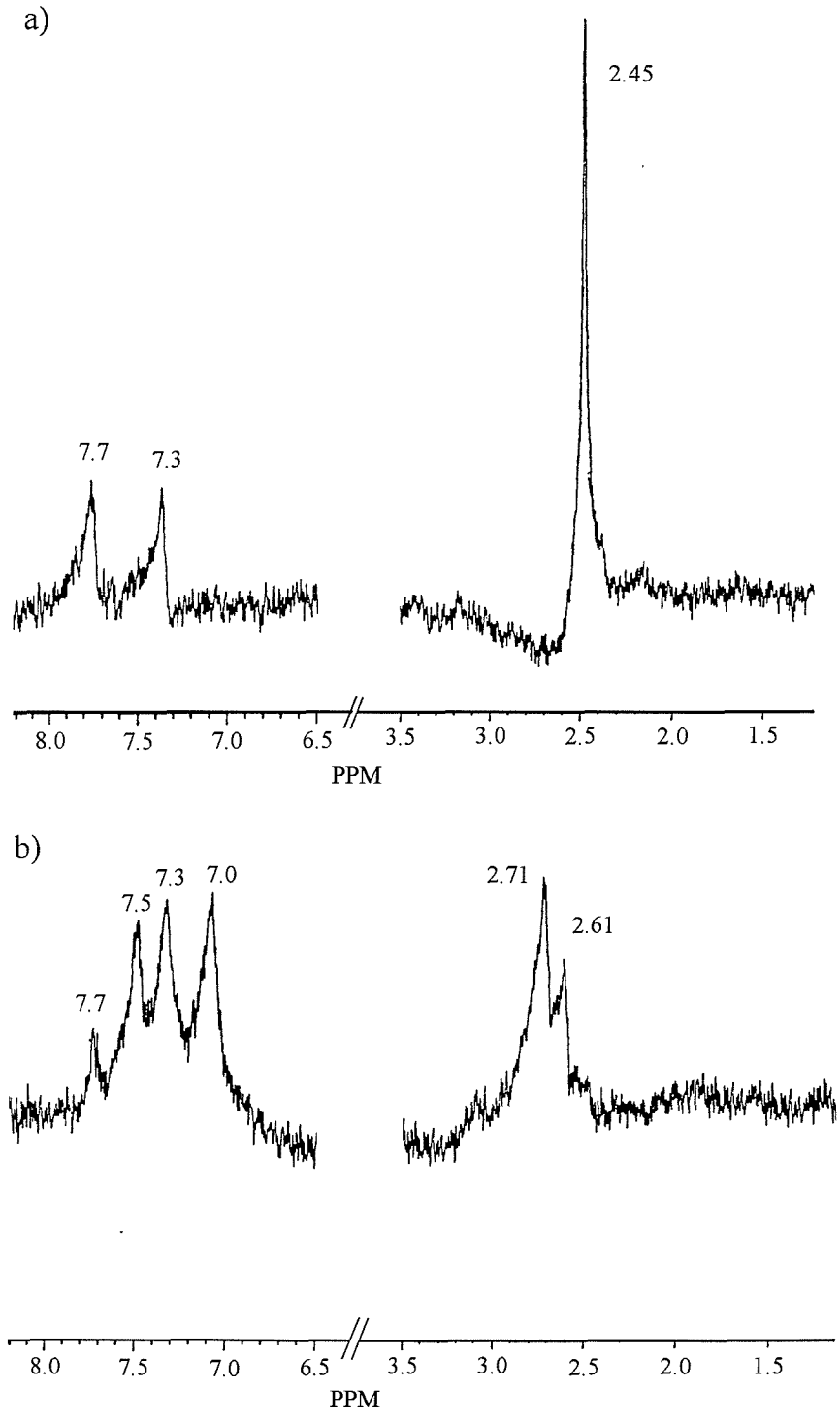

4.3. Conclusions

The products $[SnX_4(Me_2Te)_2]$ (where X = Cl, Br or I) arising from the reactions of SnX_4 with Me_2Te and those with bidentate telluroethers, $[SnX_4\{MeTe(CH_2)_3TeMe\}]$, $[SnX_4\{PhTe(CH_2)_3TePh\}]$ and $[SnX_4\{o\text{-}C_6H_4(TeMe)_2\}]$ have been prepared. A detailed examination of the variable temperature ^1H, $^{119}Sn\text{-}\{^1H\}$ and $^{125}Te\text{-}\{^1H\}$ NMR spectroscopy over the temperature range 300 – 180 K has been presented. These complexes are found to be poorly soluble, leading to the isolation of products that were not seen for the analogous thio- or selenoether systems. Conversely poor solubility means that very little NMR data were obtainable, although for $[SnCl_4\{o\text{-}C_6H_4(TeMe)_2\}]$ *meso* and *DL* diastereoisomers were observed at 180 K. The lack of data means that it is difficult to make qualitative observations, though it is still clear that the stability of these systems decreases with weakening Lewis acid, Cl > Br > I, and also that the telluroether complexes are less stable than the corresponding selenoethers.

4.4. Observed Trends for Group 16 Complexes of Tin(IV) Halides

In chapters 2, 3 and 4 a detailed study of the solution and solid state behaviours of the thio-, seleno- and telluro-ether complexes of the tin(IV) halides has been presented. As a consequence several trends become apparent.

Firstly no reaction was observed for any ligand with SnF_4. SnF_4 is a polymer consisting of SnF_6 octahedra with opposite *trans* edges shared[4], and shows poor solubility in non-coordinating solvents. The apparent lack of reactivity may therefore be attributed to kinetic factors or may be a consequence of the preference of the hard tin centre for bridging fluoride rather than the group 16 donors. It does react with some hard O- and N-donor ligands.[5-9] We have shown that O-donor solvents such as Me_2CO or thf react with [$SnCl_4$(dithioether)], for example by partial displacement of the thioether donors. Of the five structurally characterised examples, three feature a retention of the SnF_6 octahedra observed for the free halide,[5-7] with only one uncharged octahedral complex with 2,2'-bipyridine.[9]

The other three tin(IV) tetrahalides are molecular tetrahedra and thus react easily with donor ligands in non-coordinating solvents. The literature data on the coordination chemistry of these SnX_4 units show a clear trend in Lewis acidity: Cl > Br > I,[10] and consequently relatively few complexes of SnI_4 are known. Indeed a search of the CCDB for structurally characterised examples found only six examples,[11-16] of which one is the sulfoxide discussed in chapter 2 of this study,[16] and all feature harder N- or O-donors. Our solution and solid state data on the thio-, seleno- and telluro-ether adducts clearly supports this trend and demonstrates that the Sn-E (E = S, Se or Te) interactions become weaker as the halogen becomes heavier.

Turning to trends with changes of the group 16 donors. The solution NMR spectroscopic data shows the Sn-E interaction is strongest in thioether adducts, rather weaker in selenoethers, while the telluroether complexes are extensively dissociated in solution. Indeed, as discussed above, it appears that it is the poor solubility of certain [SnX_4(ditelluroether)] species which permits their isolation as solids.

Examination of the effect of varying the ligand architecture shows that, as expected, the phenyl substituted ligands are weaker donors than their methyl substituted analogues. A similar conclusion was drawn for R_2E complexes of SnX_4 by Merbach *et al.*[17] and Abel *et al.*[18]

The interdonor linkage also influences the solution characteristics of the SnX_4 adducts and, as discussed above, the complexes involving aliphatic linkages show

decreasing stability with chelate ring-size: 5 > 6 > 4, and thus the successful isolation of complexes involving four membered chelate rings was unexpected and analogous species have not been identified in transition metal chemistry. The o-phenylene linkage allows relatively straightforward isolation of adducts and this may be attributed to the o-phenylene effect.[19] Additionally these ligands facilitate increased solubility of the adducts and hence allow easier crystallisation of the products.

The variable temperature NMR spectroscopic studies have shown that at room temperature reversible ligand dissociation is rapid on the NMR timescales, and presumably occurs *via* reversible ring-opening. Experiments with added ligand show rapid intermolecular exchange. At low temperatures the NMR spectra of certain systems show exchange is slow. In these systems at low temperature we also observe slow pyramidal inversion and separate resonances for the invertomers for the invertomers are clearly evident. Upon warming these solutions it appears that onset of rapid pyramidal inversion and dissociation occurs within similar temperature ranges and hence quantitative measurements of these processes are not possible.

4.5. Experimental

The tin(IV) chloride, bromide and iodide were purchased from *Aldrich Chemicals*. The ligands Me_2Te, $MeTe(CH_2)_3TeMe$, $PhTe(CH_2)_3TePh$ and o-$C_6H_4(TeMe)_2$ were prepared by following literature methods.[2,20]

Tin(IV) halides and telluroether compounds are extremely moisture sensitive, therefore all of the reactions were carried out under an atmosphere of dry nitrogen, using standard Schlenk, vacuum-line and dry box techniques.

Single Crystal X-ray Diffraction

Single crystals of $[SnCl_4\{o\text{-}C_6H_4(TeMe)_2\}]$ and $[SnBr_4\{o\text{-}C_6H_4(TeMe)_2\}]$ were obtained from a solution of the appropriate complex in CH_2Cl_2. The compounds were extremely sensitive to hydrolysis on exposure to moist air. Therefore, in each case the selected crystal was coated with mineral oil, mounted on a glass fibre using silicone grease as adhesive, and immediately placed in a stream of cold nitrogen gas. Data collection used a Rigaku AFC7S four-circle diffractometer equipped with an Oxford Cryostreams low temperature attachment operating at 150 K, using graphite-monochromated Mo-K_α X-radiation (λ = 0.71073 Å), T = 150 K, ω-2θ scans. The intensities of three standard reflections were monitored every 150 reflections. No significant crystal decay or movement was observed. As there were no identifiable faces for $[SnCl_4\{o\text{-}C_6H_4(TeMe)_2\}]$ the raw data were corrected for absorption using psi-scans. The weighting scheme $w^{-1} = \sigma^2(F)$ gave satisfactory agreement analyses in each case.

The structures were solved by direct methods,[21] and then developed by iterative cycles of full-matrix least-squares refinement (based on *F*) and difference Fourier syntheses which located all non-H atoms in the asymmetric unit.[22] For $[SnBr_4\{o\text{-}C_6H_4(TeMe)_2\}]$ an empirical absorption correction using DIFABS[23] was applied to the raw data at isotropic convergence, as psi scans did not provide a satisfactory absorption correction. All non-H atoms in the structures were refined anisotropically (with the exception of $[SnBr_4\{o\text{-}C_6H_4(TeMe)_2\}]$ for which C(4) was refined isotropically since anisotropic refinement resulted in this atom becoming non-positive definite, probably a result of an imperfect absorption correction), and H atoms were placed in fixed, calculated positions with *d*(C-H) = 0.96 Å. Crystallographic data are presented in Table 4.5.

Table 4.5. Crystallographic Data

Compound	$[SnCl_4\{o\text{-}C_6H_4(TeMe)_2\}]$	$[SnBr_4\{o\text{-}C_6H_4(TeMe)_2\}]$
Formula	$C_8H_{10}Cl_4SnTe_2$	$C_8H_{10}Br_4SnTe_2$
Formula Weight	621.87	799.67
Colour, morphology	Yellow, column	Red-brown, block
Crystal dimensions/mm	0.40 x 0.15 x 0.10	0.30 x 0.20 x 0.20
Crystal System	Monoclinic	Monoclinic
Space Group	$P2_1/n$	$P2_1/m$
a/Å	8.064(3)	6.829(9)
b/Å	14.362(2)	11.50(1)
c/Å	13.549(2)	10.23(1)
β/°	102.10(1)	100.5(1)
U/Å^3	1534.3(6)	790(1)
Z	4	2
Scan Type	ω-2θ	ω-2θ
HKL limits		
F(000)	1120	704
D_c/g cm^{-3}	2.692	3.361
μ(Mo-K_α)/cm^{-1}	60.88	153.52
Transmission factors (max. and min.)	1.000, 0.886	1.000, 0.410
No. of Unique obs. reflections	2834	1482
R_{int} (based on F^2)	0.028	0.051
Unique obs. reflections with $[I_o > 2.0\sigma(I_o)]$	2120	1234
No. of parameters	136	68
Goodness of fit	1.33	2.67
R(F_o)	0.031	0.039
$R_w(F_o)$	0.035	0.043
Max. residual peak/eÅ^{-3}	1.60	1.70
Max. residual trough/eÅ^{-3}	-0.84	-1.90

$R = \Sigma (|F_{obs}|_i - |F_{calc}|_i)/\Sigma |F_{obs}|_i$

$R_w = \sqrt{[\Sigma w_i(|F_{obs}|_i - |F_{calc}|_i)^2 / \Sigma w_i|F_{obs}|_i^2]}$

$GOF = [\Sigma (|F_{obs}|_i - |F_{calc}|_i)/\sigma_i]/(n - m) \approx 1$

Complex Synthesis

$[SnCl_4(Me_2Te)_2]$

Dimethyl telluride (0.32 g, 2 mmol) was dissolved in anhydrous, degassed CH_2Cl_2 ($5cm^3$) in a 3-neck RB flask under an atmosphere of dry N_2 and the solution further degassed. Addition of $SnCl_4$ (0.26 g, 1 mmol) to the solution gave immediate formation of a yellow precipitate which was filtered off and dried *in vacuo*. Found: C, 8.6; H, 2.3. Calculated for $C_4H_{12}Cl_4Te_2Sn$: C, 8.3; H, 2.1 %. IR spectrum (nujol mull) ν/cm^{-1} (Sn-Cl): 312. ^1H NMR (CD_2Cl_2): δ 3.0 (s) (300 K); 3.04, 3.06 (180 K).

$[SnBr_4(Me_2Te)_2]$

A saturated solution of $SnBr_4$ (0.44 g, 1 mmol) in anhydrous, degassed CH_2Cl_2 (5 cm^3) was added dropwise to a solution of dimethyl telluride (0.32 g, 2 mmol) in anhydrous, degassed CH_2Cl_2 (5 cm^3). The complex formed as a fawn powder which was filtered off and dried *in vacuo*. Found: C, 6.7; H, 1.7. Calculated for $C_4H_{12}Br_4Te_2Sn$: C, 6.4; H, 1.6 %. IR spectrum (nujol mull) ν/cm^{-1} (Sn-Br): 220. ^1H NMR (CD_2Cl_2, 300 K): δ 2.8 (s).

$[SnCl_4\{MeTe(CH_2)_3TeMe\}]$

$SnCl_4$ (0.26 g, 1 mmol) was added to a solution of $MeTe(CH_2)_3TeMe$ (0.32 g, 1 mmol) in anhydrous, degassed CH_2Cl_2 (10 cm^3). The complex precipitated immediately as a yellow powder which was filtered off and dried *in vacuo*. Found: C, 9.9; H, 2.0. Calculated for $C_5H_{12}Cl_4Te_2Sn$: C, 10.2; H, 2.0 %. IR spectrum (nujol mull) ν/cm^{-1} (Sn-Cl): 317, 313, 309 and 305.

$[SnCl_4\{PhTe(CH_2)_3TePh\}]$

$SnCl_4$ (0.26 g, 1 mmol) was added to a solution of $PhTe(CH_2)_3TePh$ (0.45 g, 1 mmol) in anhydrous, degassed CH_2Cl_2 (10 cm^3). The complex precipitated immediately as a red-brown powder which was filtered off and dried *in vacuo*. Found: C, 25.7; H, 2.5. Calculated for $C_{15}H_{16}Cl_4Te_2Sn$: C, 25.5; H, 2.3 %. IR spectrum (nujol mull) ν/cm^{-1} (Sn-Cl): 332, 321, 314 and 309.

[$SnCl_4${o-$C_6H_4(TeMe)_2$}]

$SnCl_4$ (0.26 g, 1 mmol) was added to a solution of o-$C_6H_4(TeMe)_2$ (0.36 g, 1 mmol) in anhydrous, degassed CH_2Cl_2 (10 cm^3). The complex formed as a white crystalline precipitate which was filtered off and dried *in vacuo*. Found: C, 15.4; H, 1.7. Calculated for $C_8H_{10}Cl_4Te_2Sn$: C, 15.4; H, 1.6 %. IR spectrum (nujol mull) ν/cm^{-1} (Sn-Cl): 315, 304, 296 and 284. ^1H NMR (CD_2Cl_2): δ 2.45 (s, 3 H), 7.3, 7.7 (2 H) (300 K); 2.61, 2.71, 7.0-7.7 (180 K).

[$SnBr_4${$MeTe(CH_2)_3TeMe$}]

A saturated solution of $SnBr_4$ (0.44 g, 1 mmol) in anhydrous, degassed CH_2Cl_2 (5 cm^3) was added dropwise to a solution of $MeTe(CH_2)_3TeMe$ (0.32 g, 1 mmol) in anhydrous, degassed CH_2Cl_2 (5 cm^3). The complex precipitated immediately as a yellow powder which was filtered off and dried *in vacuo*. Found: C, 8.1; H, 2.2; Br, 42.1. Calculated for $C_5H_{12}Br_4Te_2Sn$: C, 7.9; H, 1.6; Br, 41.7 %. IR spectrum (nujol mull) ν/cm^{-1} (Sn-Br): 219, 217, 212 and 210.

[$SnBr_4${$PhTe(CH_2)_3TePh$}]

A saturated solution of $SnBr_4$ (0.44 g, 1 mmol) in anhydrous, degassed CH_2Cl_2 (5 cm^3) was added dropwise to a solution of $PhTe(CH_2)_3TePh$ (0.45 g, 1 mmol) in anhydrous, degassed CH_2Cl_2 (5 cm^3). The complex precipitated immediately as a brown powder which was filtered off and dried *in vacuo*. Found: C, 19.9; H, 1.9; Br, 37.2. Calculated for $C_{15}H_{16}Br_4Te_2Sn$: C, 20.4; H, 1.8; Br, 36.0 %. IR spectrum (nujol mull) ν/cm^{-1} (Sn-Br): 218, 215, 213 and 207.

[$SnBr_4${o-$C_6H_4(TeMe)_2$}]

A saturated solution of $SnBr_4$ (0.44 g, 1 mmol) in anhydrous, degassed CH_2Cl_2 (5 cm^3) was added dropwise to a solution of o-$C_6H_4(TeMe)_2$ (0.36 g, 1 mmol) in anhydrous, degassed CH_2Cl_2 (5 cm^3). The complex formed as a dark brown crystalline precipitate which was filtered off and dried *in vacuo*. Found: C, 12.3; H, 1.5; Br, 40.3. Calculated for $C_8H_{10}Br_4Te_2Sn$: C, 12.3; H, 1.3; Br, 39.9 %. IR spectrum (nujol mull) ν/cm^{-1} (Sn-Br): 218, 216, 214 and 207. ^1H NMR (CD_2Cl_2): δ 2.4 (13 H), 7.3, 7.7 (2 H) (300 K); 2.6, 7.5, 7.65 (180 K).

[SnI_4{$MeTe(CH_2)_3TeMe$}]

A saturated solution of SnI_4 (0.63 g, 1 mmol) in anhydrous, degassed CH_2Cl_2 (5 cm^3) was added dropwise to a solution of $MeTe(CH_2)_3TeMe$ (0.32 g, 1 mmol) in anhydrous, degassed CH_2Cl_2 (5 cm^3). The complex precipitated immediately as a brown powder which was filtered off and dried *in vacuo*. Found: C, 6.5; H, 1.5; I, 51.42. Calculated for $C_5H_{12}I_4Te_2Sn$: C, 6.3; H, 1.27; I, 53.23 %.

[SnI_4{$PhTe(CH_2)_3TePh$}]

A saturated solution of SnI_4 (0.63 g, 1 mmol) in anhydrous, degassed CH_2Cl_2 (5 cm^3) was added dropwise to a solution of $PhTe(CH_2)_3TePh$ (0.45 g, 1 mmol) in anhydrous, degassed CH_2Cl_2 (5 cm^3). A pale brown precipitate forms immediately, which was filtered off and dried *in vacuo*. Found: C, 17.1; H, 1.7. Calculated for $C_{15}H_{16}I_4Te_2Sn$: C, 16.8; H, 1.3 %.

[SnI_4{o-$C_6H_4(TeMe)_2$}]

A saturated solution of SnI_4 (0.63 g, 1 mmol) in anhydrous, degassed CH_2Cl_2 (5 cm^3) was added dropwise to a solution of o-$C_6H_4(TeMe)_2$ (0.36 g, 1 mmol) in anhydrous, degassed CH_2Cl_2 (5 cm^3). A fawn coloured precipitate forms immediately. Further precipitate is formed on reducing the volume *in vacuo* and this is filtered off and dried *in vacuo*. Found: C, 10.1; H, 1.3. Calculated for $C_8H_{10}I_4Te_2Sn$: C, 9.72; H, 1.01 %.

References

[1] H. J. Gysling, *Coord. Chem. Rev.*, 1982, **42**, 133; H. J. Gysling, in S. Patai and Z. Rappoport (Editors), *The Chemistry of Organic Selenium and Tellurium Compounds*, Wiley, New York, 1986, vol. 1, p. 365; E. G. Hope and W. Levason, *Coord. Chem. Rev.*, 1993, **122**, 109.

[2] E. G. Hope, T. Kemmitt and W. Levason, *Organometallics*, 1988, **7**, 78.

[3] T. Kemmitt, W. Levason and M. Webster, *Inorg. Chem.*, 1989, **28**, 692; T. Kemmitt and W. Levason, *Inorg. Chem.*, 1990, **29**, 731.

[4] R. Hoppe and W. Dähne, *Naturwissenschaften*, 1962, **49**, 254.

[5] U. Calov, K.-H. Jost and F. Leibnitz, *Z. Anorg. Allg. Chem.*, 1990, **598**, 199.

[6] A. Taha, B. Liautard and W. Granier, *Acta Crystallogr., Sect. C*, 1992, **48**, 1929.

[7] U. Calov, M. Schneider and P. Leibnitz, *Z. Anorg. Allg. Chem.*, 1991, **604**, 77.

[8] D. Tudela, *J. Organomet. Chem.*, 1994, **63**, 471.

[9] A. D. Adley, P. H. Bird, A. R. Fraser and M. Onyszchuk, *Inorg. Chem.*, 1972, **11**, 1402.

[10] P. G. Harrison, in P. G. Harrison (Editor), *The Chemistry of Tin*, Blackie, New York, 1989, p. 30.

[11] K. A. Paseshnitchenko, L. A. Aslanov, A. V. Yatsenko and S. V. Medvedev, *Koord. Khim.*, 1984, **10**, 1279.

[12] A. V. Jatsenko, S. V. Medvedev, K. A. Paseshnitchenko and L. A. Aslanov, *J. Organomet. Chem.*, 1985, **284**, 181.

[13] A. I. Tursina, L. A. Aslanov, V. V. Cheryshev, S. V. Medvedev, A. V. Yatsenko, *Koord. Khim.*, 1986, **12**, 420.

[14] J. Angenault, J.-C. Couturier and E. Reculeau, *Rev. Chim. Miner.*, 1979, **16**, 157.

[15] N. Bricklebank, S. M. Godfrey, C. A. McAuliffe and R. G. Pritchard, *J. Chem. Soc., Chem. Commun.*, 1994, 695.

[16] S. E. Dann, A. R. J. Genge, W. Levason and G. Reid, *J. Chem. Soc., Dalton Trans.*, 1996, 4471.

[17] S. J. Ruzicka and A. E. Merbach, *Inorg. Chim. Acta.*, 1976, **20**, 221; 1977, **22**, 191; S. J. Ruzicka, C. M. P. Favez and A. E. Merbach, *Inorg. Chim. Acta.*, 1977, **23**, 239.

[18] E. W. Abel, S. K. Bhargava, K. G. Orrell and V. Sik, *Inorg. Chim. Acta*, 1981, **49**, 25.

[19] L. F. Warren and M. A. Bennett, *Inorg. Chem.*, 1976, **15**, 3126.

[20] T. Kemmitt and W. Levason, *Organometallics*, 1989, **8**, 1303.

[21] SHELXS-86, program for crystal structure solution, G. M. Sheldrick, *Acta Crystallogr., Sect. A*, 1990, **46**, 467.

[22] TEXSAN, Crystal Structure Analysis Package, Molecular Structure Corporation, Houston, TX, 1992.

[23] N. Walker and D. Stuart, *Acta Crystallogr., Sect A.*, 1983, **39**, 158.

Chapter 5

Tin(IV) Halide Complexes of Phosphine, Arsine and Phosphine Oxide Ligands

5.1. Introduction

In chapters 2, 3 and 4 the first detailed studies of group 14 halide complexes of mono- and bidentate thio-, seleno- and telluroether ligands were described. In contrast the complexes formed with the group 15 ligands has been studied more extensively.

Tin(IV) halide complexes of group 15 donors have been known for over 50 years,[1-4] A range of phosphine and diphosphine complexes have been prepared and characterisd by vibrational and Mössbauer spectroscopy and X-ray crystallography.[1-9] As might be expected by analogy with the results of our studies of the tin(IV) complexes of the group 16 donors, complexes are formed easily with the stronger σ-donor phosphines. Direct reaction of SnX_4 (where X = Cl or Br) with ligands of the type R_3P in solution readily forms the 1:2 $[SnX_4(R_3P)_2]$ complex. Vibrational spectroscopic studies concluded[10] that the complexes existed primarily as the *trans* isomers in the solid state. This assignment was confirmed by the single crystal X-ray diffraction analysis of *trans*-$[SnCl_4(Et_3P)_2]$[11] (Figure 5.1).

Figure 5.1 View of the molecular structure of *trans*-$[SnCl_4(Et_3P)_2]$ (taken from ref. 11)

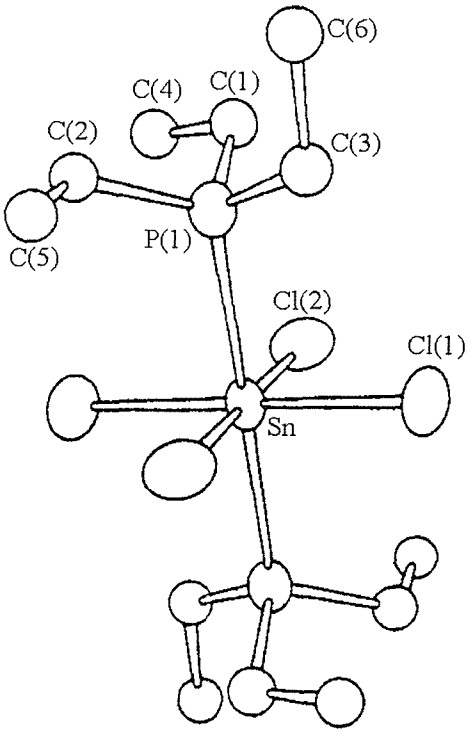

The studies also showed that while complexes of SnI_4 were formed they were too unstable to isolate from these reactions. The air sensitive complex *trans*-$[SnI_4(Pr^n{}_3P)_2]$ (Figure 5.2) has been isolated and structurally characterised, but from the reaction of tin powder with $Pr^n{}_3PI_2$ in diethyl ether.[7] These findings are consistent with the trend in SnX_4 Lewis acidity: Cl > Br > I, seen in chapters 2, 3 and 4 and literature data.[12]

Figure 5.2 View of the molecular structure of *trans*-$[SnI_4(Pr^n{}_3P)_2]$ (taken from ref. 7)

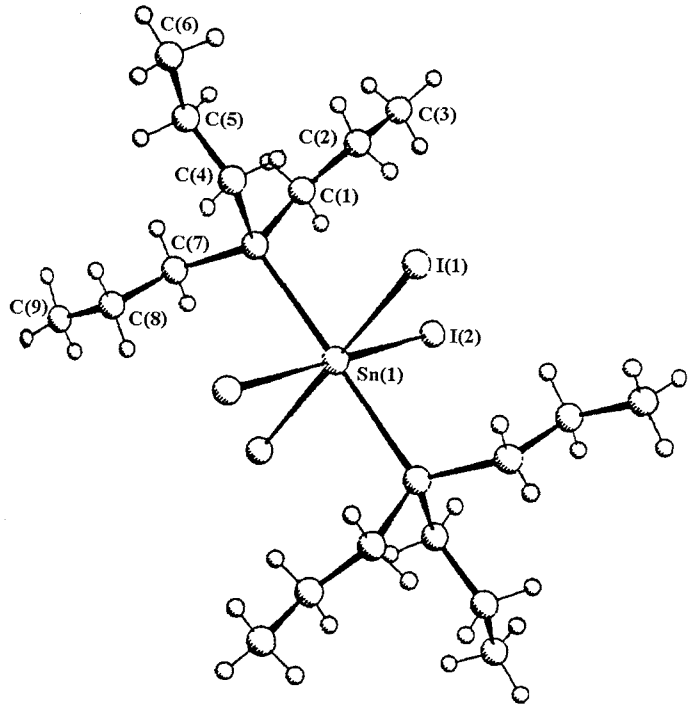

Surprisingly few studies have reported multinuclear NMR spectroscopic data.[13-17] The 1:2 tin(IV) halide complexes with monodentate phosphines have been examined by $^{31}P\text{-}\{^1H\}$ and $^{119}Sn\text{-}\{^1H\}$ NMR spectroscopy by Colton *et al.*[13] (*trans*-$[SnX_4(PBu_3)_2]$) and McFarlane *et al.*[15] and Malone *et al.*[17] (*trans*-$[SnX_4(R_3P)_2]$). All studies conclude that the *trans* isomer is the predominant species in solution. Malone and Mann[17] note that the observed trend of a large $^2J(^{31}P\text{-}^{31}P)$ for *trans* configurations

of transition metal complexes with phosphines does not extend to these octahedral tin(IV) complexes. Further to this, McFarlane *et al.*[15] also note that the *trans* coupling for tin(IV) complexes is of opposite sign to that usually found in the transition metal case. They also found that while for transition metal complexes the $^{1}J(M\text{-}^{31}P)$ is determined by the *trans* influence of groups *trans* to the phosphorus donor, for these octahedral tin(IV) complexes it is the nature of the groups *cis* to the phosphorus donor which governs the size of the coupling.

The complexes of bidentate phosphines of the tin(IV) halides, analogous to the group 16 systems studied in chapters 2, 3 and 4, have not been studied in as much detail as the monodentate systems. In the solid state Sarikhaya[9] has used vibration spectroscopy to examine a range of SnX_4 complexes with bidentate phosphines, $R_2P(CH_2)_nPR_2$ (where R = Me, Et or Ph for n = 2; R = Me or Et for n = 3). The IR spectra of these species exhibit four Sn-X bands consistent with C_{2v} symmetry and are analogous to the chelate structures seen for the equivalent group 16 bidentate ligand complexes in chapter 2, 3 and 4. The single crystal X-ray analysis of *cis*-$[SnCl_4(dppe)]$ (where dppe = 1,2-bis(diphenylphosphino)ethane) by Kunkel and Dehnicke[8] confirms this assignment. Dakternieks *et al.*[18] have also examined the complex formed between $Ph_2PCH_2PPh_2$ (dppm) and $SnCl_4$ and found that a chelate is not formed but rather the 1:2 complex is formed with two mutually *trans* η^1 dppm ligands. The $^{31}P\text{-}\{^{1}H\}$ NMR spectra of various mixtures of SnX_4 (X = Cl or Br) and $Ph_2P(CH_2)_nPPh_2$ (n = 1 - 4) have been studied *in situ* by Petrosyan *et al.*[14] but a number of their results would suggest decomposition of the complexes with the formation of phosphine oxides. Complexes of SnI_4 with group 15 bidentate ligands have been produced *in situ*[5] but have proved too unstable to be isolated as solids.

As for the phosphines a good deal of work has been done examining the complexes of the tin(IV) halides with monodentate arsines[1,5,6,19,20] using a combination of IR and ^{119}Sn Mössbauer spectroscopic techniques. The results of these studies again confirm the expected *trans* isomer as the predominant species in the 1:2 $[SnX_4(R_3As)_2]$ systems. Very few examples of bidentate arsine complexes with SnX_4 have been reported. Both involve o-phenylene backboned ligands, o-$C_6H_4(AsMe_2)_2$[1] and o-$C_6H_4(AsEt_2)_2$,[21] and are assigned as *cis* coordinated chelates on the basis of vibrational spectroscopy. No structural analyses have been carried out on either the mono- or bi-dentate arsine complexes.

5.2 Results & Discussion

5.2.1. Synthesis and Properties of Me_3P Complexes of SnX_4

The complexes $[SnX_4(Me_3P)_2]$ (X = Cl, Br or I) have been prepared by reaction of the appropriate SnX_4 with two molar equivalents of Me_3P in thoroughly degassed, anhydrous CH_2Cl_2. The solids formed are hydrolysed easily, even the briefest exposure to the laboratory atmosphere causes oxidation forming the phosphine oxide complex. All complexes were therefore stored and handled in a dinitrogen filled dry-box. The far-IR spectrum of the chloride complex shows one broad peak at 321 cm^{-1} for ν(SnCl) probably corresponding to the *trans* isomer (D_{4h}) being the principal isomer present in the solid state, consistent with the conclusions of previous studies on this compounds.[10] The same observation is made for the bromide species with a broad band observed at 220 cm^{-1}, again in agreement with previous studies.[10] Satisfactory elemental analyses were obtained for all species. IR spectroscopic and analytical data are presented in Table 5.1.

Table 5.1. Analytical and Spectroscopic data for $[SnX_4(Me_3P)_2]$ complexes

Complex	Colour	%C[a]	%H	ν(Sn-X)[b] (cm^{-1})	^{1}H NMR[c]
$[SnCl_4(Me_3P)_2]$	White	17.1(17.5)	4.3(4.4)	321	1.83(m)
$[SnBr_4(Me_3P)_2]$	Pale yellow	11.9(12.2)	3.2(3.1)	220	1.50(m)
$[SnI_4(Me_3P)_2]$	Deep yellow	9.1(9.3)	2.5(2.3)	-	1.56(m)

a. Calculated values in parentheses
b. Nujol mulls.
c. $CDCl_3$ solution at 300 K

5.2.2 Variable Temperature ^{31}P-{^{1}H} and ^{119}Sn-{^{1}H} NMR Spectroscopy

The complexes proved poorly soluble in CD_2Cl_2 necessitating long accumulation times. ^{1}H NMR spectroscopic data are presented in Table 1, ^{31}P-{^{1}H} and ^{119}Sn-{^{1}H} NMR spectroscopic data are presented in Table 5.2. $[SnCl_4(Me_3P)_2]$ exhibits a single resonance in the ^{31}P-{^{1}H} NMR spectrum (Figure 5.3a, δ = 6.8 ppm, $^{1}J(^{31}P\text{-}^{117/119}Sn)$ = 2720 Hz) indicating that only a single isomer is present in solution. As in the cases of the analogous group 16 ligands coordinating solvents were not used as they were found to partially displace the ligands in solution.[22] However, in a freshly prepared $MeNO_2$ solution of $[SnCl_4(Me_3P)_2]$ the ^{31}P-{^{1}H} NMR spectrum (Figure 5.3b) revealed two isomers in the approximate ratio 1:2, the minor isomer has δ = 8.0 and the major isomer δ = 3.6 ppm. Significantly, the minor isomer has a $^{1}J(^{31}P\text{-}^{117/119}Sn)$ coupling of the same values to that observed in CD_2Cl_2, 2720 Hz, and is therefore assigned as the same form. The same $MeNO_2$ solution in the ^{119}Sn-{^{1}H} NMR spectrum has two triplets at δ –646 and –630 ppm which have $^{1}J(^{119}Sn\text{-}^{31}P)$ couplings which can be correlated with those in the ^{31}P-{^{1}H} NMR spectrum. On standing the resonance of the isomer with δ = 8.0 diminishes and a new resonance at δ = 39.5 appears, assigned to the formation of the phosphine oxide. The two resonances are assigned as *trans* and *cis* geometrical isomers based on the relative magnitude of the coupling constants.[15] *Cis-trans* isomerisation appears slow at 300 K on the NMR timescale. The fact that two isomers are observed for the solution in $MeNO_2$ and only the *trans* isomer in CH_2Cl_2 may be due to solvent dependent isomerisation, but is more likely a consequence of the poor solubility of the *cis* isomer in chlorocarbon solvents.

This poor solubility is also found for the $SnBr_4$ complex, $[SnBr_4(Me_3P)_2]$, in CH_2Cl_2 but far better solubility is again achieved in $MeNO_2$. At 300 K a single resonance is seen in the ^{31}P-{^{1}H} NMR spectrum at δ –3.0 ppm with no evident $^{117/119}Sn$ satellites. Cooling the solution to 250 K resulted in only a slight shift to δ –2.6 ppm due to temperature effects and still no $^{117/119}Sn$ satellites observed. No resonances are observed over the same range in the ^{119}Sn-{^{1}H} NMR spectrum. It seems likely that the observed resonance in the ^{31}P-{^{1}H} NMR spectrum arises from the *trans* isomer, and the absence of $^{1}J(^{31}P\text{-}^{119}Sn)$ couplings or any resonances in the ^{119}Sn-{^{1}H} NMR spectrum reflects rapid reversible ligand dissociation. The limited temperature range of $MeNO_2$ (m.p. –29 °C) prevents the lower temperature studies that proved effective for studying the analogous group 16 donor systems (chapters 2-4).

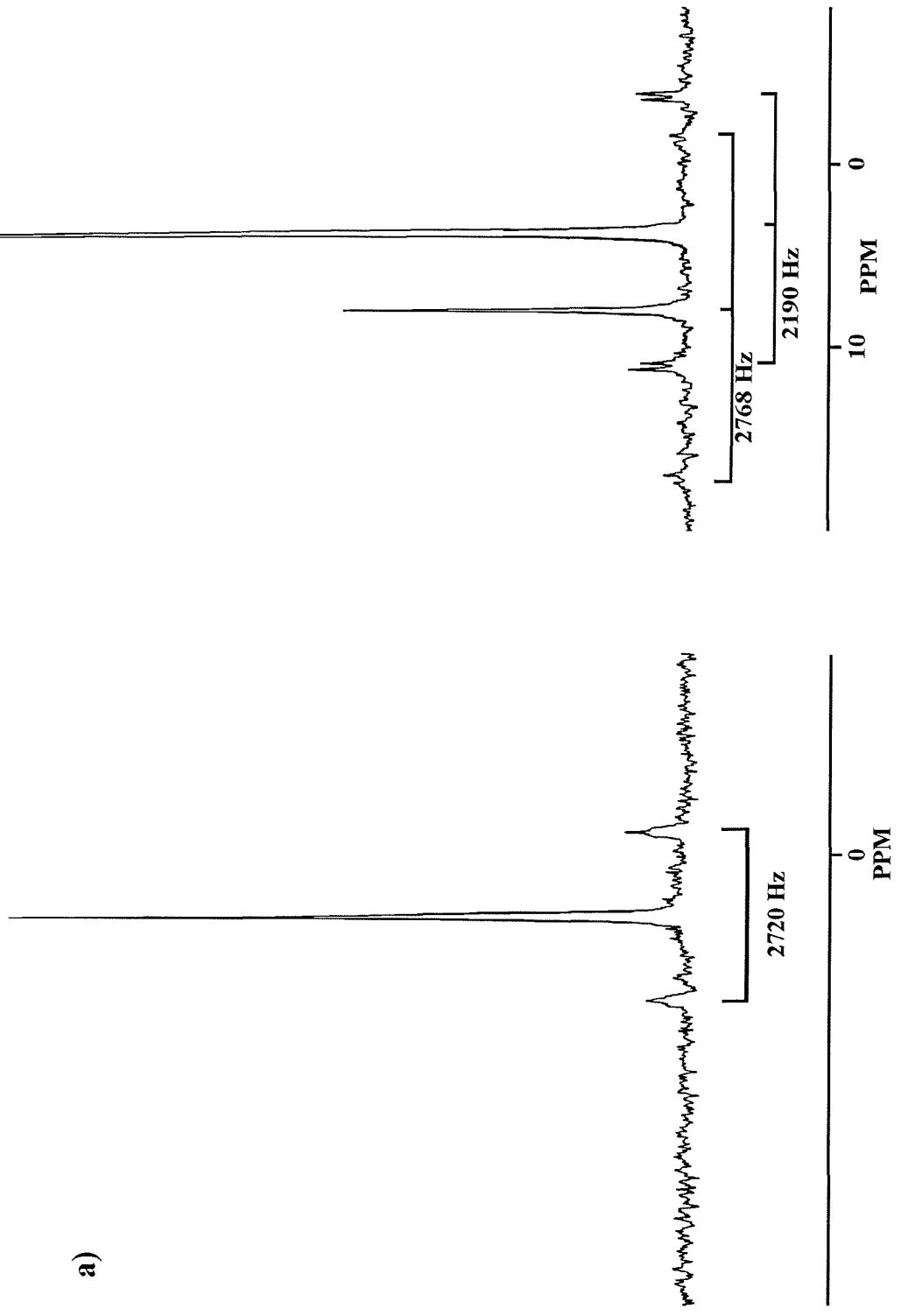

Figure 5.3. $^{31}P-\{^{1}H\}$ NMR Speetra of $[SnCl_4(Me_3P)_2]$ at 300 K in a) $CDCl_3/CH_2Cl_2$ and b) $(CD_3)_2CO/MeNO_2$ solution.

Table 5.2. ^{31}P-{^{1}H} and ^{119}Sn-{^{1}H} NMR data for $[SnX_4(Me_3P)_2]$ complexes

Complex[a]	$\delta(^{31}P$-{^{1}H}) ppm	$\delta(^{119}Sn$-{^{1}H}) ppm	$^{1}J(^{119}Sn$-$^{31}P)$ (Hz)	Solvent	Temperature (K)
$[SnCl_4(Me_3P)_2]$	(*trans*) 6.8	n.o.	2720	CH_2Cl_2	300
$[SnCl_4(Me_3P)_2]$	(*cis*) 3.6	-630(t)	2190	$MeNO_2$	300 (^{119}Sn at 250 K)
	(*trans*) 8.0	-646(t)	2768	$MeNO_2$	300 (^{119}Sn at 250 K)
$[SnBr_4(Me_3P)_2]$	(*trans*) –3.0	n.o.	n.o.	$MeNO_2$	300
$[SnI_4(Me_3P)_2]$	(*trans*) –3.7	n.o.	n.o.	$MeNO_2$	300

a. Samples made up in dried solvents and run immediately.
b. Relative to neat external 85 % H_3PO_4.
c. relative to neat external $SnMe_4$.
d. ± 6 Hz.

Similar results were observed for $[SnI_4(Me_3P)_2]$ with a single resonance observed at δ –3.5 ppm in the ^{31}P-{^{1}H} NMR spectrum (Figure 5.4), but no resonances in the ^{119}Sn-{^{1}H} NMR spectrum in the range studied (300-250 K). A second resonance was present in the ^{31}P-{^{1}H} NMR spectrum at δ 59 ppm, attributed to the formation of the phosphine oxide. This resonance was observed to grow rapidly with time as the complex decomposed.

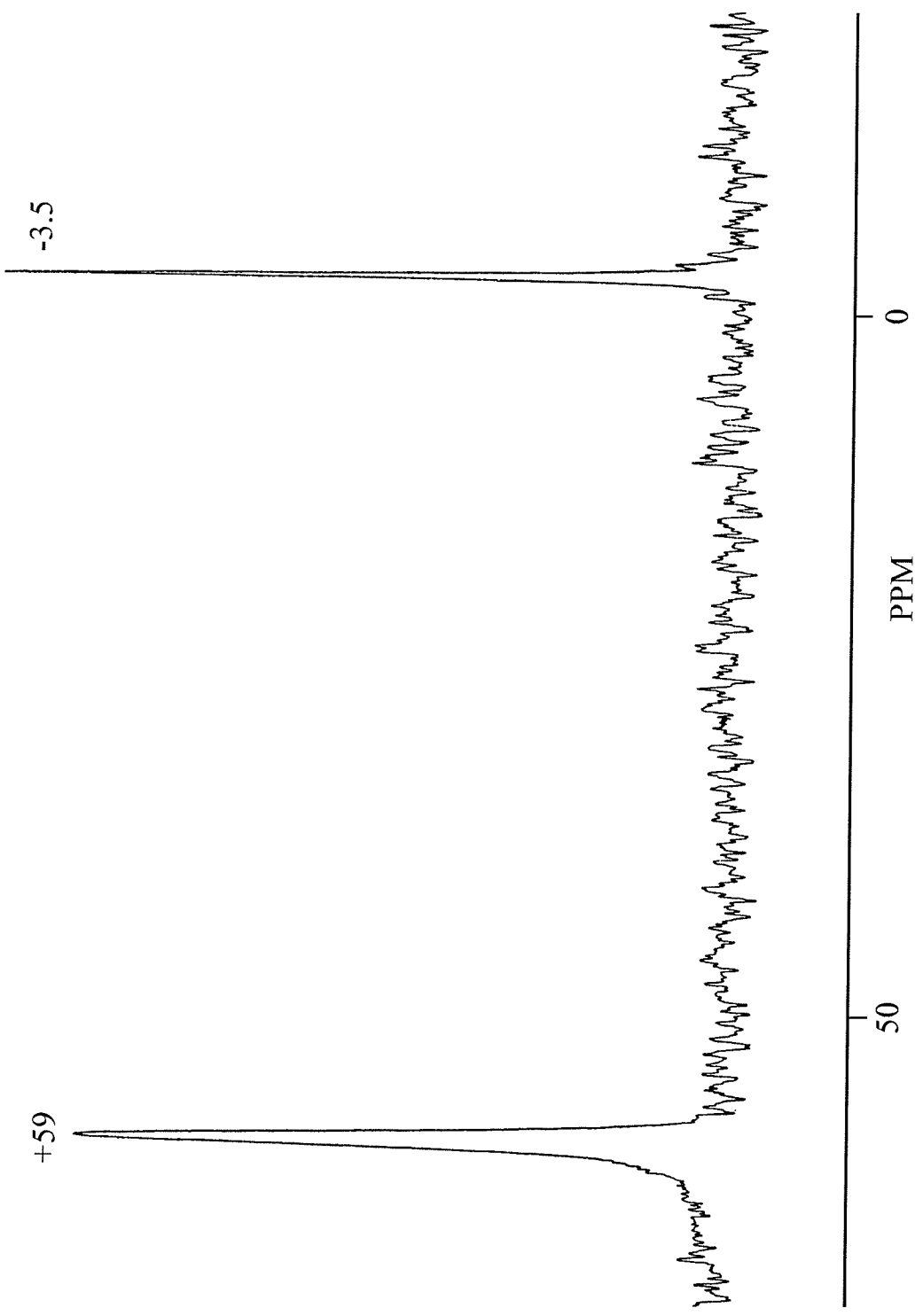

Figure 5.4. $^{31}P-\{^{1}H\}$ NMR spectrum of $[SnI_4(Me_3P)_2]$ in $CDCl_3/MeNO_2$ solution at 300 K

5.2.3. Synthesis and Properties of Bidentate Phosphine Complexes of SnX_4

A range of complexes of type $[SnX_4(L\text{-}L)]$ (where X = Cl, Br or I; L-L = $Me_2P(CH_2)_2PMe_2$ (dmpe), $Ph_2P(CH_2)_2PPh_2$ (dppe) and o-$C_6H_4(PPh_2)_2$) have been isolated from reaction in CH_2Cl_2. In most cases the poor solubility of the SnX_4-diphosphine complexes meant that the products formed immediately from solution as powdered precipitates, the exception being for the SnI_4 complex of o-$C_6H_4(PPh_2)_2$ where the reaction formed a dark red solution with a solid isolated by removal of the solvent *in vacuo*. Due to the extreme moisture sensitivity of the tin(IV) halides and phosphines when in solution, all reactions were carried out under an atmosphere of dry dinitrogen using standard Schlenk techniques. As for the $[SnX_4L_2]$ systems these complexes prove very easily hydrolysed.

IR spectra of the $SnCl_4$ complexes formed all showed the expected four ν(Sn-Cl) bands (theory: $2A_1 + B_1 + B_2$) in the range 300 - 340 cm^{-1} consistent with C_{2v} symmetry.[9] Similarly, the bromide systems also show four ν(Sn-Br) bands in the range 190 – 230 cm^{-1}.[9] Satisfactory microanalyses were obtained for all products isolated. Analytical and spectroscopic data are presented in Table 5.3. Solids were also isolated from the reactions of $Ph_2PCH_2PPh_2$ (dppm) and $Ph_2P(CH_2)_3PPh_2$ (dppp) with SnX_4 (X = Cl or Br). However, while the solids are relatively stable once isolated, with microanalyses and IR spectra confirming 1:1 adduct formation, they proved extremely susceptible to oxidation in solution, with resonances in the $^{31}P\text{-}\{^1H\}$ spectra only observed for decomposition products, and hence these complexes were not studied further.

Table 5.3. Analytical and Spectroscopic data for [SnX_4(diphosphine)] complexes

Complex	Colour	%C[a]	%H	ν(Sn-X)[b] (cm^{-1})	^{1}H NMR[c]
[$SnCl_4$(dmpe)]	White	17.4(17.6)	4.1(3.9)	325, 310, 299, 283	2.18(m), 1.57(m)
[$SnBr_4$(dmpe)]	Yellow	12.0(12.3)	2.6(2.7)	206, 199, 196, 193	2.21(m), 1.60(m)
[SnI_4(dmpe)]	Dark red	9.3(9.3)	2.1(2.1)	-	-
[$SnCl_4$(dppe)]	White	47.1(47.4)	3.8(3.7)	322, 313, 299, 294	2.2(m), 7.2-7.9(m)
[$SnBr_4$(dppe)]	Yellow	37.5(37.2)	2.7(2.9)	220, 217, 208, 205	2.2(m), 7.3-8.0(m)
[SnI_4(dppe)]	Dark red	30.3(30.5)	2.5(2.4)	-	2.25(m), 7.3-7.9(m)
[$SnCl_4${o-$C_6H_4(PPh_2)_2$}]	White	51.1(51.0)	3.5(3.4)	320, 313, 310, 300	-
[$SnBr_4${o-$C_6H_4(PPh_2)_2$}]	Yellow	40.3(40.6)	3.0(3.0)	217, 212, 208, 195	-
[SnI_4{o-$C_6H_4(PPh_2)_2$}]	Dark red	33.3(33.6)	2.4(2.3)	-	-

a. Calculated value in parentheses
b. Nujol mulls.
c. $CDCl_3$ solution 300 K.

5.2.4. Variable Temperature ^{31}P-{^{1}H} and ^{119}Sn-{^{1}H} NMR Spectroscopy

^{31}P-{^{1}H} and ^{119}Sn-{^{1}H} NMR spectroscopic data are presented in Table 5.4. ^{1}H NMR spectra were also collected for all the adducts formed but were relatively uninformative.

Table 5.4. ^{119}Sn-{^{1}H} and ^{31}P-{^{1}H} NMR data for [SnX_4(diphosphine)] complexes

Complex[a]	$\delta(^{31}P$-{^{1}H})[b] (ppm)	$\delta(^{119}Sn$-{^{1}H})[c] (ppm)	$^{1}J(^{119}Sn$-$^{31}P)$[d] (Hz)	Solvent	Temperature (K)
[$SnCl_4$(dmpe)]	-20.9	-617(t)	1080	Me_2CO	300
	-20.9	n.o.	1005	CH_2Cl_2	300
[$SnBr_4$(dmpe)]	-26.0	-1213(t)	680	Me_2CO	300
	-28.5	n.o.	645	CH_2Cl_2	300
[SnI_4(dmpe)][e]	-40 (br)	-2425(t)	~ 200	CH_2Cl_2	190
[$SnCl_4$(dppe)]	-18.8	-626(t)	890	CH_2Cl_2	300
[$SnBr_4$(dppe)]	-31.0	-1212(t)	460	CH_2Cl_2	250
[SnI_4(dppe)]	n.o.	n.o.	n.o.	CH_2Cl_2	190
[$SnCl_4${o-$C_6H_4(PPh_2)_2$}]	-13.9	-607.5(t)	717	CH_2Cl_2	300
[$SnBr_4${o-$C_6H_4(PPh_2)_2$}]	-24.2	-1218(t)	305	CH_2Cl_2	250
[SnI_4{o-$C_6H_4(PPh_2)_2$}]	-52.5	n.o.	n.o.	CH_2Cl_2	190

a. Samples made up in dried solvents and run immediately.
b. Relative to external 85 % H_3PO_4.
c. Relative to neat external $SnMe_4$.
d. ± 6 Hz.
e. Resonances only observed in the presence of excess of the group 15 ligand.

The ^{31}P-{^{1}H} NMR spectrum of [$SnCl_4${o-$C_6H_4(PPh_2)_2$}] in anhydrous CH_2Cl_2 solution at 300 K shows a singlet at δ –13.9 ppm (Figure 5.5a). Satellites from $^{1}J(^{31}P$-$^{117}Sn)$ and $^{1}J(^{31}P$-$^{119}Sn)$ coupling are also clearly visible in the spectrum with values of 690 and 717 Hz respectively. This assignment is confirmed by the ratio between these two figures, $^{1}J(^{31}P$-$^{119}Sn)/^{1}J(^{31}P$-$^{117}Sn)$ = 1.047, which is consistent with the ratio between the magnetogyric ratios of the two tin isotopes, $\gamma(^{119}Sn)/\gamma(^{117}Sn)$ = 1.046. A triplet is observed in the ^{119}Sn-{^{1}H} NMR spectrum (Figure 5.5b) at δ –607.5 ppm,

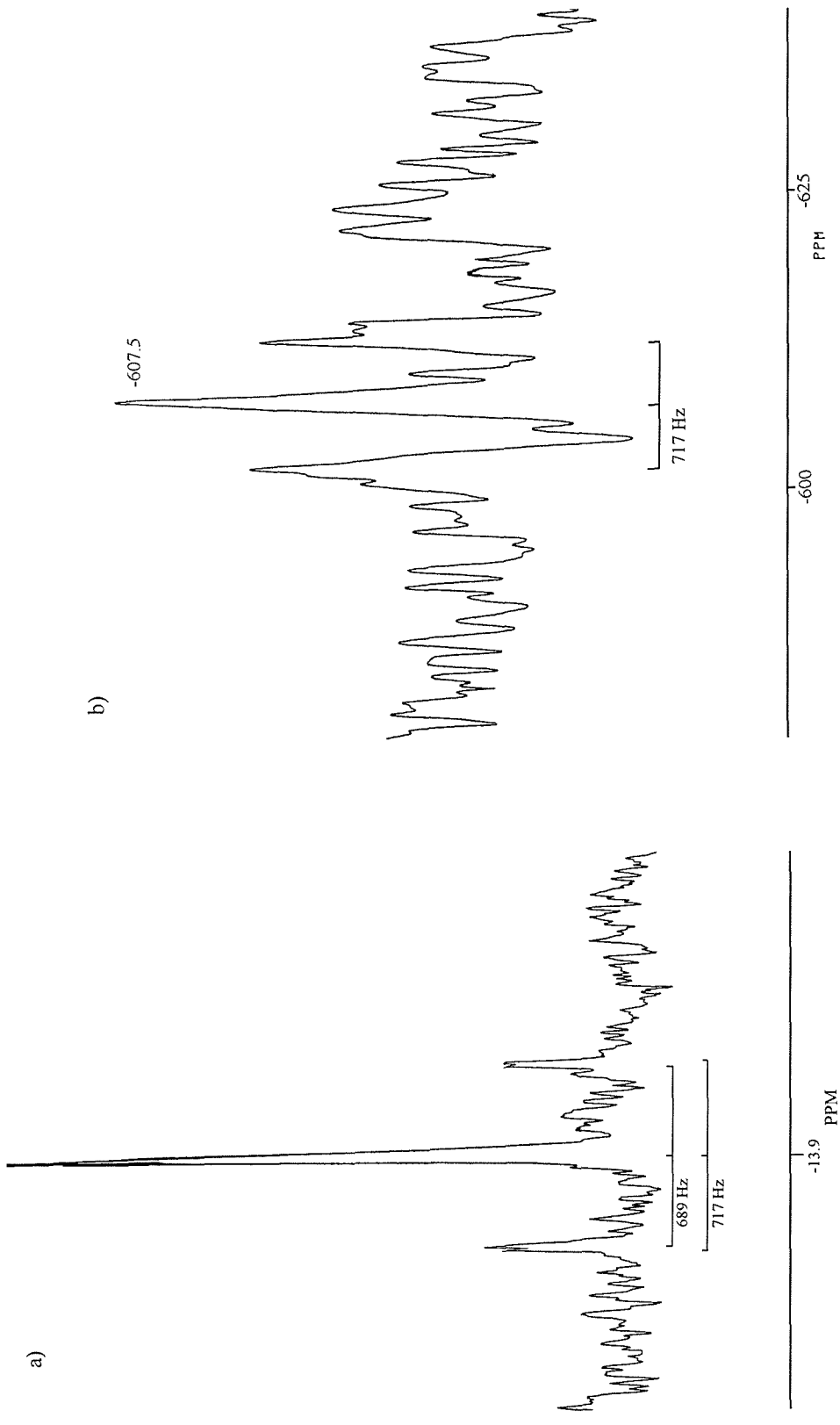

Figure 5.5. **a) ^{31}P-{^{1}H} and b) ^{119}Sn-{^{1}H} NMR spectra of [$SnCl_4${o-$C_6H_4(PPh_2)_2$}] in $CDCl_3/CH_2Cl_2$ solution at 300 K**

within the range observed for octahedral $SnCl_4$ adducts found in chapters 2-4, with the $^1J(^{119}Sn\text{-}^{31}P)$ coupling of the same value as that seen in the $^{31}P\text{-}\{^1H\}$ NMR spectrum, 717 Hz. The spectrum remains relatively unchanged on cooling the solution to 190 K. The same behaviour is seen in the $^{31}P\text{-}\{^1H\}$ NMR spectrum of $[SnBr_4\{o\text{-}C_6H_4(PPh_2)_2\}]$ with a resonance seen at δ –24.2 ppm with $^1J(^{31}P\text{-}^{117/119}Sn)$ coupling with a value of 305 Hz, the spectrum is not sufficiently resolved to distinguish the ^{117}Sn and ^{119}Sn couplings. The $^{119}Sn\text{-}\{^1H\}$ NMR spectrum exhibits a triplet at δ –1218 with $^1J(^{119}Sn\text{-}^{31}P)$ coupling matching that seen in the $^{31}P\text{-}\{^1H\}$ NMR spectrum. Once again cooling the sample to 190 K has little effect on the spectrum. Neither the $^{31}P\text{-}\{^1H\}$ nor the $^{119}Sn\text{-}\{^1H\}$ NMR spectra obtained from $[SnI_4\{o\text{-}C_6H_4(PPh_2)_2\}]$ exhibited any resonances at 300 K in CH_2Cl_2 solution. On cooling the solution to *ca.* 230 K a singlet becomes apparent in the $^{31}P\text{-}\{^1H\}$ NMR spectrum at δ –53 ppm which sharpens on cooling to 190 K. Even at this temperature tin satellites are not observed. However since the line-width at this temperature is still > 200 Hz it is possible that the couplings are obscured since the value of the $^{117/119}Sn\text{-}^{31}P$ couplings reduce rapidly with halide Cl > Br, and the couplings for the iodide species may therefore be very small. No $^{119}Sn\text{-}\{^1H\}$ NMR resonance was observed over the entire temperature range examined (300 – 190 K). Comparison between these three complexes shows that dissociation in the chloro- and bromo-complexes is minimal allowing $^{117/119}Sn\text{-}^{31}P$ couplings to be seen even at 300 K. In comparison the iodo-complex is extremely labile in solution at 300 K, and remains so on the NMR timescale until *ca.* 230 K when a signal becomes visible in the $^{31}P\text{-}\{^1H\}$ NMR spectrum. It was also observed that the iodo-complex was more prone to oxidation in solution, turning into the phosphine oxide rapidly.

Changing the ligand architecture from the rigid o-phenylene backbone to the more flexible dimethylene backbone results in an increased tendency of the $[SnX_4(diphosphine)]$ complexes to reversibly dissociate ligand in solution. This apparent stability in the o-phenylene complexes is attributed to the o-phenylene effect observed by Warren and Bennett[23] where energetically the rigid backbone resists dissociation. The $[SnX_4(dmpe)]$ complexes were very poorly soluble in CH_2Cl_2 such that extremely long accumulations were required. Even then the $^{31}P\text{-}\{^1H\}$ spectra were not clear and convincing $^{119}Sn\text{-}\{^1H\}$ resonances were not observed. Acetone offered vastly improved solubility and the $^{31}P\text{-}\{^1H\}$ NMR spectra observed were similar to those obtained from CH_2Cl_2 solution (allowing for small solvent shifts), and resonances were observed in the $^{119}Sn\text{-}\{^1H\}$ NMR spectra. At 300 K the $^{31}P\text{-}\{^1H\}$ NMR spectrum

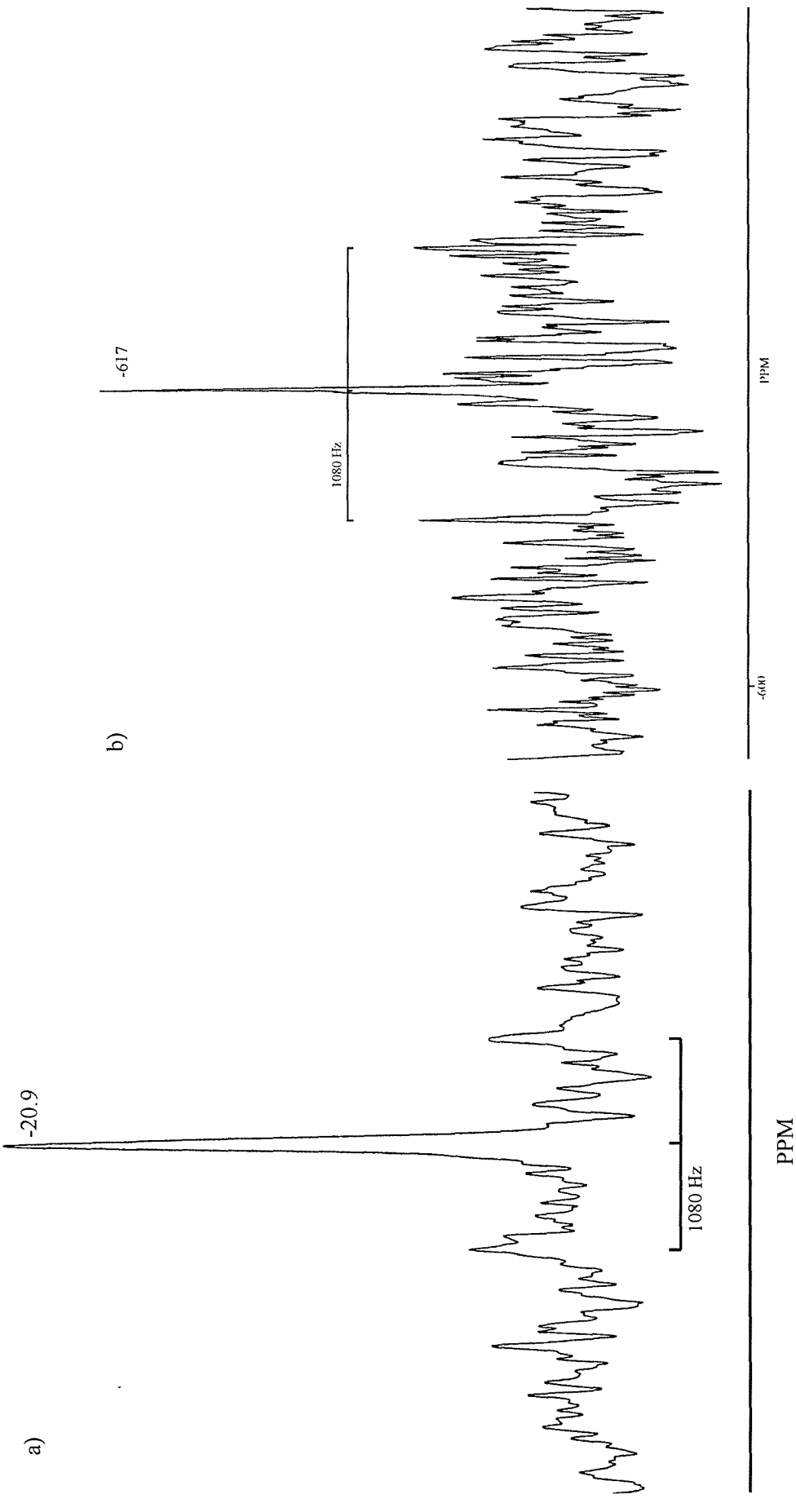

Figure 5.6. a) ^{31}P-{^{1}H} (300 K) and b) ^{119}Sn-{^{1}H} NMR spectra (270 K) of [$SnCl_4$(dmpe)] in $(CD_3)_2CO$/$(CH_3)_2CO$ solution.

of $[SnCl_4(dmpe)]$ in acetone (Figure 5.6a) has a resonance at δ –20.9 ppm with $^1J(^{31}P\text{-}^{117/119}Sn)$ coupling evident with a value of 1080 Hz. The same spectrum is observed in CH_2Cl_2 solution with $^1J(^{31}P\text{-}^{117/119}Sn)$ coupling of 1005 Hz. In CH_2Cl_2 solution no resonance is observed at any temperature (300 – 190 K) in the $^{119}Sn\text{-}\{^1H\}$ NMR spectrum. However, in Me_2CO solution at 270 K a resonance is observed at δ –617 ppm (Figure 5.6b), once again consistent with the observed range for octahedral complexes of $SnCl_4$, and does not arise from an $SnCl_4$ adduct with acetone as $^1J(^{119}Sn\text{-}^{31}P)$ couplings of equal size to those in the $^{31}P\text{-}\{^1H\}$ NMR spectrum are observed. The same behaviour is observed in $[SnBr_4(dmpe)]$ with a triplet in the $^{31}P\text{-}\{^1H\}$ NMR spectrum at δ –26.0 ppm in acetone solution (δ – 28.5 ppm in CH_2Cl_2 solution) with a clearly resolved $^1J(^{31}P\text{-}^{117/119}Sn)$ coupling of value 680 Hz (645 Hz in CH_2Cl_2). Once again the effect of changing solvent in found with no resonance observed in the $^{119}Sn\text{-}\{^1H\}$ NMR spectrum of the CH_2Cl_2 due to poor solubility, but a resonance observed from acetone solution at δ –1213 ppm. This is again consistent with the assigned ranges for octahedral $SnBr_4$ adducts observed previously (chapters 2-4) and with $^1J(^{119}Sn\text{-}^{31}P)$ coupling corresponding to those of the $^{31}P\text{-}\{^1H\}$ NMR spectra. Decomposition of the iodo-complex, $[SnI_4(dmpe)]$, is extremely rapid in solution aided by the high lability of the complex. At 300 K no resonances are observed for the adduct, though several weak signals are observed for decomposition products. After a short period a yellow precipitate is formed from the brown solution. In CH_2Cl_2 solution no resonances are observed at any temperature (300 – 190 K) in either the $^{31}P\text{-}\{^1H\}$ or $^{119}Sn\text{-}\{^1H\}$ NMR spectra. At 190 K in a Me_2CO solution with a 5-fold excess of ligand a broad resonance is observed at δ –40 ppm in the $^{31}P\text{-}\{^1H\}$ NMR spectrum and a poorly defined triplet is seen in the $^{119}Sn\text{-}\{^1H\}$ NMR spectrum at δ –2425 ppm. These values are consistent with the few resonances that were observed in the studies of group 16 systems, and the $^1J(^{119}Sn\text{-}^{31}P)$ coupling of *ca.* 200 Hz is consistent with this coupling not being observed in the spectra of $[SnI_4\{o\text{-}C_6H_4(PPh_2)_2\}]$. On warming to 230 K these signals are lost but reappear on recooling the solution, consistent with ligand dissociation becoming too rapid on the NMR timescale at this temperature.

The complex $[SnCl_4(dppe)]$ is already known to contain a chelating diphosphine from the single crystal X-ray study by Kunkel *et al.*[8] and the octahedral tin(IV) centre is confirmed in the $^{119}Sn\text{-}\{^1H\}$ NMR spectrum (Figure 5.7b) of a solution in CH_2Cl_2 where a resonance is observed at δ –626 ppm with clearly resolved $^1J(^{119}Sn\text{-}^{31}P)$ coupling of value 890 Hz. In the $^{31}P\text{-}\{^1H\}$ NMR spectrum (Figure 5.7b) a clear

Figure 5.7. a) ^{31}P-{^{1}H} (300 K) and b) ^{119}Sn-{^{1}H} NMR spectrum (250 K) of $[SnCl_4(dppe)]$ in $CDCl_3/CH_2Cl_2$ solution.

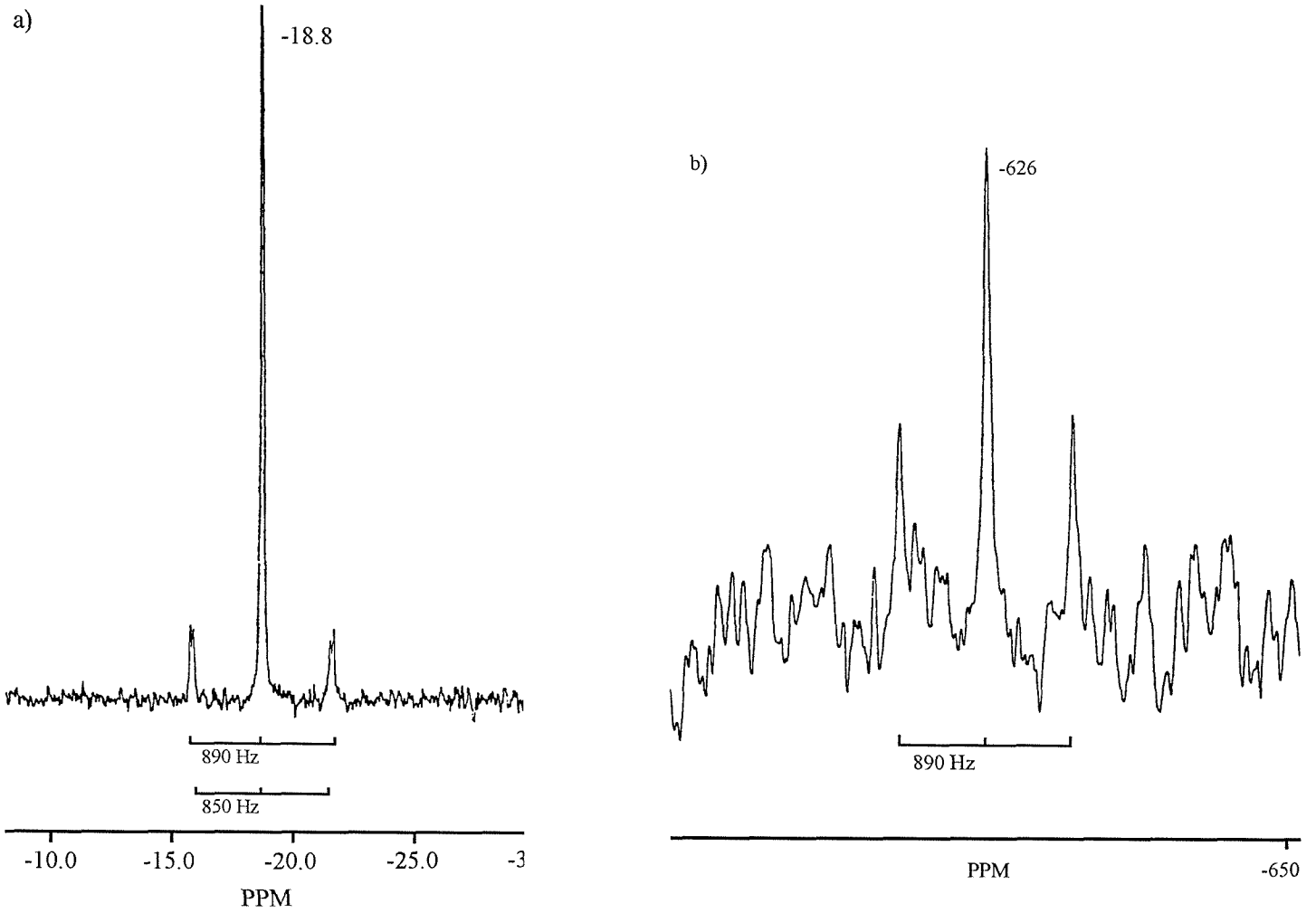

resonance is observed at δ –18.8 ppm with coupling present to both tin nuclei, $^{1}J(^{31}P\text{-}^{117}Sn)$ = 850 and $^{1}J(^{31}P\text{-}^{119}Sn)$ = 890 Hz, $^{1}J(^{31}P\text{-}^{117}Sn)/^{1}J(^{31}P\text{-}^{119}Sn)$ = 1.047. The bromo-complex, [$SnBr_4$(dppe)], was found to be very easily decomposed to the phosphine oxide in solution. The adduct was observed in a sample cooled to *ca.* 250 K at δ –31 ppm with tin satellites observed on further cooling to 190 K of 460 Hz. In the $^{119}Sn\text{-}\{^{1}H\}$ NMR spectrum no resonances were seen until the solution was cooled to 190 K when a triplet at δ –1212 ppm is observed with corresponding $^{1}J(^{119}Sn\text{-}^{31}P)$ of 460 Hz. The effect of altering ligand substituent has therefore increased the lability of the bromo-complex relative to the chloro-, consistent with the observations made previously (chapters 2-4). This trend is further continued for the iodo-complex. No resonances except those of decomposition products, such as phosphine oxides (e.g. δ 48 ppm), are observed at any temperature (300 –190 K) in either the $^{31}P\text{-}\{^{1}H\}$ or the $^{119}Sn\text{-}\{^{1}H\}$ NMR spectra, consistent with this complex still exchanging rapidly in solution.

In chapter 3 it was observed that the chelate-ring parameter, Δ*R* as first formulated by Garrou,[24] for the selenoethers follows the trend of large positive values for five-membered chelate-rings and negative values for the more strained six-membered chelate-rings observed for analogous transition metal complexes.[25] The data collected for *cis*-[$SnCl_4(Me_3P)_2$] and [$SnCl_4$(dmpe)] permits a similar calculation in this study. The coordination shift, Δ, for *cis*-[$SnCl_4(Me_3P)_2$] is 64.6 (3.6 (δ *cis*-[$SnCl_4(Me_3P)_2$]) - -61 (δ free Me_3P)) and Δ for [$SnCl_4$(dmpe)] is 28.5 (-20.9 (δ [$SnCl_4$(dmpe)]) - -49.4 (δ free dmpe)) giving a chelate-ring parameter of –36.1 for the five-membered chelate-ring in [$SnCl_4$(dmpe)]. This is the opposite to the positive value that would be expected for a five-membered chelate-ring.[24,25] The reason for this is not clear but similarly unexpected observations have been made by Schmidbaur *et al.*[26] with an upfield coordination shift in the ^{31}P NMR spectrum of the o-$C_6H_4(PPh_2)_2$ complex of indium(III) chloride rather than the normal downfield shift observed on complexation.[25] The value of the chelate ring parameter is well established as an aid to assignment of structures in transition metal complexes.[25] From our results and those of Schmidbaur *et al.*,[26] it is clear that different effects are operating in main group compounds. Studies of other main group systems and theoretical work are needed before this highly unexpected observation can be explained.

5.2.5. Synthesis and Properties of Bidentate Arsine Complexes of SnX_4

A range of complexes of type $[SnX_4(L\text{-}L)]$ (X = Cl, Br or I for L-L = o-$C_6H_4(AsMe_2)_2$ (diars); X = Cl or Br for L-L = $Ph_2As(CH_2)_2AsPh_2$ (dpae)) have been isolated from reaction in CH_2Cl_2. The adducts formed proved more soluble than those of $[SnX_4(diphosphine)]$ with only the chloro-complexes precipitating from solution. The other complexes formed were isolated by slowly removing the solvent *in vacuo* until a precipitate was formed, which was then filtered and dried *in vacuo*. Given the extreme moisture sensitivity all reactions were carried out in rigorously anhydrous solvent under an atmosphere of dry dinitrogen using standard Schlenk techniques. The arsines are known[3] not to oxidise as readily as the phosphines and while the solids formed appear less air- or moisture-sensitive than the analogous $[SnX_4(diphosphine)]$ complexes all complexes were still stored in a dinitrogen dry-box. IR spectroscopy of the chloro- and bromo- complexes again suggests chelate formation with four ν(Sn-X) bands observed, consistent with C_{2v} symmetry. Satisfactory elemental analyses were obtained for all solids formed. Analytical and spectroscopic data are presented in Table 5.5.

Table 5.5 Analytical and Spectroscopic data for Tin - Diarsine Complexes

Complex	Colour	%C[a]	%H	ν(Sn-X)[b] (cm^{-1})
$[SnCl_4(diars)]$	White	21.8(22.0)	3.0(3.0)	323, 315, 304, 300
$[SnBr_4(diars)]$	Yellow	16.9(16.6)	2.4(2.2)	217, 209, 195
$[SnI_4(diars)]$	Dark red	13.4(13.2)	2.0(1.8)	-
$[SnCl_4(dpae)]$	White	42.2(41.8)	3.4(3.2)	325, 317, 310, 303
$[SnBr_4(dpae)]$	Yellow	34.0(33.8)	2.7(2.6)	217, 212, 195

a. Calculated value in parentheses.
b. Nujol mulls.

5.2.6. Variable Temperature ^{1}H and ^{119}Sn-$\{^{1}H\}$ NMR Spectroscopy

Table 5.6 ^{1}H and ^{119}Sn-$\{^{1}H\}$ NMR data for $[SnX_4(diarsine)]$ complexes

Complex[a]	$\delta(^{1}H)$[b] (ppm)	$\delta(^{119}Sn$-$\{^{1}H\})$[c] (ppm)	Solvent	Temperature (K)
$[SnCl_4(diars)]$	1.89(s), 7.7(m)	-675	CH_2Cl_2	300
$[SnBr_4(diars)]$	1.8(s), 7.6(m)	-1354	CH_2Cl_2	270
$[SnI_4(diars)]$	1.6(s), 7.5(br, m)	-2290	CH_2Cl_2	190
$[SnCl_4(dpae)]$	2.15(s), 7.3-7.8(m)	-662	CH_2Cl_2	250
$[SnBr_4(dpae)]$	2.2(s), 7.3-7.7(m)	-1368	CH_2Cl_2	200

a. Samples made up in dried solvent and run immediately.
b. $CDCl_3$ solution.
c. Relative to neat external $SnMe_4$.

^{1}H and ^{119}Sn-$\{^{1}H\}$ NMR spectroscopic data are presented in Table 5.6. In the ^{1}H NMR spectrum of $[SnCl_4(diars)]$ in CH_2Cl_2 a sharp δ(Me) resonance at 1.89 ppm is observed which shows a significant coordination shift from the free ligand (δ 1.2 ppm). The ^{119}Sn-$\{^{1}H\}$ NMR spectrum (Figure 5.8) shows a single resonance at δ –674 ppm that shows only a small temperature drift on cooling the solution to 190 K. The ^{1}H NMR spectrum of $[SnBr_4(diars)]$ exhibits a broad resonance at δ 1.6 ppm for δ(Me) and a similarly broad feature for the aromatic resonances. Both are seen to sharpen on cooling to *ca.* 270 K. Similarly, no ^{119}Sn-$\{^{1}H\}$ resonance is observed at 300 K but at *ca.* 270 K a singlet is observed at δ –1354 ppm. The resonance is seen to drift only slightly to high frequency on cooling to 190 K. The data are consistent with some reversible ligand dissociation at ambient temperatures, which is slowed on cooling, consistent with the bromo-complexes being more labile in solution than the chloro-complex. Continuing this trend, no resonances are observed at any temperature (300 – 190 K) in the ^{119}Sn-$\{^{1}H\}$ NMR spectrum for the iodo-complex, $[SnI_4(diars)]$, despite the solution being a deep red-brown colour. Similarly, the ^{1}H NMR spectrum only exhibits broad resonances over the same range. When a 10-fold excess of diars ligand

is added to the solution a broad ^{119}Sn-{^{1}H} resonance is observed at δ –2290 ppm. This is tentatively assigned to [SnI_4(diars)] as the resonance falls within the range of previous octahedral [SnI_4(L-L)] complexes. The formation of an octahedral chelate complex was confirmed by an X-ray study (section 5.2.7) of crystals obtained from a CH_2Cl_2 solution. A further study of [$SnCl_4$(diars)] with a 10-fold excess of diars showed no change in the ^{119}Sn-{^{1}H} NMR spectrum over the range 300 – 190 K. This indicates that in marked contrast to the formation of dodecahedral $[MX_4(diars)_2]^{n+}$ by several early transition metals (e.g. Ti(IV), Mo(IV), Nb(V) or Ta(V)),[27] eight-coordinate [$SnCl_4$(diars)$_2$] does not form with tin(IV).

Figure 5.8. ^{119}Sn-{^{1}H} NMR spectrum of [$SnCl_4$(diars)] in $CDCl_3/CH_2Cl_2$ solution at 240 K

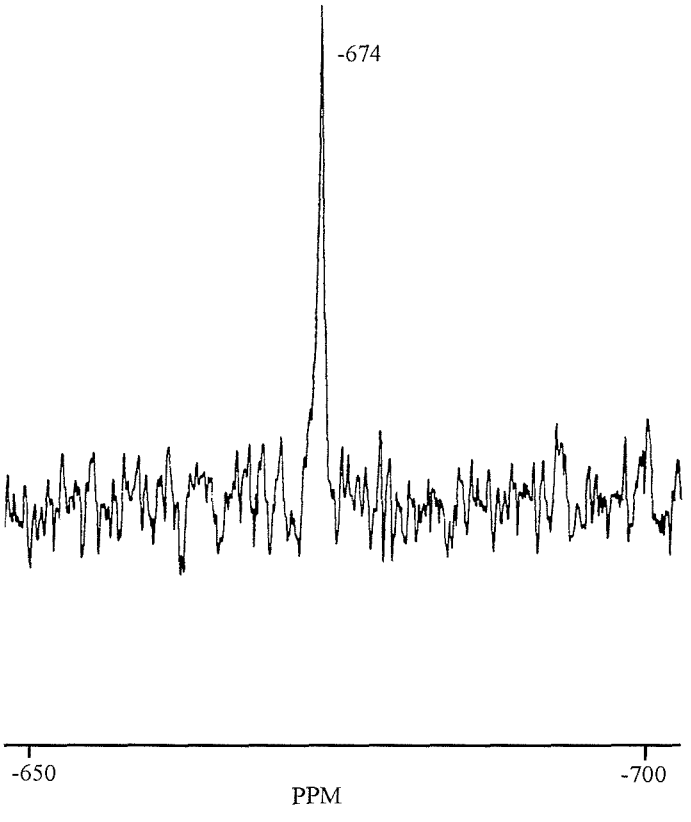

Examining the complexes of dpae, which has dramatically different ligand architecture, there are some immediate observations. The complexes of $SnCl_4$ and $SnBr_4$ were isolable as solids, but although a mixture of SnI_4 and the ligand forms a very dark red solution in CH_2Cl_2, on concentration of the solution *in vacuo* inhomogeneous products were obtained. While these may contain the complex $[SnI_4(dpae)]$ it was not possible to isolate it as a pure product. At 300 K a solution of $[SnCl_4(dpae)]$ in CH_2Cl_2 has no resonances in the ^{119}Sn-$\{^1H\}$ NMR spectrum indicative of ligand dissociation at this temperature. Cooling the solution to *ca.* 270 K a weak resonance at δ –662 ppm is observed which resolves and sharpens at 250 K (Figure 5.9). Again consistent with previous results the bromo-complex, $[SnBr_4(dpae)]$, was found to be more labile in solution such that no resonance is observed in the ^{119}Sn-$\{^1H\}$ NMR spectrum until *ca.* 200 K when a resonance is observed at δ –1368 ppm.

Figure 5.9. ^{119}Sn-$\{^1H\}$ NMR spectrum of $[SnCl_4(dpae)]$ in $CDCl_3/CH_2Cl_2$ solution at 250 K

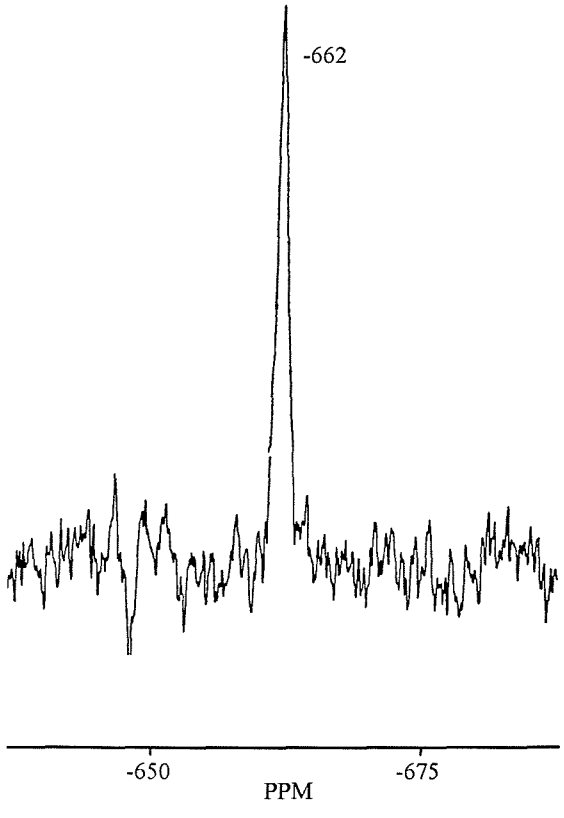

5.2.7. X-ray Structure of [SnI_4(diars)]

Figure 5.10. View of the structure of [SnI_4(diars)] with numbering scheme adopted. H atoms are omitted for clarity and ellipsoids are drawn at 40 % probability

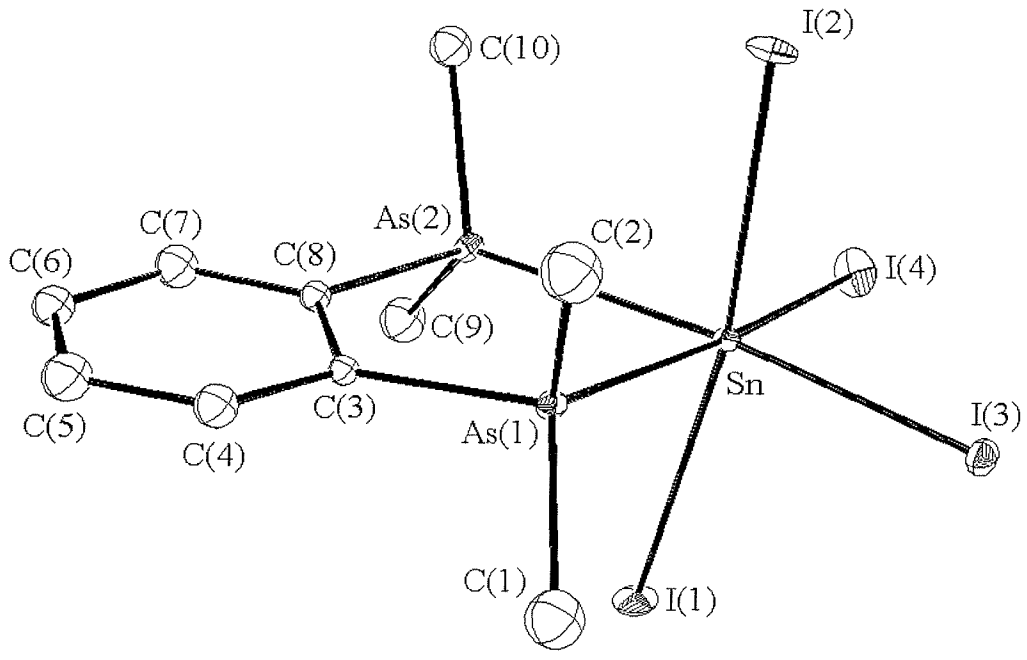

Red-brown crystals of [SnI_4(diars)] were obtained by slow evaporation of a CH_2Cl_2 solution. The structure is shown in Figure 5.10 and selected bond lengths (Å) and angles (°) are presented in Tables 5.7 and 5.8 respectively. The structure shows a distorted octahedral geometry at the tin composed of chelating diarsine and four iodines. All the (*cis*) I-Sn-I angles are greater than 90° (range 92.59(6) – 100.14(6)°) with the As-Sn-As angles of the chelate constrained to 78.47(7)°. This distortion is the same as was observed with the chelates of group 16 ligands (chapters 2-4) and common to all SnX_4 systems where the *cis* isomer is present. A search of the CCDB showed that this was the first structurally characterised example of a tin-arsine complex, and that prior to this structure only six other examples of SnI_4 adducts had been reported[7,28-32] with one structure, *cis*-[$SnI_4\{\eta^1$-*O*-MeS(O)$(CH_2)_3$SMe$\}_2$],[32] featuring previously in

this study (chapter 2). All the previous structures reported have featured harder O-,[29,30,32] N-[28,31] or P-donors.[7] The Sn-I distances present within this tin-arsine complex (Sn-I_{transI} = 2.817(2), 2.860(2) Å, Sn-$I_{transAs}$ = 2.792(2), 2.787(2) Å) may be compared with those in *trans*-$[SnI_4(Pr^n{}_3P)_2]$[7] (2.863(3), 2.872(3) Å), in *cis*-$[SnI_4(Ph_3PO)_2]$[30] (Sn-I_{transI} 2.781(-), 2.810(-), Sn-I_{transO} 2.780(-), 2.861(-) Å), and in *cis*-$[SnI_4\{\eta^1\text{-}O\text{-}MeS(O)(CH_2)_3SMe\}_2]$[32] (Sn-$I_{transI}$ 2.762(2), 2.802(2), Sn-I_{transO} 2.788(2), 2.780(2) Å). While no previous examples of tin-arsine complexes have been structurally characterised to allow comparison of Sn-As distances, the Sn-As distances (2.716(2) and 2.752(2) Å) are seen to be longer than the Sn-P distances of characterised tin-phosphine complexes ($[SnCl_4\{Ph_2P(CH_2)_2PPh_2\}]$,[8] Sn-P = 2.679(2) and 2.653(2) Å) consistent with the increased radius of As over P. For example the same trend is observed in Ni(III) systems with o-$C_6H_4(PMe)_2$ (diphos)[33] and diars.[34] In $[NiCl_2(diars)_2][Cl]$[33] the Ni-As distances (2.340 and 2.345 Å) are seen to be *ca.* 0.1 Å longer than the Sn-P distances observed in $[NiCl_2(diphos)_2][PF_6]$[34] (Ni-P = 2.255 Å).

Table 5.7. Selected bond lengths (Å) with e.s.d.s for $[SnI_4(diars)]$

I(1)	Sn	2.859(2)	I(2)	Sn	2.818(2)
I(3)	Sn	2.792(2)	I(4)	Sn	2.787(2)
Sn	As(1)	2.716(2)	Sn	As(2)	2.752(2)
As(1)	C(1)	1.90(2)	As(1)	C(2)	1.87(2)
As(1)	C(3)	1.93(2)	As(2)	C(8)	1.99(2)
As(2)	C(9)	1.92(3)	As(2)	C(10)	1.98(2)

Table 5.8. Selected bond angles (°) with e.s.d.s for [SnI_4(diars)]

I(1)	Sn	I(2)	169.76(6)	I(1)	Sn	I(3)	94.59(6)
I(1)	Sn	I(4)	92.62(5)	I(1)	Sn	As(1)	85.97(6)
I(1)	Sn	As(2)	84.89(7)	I(2)	Sn	I(3)	93.17(6)
I(2)	Sn	I(4)	92.56(5)	I(2)	Sn	As(1)	87.77(6)
I(2)	Sn	As(2)	85.93(6)	I(3)	Sn	I(4)	100.15(6)
I(3)	Sn	As(1)	87.18(6)	I(3)	Sn	As(2)	165.61(7)
I(4)	Sn	As(1)	172.63(8)	I(4)	Sn	As(2)	94.24(7)
As(1)	Sn	As(2)	78.43(7)	Sn	As(1)	C(1)	117.0(7)
Sn	As(1)	C(2)	116.4(7)	Sn	As(1)	C(3)	108.8(5)
Sn	As(2)	C(8)	107.1(6)	Sn	As(2)	C(9)	120.1(7)
Sn	As(2)	C(10)	116.2(7)				

5.2.8. Synthesis and Properties of o-$C_6H_4(P(O)Ph_2)_2$ Complexes of SnX_4

To verify that the complexes isolated with o-$C_6H_4(PPh_2)_2$ were not phosphine oxide complexes, the complexes of o-$C_6H_4(P(O)Ph_2)_2$ with SnX_4 (X = Cl, Br or I) were prepared. The ligand was easily obtained by iodine oxidation of the diphosphine, o-$C_6H_4(PPh_2)_2$, followed by base hydrolysis.[35] The phosphine oxide is a white, air-stable solid which exhibits ν(P=O) as a very strong broad feature at 1200 cm^{-1} and δ ^{31}P-{^1H} at 33.6 ppm in CH_2Cl_2 solution. The complexes were formed from direct reaction of ligand in CH_2Cl_2 solution with an equimolar solution of SnX_4. The chloro- and bromo-complexes, [SnX_4{o-$C_6H_4(P(O)Ph_2)_2$}] (X = Cl or Br), formed immediately as white and pale yellow precipitates respectively. The reaction of ligand with SnI_4 formed a dark red solution with the solid, [SnI_4{o-$C_6H_4(P(O)Ph_2)_2$}], isolated on removal of CH_2Cl_2 *in vacuo*. The effect of coordination to an SnX_4 acceptor is to lower ν(P=O) by

ca. 50-60 cm^{-1}. Satisfactory elemental analyses were obtained for all solids formed. Analytical and spectroscopic data are presented in Table 5.9.

Table 5.9. Analytical and Spectroscopic data for $[SnX_4\{o\text{-}C_6H_4(P(O)Ph_2)_2\}]$ complexes

Complex	Colour	%C[a]	%H	ν(Sn-X)[b] (cm^{-1})	ν(P-O) (cm^{-1})
$[SnCl_4\{o\text{-}C_6H_4(P(O)Ph_2)_2\}]$	White	49.0(48.8)	3.2(3.5)	318, 325(sh)	1152
$[SnBr_4\{o\text{-}C_6H_4(P(O)Ph_2)_2\}]$	Pale yellow	38.9(39.3)	2.7(2.6)	214(br)	1152
$[SnI_4\{o\text{-}C_6H_4(P(O)Ph_2)_2\}]$	Orange-red	32.8(32.6)	2.3(2.2)	-	1138

a. Calculated value in parentheses.
b. Nujol mulls.

The problems of poor solubility associated with group 16 complexes of SnX_4 which had hindered the solution studies previously proved to be a problem again. The poor solubility of the chloro- and bromo-complexes meant long accumulations were necessary for the $^{31}P\text{-}\{^1H\}$ NMR spectroscopic studies. $^{31}P\text{-}\{^1H\}$ and $^{119}Sn\text{-}\{^1H\}$ NMR spectroscopic data are presented in Table 5.10. At 300 K resonances at δ 41.6 and 42.4 ppm are observed in the $^{31}P\text{-}\{^1H\}$ NMR spectra CH_2Cl_2 solutions of the chloro- and bromo-complexes respectively. Low temperature studies were precluded by precipitation of the complexes on cooling. The poor solubility also prevented $^{119}Sn\text{-}\{^1H\}$ NMR spectra from being recorded. In contrast, the iodo-complex was found to be extremely soluble in CH_2Cl_2 and a resonance at δ 39.8 ppm is observed in the $^{31}P\text{-}\{^1H\}$ NMR spectrum which is essentially unchanged on cooling the solution to 190 K. Even at this lowest temperature no $^{31}P\text{-}^{117/119}Sn$ satellites are observed about the $^{31}P\text{-}\{^1H\}$ resonance and attempts to record $^{119}Sn\text{-}\{^1H\}$ NMR spectra were unsuccessful. This almost certainly indicates that in solution reversible ring opening and/or dissociation are occurring at a rate too rapid to be observed on the NMR timescale. The results of the $^{31}P\text{-}\{^1H\}$ NMR study that were obtained are sufficient to confirm the assignments made for the phosphine complexes were not for phosphine-oxide resonances. They

also confirm that it is these phosphine oxides that are formed when decomposition as a result of oxidation occurs in solution.

Table 5.10. ^{31}P-{^{1}H} and ^{119}Sn-{^{1}H} NMR data for [SnX_4{o-$C_6H_4(P(O)Ph_2)_2$}] complexes

Complex	$\delta(^{31}P$-{^{1}H})[a] (ppm)	$\delta(^{119}Sn$-{^{1}H}) (ppm)	Solvent
[$SnCl_4${o-$C_6H_4(P(O)Ph_2)_2$}]	42.4	n.o.	$CDCl_3/CH_2Cl_2$
[$SnBr_4${o-$C_6H_4(P(O)Ph_2)_2$}]	41.6	n.o.	$CDCl_3/CH_2Cl_2$
[SnI_4{o-$C_6H_4(P(O)Ph_2)_2$}]	39.8	n.o.	$CDCl_3/CH_2Cl_2$

a. Relative to external 85 % H_3PO_4.

5.2.9. X-ray Structure of [SnI_4{o-$C_6H_4(P(O)Ph_2)_2$}]

Crystals of [SnI_4{o-$C_6H_4(P(O)Ph_2)_2$}] were first obtained by slow evaporation of a CH_2Cl_2 solution of [SnI_4{o-$C_6H_4(PPh_2)_2$}]. The solution was prepared and stored inside a dinitrogen dry-box illustrating the extreme sensitivity of these complexes. The crystals were identified as phosphine oxide by comparison of the IR and ^{31}P-{^{1}H} NMR spectra with those of the genuine complex prepared directly from o-$C_6H_4(P(O)Ph_2)_2$.

Two different crystalline forms of [SnI_4{o-$C_6H_4(P(O)Ph_2)_2$}] were obtained. Slow evaporation of the CH_2Cl_2 solution producing red crystals of the diphosphine dioxide complex as a 1:1 CH_2Cl_2 solvate (Figure 5.11) which had a monoclinic cell ($P2_1/c$). A similar CH_2Cl_2 solution of [SnI_4{o-$C_6H_4(PPh_2)_2$}] layered with *n*-hexane produced red crystals that were characterised as an unsolvated orthorhombic form ($C222_1$) of [SnI_4{o-$C_6H_4(P(O)Ph_2)_2$}]. The geometries of the two forms showed no significant differences in bond lengths or angles so the distances quoted are for the solvated form that was the higher quality structure. Selected bond lengths (Å) and angles (°) are presented in Tables 5.11 and 5.12 respectively. The Sn-I_{transI} distances, 2.7759(7) and 2.2976(7) Å and Sn-I_{transO} distances, 2.7839(8) and 2.7796(8) Å, are in

Table 5.11. Selected bond lengths (Å) with e.s.d's for $[SnI_4\{o\text{-}C_6H_4(P(O)Ph_2)_2\}]$

I(1)	Sn	2.7759(7)	I(2)	Sn	2.7976(7)
I(3)	Sn	2.7839(8)	I(4)	Sn	2.7796(8)
Sn	O(1)	2.120(5)	Sn	O(2)	2.138(5)
P(1)	O(1)	1.509(6)	P(1)	C(1)	1.823(8)
P(1)	C(7)	1.793(8)	P(1)	C(13)	1.788(8)
P(2)	O(2)	1.513(5)	P(2)	C(6)	1.808(7)
P(2)	C(19)	1.810(8)	P(2)	C(25)	1.787(8)
C(1)	C(6)	1.42(1)			

Figure 5.11. View of the structure of $[SnI_4\{o\text{-}C_6H_4(P(O)Ph_2)_2\}]$ (monoclinic form $[P2_1/c]$) with numbering scheme adopted. Ellipsoids are drawn at 40 % and H atoms and the CH_2Cl_2 solvate are omitted for clarity

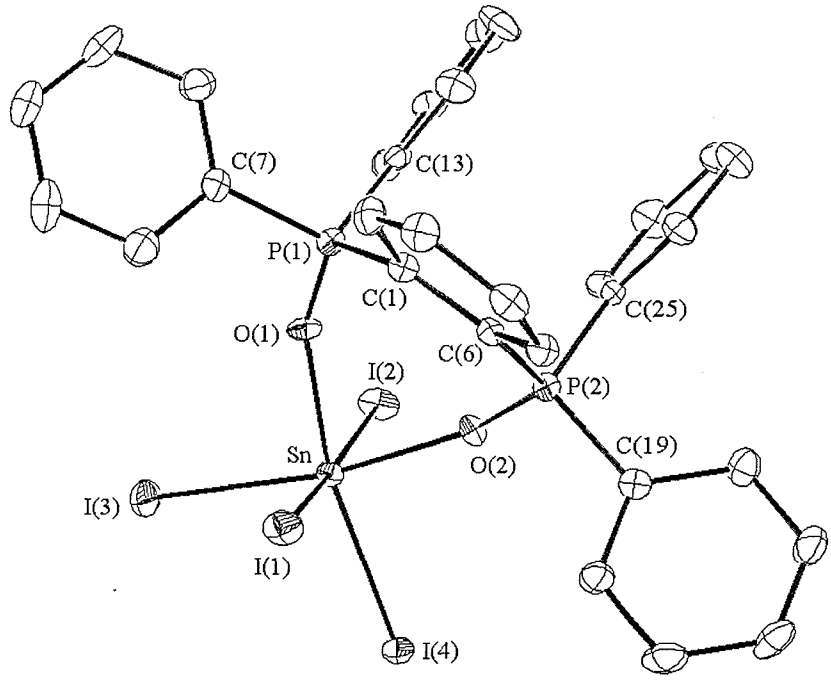

good agreement with the previous structurally characterised example of oxide complexes of SnI_4.[29,30,32] The Sn-O distances, 2.120(5) and 2.138(5) Å, are similar to those in *cis*-$[SnI_4(Ph_3PO)_2]$,[30] 2.148(-) and 2.119(-)Å. From a study of the CCDB this structure appears to be the first reported example of a complex of this diphosphine dioxide and features an unusual seven-member chelate-ring. The ring itself appears to be relatively unstrained with O-Sn-O angles of 79.6(2) and 80.6(4)° for the solvated and unsolvated forms. Seven-membered chelate-rings of this variety have been observed previously for $[Cu\{o\text{-}C_6H_4(P(O)Ph_2\}_2Cl][CuCl_4]$.[36] The angles within this complex are comparable, 84.6(4)°, and also relatively unstrained.

Table 5.12. Selected bond angles (°) with e.s.d's for $[SnI_4\{o\text{-}C_6H_4(P(O)Ph_2)_2\}]$

I(1)	Sn	I(2)	172.42(3)	I(1)	Sn	I(3)	92.25(2)
I(1)	Sn	I(4)	92.90(2)	I(1)	Sn	O(1)	87.0(1)
I(1)	Sn	O(2)	91.6(1)	I(2)	Sn	I(3)	91.67(2)
I(2)	Sn	I(4)	92.89(2)	I(2)	Sn	O(1)	86.4(1)
I(2)	Sn	O(2)	83.6(1)	I(3)	Sn	I(4)	98.93(3)
I(3)	Sn	O(1)	92.3(1)	I(3)	Sn	O(2)	170.8(1)
I(4)	Sn	O(1)	168.8(1)	I(4)	Sn	O(2)	89.2(1)
Sn	O(1)	P(1)	147.7(3)	Sn	O(2)	P(2)	149.1(3)
P(1)	C(1)	C(6)	126.4(6)	P(2)	C(6)	C(1)	124.7(6)
O(1)	Sn	O(2)	79.6(2)	O(1)	P(1)	C(1)	115.3(3)
O(1)	P(1)	C(7)	107.7(3)	O(1)	P(1)	C(13)	110.3(3)
O(2)	P(2)	C(6)	113.5(3)	O(2)	P(2)	C(19)	109.1(3)
O(2)	P(2)	C(25)	110.6(3)	C(1)	P(1)	C(7)	105.6(3)
C(1)	P(1)	C(13)	108.7(3)	C(6)	P(2)	C(19)	108.3(3)
C(6)	P(2)	C(25)	106.9(3)	C(7)	P(1)	C(13)	109.1(4)
C(19)	P(2)	C(25)	108.3(3)				

5.3. Conclusions

The products $[SnX_4(Me_3P)_2]$ (where X = Cl, Br or I) arising from the reactions of SnX_4 with Me_3P and those with bidentate phosphines, $[SnX_4\{R_2P(CH_2)_2PR_2\}]$ (where X = Cl, Br or I; R = Me or Ph) and $[SnX_4\{o\text{-}C_6H_4(PPh_2)_2\}]$ (X = Cl, Br or I) have been prepared in high yield. For comparison the complexes $[SnX_4\{o\text{-}C_6H_4(P(O)Ph_2)_2\}]$ (X = Cl, Br or I) have also been prepared in high yield. A detailed examination of the variable temperature $^{119}Sn\text{-}\{^1H\}$ and $^{31}P\text{-}\{^1H\}$ NMR spectroscopy over the temperature range 300 – 190 K has been presented. Of interest in the variable temperature NMR spectroscopic studies are the reversible ligand dissociation in solution, including ring opening for chelate complexes. The results were complicated by the easy oxidation of the phosphine ligands, but the studies do show that the phosphine complexes are more stable than the arsine complexes in strictly anhydrous, oxygen free conditions. The effects of altering the ligand architecture is clear, with methyl substituted ligands forming more stable complexes than those of the phenyl substituted ligands. It is clear that complexes involving a five-membered chelate-ring are typically more stable that those featuring four- or six-membered chelate-rings. The results also clearly illustrate that the stability of the complexes formed decreases with the SnX_4 acceptor: X = Cl > Br >> I consistent with previous studies.[12] It is also apparent that these better σ-donor group 15 ligands form more stable complexes than the equivalent group 16 ligands. X-ray studies have been used to structurally characterise the first example of a tin-arsine complex, and also $[SnI_4\{o\text{-}C_6H_4(P(O)Ph_2)_2\}].CH_2Cl_2$ and $[SnI_4\{o\text{-}C_6H_4(P(O)Ph_2)_2\}]$, featuring highly unusual seven-member chelate-rings that appear unstrained.

5.4. Experimental

The tin(IV) chloride, bromide and iodide and the ligands Me_3P, $Me_2P(CH_2)_2PMe$ (dmpe) and $Ph_2P(CH_2)_2PPh_2$ (dppe), were purchased from *Aldrich Chemicals*. The ligands *o*-$C_6H_4(PPh_2)_2$,[37] $Ph_2As(CH_2)_2AsPh_2$ (dpae)[38] and *o*-$C_6H_4(AsMe_2)_2$ (diars)[39] were all prepared by following literature methods.

All of the reactions were carried out under an atmosphere of dry nitrogen in dry solvents purchased from *Aldrich Chemicals*, using standard Schlenk, vacuum-line and dry box techniques.

Single Crystal X-ray Diffraction

Single crystals of $[SnI_4\{o\text{-}C_6H_4(AsMe_2)_2\}]$ and $[SnI_4\{o\text{-}C_6H_4(P(O)Ph_2)_2\}].CH_2Cl_2$ and $[SnI_4\{o\text{-}C_6H_4(P(O)Ph_2)_2\}]$ were obtained from a solution of the appropriate complex in CH_2Cl_2. Crystals of $[SnI_4\{o\text{-}C_6H_4(P(O)Ph_2)_2\}]$ were obtained from a CH_2Cl_2 solution of the complex layered with *n*-hexane. It was assumed that the crystals were moisture sensitive and therefore in each case the selected crystal was coated with mineral oil, mounted on a glass fibre using silicone grease as adhesive, and immediately placed in a stream of cold nitrogen gas. Data collection used a Rigaku AFC7S four-circle diffractometer equipped with an Oxford Cryostreams low temperature attachment operating at 150 K, using graphite-monochromated Mo-K_α X-radiation (λ = 0.71073 Å), ω-2θ scans. The intensities of three standard reflections were monitored every 150 reflections. No significant crystal decay or movement was observed. As there were no identifiable faces for $[SnI_4\{o\text{-}C_6H_4(P(O)Ph_2)_2\}]$ and $[SnI_4\{o\text{-}C_6H_4(P(O)Ph_2)_2\}].CH_2Cl_2$ the raw data were corrected for absorption using psi-scans. The weighting scheme $w^{-1} = \sigma^2(F)$ gave satisfactory agreement analyses in each case.

The structures were solved by direct methods,[40] and then developed by iterative cycles of full-matrix least-squares refinement (based on *F*) and difference Fourier syntheses which located all non-H atoms in the asymmetric unit.[41] For $[SnI_4\{o\text{-}C_6H_4(AsMe_2)_2\}]$ an empirical absorption correction using DIFABS[42] was applied to the raw data at isotropic convergence, as psi scans did not provide a satisfactory absorption correction. All non-H atoms in the structures were refined anisotropically and H atoms were placed in fixed, calculated positions with *d*(C-H) = 0.96 Å for $[SnI_4\{o\text{-}C_6H_4(P(O)Ph_2)_2\}]$ and $[SnI_4\{o\text{-}C_6H_4(P(O)Ph_2)_2\}].CH_2Cl_2$. Only Sn, I and As atoms

were refined anisotropically, C atoms were refined isotropically as they turn non-positive definite when refined anisotropically, probably a result of an imperfect absorption correction. For $[SnI_4\{o\text{-}C_6H_4(AsMe_2)_2\}]$ and $[SnI_4\{o\text{-}C_6H_4(P(O)Ph_2)_2\}]$ the Flack parameter was refined and indicated the correct enantiomorph in each case.

Crystallographic data for these structures are presented in Table 5.13.

Table 5.13. Crystallographic data

Compound	$[SnI_4\{o\text{-}C_6H_4(AsMe_2)_2\}]$	$[SnI_4\{o\text{-}C_6H_4(P(O)Ph_2)_2\}].CH_2Cl_2$	$[SnI_4\{o\text{-}C_6H_4(P(O)Ph_2)_2\}]$
Formula	$C_{10}H_{16}As_2SnI_4$	$C_{31}H_{26}Cl_2O_2P_2SnI_4$	$C_{30}H_{24}O_2P_2SnI_4$
Formula Weight	912.39	1189.71	1104.77
Colour, morphology	Red, plate	Red, block	Red, block
Crystal dimensions/mm	0.80 x 0.45 x 0.15	0.67 x 0.35 x 0.30	0.30 x 0.20 x 0.20
Crystal System	Orthorhombic	Monoclinic	Orthorhombic
Space Group	$P2_12_12_1$	$P2_1/c$	$C222_1$
a/Å	14.174(8)	10.119(2)	11.736(3)
b/Å	15.598(6)	20.098(2)	18.672(4)
c/Å	9.247(2)	18.054(2)	31.896(4)
β/°	90	90.37(1)	90
U/Å^3	2044(1)	3671.5(9)	6989(2)
Z	4	4	8
Scan type	ω-2θ	ω-2θ	ω-2θ
$F(000)$	1616	2216	4096
D_c/g cm^{-3}	2.964	2.152	2.100
μ(Mo-K_α)/cm^{-1}	104.91	43.20	43.82
Transmission factors (max. and min.)	1.000, 0.441	1.000, 0.578	1.000, 0.678
No. of Unique obs. reflections	2074	6670	3402
R_{int} (based on F^2)		0.023	
Unique obs. Reflections with $[I_o > 2.5\sigma(I_o)]$	1746	5349	1961
No. of parameters	104	379	202
Goodness of fit	1.94	2.62	1.45
$R(F_o)$	0.037	0.035	0.039
$R_w(F_o)$	0.040	0.043	0.039
Max. residual peak/eÅ^{-3}	1.40	1.07	0.53
Max. residual trough/eÅ^{-3}	-1.48	-1.22	-0.50

$$R = \Sigma (|F_{obs}|_i - |F_{calc}|_i)/\Sigma |F_{obs}|_i$$

$$R_w = \sqrt{[\Sigma w_i(|F_{obs}|_i - |F_{calc}|_i)^2 / \Sigma w_i|F_{obs}|_i^2]}$$

$$GOF = [\Sigma (|F_{obs}|_i - |F_{calc}|_i)/\sigma_i]/(n - m) \approx 1$$

o-$C_6H_4(P(O)Ph_2)_2$[35]

A solution of o-$C_6H_4(PPh_2)_2$ (0.9 g, 2 mmol) in $CHCl_3$ (15 cm^3) was treated with a solution of diiodine (1.05 g, 4 mmol) in $CHCl_3$ (5 cm^3). The brownish solution was transferred to a separating funnel and shaken with aqueous 2 M NaOH (20 cm^3). The colourless organic phase was separated and the $CHCl_3$ removed under reduced pressure. The oil produced was recrystallised from $CHCl_3$/EtOH to give white crystals. Yield 0.80 g, 83 %. $^{31}P\{^1H\}$ NMR (CH_2Cl_2) + 33.6, IR (Nujol mull) ν(P=O) = 1200 cm^{-1}. Found: C, 75.1; H, 5.3. Calculated for $C_{30}H_{24}O_2P_2$: C, 75.3; H, 5.0 %. EI mass spectrum *m/z* = 477, 401. Calculated P^+ = 477, $[P\text{-Ph}]^+$ = 401.

Complex Synthesis

[$SnX_4(PMe_3)_2$]

A solution of tin(IV) halide (1 mmol) in dichloromethane (20 cm^3) was added to a solution of trimethylphosphine (0.15 g, 2 mmol) in dichloromethane (20 cm^3). With tin(IV) chloride (0.26 g) the complex, [$SnCl_4(PMe_3)_2$], precipitated as a white powder which was filtered off and dried *in vacuo*. For the same method with tin(IV) bromide (0.44 g, 0.1 mmol) and iodide (0.63 g, 1 mmol), the complexes [$SnBr_4(PMe_3)_2$] and [$SnI_4(PMe_3)_2$] were produced as yellow precipitates.

[SnX_4(dmpe)]

A solution of tin(IV) chloride (0.26 g, 1 mmol) in dichloromethane (20 cm^3) was added to a solution of dmpe (0.15 g, 1 mmol) in dichloromethane (20 cm^3). The complex, [$SnCl_4$(dmpe)], precipitated as a white powder which was filtered off and dried *in vacuo*. The same method with tin(IV) bromide (0.44 g, 1 mmol) formed the complex, [$SnBr_4$(dmpe)], as a yellow precipitate. The complex [SnI_4(dmpe)] as obtained on removal of solvent from the reaction of tin(IV) iodide (0.63 g, 1 mmol) and dmpe (0.15 g, 1 mmol) in dichloromethane (40 cm^3).

[SnX_4(dppe)]

Using the same method tin(IV) chloride (0.13 g, 1 mmol) reacted with dppe (0.2 g, 0.5 mmol) to give the complex, [$SnCl_4$(dppe)], as a white precipitate which was filtered and dried *in vacuo*. The same method with tin(IV) bromide (0.22 g, 0.5 mmol) yielded the complex, [$SnBr_4$(dppe)], as a yellow precipitate. Removal of solvent from

the reaction of tin(IV) iodide (0.32 g, 0.5 mmol) with dppe (0.2 g, 0.5 mmol) in dichloromethane (40 cm^3) produced the complex [SnI_4(dppe)] as a dark red solid.

[SnX_4(o-$C_6H_4(PPh_2)_2$]

The same method for the reaction of tin(IV) chloride (0.13 g, 0.5 mmol) and (o-$C_6H_4(PPh_2)_2$ (0.23 g, 0.5 mmol) formed the complex, [$SnCl_4$(o-$C_6H_4(PPh_2)_2$], as a white precipitate. Tin(IV) bromide (0.22 g, 0.5 mmol) reacted with (o-$C_6H_4(PPh_2)_2$ (0.23 g, 0.5 mmol) to form a yellow precipitate. Tin(IV) iodide (0.32 g, 0.5 mmol) reacted with (o-$C_6H_4(PPh_2)_2$ (0.23 g, 0.5 mmol) in dichloromethane (40 cm^3) to give a red solution. The complex, [SnI_4(o-$C_6H_4(PPh_2)_2$], was isolated by removal of solvent *in vacuo*.

[SnX_4(dpae)]

Reaction of tin(IV) chloride (0.13 g, 0.5 mmol) with dpae (0.245 g, 0.5 mmol) in dichloromethane (40 cm^3) produced the complex, [$SnCl_4$(dpae)], as a white precipitate which was filtered and dried *in vacuo*. The same reaction with tin(IV) bromide (0.22 g, 0.5 mmol) produced a yellow solution which yielded the complex [$SnBr_4$(dpae)] as a yellow solid on removal of solvent *in vacuo*.

[SnX_4(diars)]

The same method for the reaction of tin(IV) chloride (0.13 g, 0.5 mmol) with diars (0.145 g, 0.5 mmol) yielded the complex, [$SnCl_4$(diars)], as a white precipitate which was filtered off and dried *in vacuo*. With tin(IV) bromide (0.22 g, 0.5 mmol) a yellow solution was produced which yielded a yellow solid, [$SnBr_4$(diars)], on removal of solvent *in vacuo*. The same reaction with tin(IV) iodide (0.33 g, 0.5 mmol) formed a red solution, with a dark red solid, [SnI_4(diars)], isolated by removal of solvent *in vacuo*.

[SnX_4(o-$C_6H_4(P(O)Ph_2)_2$)]

Following the same method reaction of tin(IV) chloride (0.13 g, 0.5 mmol) with (o-$C_6H_4(P(O)Ph_2)_2$) (0.24 g, 0.5 mmol) produced a white precipitate which was filtered and dried *in vacuo*. Tin(IV) bromide (0.22 g, 0.5 mmol) with (o-$C_6H_4(P(O)Ph_2)_2$) (0.13 g, 0.5 mmol) produced a yellow solution by the same method, from which a yellow solid was isolated by removal of solvent *in vacuo*. Similarly tin(IV) iodide (0.33 g, 0.5 mmol) formed a red solution with (o-$C_6H_4(P(O)Ph_2)_2$) (0.13 g, 0.5 mmol)

in dichloromethane (40 cm^3) which yielded a dark red solid on removal of solid *in vacuo*.

References

[1] J. A. C. Allison and F. G. Mann, *J. Chem. Soc.*, 1949, 2915.

[2] I. R. Beattie, *Q. Rev. Chem. Soc.*, 1963, **17**, 382.

[3] W.Levason and C. A. McAuliffe, *Coord. Chem. Rev.*, 1976, **19**, 173.

[4] J. D. Dumas and M. Gomel, *Bull. Soc. Chim. France*, 1974, 1885.

[5] P. G. Harrison, B. C. Lane and J. J. Zuckerman, *Inorg. Chem.*, 1972, **11**, 1537.

[6] D. Cunningham, M. J. Frazer and J. D. Donaldson, *J. Chem. Soc. A*, 1971, 2049.

[7] N. Bricklebank, S. M. Godfrey, C. A. McAuliffe and R. G. Pritchard, *J. Chem. Soc., Chem. Commun.*, 1994, 695; N. Bricklebank, S. M. Godfrey, C. A. McAuliffe and K. C. Molloy, *J. Chem. Soc., Dalton Trans.*, 1995, 1593.

[8] F. Kunkel, K. Dehnicke, H. Goesmann and D. Fenske, *Z. Naturforsch., Teil B*, 1995, **50**, 848.

[9] F. Sarikhaya, *Synth. React. Inorg. Met. Org. Chem.*, 1989, **19**, 641.

[10] I. R. Beattie and G. A. Ozin, *J. Chem. Soc. A*, 1970, 370; D. K. Frieson and G. A. Ozin, *Can. J. Chem.*, 1973, **51**, 2685.

[11] G. G. Mather, G. M. McLaughlin and A. Pidcock, *J. Chem. Soc., Dalton Trans.*, 1973, 1823.

[12] P. G. Harrison in *The Chemistry of Tin*, P. G. Harrison (Editor), Blackie, New York, 1989, p. 30.

[13] R. Colton, D. Dakternieks and C.-A. Harvey, *Inorg. Chim. Acta*, 1982, **61**, 1.

[14] V. S. Petrosyan, N. S. Yashina and E. J. Gefel, *Silicon Germanium Tin Lead Compd.*, 1985, **9**, 1387.

[15] W. McFarlane and N. H. Rees, *Polyhedron*, 1989, **8**, 2047.

[16] O. A. Reutov, V. S. Petrosyan, N. S. Yashina and E. I. Gefel, *J. Organomet. Chem.*, 1988, **341**, 31.

[17] J. F. Malone and B. E. Mann, *Inorg. Nucl. Chem. Lett.*, 1972, **8**, 819.

[18] D. Dakternieks, Hongjian Zhu and E. R. T. Tiekink, *Main Group Metal Chemistry*, 1994, **17**, 519.

[19] R. Rivest, S. Singh and C. Abraham, *Can. J. Chem.*, 1967, **45**, 3137.

[20] N. Ohkaku and K. Nakamoto, *Inorg. Chem.*, 1973, **12**, 2446.

[21] R. J. H. Clark, *J. Chem. Soc.*, 1965, 5699.

[22] S.J. Blunden, D. Searle and P.J. Smith, *Inorg. Chim. Acta*, 1985, **98**, 185.

[23] L. F. Warren and M. A. Bennett, *Inorg. Chem.*, 1976, **15**, 3126.

[24] P.E. Garrou, *Chem. Rev.*, 1981, **81**, 229.

[25] E. G. Hope and W. Levason, *Coord. Chem. Rev.*, 1993, **122**, 109.

[26] M. Sigl, A. Schier and H. Schmidbaur, *Eur. J. Inorg. Chem.*, 1998, 203.

[27] M. G. B. Drew, A. P. Walters and J. D. Wilkins, *Acta Crystallogr., Sect. B*, 1975, **31**, 324.

[28] K. A. Paseshnitchenko, L. A. Aslanov, A. V. Yatsenko and S. V. Medvedev, *Koord. Khim.*, 1984, **10**, 1279.

[29] A. V. Yatsenko, S. V. Medvedev, K. A. Paseshnitchenko and L. A. Aslanov, *J. Organomet. Chem.*, 1985, **284**, 181.

[30] A. I. Tursina, L. A. Aslanov, V. V. Chernyshev, S. V. Medvedev and A. V. Yatsenko, *Koord. Khim.*, 1986, **12**, 420.

[31] J. Angenault, J.-C. Couturier and E. Reculeau, *Rev. Chim. Miner.*, 1979, **16**, 157.

[32] S. E. Dann, A. R. J. Genge, W. Levason and G. Reid, *J. Chem. Soc., Dalton Trans.*, 4471, 1996.

[33] P. K. Bernstein, G. A. Rodley, R. Marsh and H. B. Gray, *Inorg. Chem.*, 1972, **11**, 3040.

[34] C. Mahadevan, M. Seshasayee, B. L. Ramakrishna and P. T. Manoharan, *Acta Crystallogr., Sect. C*, 1985, **41**, 38.

[35] F. Canziani, F. Zingales and U. Sartorelli, *Gazz. Chim. Ital.*, 1964, **94**, 848.

[36] M. D. Spicer, Ph. D. Thesis, Southampton University, 1988.

[37] S. J. Higgins, Ph.D Thesis, University of Southampton, 1984.

[38] A. G. Aguiar, J. T. Mague, H. J. Aguiar, T. G. Archibald and B. Prejean, *J. Org. Chem.*, 1968, **33**, 1681.

[39] R. D. Feltham, A. Kasenally and R. S. Nyholm, *J. Organomet. Chem.*, 1967, **7**, 285.

[40] SHELXS-86, program for crystal structure solution, G. M. Sheldrick, *Acta Crystallogr., Sect. A*, 1990, **46**, 467.

[41] TEXSAN, Crystal Structure Analysis Package, Molecular Structure Corporation, Houston, TX, 1992.

[42] N. Walker and D. Stuart, *Acta Crystallogr., Sect A.*, 1983, **39**, 158.

Chapter 6

Bismuth(III) Halide Complexes of Bidentate Group 15 and 16 Ligands

6.1. Introduction

The complexes of tin(IV) halides with a variety of group 15 and group 16 ligands were studied in chapters 2-5 of this work. They formed octahedral complexes with either mono- or bi-dentate ligands, even forming highly strained four-membered chelate-rings in some cases. This chapter examines the complexes formed between the bismuth(III) halides and a variety of bidentate ligands of differing architecture from groups 15 and 16.

In the +3 oxidation state the elements of group 15 have a lone pair of electrons. It is not clear whether this lone pair of electrons will be stereochemically active in a particular compound but a number of trends have been observed.[1] The stereochemical activity of this lone pair appears to decrease with increasing coordination number, increasing atomic number of the halogen (Cl > Br > I) and with increasing atomic number in group 15 (i.e., As > Sb > Bi).

A large amount of work has been done involving anionic complexes of the bismuth(III) halides. These have been discussed in detail in previous reviews[2,3] and since this study involves neutral complexes they will not be discussed here. Alonzo *et al.*[4] examined the products formed from the reactions of bismuth(III) halides with a variety of nitrogen and phosphorus chelating ligands such as 1,10-phenanthroline and 1,2-bis(diphenylphosphino)ethane (dppe). Using a combination of analytical, mass and IR spectroscopic techniques they studied a number of solids which were assigned as chelates. They also found that in some cases the reaction did not occur in a 1:1 stoichiometry. The only structurally characterised examples of multidentate amine complexes of Bi(III) involve the macrocyclic ligands Me_3[9]aneN_3 (1,4,7-trimethyl-1,4,7-triazacyclononane)[5] and [12]aneN_4 (1,4,7,10-tetraazacyclododecane)[6] with bismuth (III) chloride and perchlorate respectively. In both cases the structures feature the pyramidal bismuth(III) species with the tri- or tetra-dentate macrocycle capping the Bi(III) ion.

Figure 6.1 View of the molecular structure of $[Bi_2Br_6(dmpe)_2]$ (taken from ref. 7)

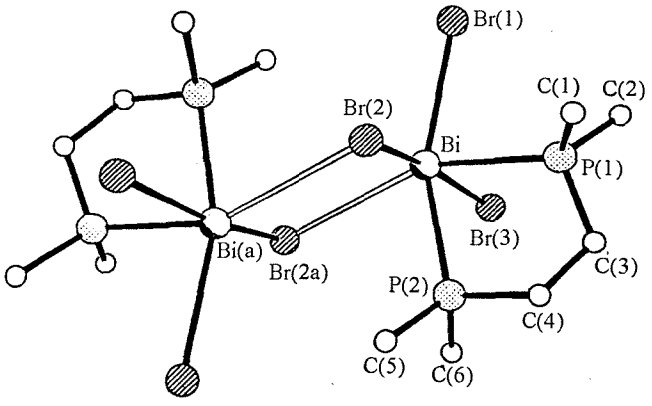

Clegg *et al.*[7] have studied various phosphine complexes of the group 15 halides including $[Bi_2Cl_6(dmpe)_2]$ (Figure 6.1), $[Bi_4Br_{12}(PEt_3)_4]$, $[Bi_2Br_6(PMe_3)_4]$ and $[Bi_2Br_6(PMe_2Ph)_2(OPMe_2Ph)_2]$. $[Bi_4Br_{12}(PEt_3)_4]$ is a tetramer with four octahedral Bi centres bound to one phosphine and five Br atoms. The other complexes all consist of an edge-shared, bioctahedral structure.

Figure 6.2 View of the centrosymmetric $[Bi_2Cl_6(dppm)_2]$ dimer (taken from ref. 8)

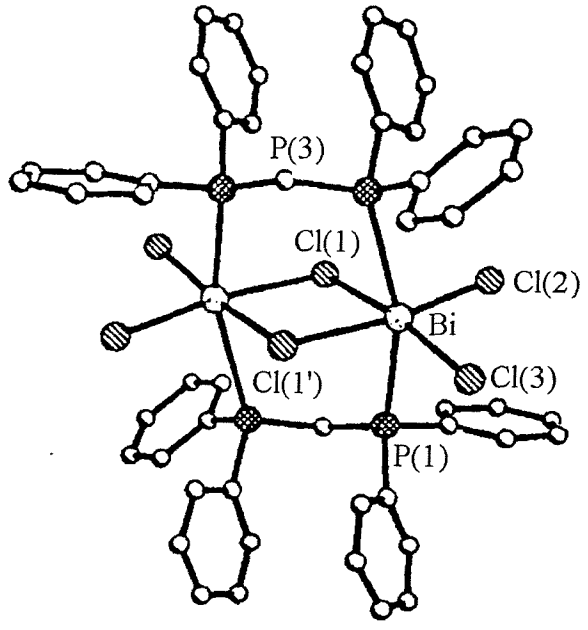

Willey *et al.*[8] have also examined the structures of crystals obtained from the reactions of $BiCl_3$ with dppe and also dppm. For the reaction of $BiCl_3$ with dppm the complex was characterised as $[Bi_2Cl_6(dppm)_2]$ (Figure 6.2) consisting of a Bi_2Cl_6 dimer with two bridging chlorides and with the two dppm molecules bridging the Bi centres. The crystal structure of the complex formed between $BiCl_3$ and dppe features two independent molecules of formula $[Bi_2Cl_6(dppe)_2]$ (Figure 6.3a) and $[Bi_2Cl_6(dppe)_3]$ (Figure 6.3b). The first is the same as that identified by Clegg *et al.*[7] for $[Bi_2Cl_6(dmpe)_2]$, while the second consists of two $BiCl_3(dppe)$ moieties bridged by a single dppe molecule, thus involving both chelating and bridging dppe ligands.

Figure 6.3 View of the centrosymmetric dimeric structures of a) $[Bi_2Cl_6(dppe)_2]$ and b) $[Bi_2Cl_6(dppe)_3]$ (taken from ref. 8)

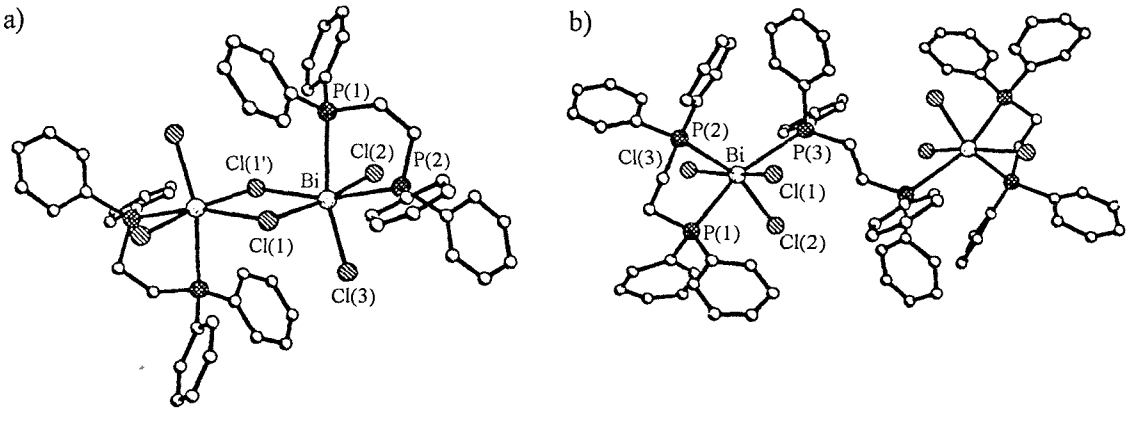

The reason for the complexes adopting these edge-shared, bioctahedral dimers in the majority of cases is unclear. Norman and Pickett[2] observe that the Bi-X *trans* to a phosphine ligand is typically *ca.* 0.2 Å greater than similar Bi-X bonds *trans* to X. This observation is attributed to the large *trans* influence of the phosphine *vs.* halide. They also note that of the four possible isomers (Figure 6.4) for structures of this type (**A-D**), isomer **A** is formed. On steric grounds isomer **C** would be the favoured isomer and Norman and Pickett suggest that the preference for isomer **A** can be assigned to an electronic effect arising from the *trans* influence of the phosphine ligands.

Figure 6.4 Possible isomers for $[Bi_2X_6(L)_4]$ (taken from ref. 1)

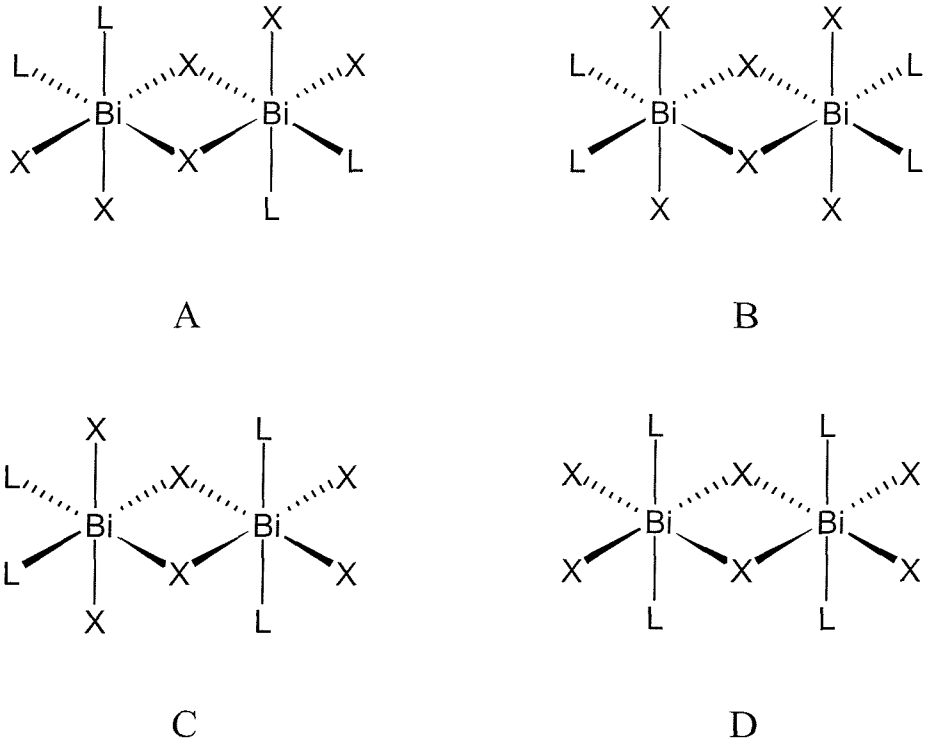

If a phosphine were placed *trans* to a bridging halide (as in isomer **B**), this would weaken the Bi-X bond, effectively creating a pair of $[BiX_2L_2]^+$ cations in close proximity, not energetically favoured. The products formed from the reactions of $BiCl_3$ and $BiBr_3$ with o-$C_6H_4(AsMe_2)_2$ (diars) have also been studied by Sutton,[9] though their characterisation was restricted to analyses.

For group 16 donor systems the preference is again for the harder oxygen-donor ligands. The crown ethers in particular have been studied in great detail and all show a monomeric BiX_3 unit capped by the multidentate ligand.[10-14] A number of monodentate ligand systems [e.g. *fac*-$[BiX_3(thf)_3]$ (where X = Cl[15] or Br[16]) *fac*-$[BiX_3(dmso)_3]$ (where X = Cl[17] or Br[18])] have also been characterised structurally, and these do not adopt the edge-shared, bioctahedral unit observed for the chelates. Instead they form mononuclear octahedral 1:3 Bi:ligand systems. A series of acyclic ethylene glycols of varying denticities have also been studied by Rogers *et al.*[11] The interdonor linkages in these species are no larger than dimethylene, and all form monomeric units with Bi centres which are 7-coordinate with O_4X_3 donor sets (e.g. Figure 6.5 –

Figure 6.5 View of the monomeric structure of [$BiCl_3$(pentaethylglycol)] (taken from ref. 11)

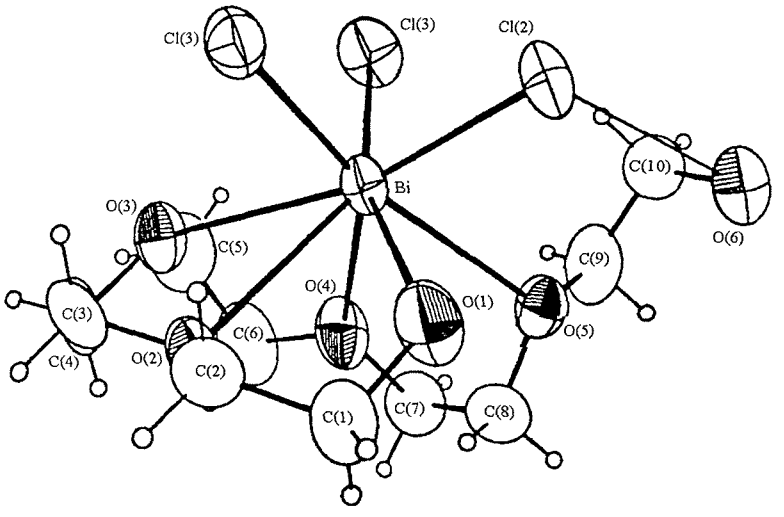

[$BiCl_3$(pentaethylglycol)]. The ether donor is preferred to the hydroxyl donor in the cases where five oxygen donors are present within the ligand. Eveland *et al.*[15] have also characterised the products formed from the reaction of $BiCl_3$ with $MeO(CH_2)_2O(CH_2)_2OMe$ and $EtO(CH_2)_2O(CH_2)_2OEt$. In both cases the product formed adopts the edge-shared, bioctahedral dimers commonly observed in Bi(III) complexes. Similarly, the edge-shared, bioctahedral structure was also found by Willey *et al.*[19] for the five-membered chelate system of [$BiCl_3\{Pr^n_2P(S)P(S)Pr^n_2\}$]. Willey *et al.*[20] have also characterised [$BiCl_3\{Ph_2P(O)CH_2P(O)Ph_2\}]_2$ (formed as a result of oxidation of [$BiCl_3$(dppm)]) (Figure 6.6) and [$BiCl_3\{As(O)MePh_2\}\{Ph_2As(O)CH_2CH_2As(O)Ph_2\}]_n$, (similarly formed by the oxidation of [$BiCl_3$(dpae)] – Figure 6.7). Interestingly, where dppm had formed a bridge between the two Bi centres of an edge-shared, bioctahedral unit, the oxide forms the more usual edge-shared, bioctahedral unit with one ligand chelated to each Bi. For the arsine-oxide, the ligand does not chelate to give a seven-membered ring, but rather bridges between Bi monomers forming an extended infinite chain.

Figure 6.6 View of the centrosymmetric dimeric structure of $[BiCl_3\{Ph_2P(O)CH_2P(O)Ph_2\}]_2$ (taken from ref. 19)

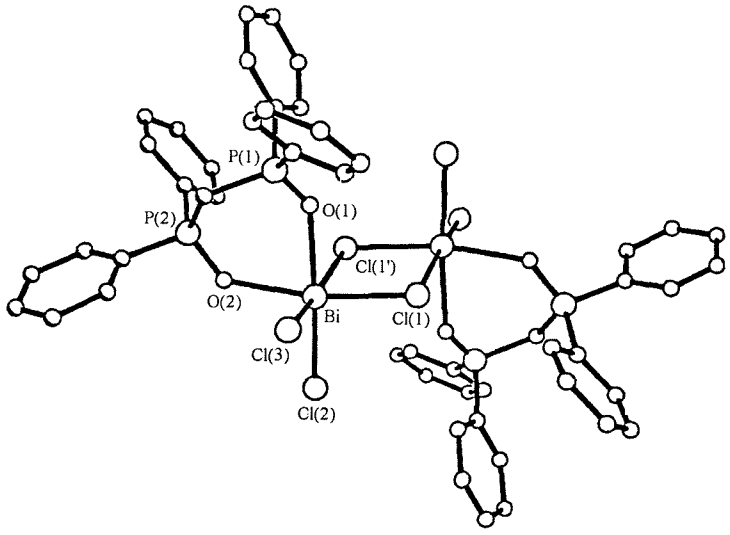

Figure 6.7 View of the polymeric structure of $[BiCl_3\{As(O)MePh_2\}\{Ph_2As(O)CH_2CH_2As(O)Ph_2\}]_n$. O(2*) is related by the symmetry operator (x – ½, ½ - y, z) and Bi(1') by (½ + x, ½ - y, z). (taken from ref. 19)

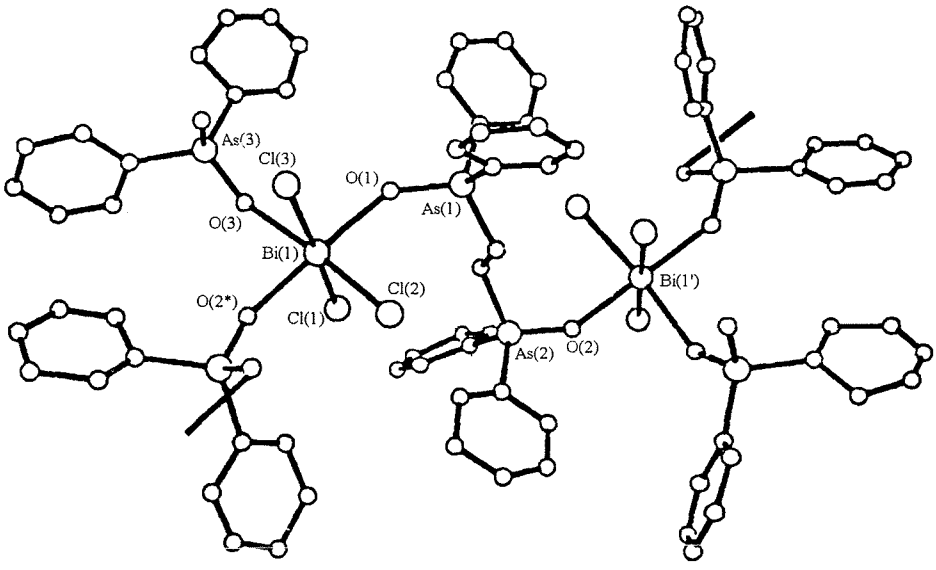

A number of thioether ligand complexes of Bi(III) halides are also known. The ionic species $[Me_3S]_2[Bi_2I_8(Me_2S)_2]$ produced from the reaction of BiI_3 in neat Me_2S has been characterised structurally by Clegg *et al.*[21] The structure features the same edge-shared bioctahedral dimer with each Bi coordinated to three terminal I atoms, two bridging I atoms and one Me_2S ligand. The bridging Bi-I distances (3.229(3) and 3.234(3) Å) for this structure are considerably longer than those of the terminal I atoms (2.934(3) – 2.955(3) Å). A number of the macrocyclic thioether systems with different denticities have also been studied and characterised structurally.[22-24] In all cases the macrocycle is found to cap the pyramidal $BiCl_3$ unit. All of these structurally characterised bismuth(III) halide complexes involving polyethylene glycols, ethers, crown ethers and crown thioethers reflect the dominance of the pyramidal BiX_3 unit on the structures adopted. The five weaker secondary halide interactions which are evident within the structure of the parent Bi(III) halide[25] (Figure 6.8) are replaced with weak Bi-O or Bi-S interactions, generating 7-, 8- or 9-coordinate compounds.

Figure 6.8 Projection of the structure of $BiCl_3$ on the *ab* plane, showing the chlorine bridging that is present between a single $BiCl_3$ molecule and its neighbours. Two units cells in the *z* direction are involved. (taken from ref. 25)

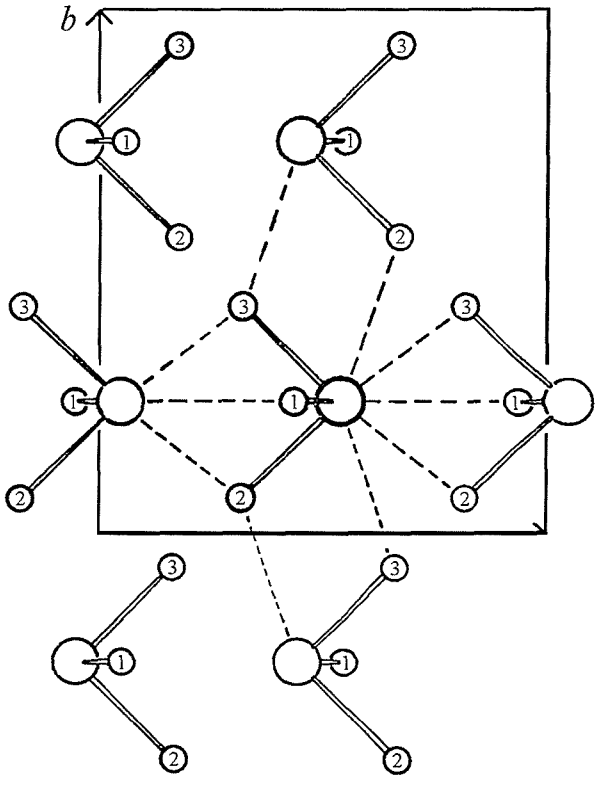

A stereochemically active lone pair on the Bi, directed towards the weakly interacting S- or O-donors can be invoked for these species. This is clearly seen in the structure of $[(BiCl_3)_2([24]aneS_8)]$[24] (Figure 6.9) which contains two such $BiCl_3$ pyramidal units, each with weak interactions to five S-donors. Further evidence for the dominance of the pyramidal BiX_3 unit in these species comes from the observation that the Bi-Cl bond distances do not change significantly upon complexation. The same model can be applied to the isomers formed with dppe,[7] dmpe[8] and all other structures adopting isomer **A** detailed above.[2] In those cases two pyramidal bismuth(III) halide units can be identified with weaker secondary interactions linking them, and other ligand donor atoms replacing the other weak secondary interactions. This behaviour is apparently independent of the ether or thioether ligand denticity, and similar results have also been observed for SbX_3 derivatives.[26]

Figure 6.9 View of $[(BiCl_3)_2([24]aneS_8)]$ (taken from ref. 23)

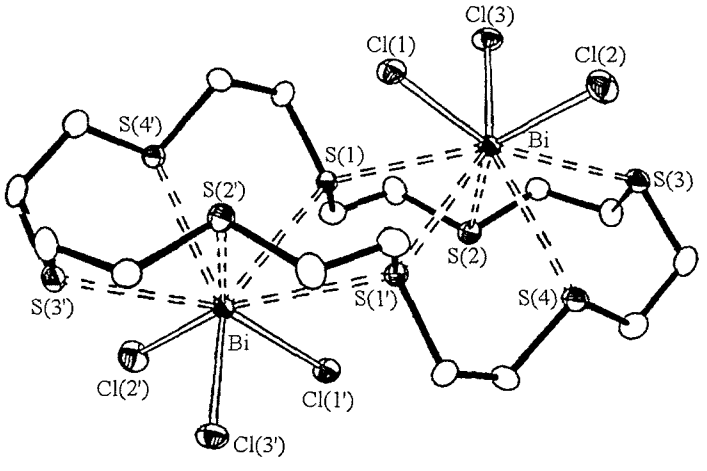

Sawyer and Gillespie[27] have reviewed the stereochemistry of Sb^{III} halides and showed that the weak interactions form around the direction of maximum electron density of the lone pair, but not directly over it. In the complexes involving edge-shared, bioctahedral dimers, this is consistent with the lone pairs of Bi lying within the plane of the bridging halides.[2,3,7,8,20,21]

The aim of this work is to conduct an investigation into the reaction of the bismuth(III) halides (Cl, Br or I) with a range of bidentate group 16 ligands, $MeE(CH_2)_nEMe$ (where n = 2 or 3; E = S or Se), $PhE(CH_2)_nEPh$ (where n = 2 or 3; E = S or Se) and o-$C_6H_4(SMe)_2$, and the group 15 ligands $Ph_2As(CH_2)_2AsPh_2$ (dpae), o-$C_6H_4(AsMe_2)_2$ (diars) and $MeC(CH_2AsMe_2)_3$ (triars). The affects of changing halide, the ligand interdonor linkage and terminal substituents are studied. Microanalysis and IR spectroscopy have been used to characterise these complexes in the solid state. The first structurally characterised example of a bismuth(III)-arsine complex, $[Bi_2I_6(diars)_2]$, is reported. The X-ray structures of the group 16 bismuth(III) halide complexes, $[BiBr_3\{MeS(CH_2)_2SMe\}_2]$, $[BiI_3\{MeS(CH_2)_2SMe\}_2]$, $[Bi_2Br_6\{PhS(CH_2)_2SPh\}]_n$, $[Bi_4Cl_{12}\{MeS(CH_2)_3SMe\}_4]_n.nH_2O$, $[BiBr_3\{MeSe(CH_2)_3SeMe\}]_n$, $[BiCl_3\{MeSe(CH_2)_3SeMe\}]_n$ and $[BiBr_3\{MeSe(CH_2)_3SeMe\}]_n$ are reported.

6.2. Results & Discussion

6.2.1. Synthesis and Properties of Bidentate Group 16 Complexes of BiX_3

A range of complexes of stoichiometry $BiX_3(L\text{-}L)_2$ (where X = Cl, Br or I; L-L = $MeE(CH_2)_2EMe$, E = S or Se), $Bi_2X_6(L\text{-}L)$ (where X = Cl, Br or I; L-L = $PhE(CH_2)_2EMe$, E = S or Se) and $BiX_3(L\text{-}L)$ (where X = Cl, Br or I; L-L = $MeE(CH_2)_3EMe$ or o-$C_6H_4(SMe)_2$) have been isolated from reaction of BiX_3 and L-L in MeCN. Concentration of the resultant coloured solutions produced solids which were filtered, washed with anhydrous CH_2Cl_2 and dried *in vacuo*. Due to the moisture sensitivity of the bismuth(III) halides, all reactions were carried out under an atmosphere of dry dinitrogen using standard Schlenk techniques. All complexes were stored in a dinitrogen purged dry-box. The thioether complexes were found to be relatively stable in moist air, but the selenoether complexes were found to change to viscous black materials over a period of a few weeks in the dry-box. Satisfactory microanalyses were recorded for all freshly prepared solids and IR spectra of the $BiCl_3$ species show several features in the range 230-280 cm^{-1} assigned to ν(Bi-Cl) (*c.f.* 242 and 288 cm^{-1} in the parent halide, $BiCl_3$[28]). The poor solubility of the complexes in non-coordinating solvents such as CH_2Cl_2 and $CHCl_3$ meant that ^1H and $^{77}Se\text{-}\{^1H\}$ NMR spectra did not provide any useful information. The reaction of $BiCl_3$ with $MeSCH_2SMe$ was attempted but, while a yellow solution was formed, no solid was isolable. The analogous ditelluroethers were also studied but the highly coloured products formed from reaction with BiX_3 proved too unstable to isolate.

6.2.2. Single Crystal X-ray Diffraction Studies

Prior to this study the only bidentate group 16 complexes of the bismuth(III) halides characterised structurally were restricted to phosphine or arsine oxides[20] (Figures 6.6 and 6.7), sulfides[19] (e.g. $[BiCl_3\{Pr^n{}_2P(S)P(S)Pr^n{}_2\}]$) or the polyethylene glycols (e.g. Figure 6.5), ethers, crown ether and crown thioether complexes[22-24] which feature pyramidal BiX_3 units capped by the macrocycle. The structures obtained for $[BiBr_3\{MeS(CH_2)_2SMe\}_2]$, $[BiI_3\{MeS(CH_2)_2SMe\}_2]$, $[BiBr_3\{MeS(CH_2)_3SMe\}]_n$, $[Bi_2Br_6\{PhS(CH_2)_2SPh\}]_n$, $[Bi_4Cl_{12}\{MeS(CH_2)_3SMe\}_4]_n.nH_2O$,

$[BiCl_3\{MeSe(CH_2)_3SeMe\}]_n$ and $[BiBr_3\{MeSe(CH_2)_3SeMe\}]_n$ exhibit a wide variety of different structural motifs for relatively small alterations in ligand architecture.

Crystals obtained from the reaction of $BiBr_3$ with $MeS(CH_2)_2SMe$ show that the 7-coordinate species $[BiBr_3\{MeS(CH_2)_2SMe\}_2]$ is formed as a monomer with two chelating ligands lying equatorially within a distorted pentagonal bipyramid (Figure 6.10). The coordination sphere created about the bismuth centre has three terminal Br atoms and four S-donors from the two chelated ligands.

Figure 6.10 View of $[BiBr_3\{MeS(CH_2)_2SMe\}_2]$ with numbering scheme adopted. Ellipsoids are drawn at 40 % probability, hydrogen atoms have been omitted for clarity

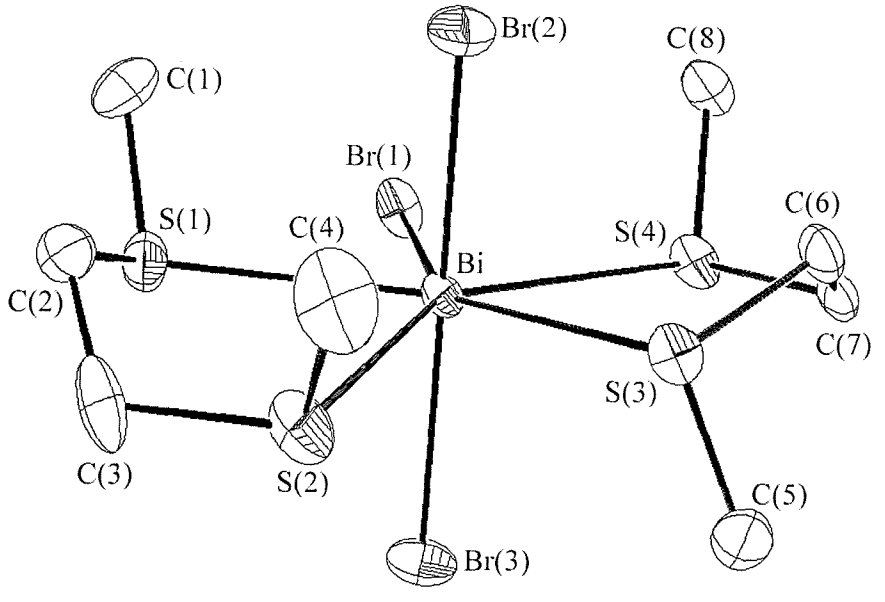

Bond lengths (Å) and angles (°) for $[BiBr_3\{MeS(CH_2)_2SMe\}_2]$ are presented in Tables 6.1 and 6.2 respectively. The pyramidal unit found in the parent halide[25] is severely disrupted here, with the $BiBr_3$ unit becoming almost planar to accommodate the two chelating ligands. One thioether ligand (S(1) and S(2)) adopts the *meso* and the other (S(3) and S(4)) the *dl* configuration. It is extremely unusual for a ligand to adopt both forms within a molecule. The only structurally characterised example where this occurs was $[Ru\{MeTe(CH_2)_3TeMe\}_2(PPh_3)Cl]PF_6$.[29] In that case it is most likely the

influence of the triphenylphosphine that determines the isomer adopted. Here it likely to be the strained nature of the 5-membered chelate ring. The S-Bi-S bond angles observed for the two ligands, 70.3(2) and 72.6(1) Å, are much less than the angle observed in chapter 2 for the octahedral species $[SnCl_4\{MeS(CH_2)_2SMe\}]$ (84(1)°) involving the same ligand.

Table 6.1 Selected bond lengths with e.s.d.s for $[BiBr_3\{MeS(CH_2)_2SMe\}_2]$

Bi	Br(1)	2.814(2)	Bi	Br(2)	2.826(2)
Bi	Br(3)	2.787(2)	Bi	S(1)	2.964(6)
Bi	S(2)	3.091(5)	Bi	S(3)	3.005(5)
Bi	S(4)	2.919(5)			

Table 6.2 Selected bond angles (°) with e.s.d.s for $[BiBr_3\{MeS(CH_2)_2SMe\}_2]$

Br(1)	Bi	Br(2)	98.95(8)	Br(1)	Bi	Br(3)	96.08(7)
Br(1)	Bi	S(1)	76.8(1)	Br(1)	Bi	S(2)	146.3(1)
Br(1)	Bi	S(3)	145.2(1)	Br(1)	Bi	S(4)	73.1(1)
Br(2)	Bi	Br(3)	164.62(8)	Br(2)	Bi	S(1)	88.3(1)
Br(2)	Bi	S(2)	87.3(1)	Br(2)	Bi	S(3)	77.3(1)
Br(2)	Bi	S(4)	93.0(1)	Br(3)	Bi	S(1)	92.0(1)
Br(3)	Bi	S(2)	78.4(1)	Br(3)	Bi	S(3)	92.1(1)
S(1)	Bi	S(2)	70.3(2)	S(2)	Bi	S(4)	140.0(2)
S(3)	Bi	S(4)	72.6(1)	S(2)	Bi	S(3)	68.5(1)

The Bi-S distances for this structure (2.918(5), 2.963(5), 3.004(5), 3.090(5) Å) are typically shorter than those observed in $[Me_3S]_2[Bi_2I_8(Me_2S)_2]$[21] (3.054(8) Å) and the macrocyclic thioether complexes (*cf.* 2.987(3) – 3.206(3) Å for $[BiCl_3([12]aneS_4)]$[22]; 3.058(7) – 3.251(7) Å for $[BiCl_3([15]aneS_5)]$[22]; 3.146(4) and 3.225(4) Å for $[BiCl_3([18]aneS_6)]$[23]; 3.134(2) – 3.313(2) Å for $[(BiCl_3)_2([24]aneS_8)]$[24]). The Bi-Br bond distances observed (2.787(2), 2.813(2) and 2.826(2) Å) are at the upper end of those observed in previous $BiBr_3$ complexes (*cf.* 2.66(1) – 2.76(1) for [$BiBr_3$(12-crown-4)][11]; 2.672(4) – 2.714(4) Å for [$BiBr_3$(15-crown-5)][11]; 2.656(2) – 2.694(2) Å for [$BiBr_3$(benzo-15-crown-5)][11]; 2.669(2) – 2.739(2) Å for [$BiBr_3$(tetraethyleneglycol)][11]). Within each of the thioether ligands chelated to the $BiBr_3$ there is one shorter and one longer Bi-S bond distance, possibly due to the presence of the stereochemically active lone pair on Bi pointing in the direction of S(2) and S(3), consistent the observations of Sawyer and Gillespie.[27]

A number of diamond-shaped crystals of the analogous iodo-complex, $[BiI_3\{MeS(CH_2)_2SMe\}_2]$ were obtained upon concentration of the reaction mix of BiI_3 and $MeS(CH_2)_2SMe$ in MeCN. Two datasets were collected from two different samples both of which turned out to be weakly diffracting. The structure was found to be enantiomorphic, with the choice of enantiomorph unclear. Depending on the direction of the screw-axis within the structure, 4_1 or 4_3, a different space group, $P4_12_12$ or $P4_32_12$, is necessary for each enantiomorph. There was also evidence of disorder within the C atoms of the thioether. These factors prevented satisfactory solution and refinement however, refinement of the heavy atoms was sufficient to show that the structure adopted was the same as was found for the mononuclear bromide analogue, $[BiBr_3\{MeS(CH_2)_2SMe\}_2]$, discussed above.

The effects of altering the terminal ligand substituent from methyl to phenyl prove quite dramatic. Rather than discrete monomeric units, the X-ray structure of crystals obtained from a 1:1 mix of $BiBr_3$ with $PhS(CH_2)_2SPh$ shows the product has a 2:1 Bi:dithioether ligand stoichiometry, with the structure forming an extended array, incorporating a form of the edge-shared, bioctahedral dimers. The asymmetric unit and nearest symmetry related atoms as shown in Figure 6.11, the extended structure for $[Bi_2Br_6\{PhS(CH_2)_2SPh\}]_n$ is shown in Figure 6.12. Bond lengths (Å) and angles (°) have been presented in Tables 6.3 and 6.4. Each Bi^{III} atom is coordinated to a slightly distorted octahedral arrangement (Br(1)-Bi-Br(2) 94.93(8)°, Br(1)-Bi-Br(3) 94.19(8)°, Br(1)-Bi-S(1) 90.3(1)°) of four μ_2-Br atoms, one terminal Br atom and one S-donor. The terminal Br atom and the S-donor are mutually *cis*. This gives infinite chains of

edge-shared octahedra formed *via* linking Bi_2Br_2 rectangles. The dihedral angle between adjacent Bi_2Br_2 units is 82.65(7) °.

Figure 6.11 View of the $[Bi_2Br_6\{PhS(CH_2)_2SPh\}]_n$ asymmetric unit with numbering scheme adopted. Ellipsoids are drawn at 40 % probability. Neighbouring atoms are included marked with an asterisk (*) (related by a crystallographic inversion centre)

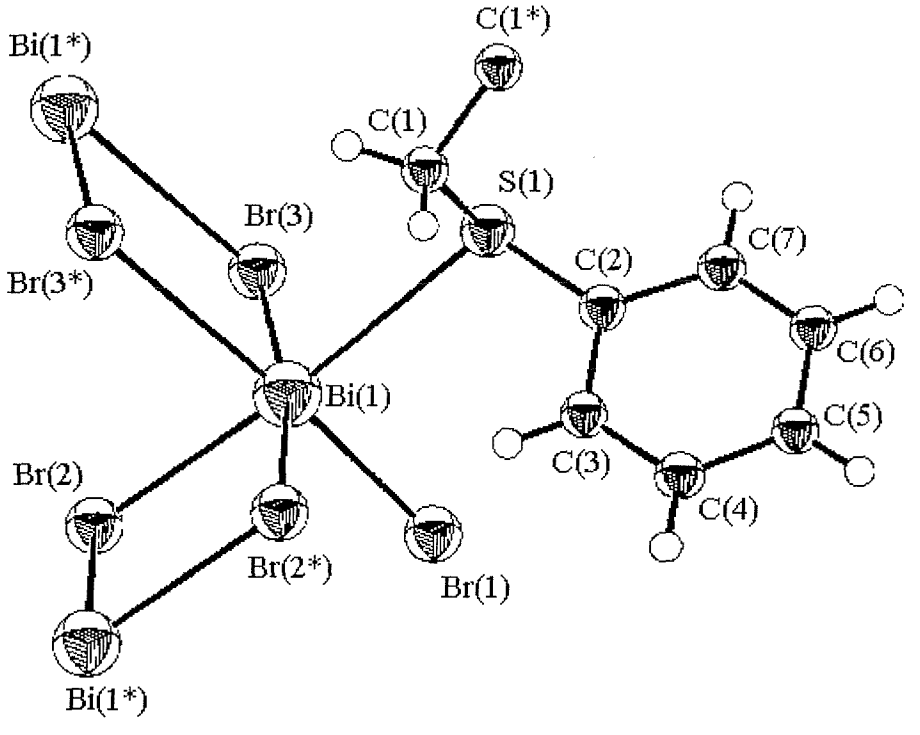

The chain retains some of the characteristics of the parent halide[25] with a pyramidal core (Bi-Br *ca.* 2.7 Å), three weaker secondary halide interactions (Bi-Br *ca.* 3 Å) and the S-donor displacing one of the other secondary interactions. The Bi-S distance, 3.082(6) Å, is consistent with previously observed values.[21,22,23,24] Of interest are the Bi-Br distances (2.596(2), 2.692(3), 2.751(3), 3.148(3) and 3.274(3) Å), which are consistent with $[BiBr_3\{MeS(CH_2)_2SMe\}_2]$ and previous examples,[11] but vary greatly within the molecule. The shortest distance (2.696(2) Å) is for the terminal Br atom, as expected, then one of the bridging Br atoms (2.692(3) Å), then the Br *trans* to the sulfur donor (2.751(3) Å). The remaining two Bi-Br distances are considerably longer and probably indicate the position of the stereochemically active lone pair on

bismuth, according to the findings of Sawyer and Gillespie.[27] Dithioether ligands of this type and other group 16 ligands have previously been shown to bind to Cu^{I} and Ag^{I} centres and in a small number of cases also yield polymeric arrays, although quite different in detail to this complex.[30]

Table 6.3 Selected bond lengths (Å) with e.s.d.s for $[Bi_2Br_6\{PhS(CH_2)_2SPh\}]_n$; atoms marked with an asterisk (*) are related by a crystallographic inversion centre

Bi(1)	Br(1) 2.596(2)	Bi(1)	Br(2) 2.751(3)
Bi(1)	Br(2*) 3.148(3)	Bi(1)	Br(3) 2.692(3)
Bi(1)	Br(3*) 3.274(3)	Bi(1)	S(1) 3.082(6)

Table 6.4 Selected bond angles (°) with e.s.d.s for $[Bi_2Br_6\{PhS(CH_2)_2SPh\}]_n$; atoms marked with an asterisk (*) are related by a crystallographic inversion centre

Br(1)	Bi(1)	Br(3)	94.20(8)	Br(1)	Bi(1)	Br(2)	94.93(8)
Br(1)	Bi(1)	S(1)	90.3(1)	Br(1)	Bi(1)	Br(2*)	97.04(9)
Br(1)	Bi(1)	Br(3*)	176.62(8)	Br(3)	Bi(1)	Br(2)	91.30(8)
Br(3)	Bi(1)	S(1)	87.5(1)	Br(3)	Bi(1)	Br(2*)	168.53(7)
Br(3)	Bi(1)	Br(3*)	87.85(7)	Br(2)	Bi(1)	S(1)	174.7(1)
Br(2)	Bi(1)	Br(2*)	85.45(8)	Br(2)	Bi(1)	Br(3*)	82.32(7)
S(1)	Bi(1)	Br(2*)	94.8(1)	S(1)	Bi(1)	Br(3*)	92.4(1)
Br(2*)	Bi(1)	Br(3*)	80.82(7)	Bi(1)	Br(2)	Bi(1*)	94.55(8)
Bi(1)	Br(3)	Bi(1*)	92.15(7)				

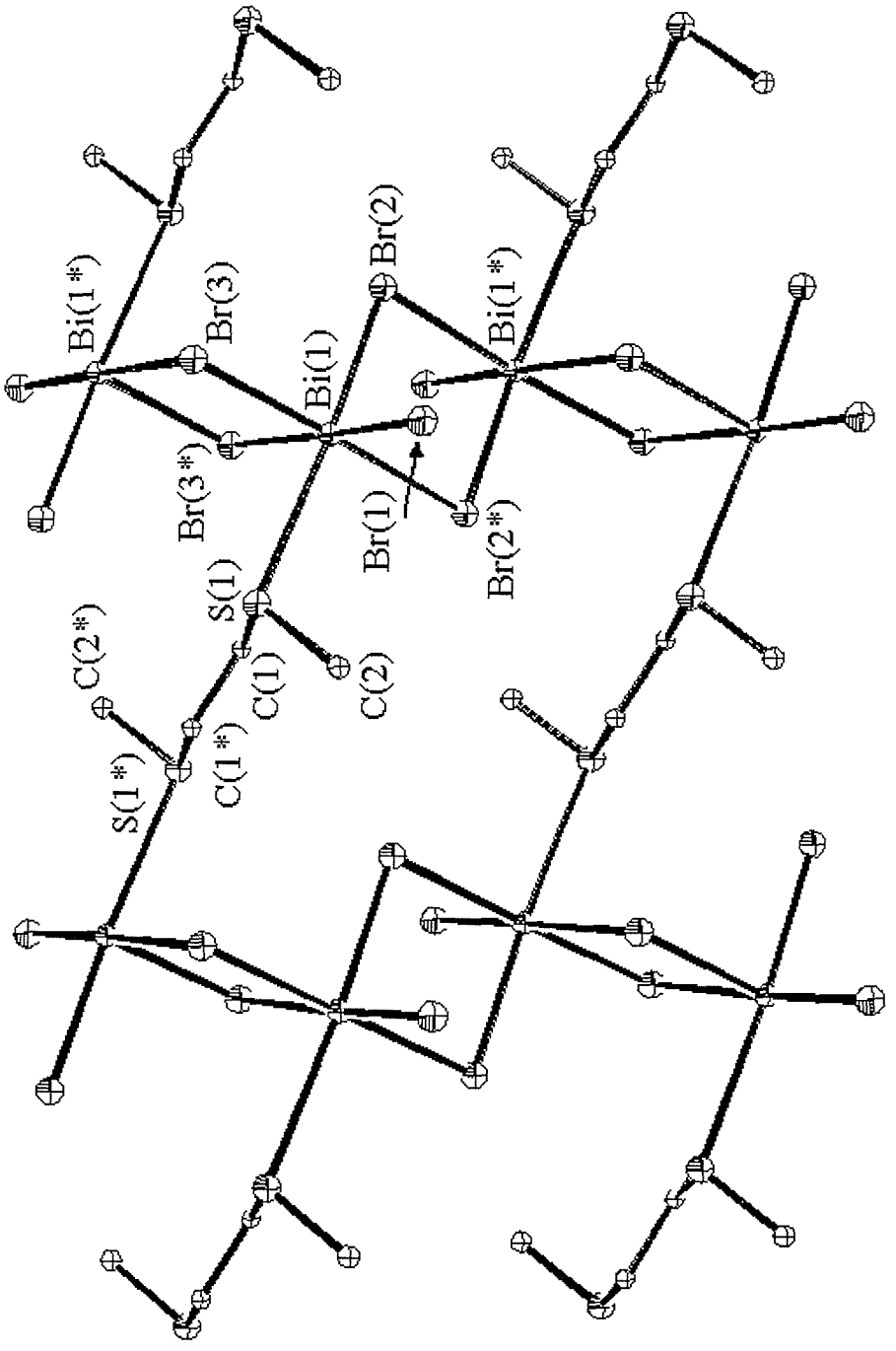

Figure 6.12 View of a portion of $[Bi_2Br_6\{PhS(CH_2)_2SPh\}]_n$ structure (phenyl rings at C(2) and C(2*) are omitted for clarity. Ellipsoids are drawn at 40 % probability. Atoms marked with an asterisk (*) are related by a crystallographic inversion centre

In chapter 2 it was seen that $PhS(CH_2)_2SPh$ was a poorer σ-donor than $MeS(CH_2)_2SMe$, and hence the structure adopted by $[Bi_2Br_6\{PhS(CH_2)_2SPh\}]_n$ is dominated by the influence of the parent $BiBr_3$ precursor, as is seen for the crown ethers[10-14] and macrocyclic thioethers.[22-24] However, further examples are necessary to prove this.

Altering the interdonor-linkage from dimethylene to trimethylene has an equally dramatic effect. The product obtained from a 1:1 mix of $BiCl_3$ with $MeS(CH_2)_3SMe$ is found to have 1:1 stoichiometry by analysis. However, rather than a simple 5- or 7-coordinate monomer featuring chelating ligands, the X-ray crystal analysis of this species shows a very different and highly unusual structure. The structure reveals a three-dimensional polymeric network with the structural formula $[Bi_4Cl_{12}\{MeS(CH_2)_3SMe\}_4]_n.nH_2O$. The asymmetric unit is shown in Figure 6.13, and a portion of the three-dimensional polymeric network is shown in Figures 6.14 and 6.15. Bond lengths (Å) and angles (°) are presented in Tables 6.5 and 6.6. Traces of moisture in the CH_2Cl_2 most likely account for the H_2O solvent molecules identified in the structure. The water molecules themselves are not involved in binding to any other centre so it is assumed they have little influence on the structure adopted.

Figure 6.13 View of the $[Bi_4Cl_{12}\{MeS(CH_2)_3SMe\}_4]$ asymmetric unit with numbering scheme adopted. Ellipsoids are drawn at 40 % probability. Neighbouring atoms are included marked with an asterisk (*) (related by a crystallographic $\bar{4}$ symmetry)

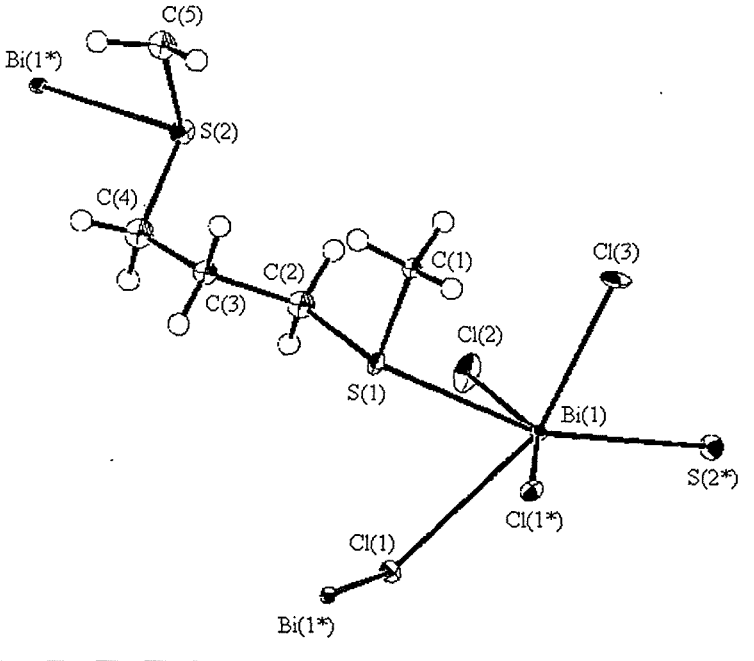

Figure 6.14 View of a portion of the $[Bi_4Cl_{12}\{MeS(CH_2)_3SMe\}_4]_n$ structure with numbering scheme adopted showing the tetramer unit (H atoms are omitted for clarity and atoms marked with an asterisk are related by a crystallographic $\bar{4}$ operation. Ellipsoids are drawn at 40 % probability

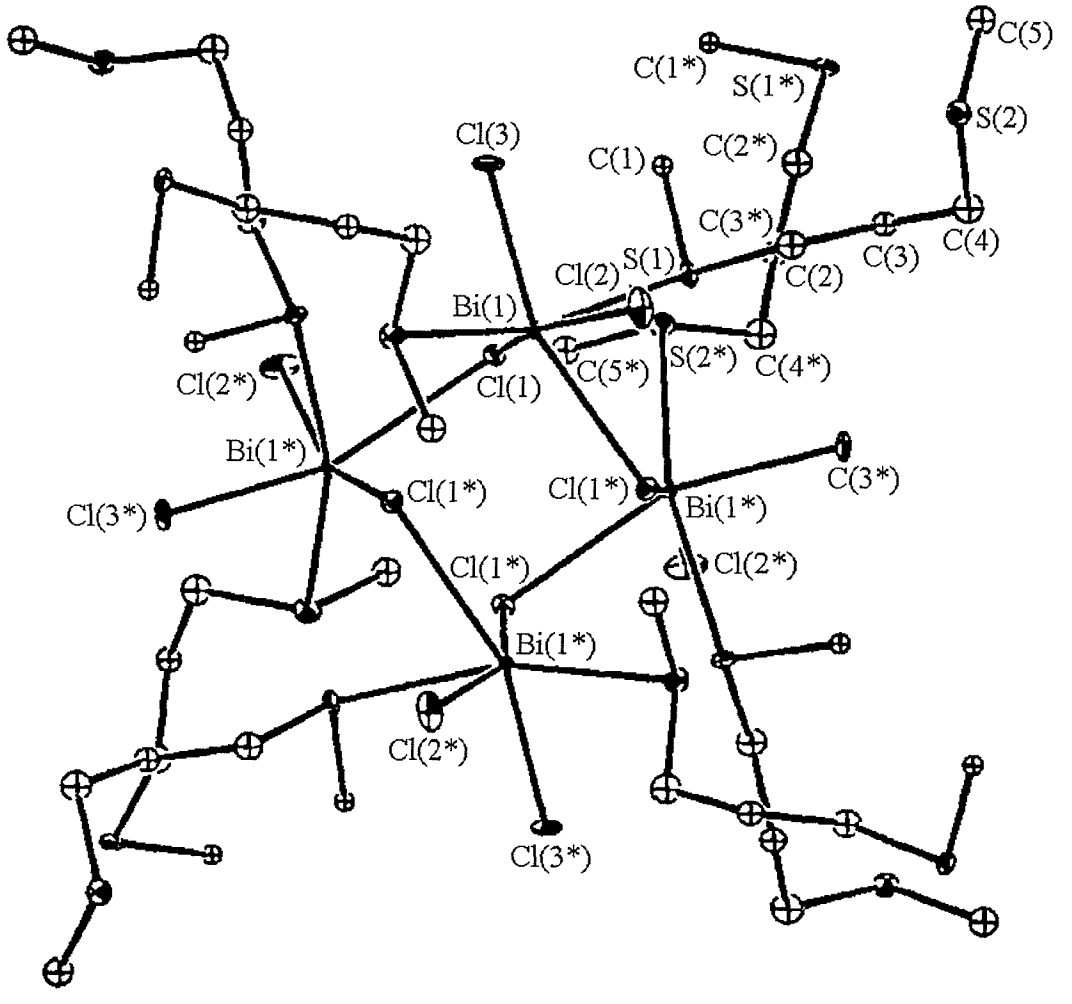

Figure 6.15 View of a portion of the $[Bi_4Cl_{12}\{MeS(CH_2)_3SMe\}_4]_n$ structure viewed down the *c*-axis of the three-dimensional polymer, illustrating the channels running through the structure (H atoms are omitted for clarity). Ellipsoids are drawn at 40 % probability

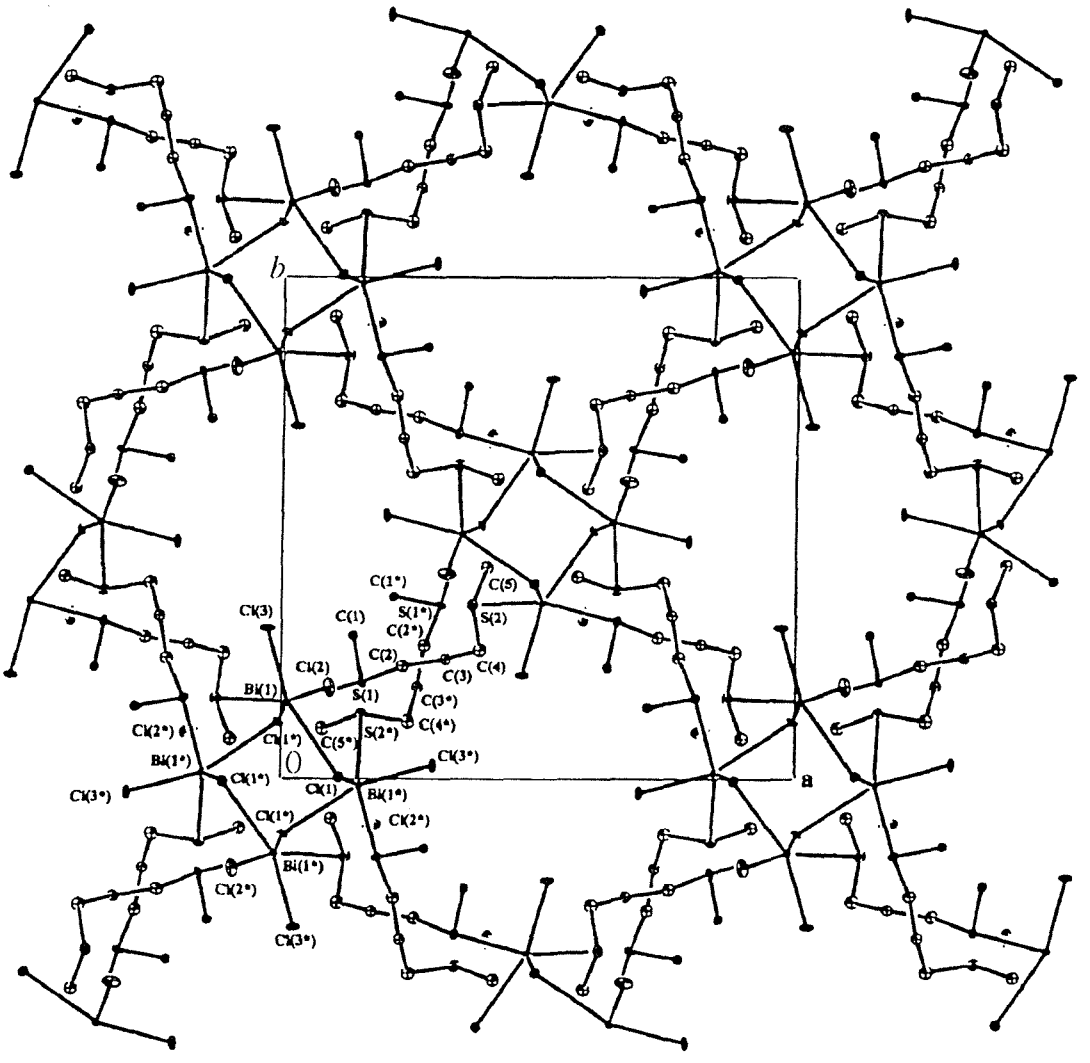

The structure involves $Bi_4Cl_{12}\{MeS(CH_2)_3SMe\}_4$ tetramer units (related by crystallographic $\bar{4}$ symmetry) which are linked by bridging dithioether ligands to give a three-dimensional polymeric network. Each Bi^{III} ion is therefore coordinated to two terminal Cl atoms, two μ_2-bridging Cl atoms and two S-donors from different bridging dithioether ligands. The geometry at each Bi atom therefore approximates to a severely distorted octahedron, with an open triangular face within which it is assumed the Bi lone pair lies. The μ_2-bridging Bi-Cl distances (2.913(7) and 2.969(6) Å) are much longer than the terminal Bi-Cl distances (2.538(7) and 2.533(7) Å), which are themselves only slightly different. Hence an alternative description of this structure is that it comprises of $[BiCl_2\{\eta^1\text{-}MeS(CH_2)_3SMe\}_2]^+$ cations loosely associated into tetramers through interactions with chloride ions, Cl(1) and Cl(1*). There are additional long range, weak interactions which link the μ_2-bridging Cl atoms to Bi centres across the Bi_4Cl_4 ring, Bi···Cl(1*) = 3.268(7) Å. This distance is significantly longer than would be expected for a genuine μ_3-bridging Cl.[31] The Bi_4Cl_4 core forms an 8-membered heterocyclic ring which, as a result of the weak Bi···Cl interactions adopts an open-cradle conformation (Figure 6.16). The secondary Bi···Cl(1*) interaction is in the general direction of the void assumed to be occupied by the lone pair, but not in the direction of the maximum electron density, again consistent with behaviour previously observed for Sb^{III} and Bi^{III} chemistry.[27] Bismuth halides often form compounds incorporating condensed Bi_4X_4 polyhedra,[31] however, the open cradle arrangement adopted by $[Bi_4Cl_{12}\{MeS(CH_2)_3SMe\}_4]_n.nH_2O$ is very unusual. The Bi-S (2.857(7) and 2.977(7) Å) and Bi-$Cl_{terminal}$ (2.538(7) and 2.533(7) Å) bond lengths are similar to those observed in the reported thioether complexes[21-24]

Table 6.5 Selected bond lengths (Å) with e.s.d.s for $[Bi_4Cl_{12}\{MeS(CH_2)_3SMe\}_4]_n$; atoms marked with an asterisk (*) are symmetry related by a crystallographic $\bar{4}$ operation

Bi(1)	Cl(1)	2.912(7)	Bi(1)	Cl(1*)	2.970(6)
Bi(1)	Cl(2)	2.535(7)	Bi(1)	Cl(3)	2.533(7)
Bi(1)	S(1)	2.853(7)	Bi(1)	S(2*)	2.973(8)

Table 6.6 Selected bond angles (°) with e.s.d.s for $[Bi_4Cl_{12}\{MeS(CH_2)_3SMe\}_4]_n$; atoms marked with an asterisk (*) are symmetry related by a crystallographic $\bar{4}$ operation

Cl(3)	Bi(1)	Cl(2)	94.5(3)	Cl(3)	Bi(1)	S(1)	85.4(2)
Cl(3)	Bi(1)	Cl(1)	91.6(2)	Cl(3)	Bi(1)	S(2)	82.5(2)
Cl(2)	Bi(1)	S(1)	87.0(2)	Cl(2)	Bi(1)	Cl(1*)	154.0(2)
Cl(2)	Bi(1)	S(2*)	81.6(2)	S(1)	Bi(1)	Cl(1*)	68.3(2)
S(1)	Bi(1)	S(2*)	162.7(2)	Cl(1*)	Bi(1)	S(2*)	124.3(2)
Bi(1)	Cl(1)	Bi(1*)	103.8(2)				

Figure 6.16 View of the Bi_4Cl_4 core, illustrating the open cradle conformation. The dashed lines indicate secondary Bi···Cl interactions

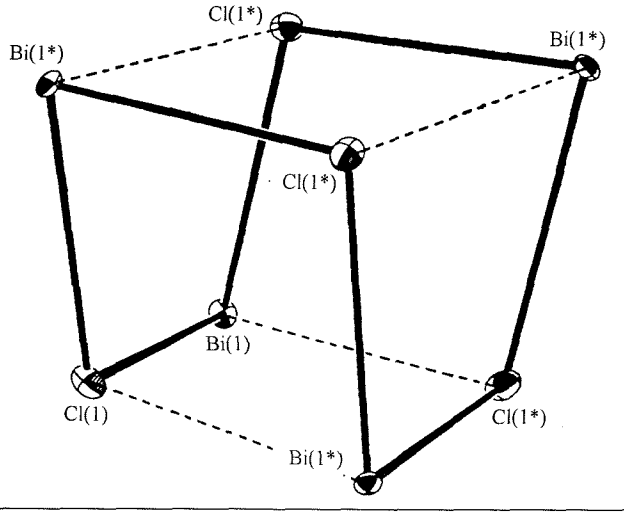

When the analogous reaction is undertaken using $BiBr_3$ in place of $BiCl_3$, a totally different structure is found. A weakly diffracting crystal was obtained from a sample which analysed as $[BiBr_3\{MeS(CH_2)_3SMe\}]_n$. The X-ray crystal structure shows that the stoichiometry remains 1:1 Bi:thioether ligand, but this time the structure incorporates the edge-shared bioctahedral dimeric unit which is commonly observed for bismuth halide complexes.[2,3,7,8,20] However, for this structure, these are not discrete dimers, but rather are linked by bridging dithioether ligands to give a two-dimensional sheet. The asymmetric unit is shown in Figure 6.17, and a portion of the extended sheet system is included in Figure 6.18. Bond lengths (Å) and angles (°) are presented in Tables 6.7 and 6.7. Each Bi^{III} atom is coordinated to distorted octahedral arrangement (two terminal Br atoms, two μ_2-bridging Br atoms and two mutually *trans* S-donors from different bridging dithioethers. The Bi_2Br_6 units are planar and, although the bond distances are somewhat asymmetric within the $Bi_2(\mu_2\text{-}Br_2)$ ring, there is a crystallographic inversion centre at the centre of this unit. One methyl substituent (C(5) on S(1)) of the ligand is disordered and has been satisfactorily modelled across the two possible sites such that 60 % of the ligand is in the *meso* configuration and the remaining 40 % in the *dl* form.

There is evidence, once again, for the stereochemically active Bi based lone pair. The bond distances for the terminal Br atoms (2.697(2) and 2.719(2) Å) are considerably shorter than those for the bridging Br atoms (2.980(2) and 3.004(2) Å). This suggests that the stereochemically active lone pair on the Bi atoms lie within the plane of the Bi_2Br_6 dimer, between the two bridging BiBr bonds.

This structure starkly contrasts with that of the chloride example, $[Bi_4Cl_{12}\{MeS(CH_2)_3SMe\}_4]_n.nH_2O$, discussed earlier and, although that structure incorporates H_2O solvent molecules, it seems unlikely that they account for the difference as they are not involved in binding and are not sterically demanding.

Figure 6.17 View of the asymmetric unit for $[BiBr_3\{MeS(CH_2)_3SMe\}]_n$ with numbering scheme adopted. Ellipsoids are drawn at 40 % probability. Neighbouring atoms are included marked with an asterisk (related by a crystallographic inversion centre). C(5) is disordered across two sites, C(5) and C(5b), in a 6:4 ratio

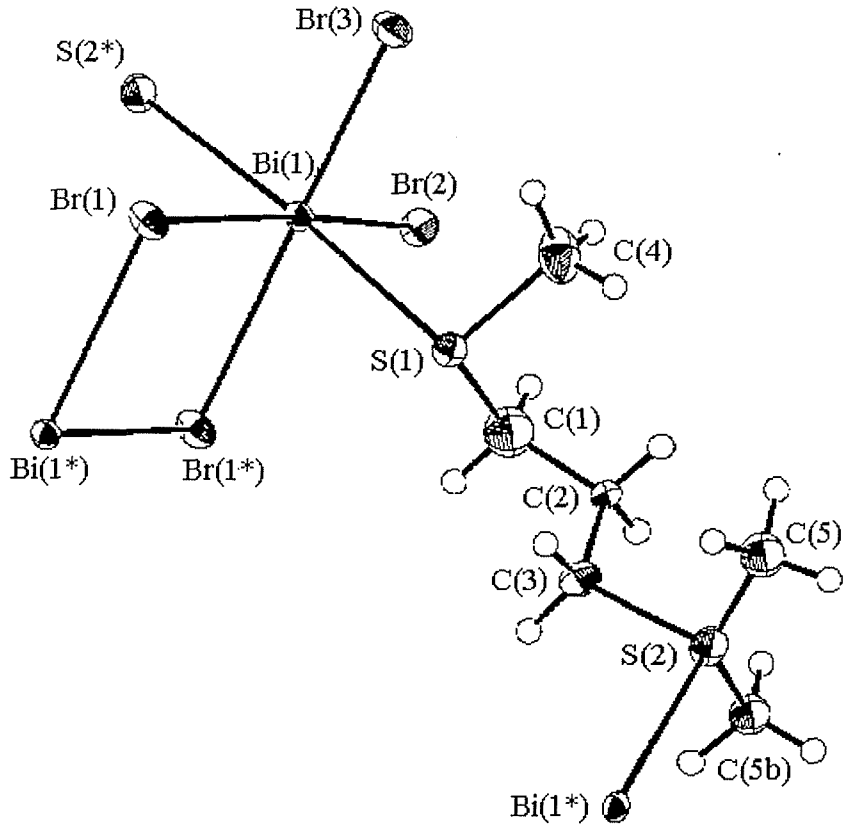

Table 6.7 Selected bond lengths (Å) with e.s.d.'s for $[BiBr_3\{MeS(CH_2)_3SMe\}]_n$; atoms marked with an asterisk (*) are symmetry related by a crystallographic inversion centre

Bi(1)	Br(1)	3.004(2)	Bi(1)	Br(1*)	2.980(2)
Bi(1)	Br(2)	2.719(2)	Bi(1)	Br(3)	2.697(2)
Bi(1)	S(2*)	2.880(4)	Bi(1)	S(1)	2.931(4)

Table 6.8 Selected bond angles (°) with e.s.d.s for $[BiBr_3\{MeS(CH_2)_3SMe\}]_n$; atoms marked with an asterisk (*) are symmetry related by a crystallographic inversion centre

Br(1*)	Bi(1)	Br(1)	83.80(5)	Br(1)	Bi(1)	Br(2)	90.16(5)
Br(1)	Bi(1)	Br(3)	175.18(6)	Br(1)	Bi(1)	S(2*)	94.4(1)
Br(1)	Bi(1)	S(1)	82.74(9)	Br(1*)	Bi(1)	Br(2)	173.40(5)
Br(1*)	Bi(1)	Br(3)	92.64(6)	Br(1*)	Bi(1)	S(2*)	88.8(1)
Br(1*)	Bi(1)	S(1)	88.35(9)	Br(2)	Bi(1)	Br(3)	93.53(6)
Br(2)	Bi(1)	S(2*)	89.0(1)	Br(2)	Bi(1)	S(1)	93.53(9)
Br(3)	Bi(1)	S(2*)	88.8(1)	Br(3)	Bi(1)	S(1)	93.9(1)
S(2*)	Bi(1)	S(1)	176.(1)	Bi(1)	Br(1)	Bi(1*)	96.20(5)

Figure 6.18 View of a portion of the *meso* form of $[BiBr_3\{MeS(CH_2)_3SMe\}]_n$ structure with the numbering scheme adopted (ellipsoids are drawn at 40 % probability; H atoms are omitted for clarity and atoms marked with an asterisk (*) are related by a crystallographic inversion centre

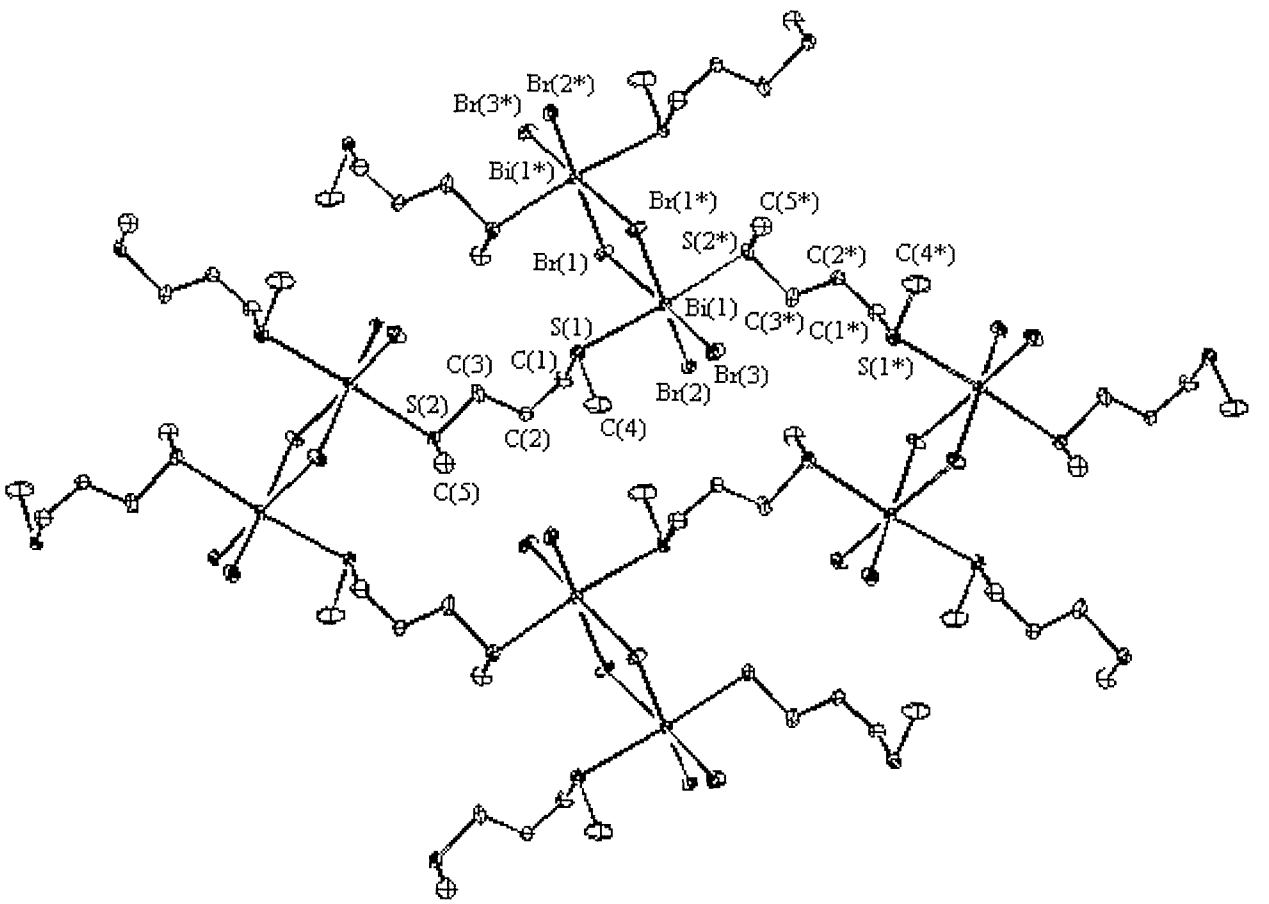

Crystals were also obtained from a 1:1 mix of $BiCl_3$ and the selenoether analogue, $MeSe(CH_2)_3SeMe$. Analysis showed that the 1:1 Bi:diselenoether ligand stoichiometry was maintained. The X-ray structure obtained for this compound, shows the same two-dimensional array as seen for $[BiBr_3\{MeS(CH_2)_3SMe\}]_n$ (Figure 6.18). The edge-shared, bioctahedral Bi_2Cl_6 dimers are linked by the diselenoether ligand which bridges between staggered Bi_2Cl_6 dimer units. The asymmetric unit for this structure is shown in Figure 6.19, with bond lengths (Å) and angles (°) presented in Tables 6.9 and 6.10. Each Bi^{III} is bound to two terminal Cl atoms, two μ_2-bridging Cl atoms and two mutually *trans* Se-donor atoms. The octahedral geometry is slightly distorted from the ideal (Se(1)-Bi-Se(2) 173.19(4)°, Se(1)-Bi-Cl(1) 89.9(1)°, Se(1)-Bi-Cl(2) 97.3(1)°, Se(1)-Bi-Cl(3) 83.6(1)°). As with $[BiBr_3\{MeS(CH_2)_3SMe\}]_n$, there is an inversion centre at the centre of the Bi_2Cl_6 dimer.

Figure 6.19 View of the asymmetric unit for $[BiCl_3\{MeSe(CH_2)_3SeMe\}]_n$ with numbering scheme adopted. Ellipsoids are drawn at 40 % probability. Neighbouring atoms are included marked with an asterisk (related by a crystallographic inversion centre)

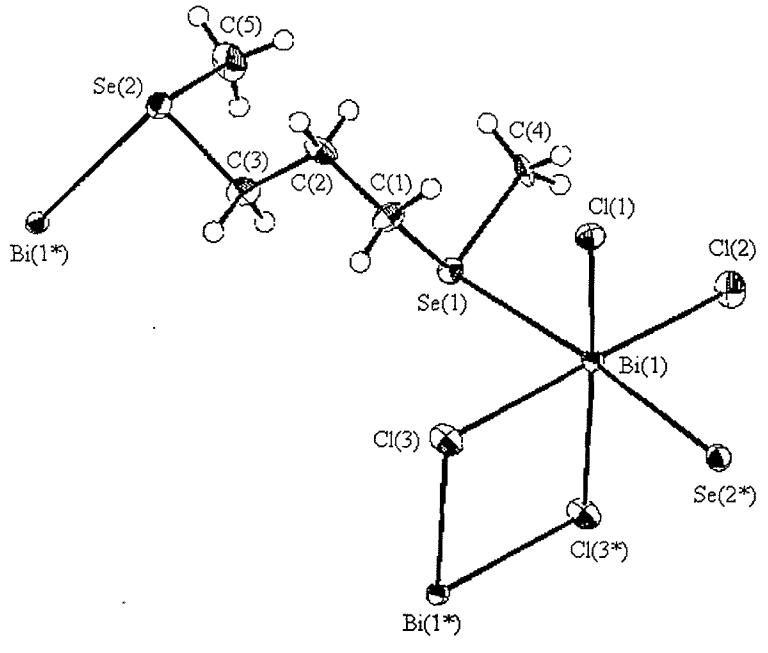

Table 6.9 Selected bond lengths (Å) with e.s.d.s for $[BiCl_3\{MeSe(CH_2)_3SeMe\}]_n$; atoms marked with an asterisk are related by a crystallographic inversion centre

Bi(1)	Se(1)	3.036(2)	Bi(1)	Se(2*)	2.988(2)
Bi(1)	Cl(1)	2.554(4)	Bi(1)	Cl(2)	2.566(4)
Bi(1)	Cl(3)	2.826(4)	Bi(1)	Cl(3*)	2.884(4)

Table 6.10 Selected bond angles (°) with e.s.d.s for $[BiCl_3\{MeSe(CH_2)_3SeMe\}]_n$; atoms marked with an asterisk are related by a crystallographic inversion centre

Cl(1)	Bi(1)	Cl(2)	89.7(1)	Cl(1)	Bi(1)	Cl(3)	90.3(1)
Cl(1)	Bi(1)	Cl(3*)	172.2(1)	Cl(1)	Bi(1)	Se(2*)	89.7(1)
Cl(1)	Bi(1)	Se(1)	89.9(1)	Cl(2)	Bi(1)	Cl(3)	179.1(1)
Cl(2)	Bi(1)	Cl(3*)	97.3(1)	Cl(2)	Bi(1)	Se(2*)	89.5(1)
Cl(2)	Bi(1)	Se(1)	97.3(1)	Cl(3)	Bi(1)	Cl(3*)	82.6(1)
Cl(3)	Bi(1)	Se(2*)	89.6(1)	Cl(3)	Bi(1)	Se(1)	83.6(1)
Cl(3*)	Bi(1)	Se(2*)	87.0(1)	Cl(3*)	Bi(1)	Se(1)	92.6(1)
Se(2)	Bi(1)	Se(1)	173.19(4)				

Figure 6.20 View of a portion of the $[BiBr_3([16]aneSe_4)]_n$ structure, illustrating the extended 'ladder' configuration. Ellipsoids are drawn at 40 % probability. Atoms marked with an asterisk (*) are related by a crystallographic inversion centre (taken from ref. 32)

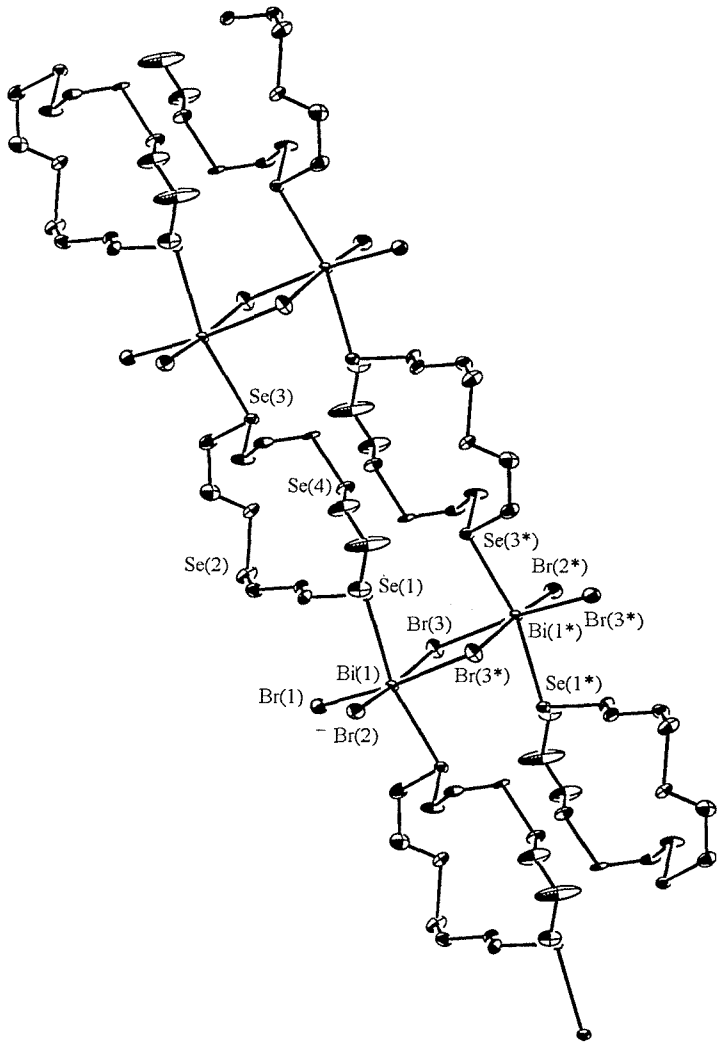

The only other structurally characterised example of a bismuth complex, $[(Me_2N)_3PSeSeP(Me_2N)_3][Bi_2Cl_8]$,[19] is ionic and the Se-donors are not coordinated. Subsequent work within the Southampton research group[32] on multidentate selenoether complexes of the bismuth(III) halides has produced further structures for comparison. The structures of $[BiCl_3([8]aneSe_2)]_n$ (where $[8]aneSe_2$ = 1,5-diselenacyclooctane), $[BiBr_3([16]aneSe_4)]_n$ (Figure 6.20; where $[16]aneSe_4$ = 1,5,9,13-tetraselenacyclohexadecane), $[Bi_2Cl_6\{MeC(CH_2SeMe)_3\}]_n$ and $[Bi_2I_6\{MeC(CH_2SeMe)_3\}]$ have been determined and all feature the edge-shared,

bioctahedral dimer subunits. The two structures involving macrocyclic ligands, $[BiCl_3([8]aneSe_2)]_n$ and $[BiBr_3([16]aneSe_4)]_n$, form one-dimensional 'ladder' structures (Figure 6.20) with the Bi_2X_6 dimers forming the 'steps' and the selenoether ligands forming the 'uprights'. The tripod selenoether, $MeC(CH_2SeMe)_3$, which might have been expected to cap the BiX_3 units in a *fac* conformation, form two very different structures. $[Bi_2I_6\{MeC(CH_2SeMe)_3\}]$ incorporates dimeric units analogous to the literature examples of dimethylene backboned diphosphine complexes,[2,3,7,8,20] with one arm of the tripod remaining uncoordinated. In contrast to this, the $BiCl_3$ adduct forms an extended two-dimensional sheet incorporating Bi_2Cl_6 dimers with bidentate selenoether coordination at each Bi centre. The third Se-donor from each tripodal ligand crosslinks these to give the sheet, and gives an Se_3Cl_4 donor set at each Bi centre. The Bi-Se bond distances (2.989(3) and 3.035(3) Å) seen in $[BiCl_3\{MeSe(CH_2)_3SeMe\}]_n$ are in good agreement with these other selenoether complexes (2.952(2) – 3.19(1) Å). Significantly, the Bi-Se bond distances for this species are similar to the Bi-S bond distances in the macrocyclic thioether complexes[22-24] (2.987(3) – 3.313(2) Å), despite the larger radius of Se over S, suggesting a stronger interaction between the Bi(III) centre and the donor atoms for this species. The Bi-Cl bond distances (2.555(7), 2.570(7), 2.829(7) and 2.883(7) Å) are also consistent with previous literature examples[22-24] and also with $[BiCl_3\{MeC(CH_2SeMe)_3\}]_n$[32] (2.55(1), 2.622(9) and 2.776(8) Å). The Bi-Cl bond distances for the terminal Cl atoms in $[BiCl_3\{MeSe(CH_2)_3SeMe\}]_n$ are also considerably shorter, 2.555(7) and 2.570(7) Å, than those of the μ_2-bridging Cl atoms, 2.829(7) and 2.883(7) Å, as has been observed for the previous examples of this study and consistent with the observations of Sawyer and Gillespie[27] that the stereochemically active lone pair of electrons of Bi lying within the Bi_2Cl_6 plane. The same pattern is seen for $[BiCl_3\{MeC(CH_2SeMe)_3\}]_n$.[32]

When the analogous reaction was undertaken using $BiBr_3$ and $MeSe(CH_2)_3SeMe$, a solid analysing as $[BiBr_3\{MeSe(CH_2)_3SeMe\}]_n$ was obtained. Crystals obtained for this compound show the same structure as $[BiBr_3\{MeS(CH_2)_3SMe\}]_n$ (Figure 6.18) with an extended two-dimensional sheet of Bi_2Br_6 edge-shared, bioctahedral dimers crosslinked by the diselenoether ligands. The asymmetric unit for this structure is shown in Figure 6.21, with bond lengths (Å) and angles (°) presented in Tables 6.11 and 6.12.

Figure 6.21 View of the asymmetric unit for $[BiBr_3\{MeSe(CH_2)_3SeMe\}]_n$ with numbering scheme adopted. Ellipsoids are drawn to 40 % probability. Neighbouring atoms are included marked with an asterisk (*) (related by a crystallographic inversion centre)

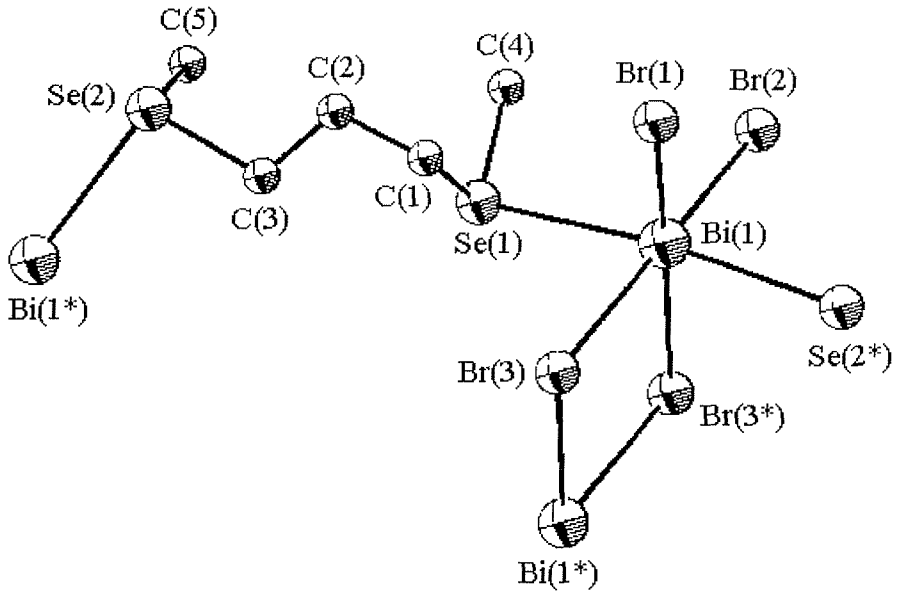

Table 6.11 Selected bond lengths (Å) with e.s.d.s for $[BiBr_3\{MeSe(CH_2)_3SeMe\}]_n$; atoms marked with an asterisk (*) are related by a crystallographic inversion centre

Bi(1)	Br(1)	2.725(3)	Bi(1)	Br(2)	2.711(3)
Bi(1)	Br(3)	2.995(3)	Bi(1)	Br(3*)	2.980(2)
Bi(1)	Se(1)	3.027(2)	Bi(1)	Se(2)	2.977(3)

Table 6.12 Selected bond angles (°) with e.s.d.s for $[BiBr_3\{MeSe(CH_2)_3SeMe\}]_n$; atoms marked with an asterisk (*) are related by a crystallographic inversion centre

Br(1)	Bi(1)	Se(2*)	89.46(8)	Br(1)	Bi(1)	Br(3*)	172.60(8)
Br(1)	Bi(1)	Br(3)	89.94(7)	Br(1)	Bi(1)	Se(1)	94.67(7)
Br(2)	Bi(1)	Br(1)	93.07(8)	Br(2)	Bi(1)	Se(2*)	90.71(8)
Br(2)	Bi(1)	Br(3*)	93.76(7)	Br(2)	Bi(1)	Br(3)	175.89(8)
Br(2)	Bi(1)	Se(1)	95.10(8)	Br(3)	Bi(1)	Br(3*)	83.38(7)
Br(3)	Bi(1)	Se(1)	81.86(7)	Br(3*)	Bi(1)	Se(1)	87.56(7)
Se(2*)	Bi(1)	Br(3*)	87.61(8)	Se(2*)	Bi(1)	Br(3)	92.12(8)
Se(2*)	Bi(1)	Se(1)	172.67(7)	Bi(1)	Br(3)	Bi(1*)	96.62(7)

The Bi-Se bond distances in this species, 2.976(3) and 3.027(2) Å, are consistent with those of the chloride analogue, 2.989(3) and 3.035(3) Å, and are similar to the Bi-S bond distances in reported macrocyclic thioether complexes[22-24] (2.987(3) – 3.313(2) Å), which again suggests that the interaction between the Bi(III) centre and the donor atoms in this system are stronger than those observed in the macrocyclic thioether systems. The bond distances within the Bi_2Br_6 dimer show the same pattern as seen in the Bi_2Cl_6 analogue. The bond distances for terminal Br atoms, 2.711(3) and 2.725(3) Å, are significantly shorter than those of the μ_2-bridging Br atoms, 2.980(2) and 2.995(3) Å, again pointing to the presence of the bismuth based lone pair within the plane of the Bi_2Br_6 dimer.

6.2.3. Synthesis and Properties of Bidentate Group 15 Complexes of BiX_3

A number of bidentate amine[4-6] and phosphine[7,8] complexes of Bi(III) have been characterised previously, but to-date very little work has been reported on arsine complexes of the bismuth(III) halides.[9] A range of complexes of type $BiX_3(L\text{-}L)$ (where X = Cl, Br or I; L-L = $Ph_2As(CH_2)_2AsPh_2$ (dpae) or o-$C_6H_4(AsMe_2)_2$) and $BiX_3(L\text{-}L\text{-}L)$ (where X = Cl, Br or I; L-L-L = $MeC(CH_2AsMe_2)_3$ (triars)) have been produced by reaction of BiX_3 with the appropriate ligand in MeCN. Concentration of the resultant coloured solutions produced solids which were filtered, washed with anhydrous CH_2Cl_2 and dried *in vacuo*. The solids were treated as air-sensitive and stored in a dinitrogen purged dry-box. However, the complexes were found to decompose only slowly in moist air, although they appear to be more easily hydrolysed in solution. Satisfactory microanalyses were recorded for all solids isolated and IR spectra of the $BiCl_3$ species show several features in the range 230-280 cm^{-1} assigned to ν(Bi-Cl). The IR spectra of all complexes formed were also checked for the formation of arsine-oxide (ν(As=O) = 800 - 860 cm^{-1} for $[BiCl_3(dpae)]$[20]). As has been seen from the complexes of group 16 ligands, however, it is difficult to formulate any structural information from the limited range of spectroscopic and analytical techniques available. Therefore it was necessary to resort to X-ray crystallography.

Figure 6.22 View of the dimeric structure of $[Bi_2I_6(diars)_2]$ with numbering scheme adopted. Ellipsoids are drawn at 40 % probability. Atoms marked with an asterisk (*) are related by a crystallographic inversion centre. H atoms omitted for clarity

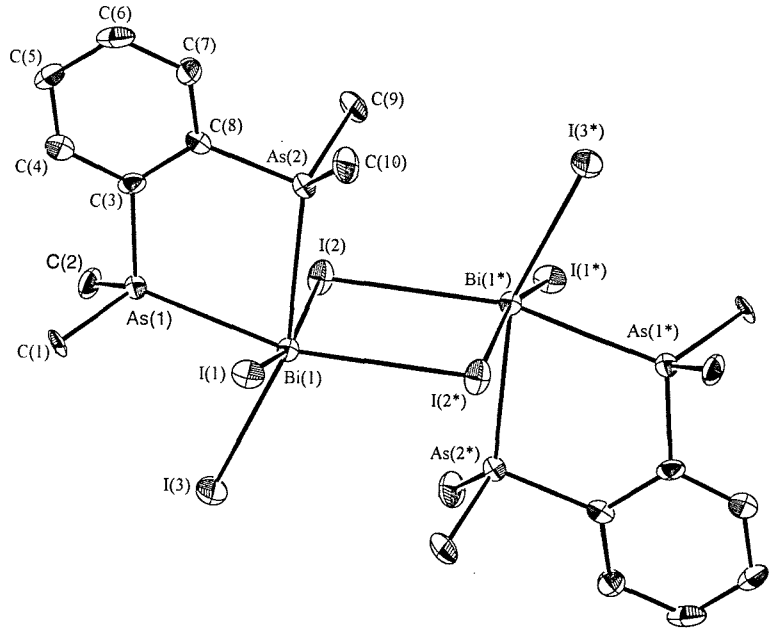

6.2.4. Single Crystal X-ray Diffraction Studies

Crystals were obtained for the solid isolated from the 1:1 mix of BiI_3 with diars. The analytical data obtained for this product indicate a 1:1 stoichiometry. The X-ray structure shows that the complex adopts the same form as the phosphine complexes previously characterised,[7,8] with formula $[Bi_2I_6(diars)_2]$. The structure for this complex is shown in Figure 6.22, with bond lengths (Å) and angles (°) are presented in Tables 6.13 and 6.14. The structure features the edge-shared, bioctahedral dimer with each Bi atoms bound to two terminal I atoms, two μ_2-bridging I atoms and two mutually *cis* As atoms from the chelating diars ligands. The fact that this ligand chelates, whereas $PhS(CH_2)_2SPh$ bridges, is not surprising, since o-phenylene backboned ligands of this type have been shown to form very stable complexes.[33] The pyramidal unit of the parent halide is retained, with one weaker, secondary Bi···I interaction and with two As atoms replacing the remaining secondary iodide interactions. This again means that the

octahedral geometry is quite severely distorted (I(1)-Bi-I(2) 164.24(4)°, I(1)-Bi-I(3) 101.97(4)°, I(1)-Bi-As(1) 84.60(4)°, I(1)-Bi-As(2) 82.95(4)°). This is the first structurally characterised example of a Bi(III) - arsine complex. The Bi-As bond distances observed for this complex, 2.801(2) and 2.974(2) Å, are *ca.* 0.2 Å longer than the Bi-P bond distances observed for $[Bi_2Br_6(dmpe)_2]$[7] (2.678(8) and 2.791(7) Å) or $[Bi_2Cl_6(dppe)_2]$[8] (2.699(8), 2.945(9) and 2.956(10) Å) consistent with the increased radius of As over P, combined with the poorer σ-donor nature of the arsine. The Bi-I bond distances for $[Bi_2I_6(diars)_2]$ (2.992(2), 3.032(1), 3.117(2) and 3.328(1) Å) are consistent with the observed values for $[Me_3S]_2[Bi_2I_8(Me_2S)_2]$[21] (2.934(3), 2.954(3), 2.955(3), 3.229(3) and 3.234(3) Å) and both have considerably longer bond lengths for the μ_2-bridging I atoms than the terminal I atoms.

Table 6.13 Selected bond lengths (Å) with e.s.d.s for $[Bi_2I_6(diars)_2]$. Atoms marked with an asterisk (*) are related by a crystallographic inversion centre

Bi(1)	I(1)	2.992(2)	Bi(1)	I(2)	3.117(2)
Bi(1)	I(2*)	3.328(2)	Bi(1)	I(3)	3.032(1)
Bi(1)	As(1)	2.801(2)	Bi(1)	As(2)	2.974(2)

Table 6.14 Selected bond angles (°) with e.s.d.s for $[Bi_2I_6(diars)_2]$. Atoms marked with an asterisk (*) are related by a crystallographic inversion centre

I(1)	Bi(1)	I(2)	164.24(4)	I(1)	Bi(1)	I(2)	93.52(4)
I(1)	Bi(1)	I(3)	101.97(4)	I(1)	Bi(1)	As(1)	84.60(4)
I(1)	Bi(1)	As(2)	82.95(4)	I(2)	Bi(1)	I(2)	90.50(3)
I(2)	Bi(1)	I(3)	90.69(5)	I(2)	Bi(1)	As(1)	87.54(4)
I(2)	Bi(1)	As(2)	81.79(5)	I(2)	Bi(1)	I(3)	111.39(4)
I(2)	Bi(1)	As(1)	164.83(4)	I(2)	Bi(1)	As(2)	90.38(5)
I(3)	Bi(1)	As(1)	83.68(4)	I(3)	Bi(1)	As(2)	157.10(5)
As(1)	Bi(1)	As(2)	74.45(5)	Bi(1)	I(2)	Bi(1*)	89.50(3)

6.3. Conclusions

This work represents the first investigation of bismuth(III) halide complexes of acyclic group 16 donor ligands and the selenoether complexes are the first examples of their type.

By the very nature of these Bi(III) species, their characterisation is restricted to analytical data, IR spectroscopy and single crystal X-ray diffraction studies. While the stoichiometry of the products is not in question, the structural motifs described here represent those species which yielded suitable quality crystals. Other motifs may be obtainable under different conditions. At present we can only discuss those structures which we have identified, but there is clearly the caveat that the discussion may need modification in light of further results. The large variety of different structural motifs for these group 16 ligand complexes means that it is not possible to formulate any structures on the basis of the analytical data or IR spectroscopy. The X-ray crystal structures obtained for these species have shown some very unexpected structural motifs in stark contrast to previous examples involving acyclic[2,3,7,8,20,21] or macrocyclic[22-24] ligand complexes. For the methyl substituted ligands, $MeS(CH_2)_nSMe$ (n = 2 or 3), when n = 2 discrete monomers are obtained of the form $[BiX_3\{MeS(CH_2)_2SMe\}]_2$ with the two ligands chelated, but for n = 3 the group 16 ligands bridge between edge-shared, bioctahedral Bi_2X_6 dimers. These Bi_2X_6 units have been identified in other bismuth(III) halide complexes[2,3,7,8,20,21] but only as discrete dimeric units. The fact that $[Bi_2Br_6\{PhS(CH_2)_2SPh\}]$ does not form the same in the same stoichiometry as the methyl substituted systems may be due to the added steric hindrance of the larger phenyl groups and the weaker σ-donor capability of the ligand over the methyl substituted analogues. Clearly more examples are required to deduce exactly why these complexes adopt such different structures.

The complex formed between diars and bismuth(III) iodide has been found to form the same dimeric structural type as previously studied group 15 ligands.[7,8] The presence of the o-phenylene backbone will promote the formation of a chelate structure. However, in light of the large number of structural motifs that have been characterised for Bi^{III} complexes, a large structural diversity may also be expected for these species depending on the arsine ligand employed.

6.4. Experimental

The bismuth(III) chloride, bromide and iodide and anhydrous CH_2Cl_2 were purchased from *Aldrich Chemicals*. The ligands $RS(CH_2)_nSR$[34] (where n = 2 or 3; R = Me or Ph), $RSe(CH2)_nSeR$[35] (where n = 2 or 3; R = Me or Ph), o-$C_6H_4(EMe)_2$ (where E = S[36] or Se[37]), $Ph_2As(CH_2)_2AsPh$,[38] o-$C_6H_4(AsMe_2)_2$[39] and were all produced by literature methods. $MeC(CH_2AsMe_2)_3$[39] was kindly produced by Professor W. Levason. MeCN was dried over P_2O_5 prior to use.

Tin(IV) halides are extremely moisture sensitive and phosphines easily oxidised in solution, therefore all of the reactions were carried out under an atmosphere of dry nitrogen in dry solvents purchased from *Aldrich Chemicals*, using standard Schlenk, vacuum-line and dry box techniques.

Single Crystal X-ray Diffraction

Single crystals of $[Bi_4Cl_{12}\{MeS(CH_2)_3SMe\}_4]_n.nH_2O$ were obtained by slow evaporation of a solution of the compound in CH_2Cl_2. Crystals of $[BiBr_3\{MeS(CH_2)_2SMe\}_2]$, $[BiI_3\{MeS(CH_2)_2SMe\}_2]$, $[Bi_2Br_6\{PhS(CH_2)_2SPh\}]$, $[BiBr_3\{MeSe(CH_2)_3SeMe\}]$, $[BiCl_3\{MeSe(CH_2)_3SeMe\}]$ and $[BiBr_3\{MeSe(CH_2)_3SeMe\}]$ and $[Bi_2I_6(diars)_2]$ were all obtained by slow evaporation of a solution of the relevant compound in MeCN. It was assumed that the crystals were moisture sensitive and therefore in each case the selected crystal was coated with mineral oil, mounted on a glass fibre using silicone grease as adhesive, and immediately placed in a stream of cold nitrogen gas. Data collection for $[BiBr_3\{MeS(CH_2)_3SMe\}]$ used an Enraf-Nonius Kappa-CCD diffractometer. Data collection for the remaining structures used a Rigaku AFC7S four-circle diffractometer equipped with an Oxford Cryostreams low temperature attachment operating at 150 K, using graphite-monochromated Mo-K_α X-radiation (λ = 0.71073 Å), T = 150 K, ω-2θ scans. The intensities of three standard reflections were monitored every 150 reflections. No significant crystal decay or movement was observed. As there were no identifiable faces for $[BiBr_3\{MeS(CH_2)_2SMe\}_2]$ and $[BiCl_3\{MeSe(CH_2)_3SeMe\}]$ the raw data were corrected for absorption using psi-scans. The weighting scheme $w^{-1} = \sigma^2(F)$ gave satisfactory agreement analyses in each case. The structures were solved by direct methods,[40] and then developed by iterative cycles of full-matrix least-

squares refinement (based on *F*) and difference Fourier syntheses which located all non-H atoms in the asymmetric unit.[41] For $[Bi_4Cl_{12}\{MeS(CH_2)_3SMe\}_4]_n.nH_2O$, $[Bi_2Br_6\{PhS(CH_2)_2SPh\}]$, $[BiBr_3\{MeSe(CH_2)_3SeMe\}]$ and $[Bi_2I_6(diars)_2]$ an empirical absorption correction using DIFABS[42] was applied to the raw data at isotropic convergence, as psi scans did not provide a satisfactory absorption correction. For $[BiBr_3(MeS(CH_2)_3SMe)]$ the raw data were corrected for absorption using SORTAV.[43] All non-H atoms in the structures were refined anisotropically (with the exception of $[Bi_4Cl_{12}\{MeS(CH_2)_3SMe\}_4]_n.nH_2O$ and $[BiBr_3\{MeSe(CH_2)_3SeMe\}]$ for which the C atoms were refined isotropically as they turn non-positive definite when refined anisotropically, probably a result of an imperfect absorption correction, and one methyl carbon {C(6)} which is disordered across two sites) and H atoms were placed in fixed, calculated positions with *d*(C-H) = 0.96 Å for $[Bi_4Cl_{12}\{MeS(CH_2)_3SMe\}_4]_n.nH_2O$, $[BiBr_3\{MeS(CH_2)_2SMe\}_2]$, $[BiBr_3\{MeS(CH_2)_3SMe\}]$, $[BiCl_3\{MeSe(CH_2)_3SeMe\}]$ and $[Bi_2I_6(diars)_2]$. For $[Bi_4Cl_{12}\{MeS(CH_2)_3SMe\}_4]_n.nH_2O$ and $[BiBr_3\{MeS(CH_2)_2SMe\}_2]$ the Flack parameter was refined and indicated the correct enantiomorph in each case.

Crystallographic data for these structures are presented in Table 6.15.

Table 6.15. Crystallographic data

Compound	$[BiBr_3\{MeS(CH_2)_2SMe\}_2]$	$[Bi_2Br_6\{PhS(CH_2)_2SPh\}]$	$[Bi_4Cl_{12}\{MeS(CH_2)_3SMe\}_4]_nH_2O$	$[BiBr_3\{MeS(CH_2)_3SMe\}]$
Formula	$C_8H_{20}S_4Br_3Bi$	$C_{14}H_{14}S_2Br_6Bi_2$	$C_5H_{14}OS_2Cl_3Bi$	$C_5H_{12}S_2Br_3Bi$
Formula Weight	693.18	1104.77	1189.71	584.96
Colour, morphology	Yellow, block	Yellow, block	Yellow, block	Yellow, block
Crystal dimensions/mm	0.59 x 0.15 x 0.13	0.26 x 0.13 x 0.11	0.67 x 0.35 x 0.30	0.20 x 0.14 x 0.05
Crystal System	Orthorhombic	Monoclinic	Monoclinic	Monoclinic
Space Group	$P2_12_12_1$	$P2_1/c$	$P\bar{4}2_1c$	C2/c
a/Å	13.040(1)	9.267(3)	16.440(10)	12.9497(4)
b/Å	14.493(2)	6.981(2)	16.440(10)	11.8967(3)
c/Å	9.883(2)	18.340(5)	11.843(7)	18.0227(4)
β/°	90	93.94(2)	90	102.895(2)
U/Å^3	1867.8(5)	1183.6(6)	3200(3)	2706.5(1)
Z	4	2	8	8
Scan type	ω-2θ	ω-2θ	ω-2θ	φ-ω
$F(000)$	1280	1012	1744	2096
D_c/g cm^{-3}	2.465	3.200	1.949	2.871
μ(Mo-K_α)/cm^{-1}	162.85	251.53	117.26	221.51
Transmission factors (max. and min.)	1.000, 0.8074	1.000, 0.5353	1.000, 0.3092	0.633, 0.222
No. of Unique obs. reflections	1907	2277	1668	2873
R_{int} (based on F^2)		0.093		0.102
Unique obs. Reflections with [$I_o > 2.0\sigma(I_o)$]	1548	1212	1183	2138
No. of parameters	145	109	79	99
Goodness of fit	1.92	1.94	1.80	1.58
$R(F_o)$	0.035	0.044	0.050	0.065
$R_w(F_o)$	0.044	0.049	0.066	0.077
Max. residual peak/eÅ^{-3}	1.57	3.11	2.40	2.45
Max. residual trough/eÅ^{-3}	-2.43	-1.72	-1.99	-4.29

$$R = \Sigma\,(|F_{obs}|_i - |F_{calc}|_i)/\Sigma\,|F_{obs}|_I$$

$$R_w = \sqrt{[\Sigma\, w_i(|F_{obs}|_i - |F_{calc}|_i)^2 / \Sigma\, w_i|F_{obs}|_i^2]}$$

$$GOF = [\Sigma\,(|F_{obs}|_i - |F_{calc}|_i)/\sigma_i]/(n - m) \approx 1$$

Table 6.15. cont. Crystallographic data

Compound	$[BiCl_3\{MeSe(CH_2)_3SeMe\}]$	$[BiBr_3\{MeSe(CH_2)_3SeMe\}]$	$[Bi_2I_6\{o\text{-}C_6H_4(AsMe_2)_2\}]$
Formula	$C_5H_{12}Cl_3Se_2Bi$	$C_5H_{12}Br_3Se_2Bi$	$C_{10}H_{16}As_2I_3Bi$
Formula Weight	545.41	678.76	875.77
Colour, morphology	Yellow, block	Yellow, plate	Orange, lathe
Crystal dimensions/mm	0.47 x 0.18 x 0.10	0.36 x 0.27 x 0.05	0.32 x 0.15 x 0.03
Crystal System	Monoclinic	Monoclinic	Monoclinic
Space Group	$P2_1/c$	$C2/c$	$P2_1/n$
a/Å	8.653(6)	13.013(2)	9.009(5)
b/Å	12.024(5)	12.012(2)	12.620(4)
c/Å	12.600(6)	18.305(4)	16.765(3)
β/°	107.70(5)	103.64(2)	90.98(2)
U/Å^3	1249(1)	2780.5(9)	1906(1)
Z	4	8	4
Scan type	ω-2θ	ω-2θ	ω-2θ
$F(000)$	976	2384	1536
D_c/g cm^{-3}	2.900	3.243	3.052
μ(Mo-K_α)/cm^{-1}	205.11	264.99	174.59
Transmission factors (max. and min.)	1.000, 0.4325	1.000, 0.4408	1.000, 0.6217
No. of Unique obs. reflections	2317	2998	3522
R_{int} (based on F^2)	0.068		0.123
Unique obs. reflections with [$I_o > 2.0\sigma(I_o)$]	1721	1056	1941
No. of parameters	100	75	145
Goodness of fit	2.47	1.75	1.13
$R(F_o)$	0.045	0.038	0.035
$R_w(F_o)$	0.049	0.040	0.038
Max. residual peak/eÅ^{-3}	3.65	1.39	1.21
Max. residual trough/eÅ^{-3}	-2.58	-1.19	-1.09

$$R = \Sigma\,(|F_{obs}|_i - |F_{calc}|_i)/\Sigma\,|F_{obs}|_i$$
$$R_w = \sqrt{[\Sigma\, w_i(|F_{obs}|_i - |F_{calc}|_i)^2 / \Sigma\, w_i|F_{obs}|_i^2]}$$
$$GOF = [\Sigma\,(|F_{obs}|_i - |F_{calc}|_i)/\sigma_i]/(n - m) \approx 1$$

Complex Synthesis

$[BiCl_3\{MeS(CH_2)_2SMe\}_2]$

A solution of $BiCl_3$ (0.160 g, 0.52 mmol) in dry, degassed MeCN (4 cm^3) was added to a stirring solution of $MeS(CH_2)_2SMe$ (0.060 g, 0.52 mmol) in CH_2Cl_2 (2 cm^3) at room temperature. A yellow solution is formed almost immediately. Concentrating the solution *in vacuo* gave a yellow solid which was filtered, washed with CH_2Cl_2 and dried *in vacuo*. Yield 0.147 g, 67 %. IR (CsI disc): $\nu_{Bi\text{-}Cl}$ 227, 250, 281 cm^{-1}. Found: C, 17.2; H, 3.3. Calculated for $C_8H_{20}S_4Cl_3Bi$: C, 11.0; H, 3.6 %.

$[BiBr_3\{MeS(CH_2)_2SMe\}_2]$

The same general method with $BiBr_3$ (0.16 g, 0.35 mmol) in MeCN (6 cm^3) and $MeS(CH_2)_2SMe$ (0.040 g, 0.35 mmol) in CH_2Cl_2 (2 cm^3) yielded a dark yellow solid. Yield 0.122 g, 61 %. Found: C, 13.5; H, 2.6. Calculated for $C_8H_{20}S_4Br_3Bi$: C, 13.9; H, 2.9 %.

$[BiI_3\{MeS(CH_2)_2SMe\}_2]$

BiI_3 (0.206 g, 0.035 mmol) in MeCN (15 cm^3) reacted with $MeS(CH_2)_2SMe$ (0.04 g, 0.035 mmol) in CH_2Cl_2 (2 cm^3) to yield dark red diamond shaped crystals on concentration. Yield 0.91, 37 %. Found: C, 11.7; H, 2.5. Calculated for $C_8H_{20}S_4I_3Bi$: C, 11.5; H, 2.4 %.

$[BiCl_3\{MeS(CH_2)_3SMe\}]$

The same general method with $BiCl_3$ (0.16 g, 0.52 mmol) and $MeS(CH_2)_3SMe$ (0.071 g, 0.52 mmol) in MeCN (10 cm^3) gave a yellow solid. Yield 0.18g, 78 %. IR (CsI disc): $\nu_{Bi\text{-}Cl}$ 245, 263, 274 cm^{-1}. Found: C, 13.1; H, 2.7. Calculated for $C_5H_{12}S_2Cl_3Bi$: C, 13.3; H, 2.7 %.

$[BiCl_3\{MeS(CH_2)_3SMe\}]_n.nH_2O$

When $BiCl_3$ (0.16 g, 0.52 mmol) was stirred with $MeS(CH_2)_3SMe$ (0.071 g, 0.52 mmol) in CH_2Cl_2 (20 cm^3) the white $BiCl_3$ solid was seen to turn yellow and a yellow solution formed. Concentration of the solution yielded yellow crystals which were filtered, washed with Na-dried petroleum ether and dried *in vacuo*. Yield 0.046 g, 20 %. IR (CsI disc): $\nu_{Bi\text{-}Cl}$ 239, 258, 279 cm^{-1}. Found: C, 13.0; H, 2.8. Calculated for $C_5H_{14}O_1S_2Cl_3Bi$: C, 12.8; H, 3.0 %.

[$BiBr_3${$MeS(CH_2)_3SMe$}]

$BiBr_3$ (0.16 g, 0.35 mmol) was treated with $MeS(CH_2)_3SMe$ (0.05 g, 0.35 mmol) in MeCN (10 cm^3) forming a yellow solution which yielded a yellow solid on concentration *in vacuo*. This was filtered, washed with CH_2Cl_2 and dried *in vacuo*. Yield 0.16 g, 76 %. Found: C, 10.4; H, 2.0. Calculated for $C_5H_{12}S_2Br_3Bi$: C, 10.3; H, 2.1 %.

[BiI_3{$MeS(CH_2)_3SMe$}]

The same reaction method with BiI_3 (0.206 g, 0.35 mmol) yielded a dark red powder. Yield 0.15 g, 59 %. Found: C, 8.5; H, 1.9. Calculated for $C_5H_{12}S_2I_3Bi$: C, 8.3; H, 1.7 %.

[Bi_2Cl_6{$PhS(CH_2)_2SPh$}]

The same reaction method with $BiCl_3$ (0.16 g, 0.52 mmol) and $PhS(CH_2)_2SPh$ (0.128 g, 0.52 mmol) in $MeCN/CH_2Cl_2$ (10 cm^3) gave an orange solid which was filtered, washed with CH_2Cl_2 and dried *in vacuo*. Yield 0.187 g, 67 %. IR (CsI disc): $\nu_{Bi\text{-}Cl}$ 219, 234, 271 cm^{-1}. Found: C, 19.6; H, 1.7. Calculated for $C_{14}H_{14}S_2Cl_6Bi_2$: C, 19.2; H, 1.6 %.

[Bi_2Br_6{$PhS(CH_2)_2SPh$}]

The same method with $BiBr_3$ (0.16 g, 0.35 mmol) and $PhS(CH_2)_2SPh$ (0.086 g, 0.35 mmol) yielded a dark orange powder. Yield 0.133 g, 54 %. Found: C, 13.4; H, 1.2. Calculated for $C_{14}H_{14}S_2Br_6Bi_2$: C, 13.6; H, 1.1 %.

[$BiCl_3${o-$C_6H_4(SMe)_2$}]

$BiCl_3$ (0.16 g, 0.52 mmol) and o-$C_6H_4(SMe)_2$ (0.09 g, 0.52 mmol) in MeCN (10 cm^3) gave an orange solid on concentration *in vacuo*. Yield 0.133 g, 53 %. IR (CsI disc): $\nu_{Bi\text{-}Cl}$ 227, 246, 282 cm^{-1}. Found: C, 19.4; H, 2.0. Calculated for $C_8H_{10}S_2Cl_3Bi$: C, 19.8; H, 2.1 %.

[$BiCl_3${$MeSe(CH_2)_2SeMe$}]

The same general method with $BiCl_3$ (0.16 g, 0.52 mmol) and $MeSe(CH_2)_2SeMe$ (0.112 g, 0.52 mmol) in MeCN (10 cm^3) gave a yellow solid. Yield 0.155 g, 57 %. IR (CsI disc): $\nu_{Bi\text{-}Cl}$ 234, 256, 279 cm^{-1}. Found: C, 10.0; H, 2.1. Calculated for $C_4H_{10}Se_2Cl_3Bi$: C, 9.7; H, 2.0 %.

[$BiBr_3${$MeSe(CH_2)_2SeMe$}]

The same general method with $BiBr_3$ (0.16 g, 0.35 mmol) and $MeSe(CH_2)_2SeMe$ (0.075 g, 0.35 mmol) in MeCN (10 cm^3) yielded a dark yellow solid. Yield 0.108 g, 46 %. Found: C, 7.0; H, 1.5. Calculated for $C_4H_{10}Se_2Br_3Bi$: C, 7.2; H, 1.5 %.

[BiI_3{$MeSe(CH_2)_2SeMe$}]

The same general method with BiI_3 (0.206 g, 0.35 mmol) and $MeSe(CH_2)_2SeMe$ (0.075 g, 0.35 mmol) in MeCN (10 cm^3) produced a blood red solid. Yield 0.045 g, 16 %. Found: C, 6.4; H, 1.4. Calculated for $C_4H_{10}Se_2I_3Bi$: C, 6.0; H, 1.2 %.

[$BiCl_3${$MeSe(CH_2)_3SeMe$}]

$BiCl_3$ (0.16 g, 0.52 mmol) and $MeSe(CH_2)_3SeMe$ (0.240 g, 1.04 mmol) in MeCN (10 cm^3) formed a yellow solid. Yield 0.21g, 75 %. IR (CsI disc): $\nu_{Bi\text{-}Cl}$ 238, 252, 263 cm^{-1}. Found: C, 10.8; H, 2.3. Calculated for $C_5H_{12}Se_2Cl_3Bi$: C, 11.0; H, 2.2 %.

[$BiBr_3${$MeSe(CH_2)_3SeMe$}]

$BiBr_3$ (0.16 g, 0.35 mmol) and $MeSe(CH_2)_3SeMe$ (0.16 g, 0.36 mmol) in MeCN (10 cm^3) gave a dark yellow solid. Yield 0.16 g, 64 %. Found: C, 9.1; H, 2.1. Calculated for $C_5H_{12}Se_2Br_3Bi$: C, 8.9; H, 1.8 %.

[$BiCl_3$(dpae)]

A solution of $BiCl_3$ (0.16 g, 0.52 mmol) in MeCN (5 cm^3) was added to dpae (0.253 g, 0.52 mmol) in CH_2Cl_2 (5 cm^3). A pale yellow solution formed immediately. On concentration *in vacuo* this gave a pale yellow solid which was filtered, washed with CH_2Cl_2 and dried *in vacuo*. Yield 0.292 g, 71 %. IR (CsI disc): $\nu_{Bi\text{-}Cl}$ 229, 247, 273 cm^{-1}. Found: C, 39.0; H, 3.1. Calculated for $C_{26}H_{24}As_2Cl_3Bi$: C, 39.0; H, 3.0 %.

[$BiBr_3$(dpae)]

The same method with $BiBr_3$ (0.16 g, 0.035 mmol) and dpae (0.170 g, 0.35 mmol) in MeCN (10 cm^3) produced a yellow solid. Yield 0.195 g, 59 %. Found: C, 32.9; H, 2.4. Calculated for $C_{26}H_{24}As_2Br_3Bi$: C, 33.4; H, 2.6 %.

[BiI_3(dpae)]

The same method with BiI_3 (0.206 g, 0.035 mmol) and dpae (0.170 g, 0.35 mmol) in MeCN (10 cm^3) gave a yellow solid. Yield 0.135 g, 36 %. Found: C, 29.3; H, 2.6. Calculated for $C_{26}H_{24}As_2I_3Bi$: C, 29.0; H, 2.3 %.

[$BiCl_3$(diars)]

$BiCl_3$ (0.16 g, 0.52 mmol) in MeCN (4 cm^3) gave a pale yellow solution when added to diars (0.150, 0.52 mmol) in CH_2Cl_2 (5 cm^3). Concentrating *in vacuo* produced a yellow solid. Yield 0.227 g, 73 %. IR (CsI disc): $\nu_{Bi\text{-}Cl}$ 232, 254, 268 cm^{-1}. Found: C, 19.6; H, 2.6. Calculated for $C_{10}H_{16}As_2Cl_3Bi$: C, 20.0; H, 2.7 %.

[$BiBr_3$(diars)]

The same method with $BiBr_3$ (0.16 g, 0.35 mmol) and diars (0.101, 0.35 mmol) formed a dark orange solid. Yield 0.167 g, 64 %. Found: C, 16.4; H, 2.2. Calculated for $C_{10}H_{16}As_2Br_3Bi$: C, 16.40; H, 2.20 %.

[BiI_3(diars)]

BiI_3 (0.206 g, 0.35 mmol) and diars (0.101, 0.35 mmol) in MeCN gave a red solid. Yield 0.175 g, 57 %. Found: C, 13.8; H, 2.0. Calculated for $C_{10}H_{16}As_2I_3Bi$: C, 13.7; H, 1.8 %.

[$BiCl_3$(triars)]

$BiCl_3$ (0.16 g, 0.52 mmol) in MeCN (5 cm^3) gave a pale yellow solution when added to a solution of triars (0.2 g, 0.52 mmol) in CH_2Cl_2 (5 cm^3). Concentration *in vacuo* gave a pale yellow solid. Yield 0.043 g, 12 %. IR (CsI disc): $\nu_{Bi\text{-}Cl}$ 236, 255, 282 cm^{-1}. Found: C, 18.5; H, 4.0. Calculated for $C_{11}H_{27}As_3Cl_3Bi$: C, 18.9; H, 3.9 %.

[$BiBr_3$(triars)]

$BiBr_3$ (0.16 g, 0.4 mmol) with triars (0.155 g, 0.4 mmol) in MeCN (5 cm^3) gave a yellow solid which was filtered and dried *in vacuo*. Yield 0.200 g, 64 %. Found: C, 15.5; H, 3.0. Calculated for $C_{11}H_{27}As_3Br_3Bi$: C, 15.9; H, 3.3 %.

[BiI_3(triars)]

BiI_3 (0.206 g, 0.4 mmol) with triars (0.155 g, 0.4 mmol) in MeCN (10 cm^3) gave an orange solution. Removal of solvent *in vacuo* produced an orange oil. Stirring

this oil in anhydrous dichloromethane (10 cm^3) produced an orange precipitate which was filtered and dried *in vacuo*. Yield 0.170 g, 47 %. Found: C, 13.7; H, 2.8. Calculated for $C_{11}H_{27}As_3I_3Bi$: C, 13.6; H, 2.8 %.

References

[1] *Advanced Inorganic Chemistry*, F. A. Cotton, G. Wilkinson, C. A. Murillo and M. Bochmann, 6th Edition, Wiley, London, 1999.

[2] N. C. Norman and N. L. Pickett, *Coord. Chem. Rev.*, 1995, **145**, 27.

[3] S. M. Godfrey, C. A. McAuliffe, A. G. Mackie and R. G. Pritchard in *Chemistry of Arsenic, Antimony and Bismuth*, N. C. Norman (Editor), Blackie, New York, 1997, p. 159.

[4] G. Alonzo, M. Consiglio, N. Bertazzi and C. Preti, *Inorg. Chim. Acta*, 1985, **105**, 51.

[5] G. R. Willey, L. T. Daly and M. D. Rudd, *Polyhedron*, 1995, **14**, 315.

[6] R. Luckay, I. Cukrowski, J. Mashishi, J. H. Reibenspies, A. H. Bond, R. D. Rogers and R. D. Hancock, *J. Chem. Soc., Dalton Trans.*, 1997, 901.

[7] W. Clegg, M. R. J. Elsegood, V. Graham, N. C. Norman, N. L. Pickett and K. Tavakkoli, *J. Chem. Soc., Dalton Trans.*, 1994, 1743.

[8] G. R. Willey, L. T. Daly and M. G. B. Drew, *J. Chem. Soc., Dalton Trans.*, 1996, 1063.

[9] G. J. Sutton, *Aust. J. Chem.*, 1958, **11**, 415.

[10] N. W. Alcock, M. Ravindran and G. R. Willey, *J.Chem.Soc.,Chem.Comm.*, 1989, 1063.

[11] R. D. Rogers, A. H. Bond, S. Aguinaga and A. Reyes, *J.Am.Chem.Soc.*, 1992, **114**, 2967.

[12] N. W. Alcock, M. Ravindran and G. R. Willey, *Acta Crystallogr.,Sect.B*, 1993, **49**, 507.

[13] R. Weber, H. Kosters and G. Bergerhoff, *Z.Kristallogr.*, 1993, **207**, 175.

[14] M. G. B. Drew, D. G. Nicholson, I. Sylte and A. Vasudevan, *Inorg.Chim.Acta*, 1990, 171, 11.

[15] J. R. Eveland and K. H. Whitmire, *Inorg. Chim. Acta*, 1996, **249**, 41.

[16] C. J. Carmalt, W. Clegg, M. R. J. Elsegood, R. J. Errington, J. Havelock, P. Lightfoot, N. C. Norman and A. J. Scott, *Inorg.Chem.*, 1996, **35**, 3709.

[17] P. G. Jones, D. Henschel, A. Weitze and A. Blaschette, *Z. Anorg. Allg. Chem.*, 1994, **620**, 1037.

[18] G. A. Bowmaker, J. M. Harrowfield, P. C. Junk, B. W. Skelton and A. H. White, *Aust.J.Chem.*, 1998, **51**, 285.

[19] G. R. Willey, J. R. Barras, M. D. Rudd and M. G. B. Drew, *J. Chem. Soc., Dalton Trans.*, 1994, 3025.

[20] G. R. Willey, M. D. Rudd, C. J. Samuel and M. G. B. Drew, *J. Chem. Soc., Dalton Trans.*, 1995, 759.

[21] W. Clegg, N. C. Norman and N. L. Pickett, *Polyhedron*, 1993, **12**, 1251.

[22] G. R. Willey, M. T. Lakin and N. W. Alcock, *J. Chem. Soc., Dalton Trans.*, 1992, 591.

[23] G. R. Willey, M. T. Lakin and N. W. Alcock, *J. Chem. Soc., Dalton Trans.*, 1992, 1339.

[24] A. J. Blake, D. Fenske, W-S. Li, V. Lippolis and M. Schröder, *J. Chem. Soc., Dalton Trans.*, 1998, 3968.

[25] S. C. Nyburg, G. A. Ozin and J. T. Szymanski, *Acta Crystallogr., Sect. B*, 1971, **27**, 2298.

[26] G. R. Willey, M. T. Lakin, M. Ravindran and N. W. Alcock, *Chem. Commun.*, 1991, 271.

[27] J. F. Sawyer and R. J. Gillespie, *Prog. Inorg. Chem.*, 1986, **34**, 65.

[28] R. P. Oertel and R. A. Plane, *Inorg. Chem.*, 1969, **8**, 1188; A. Hadni, E. Dechamps and J.-P. Herbeuval, *J. Chim. Phys.*, 1968, **65**, 959.

[29] W. Levason, S. D. Orchard, G. Reid and V.-A. Tolhurst, *J. Chem. Soc., Dalton Trans.*, 1999, 2071.

[30] J. R. Black, N. R. Champness, W. Levason and G. Reid, *J. Chem. Soc., Dalton Trans.*, 1995, 3439; J. R. Black, N. R. Champness, W. Levason and G. Reid, *Inorg. Chem.*, 1996, **35**, 1820; 1996, **35**, 4432.

[31] A. L. Rheingold, A. D. Uhler and A. G. Landers, *Inorg. Chem.*, 1983, **22**, 3255; G. R. Willey, H. Collins and M. G. B. Drew, *J. Chem. Soc., Dalton Trans.*, 1991, 961.

[32] A. J. Barton, A. R. J. Genge, W. Levason and G. Reid, unpublished results.

[33] L. F. Warren and M. A. Bennett, *Inorg. Chem.*, 1976, **15**, 3126.

[34] F. R. Hartley, S.G. Murray, W. Levason, H. E. Soutter and C. A. McAuliffe, *Inorg. Chim. Acta*, 1979, **35**, 265.

[35] D. J. Gulliver, E. G. Hope, W. Levason, S. G. Murray, D. M. Potter and G. L. Marshall, *J. Chem. Soc., Perkin Trans. 2*, 1984, 429.

[36] T. Kemmitt and W. Levason, *Organometallics*, 1989, **8**, 1303.

[37] E. G. Hope, T. Kemmitt and W. Levason, *J. Chem. Soc., Perkin Trans. 2*, 1987, 487.

[38] A. G. Aguiar, J. T. Mague, H. J. Aguiar, T. G. Archibald and B. Prejean, *J. Org. Chem.*, 1968, **33**, 1681.

[39] R. D. Feltham, A. Kasenally and R. S. Nyholm, *J. Organomet. Chem.*, 1967, **7**, 285.

[40] SHELXS-86, program for crystal structure solution, G. M. Sheldrick, *Acta Crystallogr., Sect. A*, 1990, **46**, 467.

[41] TEXSAN, Crystal Structure Analysis Package, Molecular Structure Corporation, Houston, TX, 1992.

[42] N. Walker and D. Stuart, *Acta Crystallogr., Sect A.*, 1983, **39**, 158.

[43] SORTAV, R. H. Blessing, *Acta Crystallogr., Sect A.*, 1995, **51**, 33; R. H. Blessing, *J. Appl. Cryst.*, 1997, **30**, 421.

APPENDIX

Infrared spectra were recorded on either a Perkin-Elmer 983G spectrometer or a Perkin-Elmer FTIR 1710 spectrometer in the range 4000-180 cm^{-1}. Samples were prepared as nujol mulls and mounted between caesium iodide plates.

C and H analyses were performed by the microanalytical laboratory of Imperial College, London and by Dr. W. Levason on an F&M Model 185 Analyser at the University of Southampton. Br and I analyses were performed by the microanalytical laboratory of the University of Strathclyde.

Variable temperature ^{1}H NMR spectra were recorded over the range 180 - 300 K using a Bruker AM360 spectrometer operating at 360 MHz and are referenced to TMS.

Multinuclear NMR $^{31}P-\{^{1}H\}$, $^{77}Se-\{^{1}H\}$, and $^{119}Sn-\{^{1}H\}$ NMR spectra were recorded on a Bruker AM360 spectrometer. The samples were prepared in 10 mm NMR tubes containing 10 - 15 % deuteriated solvent. $Cr(acac)_3$ was also added to the samples to as a relaxation agent prior to recording the spectra, to avoid signal diminuation *via* the Nuclear Overhauser Effect (NOE) resulting from the negative magnetogyric moment of the tin nucleus. $^{31}P-\{^{1}H\}$ spectra were recorded at 145.5 MHz and referenced to neat external 85 % H_3PO_4; $^{77}Se-\{^{1}H\}$ spectra were recorded at 68.7 MHz and are referenced to neat external Me_2Se; $^{119}Sn-\{^{1}H\}$ spectra were recorded at 134.2 MHz and are referenced to neat external Me_4Sn.

Solid state ^{119}Sn NMR spectra were obtained by Dr. Sandra Dann using a Bruker AM300 spectrometer fitted with multinuclear solid state probe at 111.9 MHz and 300 K. 400 - 500 mg of material were packed into ZrO_2 or SiN rotors and data collected using a spinning speed of 4.5 - 6.5 kHz for best spectra. In cases where insufficient material was available the rotors were topped up with spectroscopic grade KBr. Typical spectral parameters were; contact time 6 ms, recycle time 2 seconds and number of transients typically 20,000. Spectra were rerun at lower speeds (2.5 kHz) to establish central band position where spinning side bands were present. Spectra were referenced to Me_4Sn ($\delta = 0$) and a secondary reference of $SnCl_4$ ($\delta = -150$ ppm) was also employed. The magic angle was initially set using the ^{79}Br resonance of KBr.